

Mg-Al Layered Double Hydroxide: A Potential Nanofiller and Flame-Retardant for Polyethylene

Von der Fakultät Maschinenwesen
der
Technischen Universität Dresden

zur

Erlangung des akademischen Grades
Doktoringenieur (Dr.-Ing.)
angenommene Dissertation

M.Tech. Costa, Francis Reny
geb. am 17.01.1976 in Calcutta, India

Tag der Einreichung: 12.02.2007

Tag der Verteidigung: 09.11.2007

Gutachter: Prof. Dr.rer.nat.habil. Gert Heinrich

Prof. Dr.-Ing.habil Hans-Joachim Radusch

Prof. Dr.rer.nat.habil. Stefan Kaskel

Vorsitzender der Promotionskommission: Prof. Dr.-Ing.habil R. Lange

Dedicated to My Best Friend and Wife
Swapna

Acknowledgment

It is an ultimate pleasure to see the extreme hard work and dedication that I invested in my research during last four years have been acclaimed within scientific community. This success would have never been possible to achieve without the assistance from my supervisors, co-workers, friends and family members. Before presenting my Ph.D. thesis, therefore, I express my deep gratitude to all these kind hearted people.

I was extremely lucky to get Prof. Gert Heinrich and Prof. Udo Wagenknecht as supervisors in my research work at Leibniz-Institut für Polymerforschung Dresden e.V. They not only constantly helped me with inspiration and ideas, but also provided me complete freedom to pursue my own thinking. Prof. Heinrich created a deep interest in me for polymer physics, which I never studies seriously before. Prof. Wagenknecht provided all necessary technical support and infrastructures for my work. Above all, they are very nice persons and I admire their humble and friendly personality.

Besides my supervisors, I would like to remember the co-operation that I have always received from the members of processing group at IPF. Dr. Andreas Leuteritz, Herr Sven Wiessner and Frau Ulrike Jentsche-Hutschenreuter were the most helpful persons from this group on whom I relied a lot. They not only helped me while working in the chemical and processing laboratory, but also were always available in solving my personal problems. The numerous discussions with Dr. Leuteritzs were always thoughtful and productive for my work. I also thank Herr Bernd Kretzschmar, Herr Andreas Scholze, Herr Dirk Pahlitzsch, Frau Maria Auf der Landwehr and others for helping me while working in the large processing laboratory.

I specially thank Dr. Marina Grenzner who helped me in doing detail analysis and modeling of the rheological characteristics of my materials. Her strong theoretical knowledge was a great support for me in this regard.

The members from the other working groups at IPF were also helped me during my research work. Dr. Dieter Jehnichen helped me for XRD analysis of my samples, Frau Liane Haussler and Frau Kerstin Arnhold for thermal analysis, Frau Gudrum Adam for FTIR analysis, Frau Ute Reuter for mechanical testing, Frau Dr. Victoria Albrecht for BET analysis and many others for providing occasional assistance. I thank all of them from the deep of my heart. I also thank Dr. Ulrike Staudinger, Dr. Mahmoud Abdel Goad, Dr. Roland Vogel and many others for helping me in several ways.

I also acknowledge the financial support received from Deutsche Akademischer Austauschdienst (DAAD) as a DAAD-Leibniz scholar during my whole Ph.D. research period.

Forgetting the support from my family members at this moment would be a big hypocrisy for me. My parents always supported my venture into higher study through their constant inspiration, love and sacrifice. My Ph.D. work would have never been possible without the support of my wife, Swapna. She took care of all aspect of my life as a friend and a real well-wisher. Her company keeps me relaxed and in peace during the difficult situations of my life.

Contents

1	Introduction	1
1.1	Objective	1
1.2	Basics of Polymer Flammability and the Role of Flame-Retardants	2
1.3	Environmental Concerns Relating Common Flame-Retardants and the Prospect of Mg-Al-LDH	4
1.4	Synopsis of the Presented Work	5
2	Literature Review	6
2.1	Layered Double Hydroxide	6
2.2	An Overview of LDH Based Polymer Nanocomposites	8
2.2.1	Preparation	8
2.2.1.1	In-situ Polymerization	9
2.2.1.2	Solution Intercalation of Polymers within LDH Layers	12
2.2.1.3	Melt Compounding Method	13
2.2.2	Properties of Polymer/LDH Nanocomposites	14
2.2.2.1	Morphological Characteristics	14
2.2.2.2	General Properties of Polymer/LDH Nanocomposites	18
2.3	Potential Applications of LDH Materials	21
2.4	Nanoclays as Flame-Retardant in Polymer	23
2.4.1	Flammability of Layered Silicate based Polymer Nanocomposites	23
2.4.2	LDH Clay as Flame-Retardants for Polymer	25
3	Experimental: Compounding and Characterization	28
3.1	Materials Description	28
3.1.1	Mg-Al-LDH	28
3.1.2	Chemicals Used for LDH Synthesis	29
3.1.3	Surfactants	29
3.1.4	Polymers	29
3.2	Melt Processing	30
3.2.1	Introduction	30
3.2.2	Mixing in Batch Mixer (Brabender Plasticorder)	30
3.2.3	Mixing in Extruder	31
3.3	Characterizations	32
3.3.1	X-ray Diffraction Analysis	32

3.3.2	FTIR Analysis	33
3.3.3	Morphological Analysis by Electron Microscopy	33
3.3.4	Thermal Analysis	33
3.3.5	Rheological Analysis	33
3.3.5.1	Dynamic Oscillatory Shear Experiment	33
3.3.5.2	Step Strain Experiment	34
3.3.5.3	Non-linear Shearing or Flow Reversal Experiment	34
3.3.6	Mechanical Properties and Fracture Behavior	35
3.3.7	Flammability Properties	35
3.3.7.1	Limiting Oxygen Index (LOI)	35
3.3.7.2	Cone Calorimeter Test	36
3.3.7.3	UL-94 testing	38
4	LDH: Synthesis, Modification and Characterization	40
4.1	Synthesis	40
4.2	Modification of LDH	40
4.3	Characterization of LDH Materials	41
4.3.1	Characterization of the Unmodified Clays	41
4.3.2	Characterization of the Modified Clays	44
4.3.2.1	XRD Analysis	44
4.3.2.2	FTIR Analysis	46
4.3.2.3	Morphological Analysis	50
4.3.2.4	Thermal Analysis	51
4.3.2.5	SDBS Modified LDH or LDH-DBS	53
4.4	Conclusion	59
5	Characterizations of PE/LDH Nanocomposite	60
5.1	Morphological Characterizations	60
5.1.1	Introduction	60
5.1.2	PE/LDH Nanocomposite Prepared in Small Batch-Mixer	61
5.1.3	PE/LDH Nanocomposite Compositions Prepared in Twin-Screw Extruder	63
5.2	Thermal Analysis	69
5.3	Rheological Analysis	72
5.3.1	Introduction	72
5.3.2	Linear Viscoelastic Behavior	74
5.3.3	Non-Linear Viscoelastic Behavior	80
5.3.3.1	Non-linear rheological behavior of unfilled PE	81
5.3.3.2	Non-Linear Rheological Behavior of PE/LDH Nanocomposites	85
5.3.3.3	Modeling of non-linear rheological behavior of PE/LDH nanocomposites	91
5.4	Mechanical Properties and Fracture Behavior	94

6	Flammability Properties of LDH Based Composites	100
6.1	PE/LDH Nanocomposites	100
6.1.1	Flammability Study by LOI	100
6.1.2	Flammability Study by UL94	102
6.1.3	Flammability Study by Cone Calorimetry	103
6.2	PE/LDH/Mg(OH) ₂ Composites: Synergistic Effect	111
7	Conclusions and Outlooks	118
	Appendices	142
A	Theoretical Calculation of Combustion Residue	143
B	Rheological Measurements	145
C	Surface energy measurement using capillary penetration method	147
D	Curriculum Vitae of Francis Reny Costa	149

Nomenclature

LDH	layered double hydroxide
MH	magnesium hydroxide
Mg-Al-LDH	magnesium and aluminum based LDH
HRR	heat release rate
PHRR	peak heat release rate
THR	total heat released
SEA	specific extinction area
t_{ig}	ignition time
LOI	limited oxygen index
$T_{0.1}$ and $T_{0.5}$	temperature at 10.0 and 50.0 % weight loss respectively
DBS	dodecylbenzenesulfonate
DS	dodecylsulfate
BEHP	bis (2-ethylhexyl)hydrogenphosphate
CLDH	calcined LDH
LDHR	regenerated LDH
G'	storage modulus
G_{prime}	loss modulus
$ \eta^* $	complex viscosity
$G(t)$	stress relaxation modulus

INTRODUCTION

1.1 Objective

Polymers constitute a versatile class of materials that can be designed to obtain wide ranges of properties, making them an inevitable choice for large scale applications in various fields, like household commodities, transport, building, electrical, electronic, space applications, etc. However, in many applications, the intrinsic flammability of common polymers often restricts their use in spite of their enormous design flexibility and performance efficiency. Being organic in nature, both synthetic and natural polymers are usually combustible and decompose into volatile combustible products when exposed to heat. In addition to immediate fire risk posed by the polymeric materials while burning, their combustion products often cause serious threat to human health and environment. In United States alone between 1996 and 2005, an average of 3,932 human loss and another 20,919 injuries (excluding the events of September 11, 2001) were reported annually as the result of fire accidents [1]. Additionally, all these fire accidents together involve loss of properties worthy of several thousand millions of dollars. Thus, the improvement of flammability of polymeric materials continues to remain as a very fresh area of research for polymer chemists and material engineers. Such research is also highly encouraged by the polymer industries because of huge economic and sociological casualties involved each year in fire accidents. Among the various methods of improving flammability of polymeric materials, incorporation of flame-retardant chemicals is a very commonly used one. These flame-retardant chemicals called flame-retardants, execute certain specific function(s) during combustion process in order to either extinguish the flame or to slow its propagation. The present work and the relevant reporting involve the investigation of a relatively new inorganic material, namely layered double hydroxide (LDH) as potential flame-retardant for polymers. The basic reason for selecting LDH or more specifically magnesium-aluminum based LDH (Mg-Al-LDH) is their typical metal hydroxide-like chemistry and conventional clay-like layered crystalline structure. The former can be helpful in their direct participation in flame inhibition through endothermic decomposition and stable char formation. Whereas, the later makes them suitable for polymer nanocomposite preparation, which can improve their dispersion in polymer matrix. In fact, the principle used for the preparation of layered silicate based polymer nanocomposites has also been employed here to incorporate Mg-Al-LDH in polymer matrix. The polymer chosen for the present work is low density polyethylene (PE), which belongs to one of the most widely used and extremely flammable group of polymers i.e., polyolefins.

1.2 Basics of Polymer Flammability and the Role of Flame-Retardants

When both natural and synthetic polymers are exposed to a source of sufficient heat energy, a process called pyrolysis starts that liberates flammable volatiles. These volatiles then mix with air (containing oxygen) and undergo ignition when the temperature is sufficiently high. Therefore, three steps are involved for whole combustion process: heating, thermal decomposition or pyrolysis and ignition into flame [2]. If the heat of combustion is enough to sustain the pyrolysis and the subsequent ignition, polymers burn spontaneously even after the removal of the external heat source. Thus a self-sustaining combustion cycle is established, which has been schematically demonstrated in **Figure 1.1**. Pyrolysis is an endothermic process as the dissociation of chemical bonds always requires some energy. Whereas, the ignition during which the flammable products of pyrolysis reacts with oxygen, is always an exothermic process and provides a thermal feedback mechanism for the combustion process. Ignition starts when temperature reaches the characteristic ignition temperature of the volatiles and depends on factors, like availability of oxygen, chemical stability of the volatiles and obviously temperature. In a self-sustaining combustion cycle, the heat produced by the ignition propagates the pyrolysis process along the fresh polymer surface and maintains the supply of fuel to the flame front. This results in spreading of the flame over the whole polymer surface. A schematic display how flame spreads along surface is given in **Figure 1.2**, where the 'diffusion flame' (so called as oxygen is diffused into the flame to sustain it) spreads over the decomposing polymer surface. The heat of combustion is an important factor that influence the rate of flame spread.

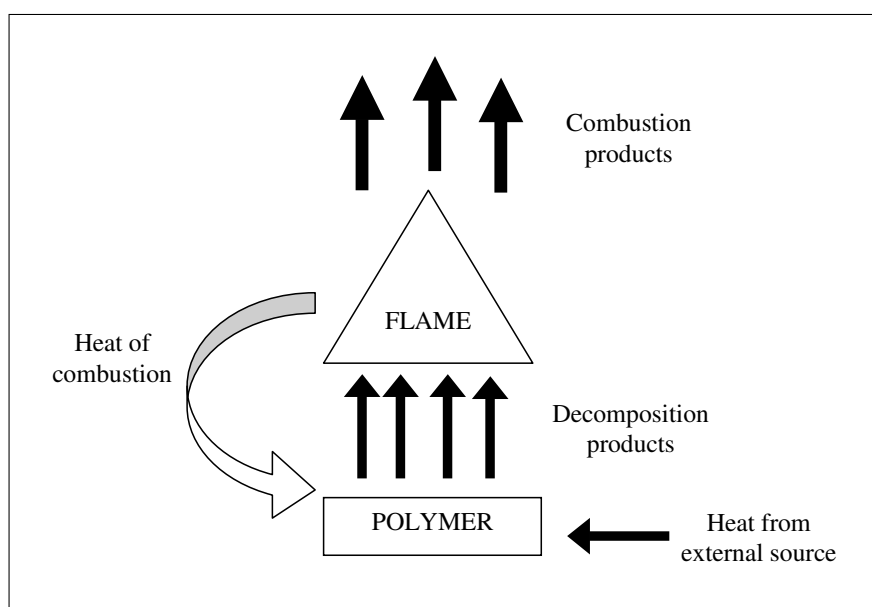


Figure 1.1 Schematic representation of polymer combustion process [2].

The flammability of a polymeric substance is determined by several factors like, the energy required to raise the temperature at which spontaneous pyrolysis and gasification of the decomposition products can occur, the amount and the nature of the pyrolysis products and the combustion residue, etc. When flame-retardants are incorporated into a polymer matrix, they execute the flame inhibition activities through different mechanisms such as the gas phase mechanism, the condensed phase mechanism and through physical effect [2, 3].

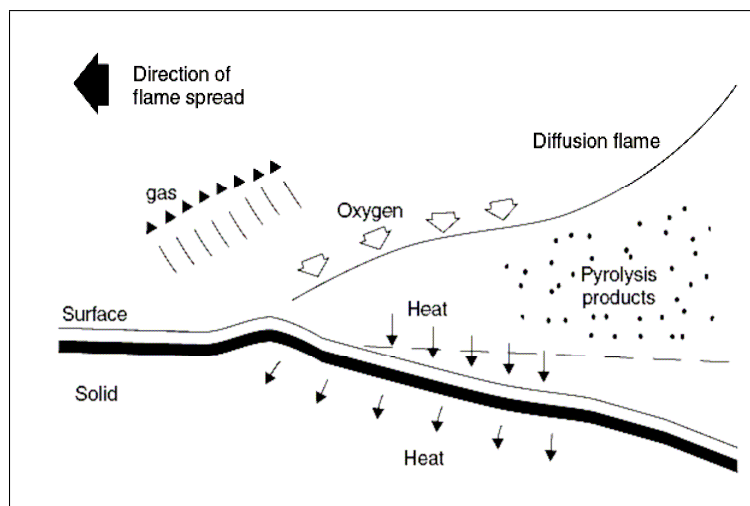


Figure 1.2 Schematic flame spread during of polymer combustion process [2].

Polymers upon pyrolysis generates active species that react with atmospheric oxygen producing H_2-O_2 radical scheme involving OH and H radicals. This radical scheme propagates the flame over the polymer surface. In gas phase mechanism, the decomposition products of the flame-retardants interact chemically with these radicals and cause flame inhibition. All halogen containing flame-retardants primarily act through this mechanism. During combustion, they produce halogen atom and hydrogen halide. The free halogen atoms, if generated, react with the combustible pyrolysis products and produce hydrogen halides. These hydrogen halides are the actual flame inhibitor that cut off the flame propagation through inactivation of the radical species, like OH, and H radicals in the H_2-O_2 radical scheme [2, 4].

In condensed phase mechanism, the flame-retardant chemicals directly react with polymer at a temperature below the pyrolysis temperature of the latter. Such interaction often occurs through non-oxidative dehydration of the polymeric matrix resulting in lowering of its oxygen content and ultimately leads to the formation of carbonaceous char. This not only reduces the formation of carbon monoxide and carbon dioxide, but also the resultant char forms a barrier layer against the flame propagation and heat conduction [2, 4]. The phosphorous containing flame-retardants usually act through this mechanism.

The flame-retardants that inhibit flame exclusively through physical effects do not usually chemically interact with polymers or pyrolysis products. They are decomposed below the pyrolysis temperature of polymers and impart flame inhibition effect both in gas phase and in condensed phase. The endothermic decomposition of these flame-retardants acts as a heat sink causing cooling effect to the surrounding and the inactive gaseous decomposition products cause dilution effect in the gas phase lowering the effective concentration of the combustible volatiles in the flame zone. The flame-retardants that act through this mechanism include various metal hydroxides, borates, talc, etc. Their thermal decomposition residue, which is most often metallic oxides, also contributes to flame inhibition through stable char formation on the burning surface and occasionally catalysing the carbonaceous char formation in case of polymers that undergoes acid catalyzed dehydration reaction [2, 4].

1.3 Environmental Concerns Relating Common Flame-Retardants and the Prospect of Mg-Al-LDH

Though the primary purpose of using flame-retardants in polymers is very noble, conventional flame-retardants have many negative effects. This includes mainly the toxic effect of the decomposition products of the flame-retardant chemicals, both direct and indirect, to the human lives and the environment. Among the conventional flame-retardants, the toxicity issue related to various halogen containing ones has drawn more attentions. The polyhalogenated diphenyl ethers, the commonly used halogen containing flame-retardants, produce highly toxic dioxins and furans during non flaming thermal decomposition [2, 3]. These toxic by products may contaminate everything from whale bladder to dolphins to human blood to household dust and to sludge. Also during combustion, halogen containing flame-retardants produce acidic and corrosive fumes causing direct health concern for lives in the immediate vicinity of a fire. The phosphorous containing flame-retardants, though mainly act in the condensed phase, may also release some gaseous phosphorous containing toxic chemical (which are often neurotoxic or carcinogenic) during combustion [2]. Because of all these environmental and health concerns related to halogenated and many phosphorous based conventional flame-retardants, the search for environment friendly and non-toxic flame-retardants has been increased in the recent years, especially after growing restriction against the use of halogen containing flame-retardants.

For years, scientists have been using the concept of nanotechnology to improve the flame retardancy of polymer composites. This approach involves the dispersing of an inorganic filler in nanoscale as flame-retardants into a polymer matrix. Usually, layered silicates and various nanoparticles (like, MgO , $\text{Mg}(\text{OH})_2$, etc) after suitable pretreatment are used for this purpose. The various research reports have already shown that such an approach indeed improves the flammability of the composites. Often satisfactory flammability improvements can be achieved in these composites when a small amount of secondary flame-retardant is incorporated along with the nanofillers. The advantages of this approach are the significant reduction of the amount of the flame-retardant loading and nontoxic decomposition products from the flame-retardants. Mg-Al-LDH is a material that combines the characteristics of $\text{Mg}(\text{OH})_2$, a commonly used flame-retardant in polyolefin, and the structural features of layered silicates, commonly used clay materials for polymer nanocomposite preparation. Like $\text{Mg}(\text{OH})_2$, Mg-Al-LDH undergoes endothermic decomposition releasing the bound water and producing a metal oxide residue. Therefore, Mg-Al-LDH has a definite potential as flame-retardant, which can act through physical effect described before. Additionally, its layered silicates-like structure, makes it suitable for preparing polymer/clay-based nanocomposites. This can lead to an improved dispersion of the filler particles through intercalation and exfoliation crystal layers by polymer chains, which is unlikely in case of $\text{Mg}(\text{OH})_2$. Because of these interesting characteristics, Mg-Al-LDH can be an interesting material to be investigated as potential flame-retardant nanofillers for polymers. Besides, non toxic nature of Mg-Al-LDH makes it an environment-friendly additive for polymers. Therefore, the aim of the present work was to investigate the potential of this Mg-Al-LDH clay as a nanofiller for PE and its ability to improve the flammability properties of the polymer.

1.4 Synopsis of the Presented Work

In the presented work, Mg-Al-LDH has been used as a nanofiller and a potential flame-retardant additive in a commercially available low-density polyethylene (PE) matrix. The investigation started with a thorough literature review of the present art of work involving LDH and LDH-based polymer nanocomposites. An overview of LDH preparation, its organic modification and polymer/LDH-based nanocomposite preparation are given at the beginning. Then various characteristic features of LDH-based polymer nanocomposites in terms of particle dispersion, properties, etc are described in details. Also a general overview of various potential applications of LDH materials is given. The use of nanoclay as flame-retardants in polymer is an upcoming field with many interesting developments. Usually, layered silicate type of clays are used for this purpose. So, a brief review of nanoclay in general as flame-retardant and their comparison with LDH as potential flame-retardant nanofiller have also been given.

The various materials used in the present study and their basic features are described in Chapter 3. The experimental methods and analytical tools used for characterization of the LDH materials and the nanocomposites are also presented.

The actual experimental work started with the synthesis and the organic modification of Mg-Al-LDH, which are reported in Chapter 4. The main purpose of this section was to study the intercalation behavior of Mg-Al-LDH with various organic surfactants. Both the pristine and the modified clay materials have been characterized in details using various analytical techniques. The organically modified Mg-Al-LDH that showed best properties, mainly in terms of interlayer separation, was chosen for the preparation of PE/Mg-Al-LDH (henceforth will be designated as PE/LDH) nanocomposites using melt compounding technique. This particular organically modified Mg-Al-LDH was characterized in details.

The characterization of PE/LDH nanocomposite compositions have discussed in details in Chapter 5. Primarily, X-ray diffraction (XRD) and electron microscopy were used to investigate morphological features and the nature of LDH particle dispersion in PE matrix. Also thermal properties of the nanocomposites studied in details to investigate the influence of LDH clay on the thermal stability of the final composites. The melt rheological analysis is a very useful method to study flow behavior of the polymeric melts. This method is also a complementary method to the XRD and electron microscopy for studying the nature of filler particle dispersion in matrix. Therefore, a detailed rheological investigation of the PE/LDH nanocomposite melts were performed. The performance of a flame-retardant also depends on how it influences the mechanical properties of the final composites. This is because often higher loading of the flame-retardants is limited by the deterioration of the mechanical properties and processing irregularities. Therefore, the mechanical characteristics and the fracture behavior of the nanocomposite compositions were also studied in details.

Chapter 6 has been devoted to the discussion of the flammability properties of the PE/LDH nanocomposites. The flammability performance of this material has been investigated using various standard techniques, like cone-calorimetry, UL-94 test methods, limited oxygen index (LOI) determination, etc. The synergistic effect of the LDH nanoparticles with conventional $\text{Mg}(\text{OH})_2$ flame-retardant was also investigated.

Finally, the summary of the whole work and future outlooks regarding the use of LDH as flame-retardant nanofillers are presented in Chapter 7.

LITERATURE REVIEW

2.1 Layered Double Hydroxide

Layered double hydroxides (LDHs) belong to a general class called anionic clay minerals. They can be of both synthetic and natural origin. The most commonly known naturally occurring LDH clay is hydrotalcite having chemical formula $\text{Mg}_6\text{Al}_2(\text{OH})_{16}\text{CO}_3 \cdot 0.4\text{H}_2\text{O}$. Hydrotalcite is the first mineral of this group whose structure and properties were studied extensively and often taken as the representative of the LDH clay materials. Hence, the LDHs are also known as hydrotalcite-like-compounds. The general chemical formula of LDH clays is written as $[\text{M}^{\text{II}}_{1-x}\text{M}^{\text{III}}_x(\text{OH})_2]^{x+}(\text{A}^{n-})_{x/n} \cdot y\text{H}_2\text{O}$, where M^{II} is a divalent metal ion, such as Mg^{2+} , Ca^{2+} , Zn^{2+} , etc, M^{III} is a trivalent metal ion, such as Al^{3+} , Cr^{3+} , Fe^{3+} , Co^{3+} , etc and A^{n-} is an anion, such as Cl^- , CO_3^{2-} , NO_3^- , etc. The anions occupy the interlayer region of these layered crystalline materials. Although a wide range of values of x is claimed to provide LDH structure, the pure phase of LDH clays is usually obtained for a limited range as $0.2 \leq x \leq 0.33$ [5].

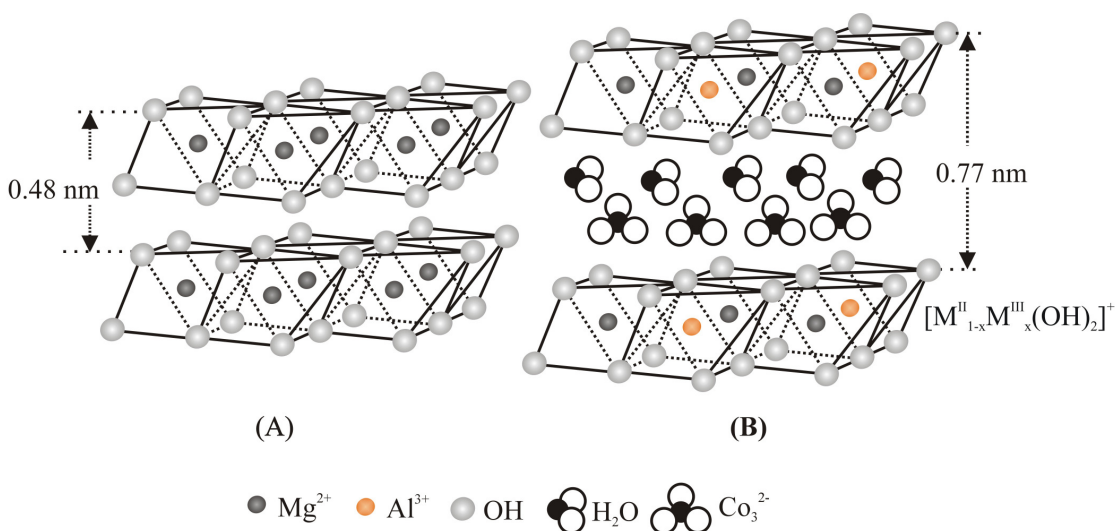


Figure 2.1 Schematic Representation comparing the crystal structure of brucite (A) and LDH (B)

The structure of LDHs can best be explained by drawing analogy with the structural features of the metal hydroxide layers in mineral brucite or simply the $\text{Mg}(\text{OH})_2$ crystal structure. Brucite consists of a hexagonal close packing of hydroxyl ions with alternate octahedral sites occupied by Mg^{2+} ions. The

metal hydroxide sheets in brucite crystal are neutral in charge and stack one upon another by Van der Waal's interaction. The interlayer distance or the basal spacing in brucite has a value of about 0.48 nm. In LDH, some of the divalent cations of these brucite-like sheets are isomorphously substituted by a trivalent cation and the mixed metal hydroxide layers, $[M^{II}_{1-x}M^{III}_x(OH)_2]^{x+}$, thus formed acquire a net positive charge. This excess charge on the metal hydroxide layers is neutralized by the anions accumulated in the interlayer region. The interlayer region in LDHs also contains some water molecules for the stabilization of the crystal structure. The presence of anions and water molecules leads to an enlargement of the basal spacing from 0.48 nm in brucite to about 0.77 nm in Mg-Al-LDH. A schematic representation comparing the brucite and the LDH structures is shown in **Figure 2.1**.

Although LDHs have layered structure like layered silicates, the two are quite significantly different from each other. While LDHs have positively charged layers with anionic interlayer species (so they are called anionic clay), the layered silicates have negatively charged layers with cationic interlayer species (hence called cationic clay). In terms of compositions, geometry and layer thickness, LDHs are vastly different from layered silicates. In LDH, as described earlier, each crystal layer is composed of a single octahedral metal hydroxide sheet. Whereas, in layered silicates, it is a sandwiched structure of two or more sheets of metal oxides. For example, montmorillonite crystal layer is made up of three sheets. One octahedral sheet containing oxides of Fe, Al, Mg, etc remains sandwiched between two silica tetrahedral sheets. This difference in layer structure results much lower crystal layer thickness and rigidity in case of LDHs.

The charge density of hydroxide sheets in LDHs is in the range of $0.33 - 0.25 \text{ Cm}^{-2}$ (as high as in mica, $0.32 - 0.34 \text{ Cm}^{-2}$) [6], which is much higher compared to that observed in various cationic clays of both natural and synthetic origin. However, the remarkable behavior of LDH is their high reactivity toward various organic anions, which can exchange as much as 80 – 100% of the interlayer anions in LDHs [6].

Many LDH materials show unique phenomenon called 'memory effect', which involves the regeneration of the layered crystalline structure from their calcined form, when the later is dispersed in an aqueous solution containing suitable anion [7]. This property is often used to synthesize and modify LDHs with different types of intercalating anions. Typically, LDHs containing carbonate anion are heated to a temperature in the range of 350–800 °C for several hours and the resultant mixed metal oxide (more precisely a solid solution of the two metal oxides) is then dispersed in an aqueous solution of the desired anionic species. The dispersion is stirred mechanically for overnight at room temperature to ensure completion of the regeneration process. The regeneration property shown by LDHs is extensively reported in numerous literatures [5, 6, 8, 9]. There are several methods by which LDHs can be synthesized. However, all these methods may not be suitable and equally efficient for every combination of metal ions. Some of the methods described in literatures are listed below.

The co-precipitation method involves co-precipitation of selected pairs of metal ions from their aqueous solution by a dilute NaOH or NaHCO_3 or Na_2CO_3 or NH_4OH solution. The pH of the reaction medium is maintained in the range of 8 to 10 depending on the nature of the metal ions. To obtain well crystallized materials the final suspension is subjected to hydrothermal treatment for a long period. The detail description of the process is available in numerous reports available in literature [10–13].

The homogeneous precipitation method using urea hydrolysis for synthesis provides LDH with a high degree of crystallinity and a narrow distribution of particle size. Usually, an aqueous solution

of desired metal ions and urea in calculated molar ratio is heated in the temperature range 90 °C to reflux condition for 24 – 36 hours. The urea molecules undergo decomposition producing ammonium carbonate, which finally causes the precipitation of LDH containing CO_3^{2-} as intercalating anion. More descriptive procedure of this method can be found in several literatures cited in reference [14–16].

The ion exchange method takes the advantage of exchangeable interlayer anions present in LDHs by other anionic species. Based on this property, the LDHs containing one type of intercalating anionic species can be synthesized from the LDHs containing another type of intercalating anion. Usually, the original LDH is dispersed in an aqueous solution of the desired anionic species and the dispersion is stirred at room temperature for several hours. However, some anionic species show more affinity to the inter gallery region of LDH than the other. More intensive literatures dealing with this method of synthesis of LDH are given in reference [17–19].

Hydrothermal crystallization method involves the crystallization of amorphous $\text{M}^{\text{III}}_2\text{O}_3$ precursor in presence of a suitable $\text{M}^{\text{II}}\text{O}$, the latter acting as a crystallizing agent [20]. The precursor $\text{M}^{\text{III}}_2\text{O}_3$ is an amorphous hydrated oxide of the trivalent metal component of LDH whereas the crystallizing agent $\text{M}^{\text{II}}\text{O}$ is a reactive and basic oxide of the divalent metal component. The actual synthesis is carried out by hydrothermal treatment of an aqueous suspension of these two metal oxides in a pressurized vessel at elevated temperature for several days.

2.2 An Overview of LDH Based Polymer Nanocomposites

2.2.1 Preparation

Although the usages of LDHs in different fields, like catalysis, acid scavenger, controlled chemical release, etc. are well known, their potential as nanofillers in preparing polymer nanocomposites is very recently realized by researchers. In this regard, unlike conventional layered silicates (which is widely used so far as nanofiller in polymer), LDHs possess certain inherent advantages. For example, being mostly of synthetic origin, the presence of impurity in LDHs is far less and also a wide range of chemical compositions can be obtained by changing the type and molar ratio of the metal ion pairs during the synthesis process. Additionally, the positive nature of the crystal layers in LDHs provides a greater flexibility in selecting the suitable modifier from several groups of organic compounds, like fatty acid salts, sulfonates, sulfates, phosphates, etc [6, 21, 22]. The LDHs apparently resemble many cationic clay minerals (like layered silicates) so far as the principle of polymer nanocomposite preparation is concerned. But, the major disadvantage of LDHs is the high charge density of layers, which firmly holds the metal hydroxide layers in the crystalline stacks and makes the intercalation of the polymeric materials into the interlayer region difficult. However, the strong affinity of LDHs for anion exchange reaction even with oligomeric anionic species gives an opportunity to convert these materials into suitable precursors for polymer nanocomposite preparation. In literatures, several methods for the preparation of polymer/LDH nanocomposites have been reported [23], which are described briefly in the following sections.

2.2.1.1 In-situ Polymerization

In-situ polymerisation is the most widely referred technique for polymer/LDH nanocomposites preparation. This method is solution based and is usually carried out in an aqueous system. The scheme shown in **Figure 2.2** indicates the general principle for carrying out in-situ polymerization within the layers of LDH crystals. The primary step is the preparation of monomer intercalated LDH hybrids, which are then subjected to excitation by heat [24, 25], initiating chemicals [26], etc. for carrying out the polymerization reaction. Various methods of intercalation of monomers into the interlayer region of LDHs and their subsequent polymerization have been reported in literatures, which are summarized in **Figure 2.2**.

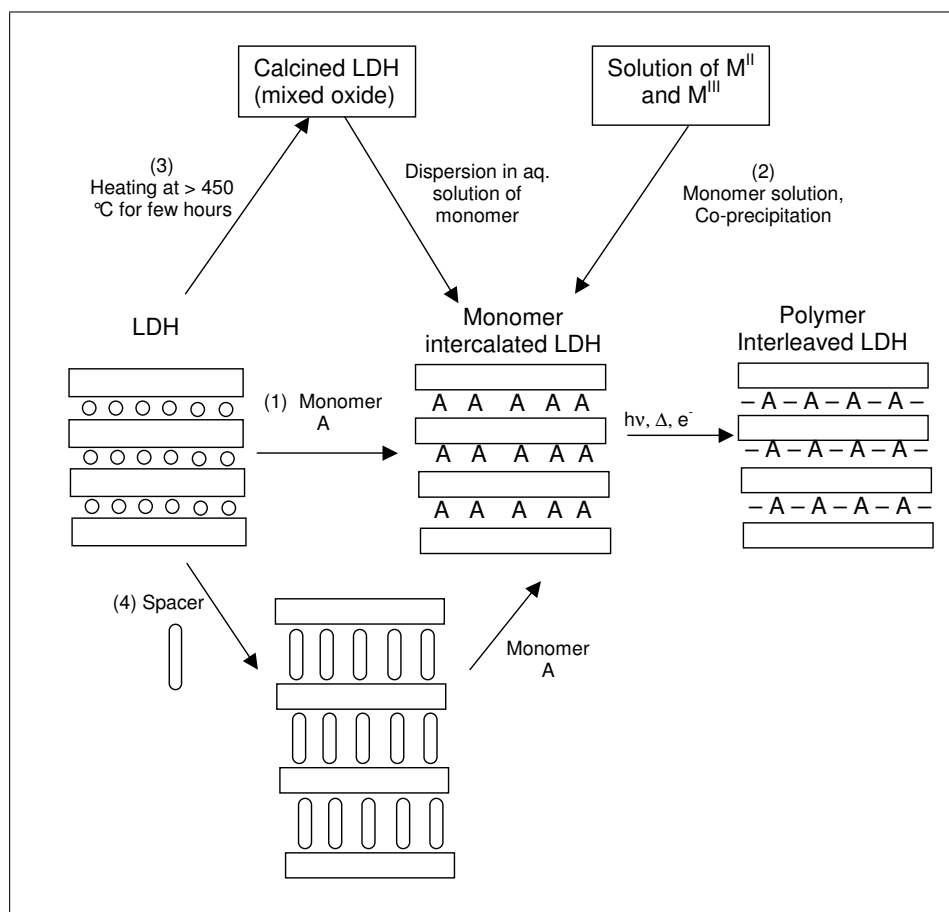


Figure 2.2 Schematic pathways of in-situ polymerization within LDH layers to synthesize polymer-LDH nanocomposites

The anionic interchange method involves the dispersion of LDHs into a monomer solution, most often in aqueous medium (path 1 in **Figure 2.2**) [26–29]. The dispersion is then stirred for several hours with mild heating. The monomer molecules must have anionic functionality or strong nucleophilic sites in order to replace the interlayer anions in LDHs and to stabilize the layered stacking of the hydroxide sheets by neutralizing their excess positive charge. For example, acrylate anions can be easily intercalated into Mg-Al-LDH through ion exchanges with Cl^- or NO_3^- present in LDH [29]. Isupov et al. reported the intercalation of various isomeric anions of amino benzoic acid into Li-Al-LDH and their subsequent polymerisation [30]. Similarly, Leroux and co-workers have intercalated vinyl benzene sulfonate monomer into Zn-Al-LDH [27] and aminobenzenesulfonate monomer into Cu-Cr-LDH [28].

Recently, Lee and Chen have synthesized polyacrylate/LDH-based superabsorbent xerogels using in-situ suspension polymerization technique [26]. They used two different types of monomer intercalated LDH based on acrylate and 2-acryloamido-2-methyl propane sulfonate. These monomer-LDH hybrids were then dispersed in an aqueous solution of sodium acrylate and the polymerization was carried out in presence of a crosslinking agent (N,N'-methylene-bis-acrylamide) and an initiator under stirring at 70 °C for 4 h. The purpose of using the crosslinking agent was to provide a means to crosslink the intercalated monomers with the growing polyacrylate chains.

The most common and successful method of preparation of monomer-LDH hybrid is synthesis of LDH by co-precipitation of metal ions from their mixed solution containing dissolved monomer (usually in form of salt) (path 2, **Figure 2.2**). To minimize the interference with CO_3^{2-} , the reaction mixture is often purged with nitrogen. The formation of hydroxide layers and the inclusion of monomer anion in the interlayer region take place simultaneously. Whilton and co-workers prepared polyamino acid/LDH based nanocomposites following this method [24]. An amino acid intercalated Mg-Al-LDH was prepared by reacting a mixed Mg and Al nitrate solution with a basic solution containing aspartate anion under nitrogen atmosphere. The aspartate-LDH hybrid thus obtained was subjected first to heating at 220 °C for 24 hours followed by the treatment with basic solution. The heat treatment in the first step provides condensation of the aspartate monomer within the interlayer region into polysuccinimide, which in the second step undergoes hydrolysis to form poly(α,β -aspartate) [24]. The other examples of the synthesis of polymer-LDH nanocomposites by co-precipitation method are intercalation and subsequent polymerization of styrene-4-sulfonate within Ca-Al-LDH [31], styrene sulfonate into Zn-Al and Ca-Al-LDH [32], 3-sulfopropyl methacrylate within Zn-Al-LDH [33], etc.

The property of LDH materials to regenerate from an aqueous dispersion of their mixed oxide form is also applied to prepare the monomer-intercalated hybrids (path 3, **Figure 2.2**). This is called regeneration method, which is similar to that used for converting LDH containing CO_3^{2-} to the other forms. This method is very common for the modification of LDH materials with organic molecules, which are then used as a precursor for polymer intercalation by various methods.

The organic/inorganic pillar method (path 4, **Figure 2.2**) differs from the anion exchange method in the sense that an anionic species (other than the monomers) is used in this method as a spacer or pillaring agent to increase the interlayer distance before the intercalation of monomer. Therefore, the monomers in this case interact with a pillared LDH species. Wang et al. [34] used 10-undecenoate pillared Mg-Al-LDH hybrid (prepared by co-precipitation method) as the precursor for methyl methacrylate (MMA) intercalation into LDH and subsequently polymerized the intercalated MMA using a two-step bulk polymerization technique. In the first step called prepolymerization step, a homogeneous mixture of organically pillared LDH and MMA monomer was prepared through constant stirring, which resulted intercalation of MMA into LDH layer. The mixture was then heated at 50°C under nitrogen atmosphere in the presence of small amount of catalyst 2,2'-azobisisobutyronitrile (AIBN) to prepolymerize the MMA monomers. In the second step called casting polymerization, AIBN was again added to the prepolymer mixture at room temperature and injected into a glass mold at 60°C for 4h. The glass mold was then kept in an oven at 120°C for 1h to complete the polymerization process. In another variation they used amino benzoate pillared LDH to prepare poly (methyl methacrylate) (PMMA)/LDH nanocomposite using a single step solution polymerization technique [35]. Challier and Slade [36] reported intercalation of aniline molecule into terephthalate or hexacyanoferate pillared Cu-Cr and Cu-Al-LDH. The

interlamellar oxidative polymerization of aniline molecules yields polyaniline intercalated LDH with retention of the framework of the later. Sugahara and co-workers [37] intercalated acrylonitrile monomer into a dodecylsulfate pillared Mg-Al-LDH to synthesize polyacrylonitrile in the interlayer region. Similarly, O'Leary and co-worker [39] also used dodecylsulfate pillared Mg-Al-LDH to intercalate acry-

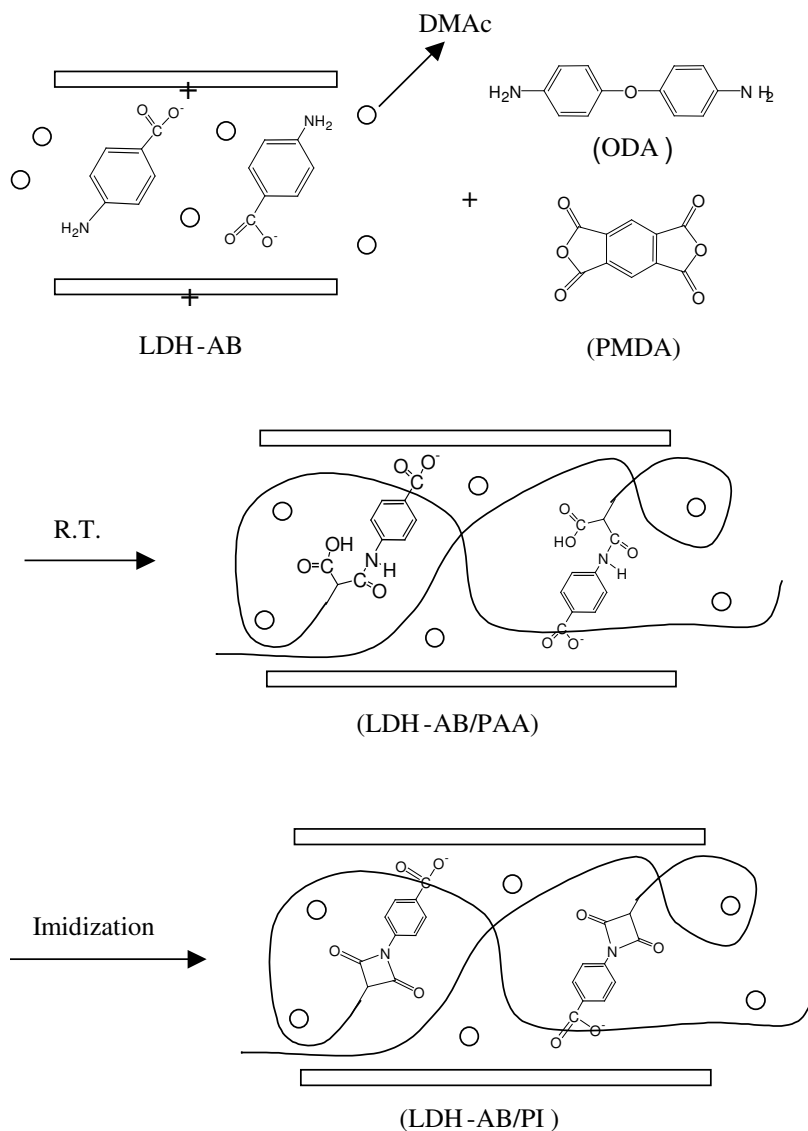


Figure 2.3 Preparation of LDH-polyimide (LDH-AB/PI) nanocomposites (LDH-AB: aminobenzoate intercalated LDH, ODA: 4,4'-oxydianiline, PMDA: pyromellitic anhydride [38].

late monomer and its subsequent polymerization. Although the primary function of the pillaring agent is the expansion of the interlayer distance, it may also actively participate in the interlayer polymerization reaction. The pillaring agent in such case has a functional group similar to the monomer molecules by which it interacts with the growing polymer chains and attach them to the LDH sheet. Hsueh and Chen [38] synthesized LDHs/polyimide nanocomposites an active pillaring agent amino benzoate. The Amino benzoate modified Mg-Al-LDH was used as the precursor for intercalation of monomers (pyromellitic anhydride and 4,4'-oxydianiline). The formation of polyimide in the interlayer region takes place in two

steps through the formation of polyamic acid. The possible mechanism of interlayer polymerization is shown in **Figure 2.3**.

2.2.1.2 Solution Intercalation of Polymers within LDH Layers

The direct intercalation of the polymeric species having functional groups that can interact with the hydroxide layers of LDH is also an effective way to prepare polymer/LDH nanocomposites. Principally, the methods used for intercalation of monomer or small oligomeric organic molecules into LDH, are also applicable for high molecular weight species. But, due to a very small interlayer distance and high charge density of the LDH layers, the direct intercalation of large polymeric chains is more difficult.

Messersmith and Stupp [40] prepared poly(vinyl alcohol) (PVA) intercalated Ca-Al-LDH by precipitating the later in the presence of dissolved PVA. The process involved mixing of a $\text{Ca}(\text{OH})_2/\text{PVA}$ solution to a solution containing $\text{Ca}(\text{OH})_2$ and $\text{Al}(\text{OH})_3$. It was suggested by them that the PVA molecules facilitate the nucleation and the growth of the metal hydroxide layers. Further, Oriakhi and co-workers [41] reported the incorporation of poly(acrylic acid), poly(vinylsulfonate) and poly(styrenesulfonate) into the LDHs, like $\text{M}_{1-x}\text{Al}_x(\text{OH})_2^{x+}$ (where, M is Mg, Ca, Co) and $\text{Zn}_{1-x}\text{M}_x(\text{OH})_2^{x+}$ (where, M is Al, Cr) by precipitating LDH from a deaerated aqueous basic solution containing mixed metal nitrates and dissolved polymer. Other examples of polymer-LDH nanocomposites prepared by direct intercalation through co-precipitation technique are Mg-Al-LDH intercalated with poly(styrenesulfonate), poly(vinylsulfonate) [42], polyaspartate [24], poly(ethyleneoxide) derivatives [43], etc.

Often for the intercalation of polymeric species in solution, organically modified LDH clays are used. Various anionic surfactants, like the salts of the fatty acids with different chain lengths, alkyl or alkyl-aryl sulfonates, etc are usually used for LDH modification. This modification involves the exchange of anionic species present in the unmodified LDH by a suitable organic anion, which is carried out by the similar methods used for LDH synthesis. The organically modified LDHs show higher interlayer separation and increased hydrophobicity, both of which make the polymer intercalation process easier. The high reactivity of LDHs toward various organic surfactant anions, in spite of their high surface charge density, makes the modification process feasible. Intercalation behavior of LDHs toward various organic anionic surfactants is extensively reported in literatures [6, 22, 44–46]. Carlino [22] reviewed different methods for modification of LDHs by long chain carboxylic acids. To prepare polymer nanocomposites, typically the organically modified LDH is dispersed in a solution containing polymer. The resultant dispersion is then stirred or aged under nitrogen atmosphere to accomplish the polymer intercalation. Qu and co-workers prepared and characterized polyethylene/LDH [47, 48] and polystyrene/LDH nanocomposites [49] by this method using dodecylsulfate modified LDH (LDH-DS). The nanocomposites were obtained by refluxing the mixture of LDH-DS and the polymers solution in xylene. Buniak and co-workers [50] also used LDH-DS to prepare poly(ethylene oxide) (PEO)/LDH nanocomposites. The modification of Mg-Al-LDH was carried out using ion-exchange method and the modified LDH was later treated with aqueous solution of PEO to prepare the nanocomposite. Recently, Liao and Ye [51] prepared PEO/LDH based nanocomposite electrolyte by solution intercalation method. First, using the co-precipitation method they modified Mg-Al-LDH with two different types of anionic surfactants: n-alkyl 3-sulfopropyl ether salt (containing about 11 ethylene oxide/mole and $\text{C}_{13} - \text{C}_{15}$ alkyl chain) and oligomeric hydroxy poly(ethylene oxide) phosphate. Then the nanocomposites were obtained by mixing PEO, the modified LDH and lithium perchlorate in anhydrous acetonitrile at 70 °C with constant

stirring for several hours. Further, Li and co-workers [52] prepared glycine intercalated Mg-Al-LDH and modified with formamide, which was then treated with an acetone solution of PMMA to form the nanocomposites. All these cases mentioned so far produce mostly polymer-intercalated LDH particle in the nanocomposite matrix. But, Hsuesh and Chen [53] reported the synthesis of exfoliated epoxy/LDH nanocomposites by treating amino laurate intercalated Mg-Al-LDH with a mixture of epoxy resin and curing agent. The resin and the curing agent diffused into the LDH interlayer region after heating the mixture for few hours. The thermal aging of this reaction mixture causes exfoliation of the LDH layers due to curing of the epoxy resin in between the layers, which results in formation of crosslinked network of epoxy resin.

The direct ion exchange with LDHs by the polymers having anionic functional groups is also a feasible method for the preparation of polymer/LDH nanocomposites. This method does not involve the organic modification of the pristine LDH. Yang and co-worker [54] reported the intercalation of poly(ethylene oxide) sulfate and poly(ethylene glycol) within Mg-Al-LDH by aging a polymer-LDH aqueous suspension at 65 °C for 4 days. Costa and co-workers [55] prepared nanocomposites through intercalation of dendrimers (carboxylate terminated polyamidoamide) into LDH. They observed saturation of dendrimer intercalation into host LDH when the mixing ratio of the two ingredients exceeded 1 : 2 (charge ratio of anionic clay and carboxylate group of the dendrimer). The dendrimers remained densely packed in the interlayer region of LDH with an ellipsoidal shape. When excess dendrimers was used (mixing ratio 1 : 8), in addition to intercalation they were also adsorbed on the clay surface. Similarly, Leroux and co-workers [43] intercalated poly(ethylene oxide) derivatives into Cu-Cr-LDH by replacing Cl^- anion from the interlayer region. They first ultrasonicated the LDH material in decarbonised water, which was then added to a neutralized polymer solution containing an amount of polymer equivalent to twice the anion exchange capacity of the clay.

2.2.1.3 Melt Compounding Method

Perhaps the most challenging method of preparing polymer/clay nanocomposites is the melt compounding method. With non-polar polymers, like polyolefin, it becomes more difficult due to high thermodynamic incompatibility between the non-polar matrix and the polar clay materials. There are not many reports available till today that exclusively deal with the preparation of polymer/LDH nanocomposites using melt-compounding technique. This method has definite technological advantage over the solution method as it can be easily adopted for industrial product manufacture using conventional polymer processing equipments. Therefore, in spite of being most difficult method, melt-compounding method always finds special interest among researchers. Use of Mg-Al-LDH in the preparation of polymer composites using this method is very common, where it is treated as simple metal hydroxide whose basic nature and endothermic decomposition serves two-fold purpose: as acid scavengers in halogenated polymers [56, 57] and as flame-retardant [58]. However, in none of these applications any reference was made to exploit the efficiency of Mg-Al-LDH as nanofiller.

The melt-compounding method used for the preparation of polymer/LDH nanocomposites is similar to that used for conventional polymer/clay nanocomposites. The organically modified LDHs are the suitable precursor for this process, which are mixed with molten polymer in the typical plastic processing equipments. Nichols and co-workers [59] first reported the melt-compounding method for preparing polymer/LDH nanocomposites. Very recently, researchers are showing more interests in this method to

prepare nanocomposites based on different types of matrices. For examples, Zammarano et al. prepared polyamide 6/LDH nanocomposites using organically modified Mg-Al-LDH [60]. They observed that high degree of exfoliation of the LDH particles can be obtained using LDHs with low anion exchange capacity. Lee et al. [61] prepared poly(ethyleneterephthalate)/LDH nanocomposites with Mg-Al-LDH modified with various organic surfactants. They observed improved thermal and mechanical properties of these nanocomposite composition compared to the unfilled polymer. The other reported polymer/LDH nanocomposites systems prepared by melt-compounding methods includes polypropylene/Zn-Al-LDH [62], polyethylene/Mg-Al-LDH [63], polyethylene/Zn-Al-LDH [64], etc.

2.2.2 Properties of Polymer/LDH Nanocomposites

2.2.2.1 Morphological Characteristics

In polymer/clay nanocomposites, complete exfoliation of clay layers results in disappearance of the diffraction maxima in their XRD patterns. However, this can also occur due to other reasons, like extremely low concentration of clay materials in the composites, crystal defects, etc. The majority of the reports on polymer/LDH nanocomposites show the intercalated or swollen nature of the clay structures. The presence of the basal reflections in the XRD patterns of such type of nanocomposites indicates that the LDH crystal structure is not destroyed completely. But, shifting of their positions to lower 2θ values is interpreted as an expansion of the interlayer region by the polymer chains. Besides, broadening of the characteristic reflections in nanocomposites is often related to the defects in the crystal layer stacking caused by the interlayer polymeric species. The information on the arrangements of the polymer chains within the interlayer region can also be obtained from the XRD data, which suggest that both bi-layer and mono-layer arrangements of polymer chains are possible depending on the nature of the chain backbone

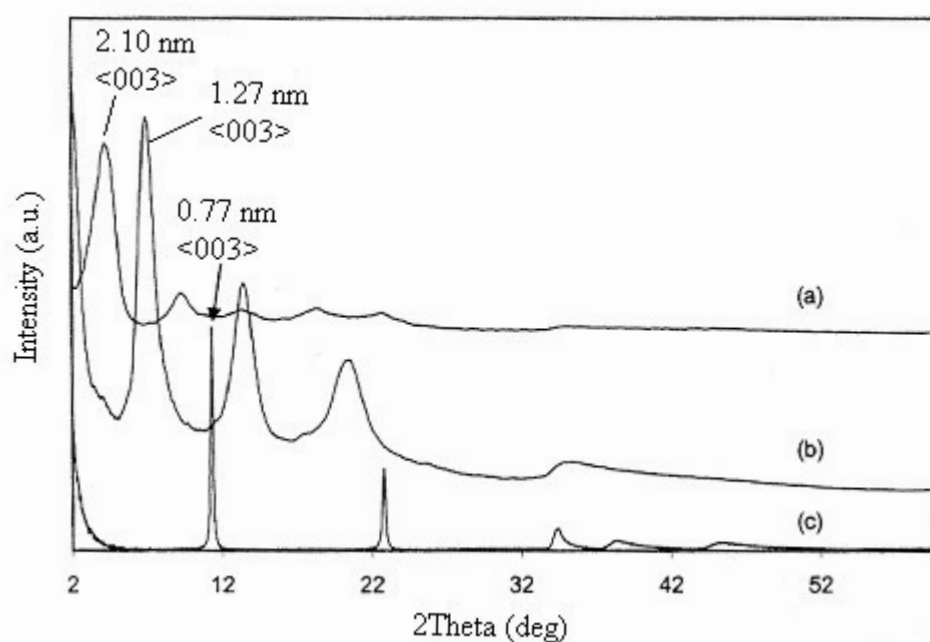


Figure 2.4 XRD patterns of LDH and LDH nanocomposites: (a) LDH-PSS, (b) LDH-PVS and (c) LDH-CO₃ [41].

and the pendent functionalities. For example, **Figure 2.4** shows the XRD patterns of polystyrenesulfonate (PSS) and polyvinylsulfonate (PVS) intercalated Mg-Al-LDH nanocomposites. The theoretical calculations based on these XRD results and molecular dimensions (which gives thickness of the metal hydroxide sheet equal to about 0.48 nm and interlayer gap 0.28 nm) reveal that the interlayer distance increases from 0.76 nm in the original LDH to 1.27 nm to the LDH-PVS hybrid and to 2.10 nm in the LDH-PSS hybrid. The bi-layer thickness of these polymers based on molecular dimensions matches the expanded interlayer distance [41, 42]. Again, the nature of arrangement of the pendent anionic functionality or electron rich moiety (like phenyl ring) on the polymer backbone can also influence the packing nature of the polymers in the interlayer region. For example, syndiotactic polystyrenesulfonate with alternating anionic groups projecting to the opposite sides of polymer backbone forms a monolayer arrangement in Ca-Al LDH host [31].

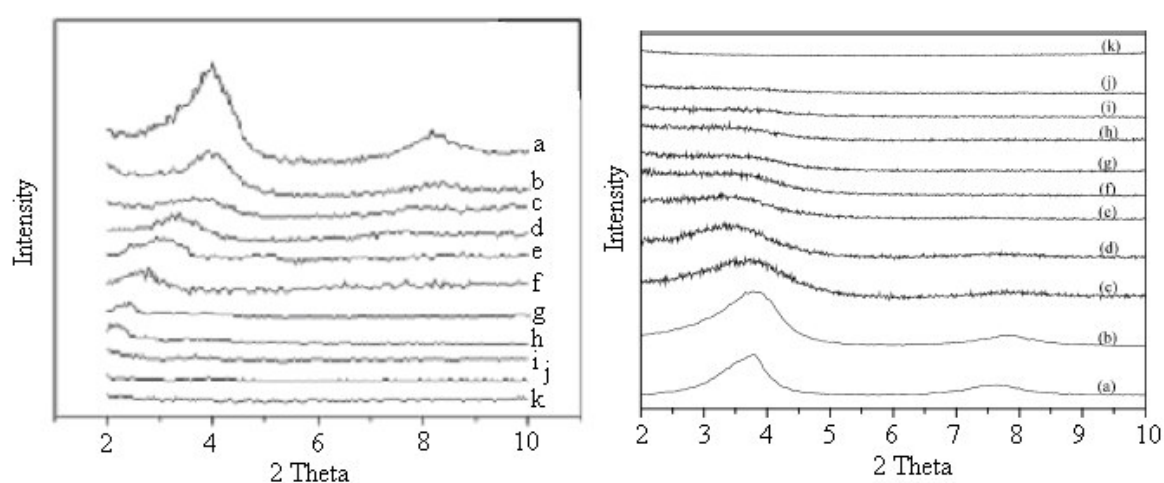


Figure 2.5 (left) The x-ray diffraction patterns of LDHs-aminolaurate (a), LDHs/Epoxy resin (b - e) [(b) - stirred at room temperature for 60 min, (c) - at 55°C for 30 min, (d) - at 55°C for 60 min and (e) - 55°C for 180 min] and LDHs/Epoxy/Curing agent (f - k) [(f) - stirred at room temperature for 60min, (g) - at 75°C for 30 min, (h) - at 75°C for 60 min, (i) - at 75°C for 120 min, (j) - at 135°C for 30 min and (k) - at 135°C for 60 min.] [53]. (right) The XRD patterns of at different stages during two-step bulk polymerization of MMA in presence of organically pillared LDH (LDH-U) and catalysts (a) unmodified LDH-U; (b) mixture of LDH-U, MMA and catalyst stirring at room temperature; at various conversions of MMA during the prepolymerization process (c) 6.3 wt%, (d) 8.4 wt%, (e) 10.5 wt%, (f) 13.2 wt%, (g) 16.2 wt%, (h) 17.1 wt%, (i) 18.3 wt%, (j) 19.6 wt% and (k) LDHs/PMMA nanocomposite [34].

The high degree of exfoliation of the LDH clay layers in polymer nanocomposites has also been reported by several groups [34, 38, 47–49, 60, 65]. When in-situ polymerization technique is used for the synthesis of nanocomposites based on PMMA or epoxy, the development of morphological features can monitored with reaction time using XRD analysis. Usually, the XRD analysis of the reaction aliquots taken at the different stages of such polymerization process reveals progressive delamination of the LDH clay layers with increasing degree of conversion. **Figure 2.5** demonstrates such XRD patterns

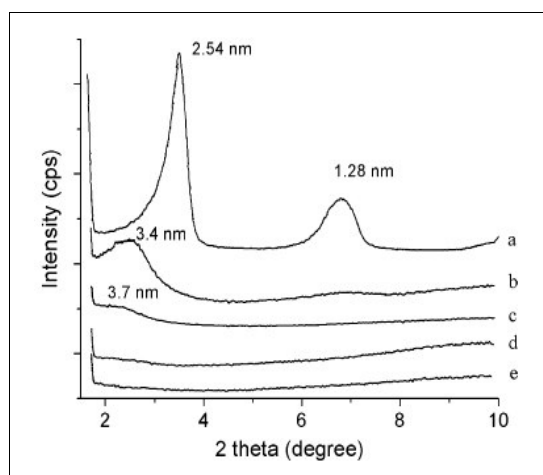


Figure 2.6 Change of XRD patterns with the different contents of LDH content in polystyrene/LDH nanocomposite sample: (a) 100 wt%, (b) 50 wt%, (c) 20 wt%, (d) 10 wt%, (e) 5 wt% [49].

for PMMA and epoxides based nanocomposites. The high degree of exfoliation is not only confirmed from the disappearance of all the characteristic peaks corresponding to LDH after expected conversion, but also from the large extent of polymer fraction unextractable by a suitable solvent from the resultant nanocomposite [65]. When the melt-compounding method is employed for polymer/LDH nanocompos-

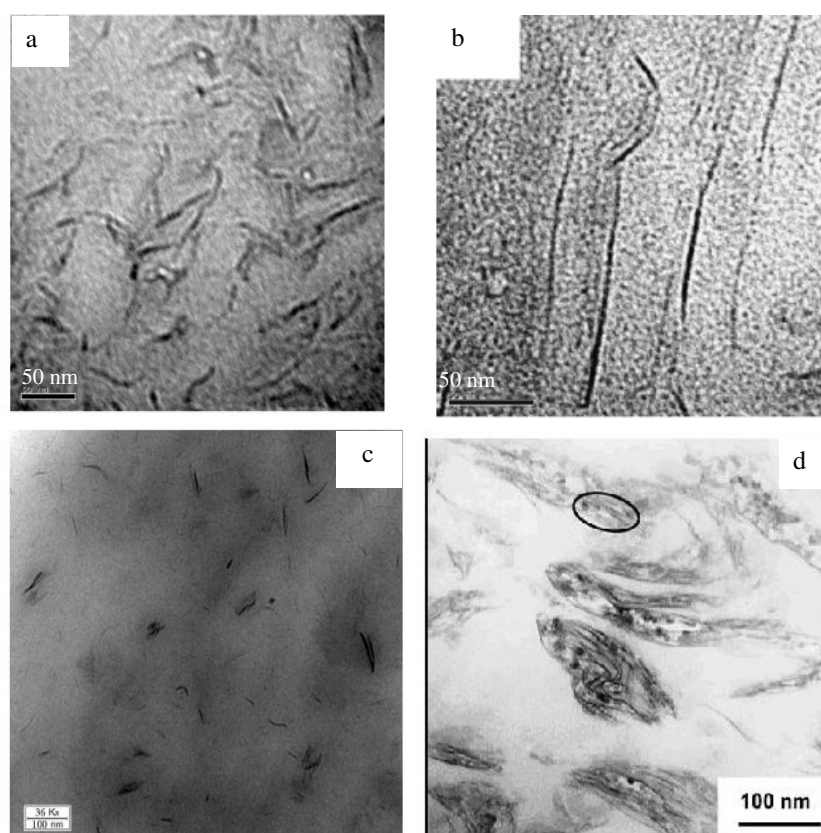


Figure 2.7 TEM micrographs showing LDH particle dispersion in different polymer (a) PMMA [34], (b) epoxy [53], (c) polyamide 6 [60] and (d) polystyrene containing 5 wt% LDH [49]

ites preparation, processing conditions such as temperature, degree of shearing, etc influence the degree of exfoliation of the LDH particles [60]. Besides, the concentration of LDH and the nature of polymer matrix also influence the state of particle dispersion in the nanocomposite. In general, with highly polar matrices, like epoxies, PMMA, polyimide, polyamide, etc the high degree of exfoliation of the LDH clay layers is achieved up to much higher LDH concentration compared to the relatively less polar or non-polar polymers. In later case, the high degree of exfoliation exists at lower concentration of LDH and with increasing concentration agglomerate formation takes place. Chen and co-workers reported that in polystyrene/LDH nanocomposites, fully exfoliated LDH particles are observed at the low concentrations of LDH whereas at high concentrations, the LDH particles mostly have intercalated nature [47–49]. **Figure 2.6** reveals the variation of interlayer separation of Zn-Al–LDH in polystyrene based nanocomposites with LDH concentration. The fully exfoliated nature of the composites containing 5.0 and 10.0 wt% LDH can be speculated from the loss of basal reflection in their XRD pattern.

The analysis of the TEM micrographs of the polymer/LDH nanocomposites presents direct information about the nature of clay particle dispersion. In the exfoliated nanocomposites based on PMMA, epoxy and polyimide, the dispersed particles mostly exist as exfoliated layers or small tactoids (stacks of small number of single layer). But, in case of the intercalated nanocomposites, they exhibit a tendency to

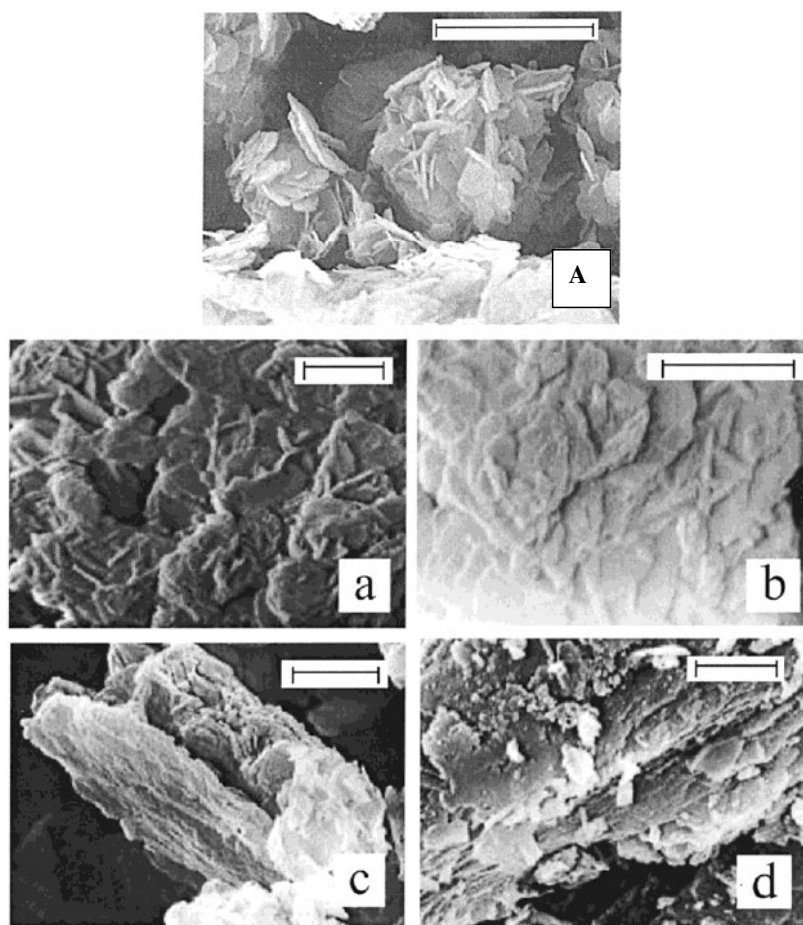


Figure 2.8 SEM micrographs of Zn-Al LDH prepared by co-precipitation method (A) and Zn-Al/polystyrene sulfonate nanocomposites prepared by (a) in situ polymerization, (b) reconstruction, (c) direct exchange and (d) restacking. The bars represent $2\mu\text{m}$. [23]

form aggregates or physically associated structures. This has been vividly demonstrated in **Figure 2.7**, where TEM images of the nanocomposites containing 5.0 wt% LDH in different matrices are shown at comparable magnification. In case polar matrix (epoxy, PMMA and polyamide), complete exfoliation of the LDH particles can be observed whereas in polystyrene matrix LDH particles are mostly intercalated. In addition to the polarity of matrix polymer, the method of preparation of the nanocomposites significantly influences the crystallinity and the morphology of the dispersed LDH particles. **Figure 2.8** demonstrates the morphological features of Zn-Al-LDH-polystyrene sulfonate intercalated nanocomposites prepared by different methods [23]. Irrespective of the the method used, a complete change in the LDH particle morphology can be observed after the polymer intercalation. The original platelet-like primary structure of the LDH crystallites no longer exists in the nanocomposites, rather the sheet are more or less crumpled over one another. As clear from **Figure 2.8**, this reorganization of particle structure is greatly influenced by the preparation method.

2.2.2.2 General Properties of Polymer/LDH Nanocomposites

In general, when compared with the conventional polymer composites, polymer nanocomposites exhibit significant improvements in different properties at relatively much lower concentration of filler. They usually differ from the conventional composites in different aspects, like size of the dispersed filler particles, nature and extent of interaction at the particle-polymer interface, etc. The efficiency of various

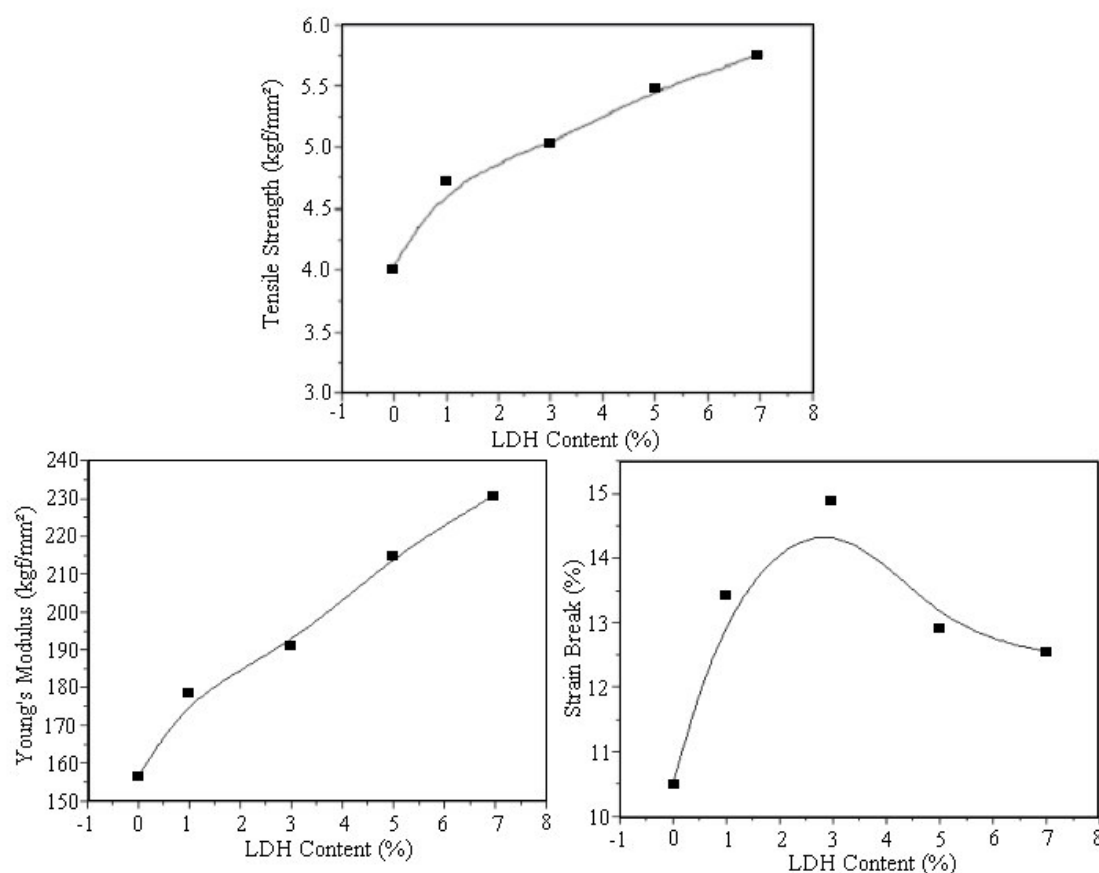


Figure 2.9 Effects of the LDHs content on the tensile properties (tensile strength, Young's modulus and strain at break) of the epoxy/LDH nanocomposites. [53]

additives in polymer composites can be increased many folds when dispersed in the nanoscale. This becomes more noteworthy when the additive is used to address any specific property of the final composites such as mechanical properties, conductivity, gas permeability, thermal stability, etc. In case of polymer/LDH nanocomposites, similar improvements are also observed in many occasion.

The mechanical properties of epoxy/LDH nanocomposites are shown in **Figure 2.9**. It is evident that the presence of a small amount of LDH significantly increases the tensile strength and the modulus showing the strong reinforcing nature of LDH on the epoxy matrix. This highly reinforcing nature of LDH particles in epoxy is related to their exfoliated structure in the nanocomposite, where the highly anisometric LDH layers remain strongly attached to the polar epoxy matrix. This becomes possible due favorable chemical and electrostatic interaction between LDH surface and oxygen rich backbone of epoxy matrix. Thus each individual exfoliated layer imparts reinforcing effect on the matrix. However, Such strong interaction often acts negatively on the impact strength of the nanocomposites resulting sharp decrease in elongation at break after a certain level of LDH concentration. In case of relatively less polar polymer, aggregation of the dispersed particles leads to a reduction in the mechanical properties after an initial improvement observed at low concentration of LDH. Hsueh and Chen [38] have observed this behavior in polyimide/LDH based nanocomposites. They reported that beyond 5 wt% LDH content, the dispersed nanolayers form aggregates and the tensile properties of the nanocomposites are reduced. In case of exfoliated PMMA/LDH nanocomposites, Wang et al. [65] have observed a strong reinforcing nature of the exfoliated LDH clay particles. In presence of 5 wt% LDH, such composite shows above 60% and 80% increase in tensile strength and modulus, respectively in comparison to unfilled PMMA. However, flexibility and the impact properties of such nanocomposites are significantly affected, which is reflected in over 50 % lowering in elongation at break during tensile testing.

The improvement of thermal properties compared to the unfilled polymer is a very important aspect of polymer/LDH nanocomposites. LDHs contain large amount of bound water due to the presence of -OH group on the metal hydroxide sheets and some free water molecules in the interlayer region. The mechanism by which LDH clays improves the thermal stability and flammability of polymer matrix is similar to that observed in case of conventional metal hydroxide type fillers, like $\text{Mg}(\text{OH})_2$ and $\text{Al}(\text{OH})_3$. The endothermic decomposition of LDHs takes off heat from the surrounding and the liberated water vapor reduces the concentration of combustible volatile in the vicinity of the polymer surface. As a result, the decomposition temperature of the polymer is increased. Interestingly, such improvement is quite significant even at low concentrations of LDH. This is probably due to better dispersion of the LDH particles compared to that observed in conventional composites based on simple metal hydroxide. Again, when the more basic interlayer anions in the unmodified LDHs are replaced by less basic organo anionic species in the modified LDHs, the thermal stability of the metal hydroxide layers are enhanced [66]. Additionally, the nanoscale dispersion of the clay materials in polymer nanocomposites improves the compactness of the char formed after burning of the surface region. This hinders the conduction of heat and the diffusion of oxygen into the bulk region [67, 68]. The improved thermal stability of LDH based nanocomposites has been reported by many researchers [38, 46–49, 53]. In all these cases, thermogravimetric analysis (TGA) showed significant increase in the temperature at which 50% weight loss occurs.

Figure 2.10 shows TGA results of polyimide-LDH nanocomposites. The addition of 5 wt% LDH causes significant enhancement of the thermal stability of the composites, which is attributed to the

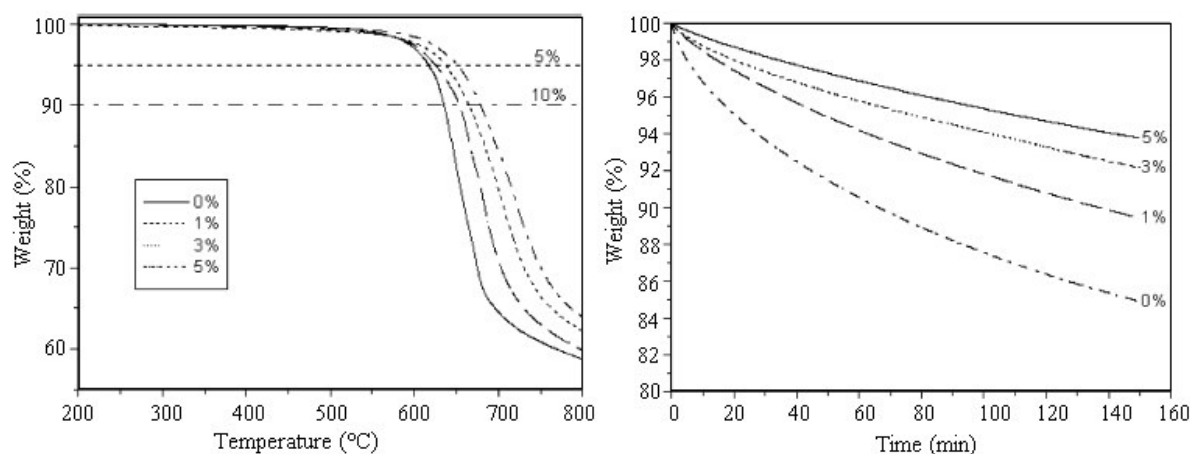


Figure 2.10 Left: TGA curves of LDH/polyimide nanocomposites with various LDH loadings, Right: Effects of LDH content on the decomposition temperatures at 5 and 10 % weight loss of LDH/polyimide nanocomposites [38].

nanoscale dispersion of the LDH hydroxide layers in the polyimide matrix. However, beyond 5 wt% LDH loading decomposition temperature does not change much with further increase in LDH concentration. The morphological analysis of these nanocomposites reveals that above 5 wt% concentration, the dispersed LDH particles form aggregates and remains mainly in the intercalated forms. This type of behavior has also been observed with other LDH based nanocomposites, like Zn–Al/polystyrene [49] and Zn–Al/polyethylene [48] nanocomposites. In these cases, decomposition temperature, though remain higher than the pure polymer, exhibits a decreasing trend after certain level of LDH content.

The electrical conductive properties of polymer/LDH nanocomposite electrolytes have also been reported in some recent literatures [51, 54, 69, 70]. The nanocomposite, based on poly(ethylene oxide) (PEO) type polymers shows high electrical conductivity at ambient temperature. In preparing such nanocomposite, the unmodified LDH clay is first modified by oligomeric PEO containing phosphate

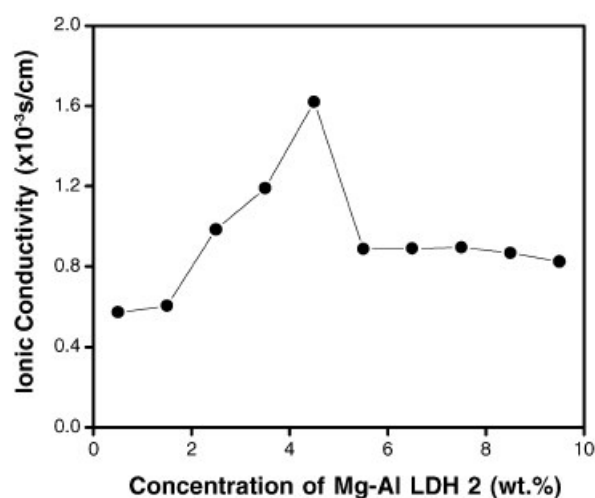


Figure 2.11 The effect of LDH on ionic conductivity of Poly(ethylene glycol diacrylate)/Mg-Al-LDH/ LiClO₄ based polymer nanocomposite [69].

groups and this modified LDH is then mixed with a high molecular weight PEO and LiClO_4 . The exfoliation of clay layers causes fine dispersion of the clays particles into PEO matrix, which reduces the crystallinity of the matrix and forms PEO/ LiClO_4 amorphous phase. This results in an easier mobility of the Li^+ ions within the polymer matrix. Usually, the ionic conductivity of such polymer nanocomposite electrolytes increases with increasing clay loading up to an optimum level beyond which the additional clay merely acts as an insulator and impedes ionic movements. **Figure 2.11** shows the effects of LDH loading on the ionic conductivity of poly(ethylene glycol diacrylate)/Mg-Al-LDH/ LiClO_4 based nanocomposite electrolyte.

2.3 Potential Applications of LDH Materials

LDHs provide a battery of advantages, like tunable chemical compositions and its purity, non-toxicity, large amount of bound water in their structure, possibility of modification by a large number of organic anionic species, etc. This makes them a potential candidate for various applications. Although the application of LDH clays or in general anionic clays is still in growing stage, their huge potential can be imagined from their properties. **Figure 2.12** shows an overview of various fields of application of LDH materials.

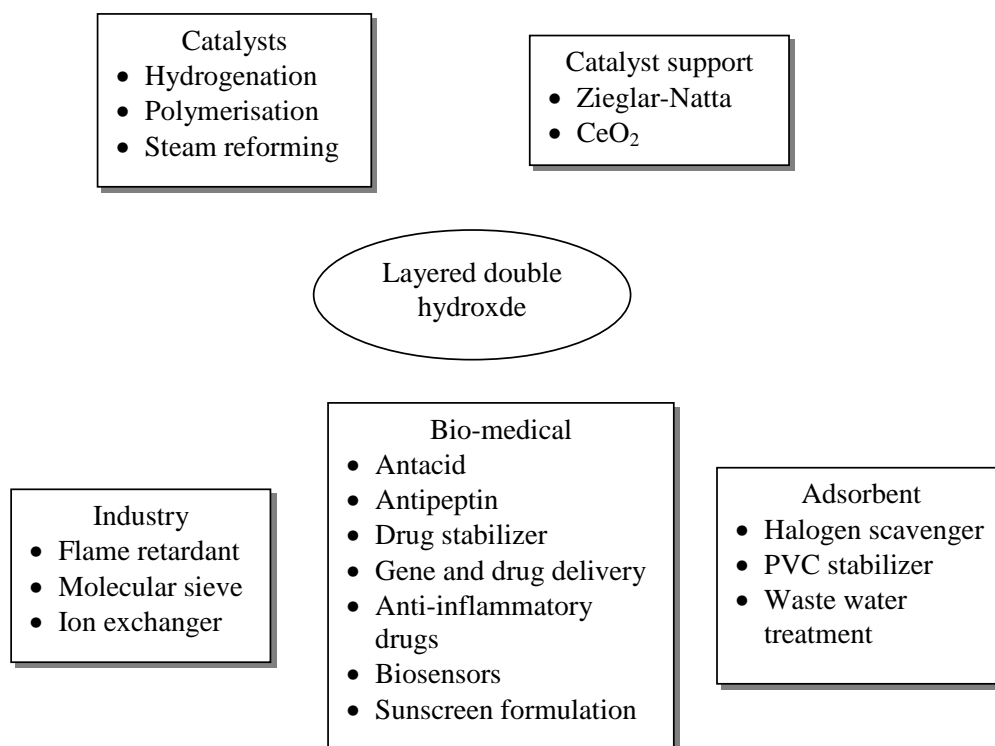


Figure 2.12 Various fields of application of LDH materials [5].

The use of LDH materials in the field of catalysis is well known and have been reported for basic catalysis (eg. Polymerization of alkene oxide, aldol condensation, transesterification reactions, etc), reforming of hydrocarbons with H_2O , hydrogenation (production of methane, alcohols, paraffins, olefins, etc), oxidation reactions, support for Ziegler-Natta catalysts during polymerization of olefins, etc [5, 71].

Because of bio-compatible nature, the use of LDH materials in bio-medical field is wide spread. One important and very promising field of application is the controlled release of drugs and various active chemical species. In this regard, the intercalation chemistry of LDH type clay is of special interest in stabilizing and sequestration of highly active or toxic molecules. Such bio-nanohybrid can then be administered into the body system, where the active ingredients are released at desired location via a chemical switch such as change in pH. For example, for controlled release of various inflammatory drugs the use of this techniques provides better results [72]. The use Mg-Al-LDH in formulating anti-gastric medicine is another popular biomedical application. Recently, Lee and Chen [73] reported the drug release behavior of nanocomposite hydrogels prepared from Mg-Al-LDH and poly[acrylic acid-co-poly(ethylene glycol methyl ethyl acrylate)]. Other important bio-medical application of LDH based organic hybrids as bio-macromolecule carriers. Choy and co-workers [74] used LDH to encapsulate DNA molecules by simple ion-exchange method in aqueous medium. These bio-LDH nanohybrids are then used for release of DNA molecules inside cells. LDH-organic hybrids can also be used in designing of electrochemical biosensors for various chemicals. For examples, polyphenylene oxidase intercalated Zn-Al-LDH hybrids for phenol determination [75], urease intercalated Zn-Al-LDH for urea detection [76], etc.

The Mg-Al-LDH is also used as stabilizer and halogen scavenger in polyvinylchloride (PVC) formulation [56, 77]. The incorporation of small amount of LDH into PVC significantly improves the thermal stability of the resin and suppresses its degradation. This happens through mainly two processes: the interaction of Cl^- ions into the interlayer region of LDH followed by the reaction of HCl (produced due to dehydrochlorination of PVC) with the hydroxide groups of the metal hydroxide layers producing metal chloride.

Recently, the use of LDH clays to prepare polymer nanocomposites electrolytes has been reported [51, 54, 69, 70]. These nanocomposites shows high ionic conductivity at ambient temperature and can be a suitable material for designing thin-film type of Li-polymer secondary battery cells.

LDHs could be treated as a carrier for specific chemical agent such as UV or photo stabilizer, dye or coloring agents, fluorescent chemicals, antioxidants, etc used in polymer composites. These chemicals are often water soluble and contains functional groups that can favourably interact with LDH. As a results, they can be easily intercalated within the gallery space of nanostructured LDH particles. The hybrid thus formed can be incorporated into the polymer matrix, where these specific chemicals can exhibit their intended functions. The basic purpose of using LDH as carrier is to prevent unwanted release of these chemicals (commonly known as leaching) from the matrix thus maintaining the life time of the final composites [78]. Additionally, due to entrapment within the LDH crystal layers, the overall (thermal, chemical and photostability) of these chemicals will be enhanced [79, 80]. Evans et al. have made extensive investigation on the intercalation of various organic dyes and UV stabilizers within LDH [80–82]. Such intercalated LDH-dye hybrids can also dispersed in polymer matrix, where the hybrid fillers simultaneously exhibit the functions of the nanofiller and the organic dye [83]. Various rare-earth metal complex based on Ce, Eu, Tb, etc can be intercalated into LDH to synthesize luminescent materials [84, 85]. These LDH based luminescent materials can be ideal materials for application in the field of signal lights and optical sensors.

The concept of nanotechnology in designing flame-retardant polymer composites is an upcoming field. It has already been established that polymer nanocomposites based on layered silicates type clays

show certain improvements in flame retardancy of polymers. In many cases partially exfoliated and intercalated clay structure show better results compared to completely exfoliated one [67]. LDH clays, especially those based on Mg–Al and Zn–Al also have a definite potential as flame-retardant fillers. The mechanism by which they delay or restrict the burning process of polymer is similar to that followed by conventional metal hydroxides. But, the added advantages are their improved dispersion into polymer matrices and confinement of polymer chains within the metal hydroxide layers through intercalation. This can improve their efficiency as compared to the conventional metal hydroxides (like $\text{Mg}(\text{OH})_2$ and aluminum trihydrate) by reducing the loading requirement for meeting certain flame-retardancy rating. Another important aspect is the choice of clay modifying surfactants. Usually, in case of LDH clays, the amount of any surfactant used for such purpose is theoretically equivalent to the amount of interlayer anions present in the unmodified materials. Since the commonly used anionic surfactants for LDH clays possess oligomeric structure, their incorporation even in small percentage (of the amount required for complete replacement of the interlayer anionic species) produce organically modified LDHs that contain substantial amount of organic portion. Therefore, choice of these surfactants can be made in such a way that they serve a dual purpose, such as modification of unmodified clays by enlarging the interlayer region and the improvement of the flame-retardancy of the final composites. In this regard, organic surfactant containing phosphorous and aromatic moieties are the ideal candidates.

The potential of LDH clays in preparing polymer nanocomposites with special properties has drawn considerable attentions among researchers in the recent years. The most widely reported a method in literature is solution intercalation process, which gives nanocomposites with intercalated to exfoliated clays structures. The melt-compounding method employed in the present study is still to be explored in details with these materials.

2.4 Nanoclays as Flame-Retardant in Polymer

2.4.1 Flammability of Layered Silicate based Polymer Nanocomposites

Polymer nanocomposites constitute a recent and promising development in the area of flame retardancy. The improvement in thermal stability and flammability properties of polymer nanocomposites have been reported by several research groups [67, 86–90]. These hybrid materials find special interest because of their unique way of preparation and improvements in various properties, like mechanical properties, gas barrier efficiency, electrical conductivity, etc in comparison to conventional polymer-inorganic filler composites [91–93]. The most widely used fillers in preparing polymer/clay nanocomposites are the layered silicates belonging to the family of 2:1 layered phyllosilicates. The crystal structure of these layered silicates consists of two sheets of silica tetrahedra sandwiching one sheet of alumina octahedra. Occasionally, elements besides aluminum and silicon sneak into the clay structure, creating a net negative charge. Positive ions infiltrate through the clay layers to balance this excess charge on the layers. The layer thickness is about 1 nm and the lateral dimension lies up to few microns. To prepare polymer nanocomposites, the unmodified layered silicate clay is first modified with suitable organic species (commonly various organic amines) containing positively charged functional groups to replace the small cations in the interlayer region. These organically modified clay is then incorporated into polymer matrix using different methods, like solution intercalation, melt-compounding, etc to obtain the nanocomposites. The morphology of the dispersed clay particles in these polymer nanocomposites may vary from an

intercalated structure (where the polymer chains remains intercalated within the clay layers) to a completely exfoliated structure (where individual clay layers remains completely separated from each other and dispersed homogeneously throughout the matrix). Technologically, all these types of clay particle morphology are useful for final applications of the end materials. Usually, with non-polar polymers like polyolefins, clay particles show less degree of exfoliation compared to polar polymers like polyamide.

The thermal stability of the clay based polymer nanocomposites have been extensively studied by several research groups [67, 94, 95]. The most common technique to investigate the thermal stability is thermogravimetric analysis (TGA). The results of TGA analysis is interpreted in terms of two temperatures: one is $T_{0.1}$ representing the temperature at which 10% weight loss occurs, which is taken as the onset of thermal degradation and the other is $T_{0.5}$ representing the temperature at which 50% weight loss occurs, which is usually treated as the degradation temperature [90]. The amount of residue left above 600 °C gives a measure of char produced after combustion. Thermogravimetric analysis of polymer/clay nanocomposites, in many cases, show higher thermal stability compared to the unfilled polymer matrix. This is manifested as the higher values $T_{0.1}$ and $T_{0.5}$ in the nanocomposites. For example, Wilkie et al. [90] reported polystyrene/montmorillonite based nanocomposites showing about 40 – 50 °C increase in both $T_{0.1}$ and $T_{0.5}$. They have also shown that the nature of the organic modifiers used for clay modification influences the thermal stability of the nanocomposites. Similar enhancement of thermal stability have also been reported for other polymer/clay nanocomposites based on polydimethylsiloxane [96], polyimide [97, 98], polyurethane [99], polycaprolactum [100], PMMA [94, 101], etc. The delay in the onset of decomposition is often related to barrier effect caused by the dispersed clay particles and their combustion residue against the diffusion of volatile gas and oxygen across the burning surface [102].

The heat release test usually carried out by cone-calorimeter is a very important method to analysis the flammability performance of polymeric materials [4, 67]. Cone-calorimeter analysis of different polymer nanocomposites reveals significant improvements in flammability properties. The results of this analysis are expressed in terms of various combustion relevant properties, like heat release rate (HRR) and its maximum value (called peak HRR or PHRR), carbon monoxide yield, smoke release rate, etc. Gilman and co-workers [67] have extensively investigated several polymer nanocomposite systems using cone calorimetry and some of their results are summarized in **Table 2.1**. It is apparent that in all these nanocomposites PHRR and mean HRR are significantly reduced indicating their improved flammability performance. Interestingly the parameters like, heat of combustion (H_c), specific extinction area (SEA, a measure of smoke yield) and carbon monoxide yield, are not significantly changed in presence of layered silicates. This means the chemistry of decomposition during combustion is not influenced by the silicates. The intercalated and the exfoliated nanocomposites show comparable results in cone calorimeter analysis [103]. Further, Wilkie and co-workers [90] have observed that in polyethylene/clay nanocomposites, presence of 3.0 wt% clay causes 30.0 – 40.0% reduction in PHRR compared to pure polyethylene. All these results when compared with conventional composites or micro composites indicate that polymer nanocomposites certainly exhibit improved flammability properties at similar filler concentrations. The layered silicate influence the flammability of the nanocomposites primarily through condensed phase mechanism [67, 86]. This involves the formation of compact char at the surface of burning material that provides mainly the two-way barrier effect to the diffusing gases and volatiles through the surface: first against the diffusion of oxygen from surrounding atmosphere to the surface beneath the char and the second the flammable volatile from the polymer to the flame front. When these two diffusion processes

Table 2.1 Selected cone calorimeter investigation results for polymer/layered silicate nanocomposites at 35 kW/m² heat flux [67]

Sample	Residue Yield	PHRR ^a	Mean HRR ^b	Mean H _c ^c	Mean SEA ^d	Mean CO Yield
	%	kW/m ²	kW/m ²	MJ/kg	m ² /kg	kg/kg
Nylon-6 (N6)	1	1010	603	27	197	0.01
N6/silicate(2%)exfoliated	3	686	390	27	271	0.01
N6/silicate(5%)exfoliated	6	378	304	27	296	0.02
Nylon-12 (N12)	0	1710	846	40	387	0.02
N12/silicate(2%)exfoliated	2	1060	719	40	435	0.02
Polystyrene (PS)	0	1120	703	29	1460	0.09
PS/silicate (3%)immiscible	3	1080	715	29	1840	0.09
PS/silicate (3%)intercalated	4	567	444	27	1730	0.08
Polypropylene (PP)	0	1525	536	39	704	0.02
PP/silicate(2%)intercalated	5	450	322	44	1028	0.02

^a Peak heat release rate^b Heat release rate^c Heat of combustion^d Specific extinction area

are severely obstructed, material can show self extinguishing behaviour [4]. The secondary mechanism of flame inhibition can be that at high temperatures, the inorganic fillers act as radical scavengers due to their Lewis acidic nature resulting in the inactivation of the flame propagating radicals formed during pyrolysis of the polymer chains [86, 103].

2.4.2 LDH Clay as Flame-Retardants for Polymer

Though the uses of LDH clay as heat stabilizer and acid scavenger in halogenated polymers (such as PVC) are well known [57, 104] its use as inorganic flame-retardant is not very common. The flame-retardant characteristics of LDH clays originate from their Mg(OH)₂ like chemistry, which involves endothermic decomposition with the liberation of water vapor and often carbon dioxide. The residue of such combustion is the metallic oxides that impedes the burning process by reducing the oxygen supply to the fresh surface beneath. The early report on the flame-retardant application of LDH was published by Miyata et al [58]. The idea was to add hydrotalcite (naturally occurring LDH clay) both in unmodified or in surface treated form at high concentrations (> 50 wt%) in polymers, like polyolefins, polystyrene, nylon, polycarbonate, etc to obtain flame-retardant compositions. In fact, such high concentrations though often provided various industrial acceptable flammability ratings (such as UL94 V0), the mechanical properties of the final composites were drastically affected. The treatment of LDH clays as flame-retardant as well as a nanofiller can be a potential development in this regard. In the recent years, many reports have been published that highlight the improved thermal and flammable properties of LDH clay based polymer nanocomposites. Recently, Zammarano and co-workers [105] have reported synthesis of self-extinguishing epoxy/LDH nanocomposites. They have also observed a synergistic ef-

fect between LDH clay and ammonium polyphosphate in such nanocomposites, where reduction of APP concentration from about 30.0 wt% to about 16.0 – 20.0 wt% can be tolerated in presence of a small amount of LDH without sacrificing the flammability performance.

The comparison of LDH with layered silicates with respect to their flame retarding efficiency in polymer nanocomposites is noteworthy. The layered silicates are usually thermally stable and do not undergo degradation in the temperature range where most of the polymers decompose. They mainly act through physical barrier effect during combustion. On the other hand, LDH undergoes thermal degradation in the vicinity of polyolefin degradation temperature, thus actively participating in flame inhibition process. Additionally, like layered silicates, the decomposition residue of LDH (mixed metal oxide) provides physical barrier effect during burning. Qui et al. [106] reported a comparative study between polyethylene nanocomposites based on LDH and montmorillinite in terms of their thermal degradation activation energy as shown in **Figure 2.13**. They presented evidence to prove the different mechanisms of thermal

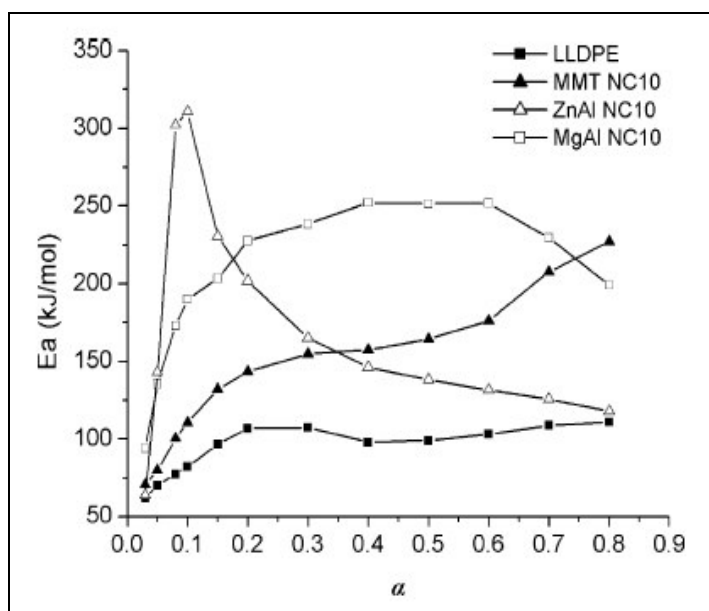


Figure 2.13 Dependence of the effective activation energy (E_a) on the extent of conversion (α) for the thermo-oxidative degradation of virgin LLDPE and its nanocomposites. (MMT NC 10 = LLDPE/montmorillinite, ZnAl NC 10 = LLDPE/Zn-Al-LDH and MgAl NC 10 = LLDPE/Mg-Al-LDH; the filler contents are 10 wt%) [106]

stabilization by these two clay materials. The linear-low-density polyethylene (LLDPE)/montmorillinite nanocomposites shows lower activation energy because of easy dehydrogenation of LLDPE matrix catalyzed by montmorillinite. However, at the later stage of decomposition the ceramic-carboneous char formed acts as excellent mass transport barrier. On the other hand, due to energy requirement for thermal degradation of LDH, the activation energy for LLDPE/LDH system is much higher during the initial phase of degradation. The large amount of water vapour may cause a dilution effect on oxygen concentration in the flame zone. Also the metal oxide residue formed acts as excellent mass and heat transport barrier. The thermogravimetric analysis of such systems also reveals the higher thermal stability of LDH based system [106]. The limitation of layered silicate type clays as flame-retardant has also been re-

ported others in literature [107]. As these clays remain inert during degradation of polymer, can not reduce the total heat released during combustion process and hence cannot reduce the propensity to form a long-duration flame. But, LDH because of its endothermic decomposition acts as heat sink, effectively reducing the heat released during combustion of the nanocomposites.

The major drawback with metal hydroxide type conventional fillers (like $\text{Mg}(\text{OH})_2$ and aluminum trihydroxide) is their high concentration (usually above 50 wt%) requirements to obtain satisfactory flame-retardant effects. Although polar polymers, like polyesters, alkyd resins, etc can tolerate such high concentration, non polar polymers, like polyolefins show deterioration of their mechanical properties and processibility [108, 109]. The poor dispersion of these highly polar inorganic materials within a hydrophobic polymer matrix is often held responsible for the high concentration dosing to obtain satisfactory flame retardancy. Several attempts, like surface treatment [110], use of compatibilizer [111–113], etc are therefore made to improve the dispersibility of these fillers in non polar matrix. In spite of all these attempts, the problem still persists and needs to be further addressed. Therefore, there exists a constant urge to develop flame-retardants, which at low concentration can provide desired flame retardancy and also will not affect the mechanical properties significantly, if not improved further. LDH can be an interesting material to investigate and study in this regard, The layered structure and exchangeable inter-layer species make them suitable precursor for preparation of polymer nanocomposites, where improved dispersion can be achieved through intercalation and delamination. Again, having cationic hydroxide layers with anionic interlayer ions, there exists several types of anionic surfactants, like carboxylate, sulfonate, phosphate, etc that can be used to modify unmodified LDH materials. The critical choice of clay modifying surfactants may provide the added contribution to flame retardancy. For examples, surfactants containing elements like, P, S, B, etc can act as radical scavengers during combustion process. Such effects have already been observed in case layered silicate based nanocomposites, where the clay materials are intercalated with triphenylphosphate [114, 115].

EXPERIMENTAL: COMPOUNDING AND CHARACTERIZATION

3.1 Materials Description

3.1.1 Mg-Al-LDH

Preliminary investigations on the intercalation behavior of LDH with different anionic surfactants was carried out using the synthesized Mg-Al-LDH. However, preparation of polymer based composites in kilogram size batches needs a sizable amount of Mg-Al-LDH. Therefore, the commercially available varieties of this LDH clay were also used, especially for carrying out compounding in twin-screw extruder. The Mg:Al ratio in the synthesized LDH is approximately 2:1 and hence a commercial grade of Mg-Al-LDH with similar Mg:Al ratio was selected. Both the Mg-Al-LDH samples were white powders with similar bulk density. The various characteristics of the industrial materials used are listed in Table 3.1.

Table 3.1 Various technical details of the commercial Mg-Al-LDH used in the present study

Description	Mg-Al-LDH	
Trade name	Dualmag HT	Hycite 713
Producer	Dulso a.s. Slovak Republic	Südchemie AG Germany
Chemical formula	$Mg_{1-x}Al_x(OH)_2(CO_3)_{x/2} \cdot nH_2O$	
MgO/Al ₂ O ₃ ratio	4.4	4.7
Loss on drying (%)	0.19	0.20
BET surface (N ₂) (m ² /g)	9.2	9.0
pH (1g/50 ml EtOH/H ₂ O)	8.5	9.2
Bulk density (g/l)	300	330
Heavy metals (ppm)	< 0.1	< 10

Mg-Al-LDH was also used in combination with a conventional metal hydroxide type flame-retardant magnesium hydroxide (MH) in the PE matrix. The product used was Magnifin-H5 supplied by Magnesiumprodukte GmbH and Co KG - Qualitätswesen, Germany.

3.1.2 Chemicals Used for LDH Synthesis

The various chemicals used for the synthesis of Mg-Al-LDH were synthetic grade and are described below.

Magnesium Chloride (MgCl_2) and Aluminum Chloride (AlCl_3): Both were in hexahydrated form with 98% purity and were purchased from Aldrich chemical company.

Urea: This is white solid and completely soluble in water at ambient condition. It was also purchased from Aldrich chemical company and as 98% pure form.

3.1.3 Surfactants

Since the interlayer region of the Mg-Al-LDH clay accommodates anionic species, anionic surfactants are most suitable to modify for its modification. Primarily, four different surfactants were used for the modification of Mg-Al-LDH to study its intercalation behavior. The choice of surfactants was made based on different anionic functional groups, solubility in aqueous medium and structure of the hydrocarbon chain. The surfactants used are sodium dodecylbenzenesulfonate (SDBS), lauric acid, sodium dodecylsulfate (SDS) and bis(2-ethylhexyl)hydrogen phosphate. All these surfactants were purchased from Aldrich chemical company, Germany and used without further purification. The various properties of these surfactants are given in **Table 3.2**.

Table 3.2 Various technical details of the surfactants used for the modification of Mg-Al-LDH

Materials	Symbol for anionic form	Purity (%)	Density (g/cc)
sodium dodecylsulfate	DS	98.0	N/A
sodium dodecylbenzene sulfonate	DBS	N/A	N/A
lauric acid	laurate	99.5	0.883
bis(2-ethylhexyl) hydrogen phosphate	BEHP	97.0	1.06

The anionic forms of these surfactants are the actual species that enter the interlayer region of the LDH clay. Both SDS and SDBS are highly water soluble producing their anionic forms dodecylsulfate (DS) and dodecylbenzenesulfonate (DBS) respectively in solution. The other two surfactants, namely lauric acid and bis(2-ethylhexyl)hydrogen phosphate are sparingly soluble in water at room temperature. Therefore, to obtain their water soluble forms and the corresponding anions, they were treated with NaOH and NH_4OH solutions respectively. These aqueous solutions containing respective anions were then used for LDH modification.

3.1.4 Polymers

The main polymer matrix used in the whole study is polyethylene (PE), which is a commercially available general purpose grade of low-density polyethylene LD263 from Exxonmobil chemical company. It is a high molecular weight grade with a high value of polydispersity index. Typically, this type of

polyethylene possesses long chain branching that causes complex flow behavior of the unfilled polymer melt. The extrusion of the unfilled polymer causes significant increase in average molecular weight and decrease in polydispersity index. This means intense shearing action by the extruder screws at elevated temperature promotes chemical reaction that leads to increasing molecular weight. Various characteristics of the virgin PE and its extruded form are given in **Table 3.3**.

Table 3.3 Description of the different polymeric materials used

Polymer	Trade name	Density	Molecular weights ^a			MFI ^b	T _m ^d
		g/cc	M _n	M _w	M _w /M _n	g/10 min	°C
PE	LD263	0.9185	88000	406500	4.62	8.2	110
PE (extruded)	-	-	124400	463800	3.72	6.5	110
MAH-g-PE ^c	Polybond 3109	0.9260	24300	41100	1.75	30	123

^a Measured by Gel Permeation Chromatography (GPC)

^b Melt Flow Index, ASTM D 1238

^c Maleic anhydride grafted polyethylene

^d Measured by differential scanning calorimetry (DSC)

Maleic anhydride grafted polyethylene (PE-g-MAH) was used as a compatibilizer to obtain better dispersion of LDH clay particles in polyethylene matrix. The PE-g-MAH used was of lower molecular weight and of higher melt index compared to the base matrix. The details of these polymeric materials used are shown in **Table 3.3**.

3.2 Melt Processing

3.2.1 Introduction

Melt processing technique is the most popular and economic method for thermoplastics and the composites based on them. In the present case, melt processing was carried out both in small scale using a batch mixture and in kilogram size scale using a twin-screw extruder. There are several parameters associated with melt processing technique that control the quality of the processed materials. For example, temperature, mixing time, shear rate applied (speed of screw elements), design of the mixing equipments, etc all critically control the extrudate quality of thermoplastics. For preparing PE/LDH based nanocomposites the similar processing conditions were maintained for all compositions.

The nanocomposites were melt-compounded in two steps. At first, the modified clay was mixed with compatibilizer (PE-g-MAH) in 1:1 weight ratio to prepare a masterbatch and the masterbatch was diluted with PE in the same mixing equipment.

3.2.2 Mixing in Batch Mixer (Brabender Plasticorder)

Brabender plasticorder (shown in **Figure 3.1**) is a laboratory sized batch compounder and is suitable for preparing small batches of samples sufficient for carrying out most of the preliminary analysis required

for material characterization. The rotor used for compounding PE/LDH system was a sigma type. In the first step, PE-g-MAH was melted in the mixing chamber. When nearly constant torque was achieved, a desired amount of modified Mg-Al-LDH was fed into the mixing chamber and compounded for further 6 minutes. The masterbatch thus obtained was then granulated, premixed with desired amount of PE and again compounded in the mixing chamber for another 6 minutes to prepare the final compositions. The temperature and the rotor speed applied during both the steps were 200 °C and 100 rpm respectively.



Figure 3.1 Brabender plasticorder: (left) the mixing chamber and (right) sigma type screw used for melt-compounding

3.2.3 Mixing in Extruder

Large batch (up to few kg) of the compounds was prepared in a tightly intermeshing, corotating twin-screw extruder (Leistritz Micro 27) having screw diameter of 27 mm and L/D ratio equal to 36. In the first step, modified Mg-Al-LDH and PE-g-MAH were mixed in the extruder in 1:1 weight ratio. The extruded masterbatch strands were water cooled as they emerged from the extruder die and were then granulated. The masterbatch granules were dried at 60 °C for about two hours. In the second step, the dried masterbatch granules and desired amount of PE were premixed and compounded in the extruder. All the ingredients were dried in vacuum at 80 °C for 2h prior to extrusion. The processing conditions used for both these steps are

- 160 – 210 °C temperature profile from the feed to the die section of the extruder barrel
- 200 rpm screw speed
- 6 kg/h feed rate
- vacuum outlet in the mixing section of the extruder barrel to take out any volatiles formed during the compounding process

The final composites as extruded was water cooled, granulated and dried at 60 °C for two hours.

The concentrations in the final composites were determined based on the metal hydroxide content of the modified clay. It has been estimated that the SDBS modified Mg-Al-LDH contains about 46.0 wt% metal hydroxide (see Appendix A). The LDH content of the nanocomposite compositions has been

interpreted in terms of its metal hydroxide content and the sum of the amounts of PE matrix and PE-g-MAH has been taken as the total polymer content of the system. The sample designation and also the actual amount of metal hydroxide content in each samples are described in **Table 3.4**. The amount of metal hydroxide per 100 gm of metal hydroxide plus polymer content (without considering the organic content of the filler) has also been shown. It is obvious that due to high molecular weight of the organic surfactant SDBS, the modified LDH content large proportion of organic species.

Table 3.4 Designation of PE/LDH nanocomposite composition and the actual metal hydroxide content in each composition

Nanocomposite Composition	Metal hydroxide content per 100 g polymer+ metal hydroxide	Metal hydroxide content per 100 g batch
	g	g
PE-LDH1	2.5	2.43
PE-LDH2	5.0	4.72
PE-LDH3	7.5	6.89
PE-LDH4	10.0	8.95
PE-LDH5	15.0	12.75
PE-LDH6	20.0	16.20

3.3 Characterizations

3.3.1 X-ray Diffraction Analysis

X-ray diffraction analysis (XRD) using wide angle x-ray scattering (WAXS) over $2\theta = 1.8$ to 40° , in steps of 0.1 or 0.02° was carried out using 4-circle wide-angle diffractometer P4 (Bruker-AXS, Karlsruhe, Germany, formerly Siemens AG) with Cu- K_α radiation ($\lambda = 0.154$ nm, monochromatization by primary graphite crystal) generated at 30 mA and 40 kV. The primary pin hole diameter was set 0.5 mm (detector distance 12 cm) and measuring time was kept 600 s. The calculation of the interlayer distance (d) was carried out from the measured value of diffraction angle 2θ using bragg equation given by

$$2d\sin\theta = n\lambda \quad (3.1)$$

where, λ represents the wave length of the incident X-ray beam and n is a positive integer. XRD spectra were interpreted with respect to the position of the first order basal reflection $<003>$, which depends on the distance between two adjacent metal hydroxide sheets in the LDH crystal lattice (i.e. d). The higher order reflections of the same $<hkl>$ series (i.e. $<006>$, $<009>$ and so on) were also reported as they indicate the presence of repeating crystal planes and symmetry in a specific crystallographic direction.

3.3.2 FTIR Analysis

Fourier transform infrared (FTIR) spectra for unmodified LDH, its calcined and organically modified forms were recorded over the wave number range $400 - 4000 \text{ cm}^{-1}$ using Equinox 55 FTIR spectrometer. The powdered samples were mixed with KBR in a 1:200 ratio of their weight and pressed in the form of pellets for measurement. For measuring FTIR of the polymeric composites thin films of thickness in the range $100 - 250 \text{ }\mu\text{m}$ were compression molded at about $150 \text{ }^{\circ}\text{C}$.

3.3.3 Morphological Analysis by Electron Microscopy

To observe the particle morphology of unmodified LDH and its surfactant modified forms scanning electron microscopy (SEM) was used (model: LEO 435 VP, Carl Zeiss SMT). The powder samples were first gold coated using a sputter coater. At first, the powder sample was sprinkled over a sticky surface made by adhering conductive carbon cement on a SEM sample holder; then loose powers were removed by shaking the sample holder and finally the adhered particles were gold coated. SEM was also used to investigate the surface morphology of the fractured surface of the nanocomposites. To observe the state of dispersion of the LDH particles in the polyethylene matrix, transmission electron microscope (TEM, model: Zeiss EM 912) was used at different magnification. TEM was carried out at room temperature with an acceleration voltage of 120keV and bright field illumination. The ultra thin sections of samples were prepared by ultramicrotomy at $-130 \text{ }^{\circ}\text{C}$ using Reichert Ultracut S (Leica, Austria). The thickness of the section cut was in the range 100 to 130 nm .

3.3.4 Thermal Analysis

The thermal analysis were carried out by thermogravimetric analyser (TGA 6 from Perkin Elmer) using a heating rate of 10 K/min . Both air and nitrogen atmospheres were used for the thermal degradation study. TGA analysis of LDH clay and the composites provides useful information regarding the thermal stability and thermal decomposition temperature of the materials. The residue left after heating beyond 700°C in the TGA chamber is considered to be the char yield of the combustion process for the respective material.

3.3.5 Rheological Analysis

The rheological measurements were carried out by an ARES rheometer (Rheometrics Scientific, USA) with torque transducers having a torque range from 0.02 g.cm to 2000 g.cm . During each experiment, the temperature maintained at the desired value by constant heating of the sample under nitrogen atmosphere. The various rheological measurements that were carried out using different strain input program are described below.

3.3.5.1 Dynamic Oscillatory Shear Experiment

Linear viscoelastic properties of the composites were studied under dynamic oscillatory shearing using parallel plates geometry (diameter 25 mm) and sample thickness of 2 mm . During each measurement the samples were subjected to an input strain function given by equation 3.2.

$$\gamma(t) = \gamma_0 \sin(\omega t) \quad (3.2)$$

The strain amplitude, γ_0 was maintained below 5% to ensure the linear viscoelastic regime of measurement for all the samples. The frequency-temperature sweep was carried out within the frequency (ω) range 0.056 rad/s to 100 rad/s and the temperature range 160 – 240 °C. The resulting time dependent stress response by the sample is given by

$$\sigma(t) = \gamma_0 [G' \sin(\omega t) + G'' \cos(\omega t)] \quad (3.3)$$

where, $\sigma(t)$ is the shear stress, G' is the storage or elastic modulus and G'' is the loss or viscous modulus. The response of the sample melt under dynamic oscillatory shear was also interpreted in terms of other parameters, like complex viscosity $|\eta^*|$ and $\tan\delta$, where δ is phase angle (phase shift between stress and strain vector). The definition of these two parameters are given by the following equations.

$$\tan\delta = \frac{G''}{G'} \quad (3.4)$$

$$|\eta^*| = \sqrt{\left[\frac{G''}{\omega}\right]^2 + \left[\frac{G'}{\omega}\right]^2} \quad (3.5)$$

3.3.5.2 Step Strain Experiment

The stress relaxation behavior of the polymeric melts was investigated by subjecting the melts to a step strain experiments. The samples were melted at 240 °C within the parallel plates and were allowed to attain equilibrium state under quiescent condition. Then a sudden strain of magnitude γ was applied. The strain was maintained at that value and the decay of modulus, called stress relaxation modulus $G(t)$, was then monitored with time. $G(t)$ is defined as

$$G(t) = \frac{\tau(t)}{\gamma} \quad (3.6)$$

where, $\tau(t)$ represent the time dependent stress.

3.3.5.3 Non-linear Shearing or Flow Reversal Experiment

To carry out the non-linear shear experiments, polymer melts were subjected to a steady shearing step (called preshearing step) at a constant shear rate till the apparent steady state is reached. The shearing was then stopped for an interval of specified duration (called rest period) and finally subjected to a second steady shearing step (called flow reversal step) at the same shear rate like the preshearing step, but in the opposite direction. This protocol of non-linear shearing was repeated with increasing rest period for each composition with the fresh sample each time. The shear cycle is schematically represented in **Figure 3.2**. Results obtained in the preshearing cycle are then discarded due to their non-reproducibility, while the data measured in the flow reversal step are used to study the influence of shear rate and the rest period on the state of the filler structure.

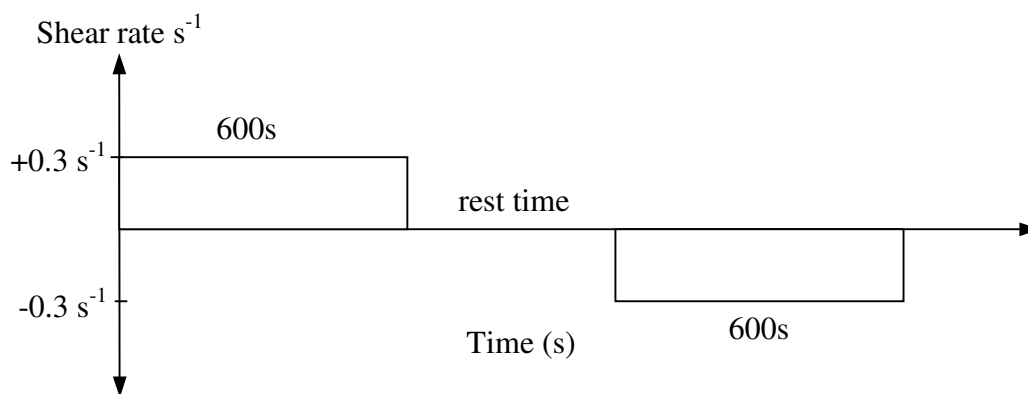


Figure 3.2 Shear cycle used during non-linear shear or flow reversal experiments

3.3.6 Mechanical Properties and Fracture Behavior

The tensile properties and the fracture behavior of all the samples were investigated using an universal testing machine [Zwick]. The load cell used for tensile testing was an Instron Static Load Cell with a 2.5 kN capacity. The ISO standard 527-3/2/5-Clip-On was followed for the tensile testing. The test speed was 5 mm/min for measuring the tensile strength, the yield strength and the elongation at break. The E-modulus (called elastic modulus) was measured at the very beginning of the strain application within 0.05 – 0.25% strain and using a cross-head speed of 1 mm/min. All of the samples were prepared by injection molding and has a has the basic shape of a typical tensile dumbbell with the following average dimensions: 7.5 cm long, 4.0 mm wide and 2.0 mm thickness. For statistical analysis of the results at least five specimens were tested for each samples.

3.3.7 Flammability Properties

3.3.7.1 Limiting Oxygen Index (LOI)

Limiting oxygen index is used to determine the minimum concentration (in a flowing mixture of nitrogen and oxygen) of oxygen required to sustain a candle-like burning process of any material. It is expressed by a number indicating percentage of oxygen in a nitrogen-oxygen mixture and gives a qualitative measure or indication of materials' susceptibility to continuous burning after ignition. LOI is often useful in comparative investigation and quality control during product design. Usually, a material having LOI value 21 or less burns spontaneously in air. So, the efficiency of a flame-retardant is often interpreted by the increase in the LOI value (from that in the pure polymer) when it is incorporated into a polymer. Although the relevance of this test to the real fire conditions is questionable, this test method is widely practiced both in industry and in academics because of inexpensive test equipments and a small sample requirement.

The typical LOI test apparatus, as shown in **Figure 3.3** consists of a glass tube of 75 to 100 mm in diameter and of 450 to 500 mm in height. A specimen with a specified dimension is supported inside the glass tube. A gas mixture of oxygen and nitrogen is supplied at the bottom of the tube and a small candle-like flame is applied to the top of the specimen in an attempt to ignite it. The composition of the gas mixture can be controlled (up to minimum 0.1 volume percent) by varying the flow pressure

of the oxygen and nitrogen stream. The LOI values of the LDH based composites were measured by a LOI tester from Raczek Analysentechnik GmbH Scientific Instruments using injection molded strips (125 x 6.5 x 3.2 mm) according to ASTM 2863.

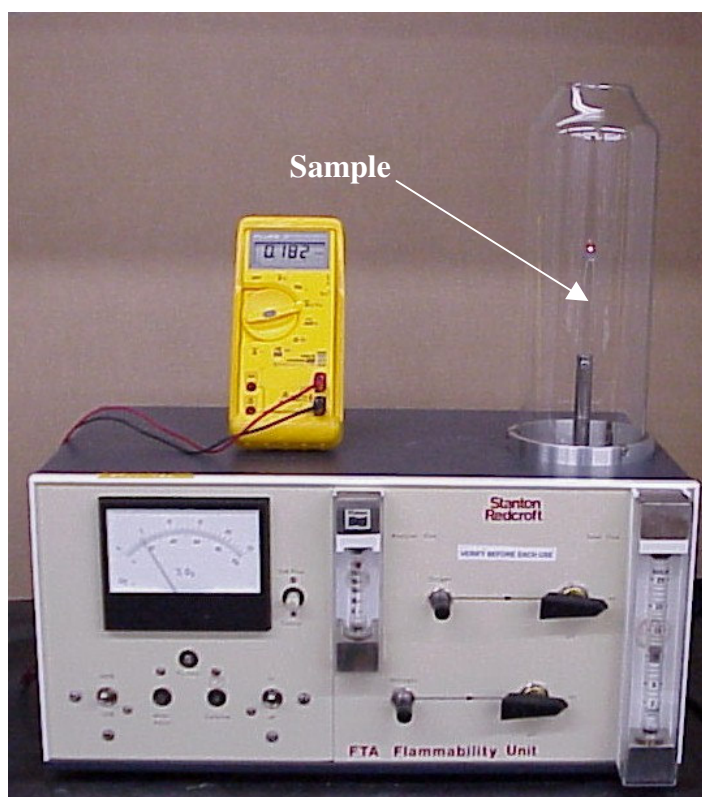


Figure 3.3 A typical LOI measuring instrument

3.3.7.2 Cone Calorimeter Test

The cone calorimeter test is an advanced and widely used test method for assessing flammability of polymeric materials. The method followed is described in international standard ISO 5660. The test specimen used according to this standard has a surface area of $100 \times 100 \text{ mm}^2$ and thickness below 50 mm. The test specimen with dimension of $100 \times 100 \times 4 \text{ mm}$ were used in the present work and were prepared by injection molding. During the actual test, an external heat flux of 30 kW/m^2 was applied. All the samples were preconditioned for 24 h at 23 C and 50% relative humidity.

The test apparatus basically consists of a radiant heat source in the shape of a truncated cone, a load cell and a gas collection system as shown in **Figure 3.4**. After the sample is mounted on sample holder, it is exposed to a heat flux (chosen in the range $0 - 100 \text{ kW/m}^2$, but typically within the range $25 - 75 \text{ kW/m}^2$). The test specimen is placed horizontally on the sample mount using an aluminum pan, which just cover the volume of the sample with top surface exposed (the aluminum pan prevents the spilling of the melt when the sample burns). With this set up, it was not possible to analysis the unfilled PE as the melt overflow the aluminum pan). An electric spark is then used to ignite the volatile gases liberated from the heated sample. The gases and smokes liberated during burning are collected in an exhaust pipe, where at the same time consumption of oxygen, temperature and opacity of the smoke are determined

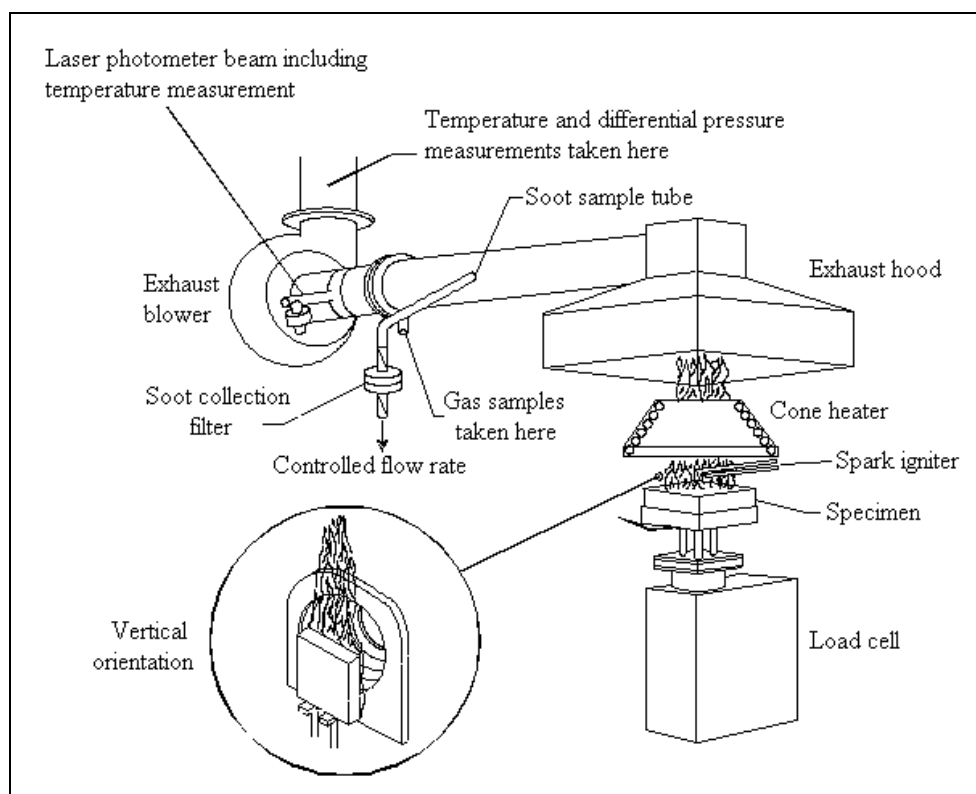


Figure 3.4 Schematic representation of a cone calorimeter unit

simultaneously. The smoke production is analyzed by the attenuation of a laser beam by the smoke in the exhaust duct and expressed as specific extinction area.

The cone-calorimeter primarily measures the parameter called heat release rate (HRR) during the whole combustion process. The calculation of the HRR is based on oxygen consumption principle described by Hugget [116]. According to this principle, for a given amount of oxygen consumption during any combustion process the amount of heat released is always constant being independent of type of the material undergoing combustion. This means in case of polymeric materials, the amount of heat released per unit amount of oxygen consumption will always be constant in spite of their different heat of combustion. The value determined for a wide range of organic fuels is 13.1 kJ per gram of oxygen consumed with an accuracy of $\pm 5\%$. To implement the principle of oxygen consumption in cone-calorimeter, the difference in the oxygen mass flow rates between the initial air flow into the combustion chamber and the combustion product stream is determined. This difference is related to the heat release rate using the relation in equation 3.7 [117].

$$\dot{q} = 13.1(\dot{m}_{O_2, \infty} - \dot{m}_{O_2}) \quad (3.7)$$

where, \dot{m}_{O_2} , indicates the mass flow rate of oxygen in the gas streams and ∞ indicates the base line ambient condition prior to the start of the test.

Several aspects related to burning process can be evaluated from cone calorimeter tests, such as ignitability, heat of combustion, heat release rate, smoke production, production of toxic gases, etc. The test results are interpreted in terms of parameters described in **Table 3.5**.

Table 3.5 Different parameters measured during cone calorimeter tests

Parameter	Symbol	Unit	Description
Time of ignition	t_{ig}	s	Time required for igniting is triggered by the electric spark
Total heat release	THR	MJ/m ²	The cumulative heat release during the whole combustion process (area under the heat release curve)
Heat release rate	HRR	kW/m ²	The instantaneous heat released during combustion process
Peak heat release rate	PHRR	kW/m ²	Maximum in the heat release curve
Heat of combustion	H_c	MJ/kg	Ratio between heat release and mass loss
Specific extinction area	SEA	m ² /kg	A measure of smoke released measured from smoke obstruction data
Production of CO	CO _{6min}	kg/kg	Production of carbon monoxide during first 6 minutes of combustion
Mass loss rate	MLR	g/s	Instantaneous mass loss during combustion

3.3.7.3 UL-94 testing

UL-94 test is widely practiced for determining relative flammability and dripping behavior during burning process. This test rating is important for plastics applications in electrical and electronic equipments. This method serves the preliminary indication of the acceptability of plastic materials with respect to flammability for a particular application. There are three types of UL-94 testing methods practiced, such as UL-94 V, UL-94 HB and UL-94 5V. In this study, only the first two methods have been used to

Table 3.6 UL-94 vertical and horizontal test criteria

Criteria	V-2	V-1	V-0	HB
Number of ignition time	2	2	2	1
Maximum flaming time per specimen per flame application, sec	30	30	10	-
Maximum total flaming time, 5 specimens, 2 ignitions, sec	250	250	50	-
Specimen drips, ignites cotton	Yes	No	No	-
Maximum afterglow time, per specimen, sec	60	60	30	-
Burn to the holding clamp	No	No	No	-
Maximum burning rate for specimens 3.0 mm to 13.0 mm, mm/min	-	-	-	40
Maximum burning rate for specimen less than 3.0 mm, mm/min	-	-	-	75

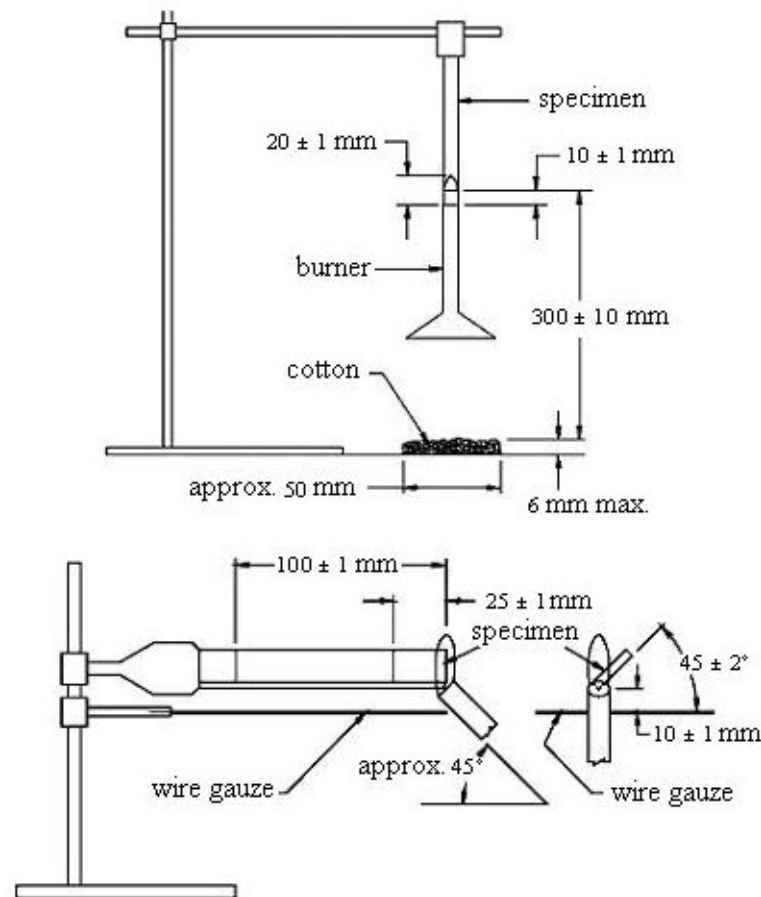


Figure 3.5 Schematic representation of a UL-94 VB (top) and UL-94 HB (bottom) test methods

characterize LDH based composites. Various kind of UL-94 V and UL-94 HB ratings are discussed in **Table 3.6** and the test procedures are schematically shown in **Figure 3.5**. The samples size used in both cases are similar and have dimension of $130 \times 12.5 - 13.0 \times 4$ mm. In case of UL-94 V test, the sample is clamped vertically with the bottom end exposed to the flame for two times each with 10 s duration. The UL-94 rating or no rating is then determined observing the burning time and burning behavior after each of the two flame exposures. In case of UL-94 HB test, the sample is clamped horizontally on the sample holder at one end and subjected to flame for 30 s at the other end. The rating is determined by observing the speed of flame propagation (how fast the sample burns) between two specified marks on the samples. For each composition, total five samples were tested and the average was calculated. All the samples were preconditioned for 72 h at at 23 C and 60% relative humidity.

LDH: SYNTHESIS, MODIFICATION AND CHARACTERIZATION

4.1 Synthesis

LDH based on magnesium and aluminum (Mg-Al-LDH, henceforth will also be represented by LDH) was synthesized using coprecipitation method from a homogeneous aqueous solution of Mg^{2+} and Al^{3+} with urea as the precipitating agent. At first, an aqueous solution of Al^{3+} and Mg^{2+} with the molar fraction $\text{Al}^{3+}/(\text{Al}^{3+} + \text{Mg}^{2+})$ equal to 0.33 was prepared by dissolving AlCl_3 and MgCl_2 in distilled water. To this solution solid urea was added until the molar fraction $\text{urea}/(\text{Al}^{3+} + \text{Mg}^{2+})$ reached 3.3. The clear solution was refluxed for 36 hours. LDH is precipitated as a white mass, which was then filtered, washed until chloride free and dried in vacuum at 60 °C till the constant weight. This method has been described in literature and is suitable for synthesizing highly crystalline Mg-Al-LDH with narrow particle size distribution [14]. The conditions chosen for the synthesis provides Mg-Al-LDH with 'x' around 0.33, i.e. the composition is more likely represented by $\text{Mg}_{0.67}\text{Al}_{0.33}(\text{OH})_2(\text{CO}_3)_{0.165}0.4\text{H}_2\text{O}$ [14].

4.2 Modification of LDH

Like layered silicate based nanoclay materials, modification of Mg-Al-LDH is an inevitable step in the preparation of polymer nanocomposites, specially when melt-compounding technique is used. Since, the hydroxide layers of LDH clays are positively charged, the modifying surfactants should contain at least one negatively charged functionalities or highly nucleophilic sites in their chemical structure. In the present work, Mg-Al-LDH has been modified by four different surfactants having different anionic functional groups. The structure and chemical formula of these surfactant anions are given in **Figure 4.1**. The length and nature of the hydrophobic tail of these surfactants are not same. While dodecyl sulfate (DS) and laurate has same tail of n- C_{12} , dodecylbenzenesulfate (DBS) contains a benzene ring in the tail backbone and Bis (2-ethylhexyl)hydrogenphosphate (BEHP) contains two branched hydrocarbon chains. These differences in the surfactant tail and functional groups certainly influence their efficiency to modify Mg-Al-LDH clay and will be discussed in details in the subsequent sections.

The modification of LDH was carried out by regeneration method, which is based on the well known 'memory effect' shown by LDHs. When the CO_3^{2-} containing LDH is heated above 450 °C for several hours, it is converted into an amorphous mixed oxide (designated as CLDH). This mixed oxide regenerates the original layered metal hydroxide structure when dispersed in an aqueous solution containing CO_3^{2-}

and stirred for sufficient time. If an anion other than CO_3^{2-} remains in the solution, the regeneration leads to intercalation of that anion in the LDH structure. The same principle was used for the modification of LDH with organic surfactants. The mixed oxide is dispersed in an aqueous solution of the desired surfactant and stirred for about 24 h at ambient temperature. The concentration of the surfactant solution was maintained around 0.1 – 0.2 M and CLDH was added to a specified volume of this surfactant solution in such an amount that there is enough surfactant anion available for 100% substitution of the interlayer carbonate anion after regeneration. The modified solid was then separated by repeated washing and centrifugation and dried at 60 °C till constant weight. To check the 'memory effect' of the LDH clay, CLDH was also dispersed in an aqueous solution of Na_2CO_3 and treated similarly as before. The so called regenerated solid was called LDHR.

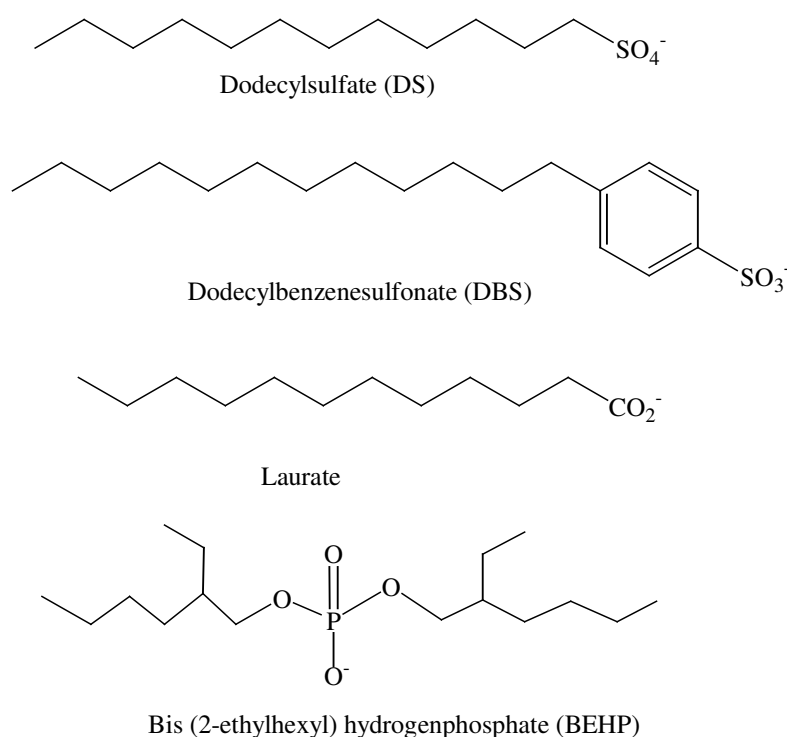


Figure 4.1 Different surfactants used for intercalation within the LDH gallery

4.3 Characterization of LDH Materials

4.3.1 Characterization of the Unmodified Clays

The XRD patterns of the synthesized and unmodified Mg-Al-LDH, its calcined form (CLDH) and the regenerated form (LDHR) are shown in **Figure 4.2**. The first three reflections assigned belong to the common $\langle hkl \rangle$ series i.e. $\langle 00l \rangle$ and resemble those reported in literature for synthetic Mg-Al-LDH [14] and hydrotalcite minerals [5]. The basal reflection $\langle 003 \rangle$ has the value of 2θ about 11.8° . This corresponds to a basal spacing or interlayer distance of about 0.76 nm, which is equal to the sum of the thickness of interlayer region and one metal hydroxide layer. These characteristic reflections of Mg-

Al-LDH are lost after calcination as indicated by the XRD pattern of CLDH and it is converted into an amorphous material closely resembling MgO (the strong reflections observed for CLDH are those typical of MgO). In the regenerated clay LDHR, the reappearance of the crystalline reflections corresponding to those in synthesized Mg-Al-LDH, indicates the reformation of the layered structure. However, the broadening of the crystalline reflections in the regenerated material is caused by partial loss in the degree of crystallinity. The overlapping of the mean position of the basal reflection of the regenerated LDH with that of the original means the LDH and LDHR have similar interlayer distance. The presence of the reflections of mixed $\langle hkl \rangle$ series, i.e. $\langle 003 \rangle$, $\langle 006 \rangle$, $\langle 012 \rangle$, $\langle 015 \rangle$, $\langle 018 \rangle$ in the synthesized LDH clay indicates the presence of coherence condition in all direction with respect to x-ray scattering. **Figure 4.2** also shows a comparison between the synthesized Mg-Al-LDH and a Mg-Al-LDH sample from industry. The similarity in XRD pattern of these samples can be observed both before and after calcination. This means the different Mg-Al-LDH samples used in the present study are similar in crystal structure and composition providing a similar oxide form after calcination.

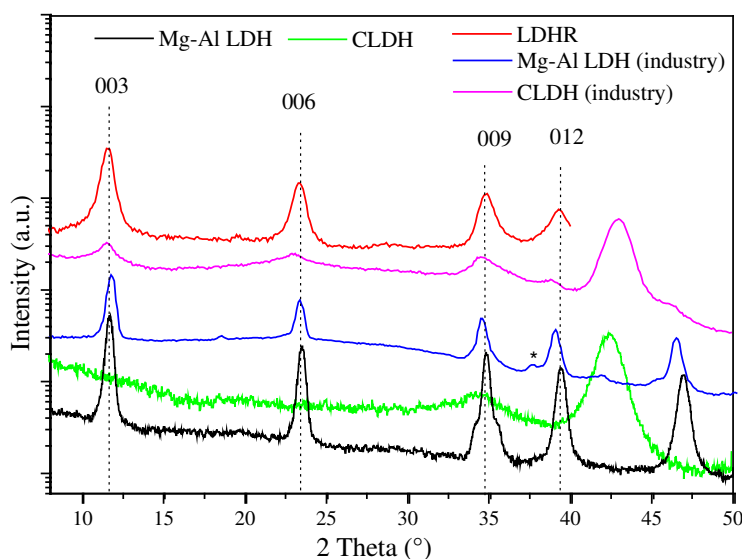


Figure 4.2 XRD patterns of different Mg-Al-LDH clay materials without interlayer modification (* indicates the unknown reflections in the industrial samples).

The FTIR spectra of LDH materials provide many important information, especially about the interlayer anions and hence are very useful to understand the structure of these materials. Mg-Al-LDH containing CO_3^{2-} has characteristic bands for various modes of infrared sensitive vibration shown by the anion. Free CO_3^{2-} shows three different IR sensitive vibrations: bending non-planar mode (γ_2), the asymmetric stretching mode (γ_3) and the bending angular mode (γ_4). These three modes in free anion present in solution are observed at 880, 1415 and 680 cm^{-1} , respectively [118]. The CO_3^{2-} present in the interlayer region in LDH shows shifting of these vibration bands to lower values and also splitting of the bands in comparison to the free anions. This is because of the fact that intercalation and also ionic interaction of the CO_3^{2-} ions with metal hydroxide layers impose steric hindrance on the normal vibration of the bonds. In most Mg-Al-LDH, these characteristics bands are observed in the range 850 – 880 cm^{-1} (γ_2), 1350 – 1380 cm^{-1} (γ_3) and 670 – 690 cm^{-1} (γ_4) [5]. Sometimes, the lowering in

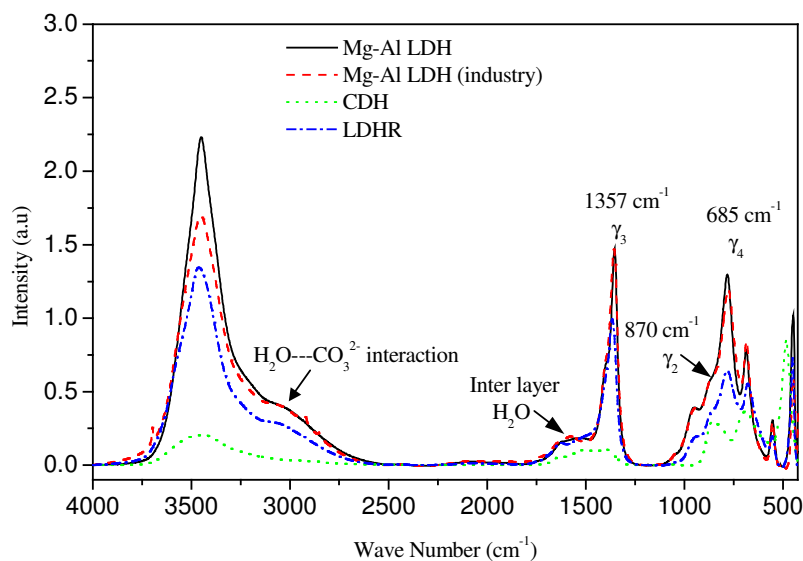


Figure 4.3 Comparison of the FTIR spectra of synthesized Mg-Al-LDH, CLDH, LDHR and an industrial Mg-Al-LDH showing the recovery of original structure LDH after regeneration process.

symmetry of the interlayer CO_3^{2-} causes degeneration or splitting of the γ_3 band into a doublet band [119, 120]. This lowering of symmetry, additionally, can activate γ_1 vibration mode around 1050 cm^{-1} and the absence of this vibration can be taken as an indication of retaining full symmetry by the CO_3^{2-} anions in the interlayer region [121]. Both the synthesized and industrial LDH samples show a sharp band at 1357 cm^{-1} corresponding to γ_3 vibration appears without any distinct shoulder or degeneration indicating the absence of splitting of the γ_3 band (**Figure 4.3**). Besides, no band or shoulder around 1050 cm^{-1} means highly symmetric nature of the interlayer CO_3^{2-} ions. The γ_3 band is the most sensitive CO_3^{2-} band and from its position depends on the M^{II}/M^{III} ratio i.e. the value of x in the LDH chemical formula. The lowering of this ratio (increasing the value of x) means higher is the electrostatic attraction (through hydrogen bonding) on the interlayer anions by the metal hydroxide sheets. As a result, with decreasing M^{II}/M^{III} ratio, position of the γ_3 band shifts to lower value of wave number indicating higher energy required for desired vibration. For M^{II}/M^{III} ratio equal to 3/1 and 2/1 the positions of γ_3 band is observed at about 1370 cm^{-1} and 1355 cm^{-1} respectively [121]. The synthesized LDH shows a strong γ_3 band around 1357 cm^{-1} indicating the $\text{Mg}^{2+}/\text{Al}^{3+}$ ratio is close to 2/1 i.e. x is close to 0.33. The bands corresponding to other two modes of vibration are also visible in **Figure 4.3**, such as a sharp band around 685 cm^{-1} indicates γ_4 mode and a small shoulder around 870 cm^{-1} for γ_2 mode. The broad band in the range $3200 - 3700\text{ cm}^{-1}$ originates from the O-H stretching of the metal hydroxide layer and interlayer water molecules. A shoulder present around $3000 - 3100\text{ cm}^{-1}$ is caused by the interaction between the CO_3^{2-} and H_2O present in the interlayer region, which involves mostly hydrogen bonding [5, 122]. The bending vibration of the interlayer H_2O is also reflected in the broad bands around 1600 cm^{-1} . The bands characteristic of the metal-oxygen bond stretching appear below 700 cm^{-1} . The sharp bands around 780, 554 and $430 - 450\text{ cm}^{-1}$ originate from various lattice vibration associated with metal hydroxide sheet. A comparison with the commercial LDH sample used for the nanocomposite preparation is also shown in **Figure 4.3**. This sample has known $\text{Mg}^{2+}/\text{Al}^{3+}$ ratio of about 2.3 (that means x is equal to 0.30) in its

composition (**Table 3.1**). The FTIR spectra of this material exactly overlap that of the synthesized LDH showing close similarity in their chemical composition.

The close similarity between the FTIR spectra of the regenerated LDH with the original LDH in **Figure 4.3** confirms the recovery of chemical structure of the LDH during the regeneration process. However, the FTIR spectra for calcined LDH indicates, though in much reduced intensity, the presence of all three modes of vibration of the carbonate ion and also a O–H stretching band. This means calcination at 450 °C though destroys the crystal structure of LDH (as confirmed from the XRD pattern in **Figure 4.2**), there still exist some carbonate ions and water molecules in the material. This may arise either due to adsorption of carbon dioxide and water vapor at the surface of highly porous CLDH or due to incomplete degradation of LDH at 450 °C.

4.3.2 Characterization of the Modified Clays

4.3.2.1 XRD Analysis

The XRD patterns of the surfactant modified LDH is shown in **Figure 4.4**. As expected, the position of the first order basal reflection $< 003 >$ in all modified samples is shifted to a higher d-value indicating an expansion in the interlayer distance. Although none of the modified samples show distinct reflection at $d = 0.76$ nm, there exists a weak and broad reflection in the close vicinity, which may be either due to the presence of small fraction of the unmodified LDH or due to a higher order reflection in $< 00l >$ series in the modified samples. However, the first option seems most probable as the XRD pattern of all the modified sample show reflections corresponding to single $< 00l >$ series and no mixed $< hkl >$ as compared to the unmodified LDH. The absence of reflection corresponding to mixed $< hkl >$ series also indicates a loss of crystallinity of LDH after organic modification. This may be due to presence of only small crystallites and/or the loss of coherent conditions for all other directions (i.e. no repeat units) in the sense of scattering.

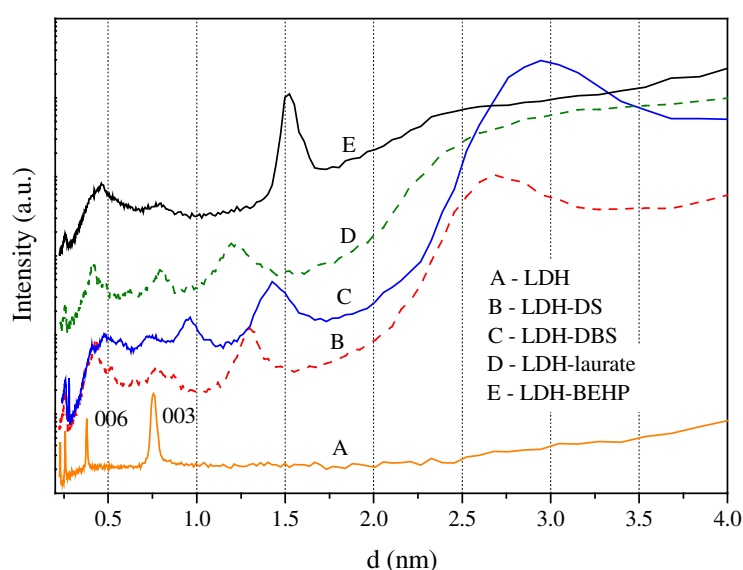


Figure 4.4 XRD patterns of modified LDH obtained using regeneration methods in presence of various surfactants.

The identification of the various reflections observed in modified LDH in **Figure 4.4** and their position are shown in **Table 4.1**. The presence of $< 00l >$ reflections up to several order in all the modified sample indicates the regeneration of the crystal layers even in the presence of large intercalating anions. The interlayer distance increases from 0.76 nm in the unmodified LDH to 1.52 nm in BEHP modified LDH (LDH-BEHP), to 2.45 nm in laurate modified LDH (LDH-laurate), to 2.68 nm in SDS modified LDH (LDH-DS) and to 2.95 nm in SDBS modified LDH (LDH-DBS). These values are in good agreement with those reported in literature for the same surfactants and the similar or different chemical procedure for organic modification. For example, LDH-DBS and LDH-DS prepared by direct ion exchange reaction in aqueous solution of the surfactants results in an interlayer separation of 2.95 nm [6] and 2.62 nm [50] respectively. Theoretical calculation of interlayer distance in the modified LDH

Table 4.1 Assignment of various XRD reflections obtained for LDH and its modified forms

Materials	reflections in $< 00l >$ series					
	$< 003 >^a$		$< 006 >$		$< 009 >^b$	
	$2\theta(\text{deg})$	$d(\text{nm})$	$2\theta(\text{deg})$	$d(\text{nm})$	$2\theta(\text{deg})$	$d(\text{nm})$
LDH	11.60	0.76	23.40	0.34	34.50	0.26
LDH-DS	3.30	2.68	6.80	1.30	10.17	0.876
LDH-DBS	2.99	2.95	6.18	1.43	9.21	0.96
LDH-laurate	3.60	2.45 ^c	7.19	1.23	10.79	0.82
LDH-BEHP	5.81	1.52	11.06	0.86 ^d	19.30	0.46

^a In all the modified sample except LDH-BEHP, the $< 003 >$ reflection appeared as a broad and diffused. The exact assignment was made following a relation existing among the various reflections in the $< 00l >$ series.

^b this reflection in unmodified LDH is assigned as $< 012 >$ and hence does not belongs to $< 00l >$ series.

^c The $< 003 >$ reflection of LDH-Laurate appears as broad shoulder around 2.45 nm

^d The $< 006 >$ reflection in LDH-BEHP seems overlapped with the $< 003 >$ reflection of the unmodified fraction

is made from the information regarding the thickness of metal hydroxide sheet, size of the surfactant molecules and their nature of orientation in the interlayer region. Such calculations have already been carried out by Lagaly and co-workers [6, 44] for a wide ranges of LDH and surfactants. The interlayer distance of the LDHs modified with primary alkyl sulfonates and carboxylic acids is given by equation (4.1). This equation is valid only in case monolayer arrangement of the surfactant in the interlayer region.

$$d_L(\text{nm}) = 0.96 + 0.127 * n_c + \sin\alpha \quad (4.1)$$

Where, d_L is the basal spacing in nm, n_c is the number of carbon atom in the alkyl chain of the

surfactant and α is the tilt angle of the alkyl chain from the normal of the metal hydroxide sheet. The value of the tilt angle has been found to be 56° [6]. In case of DBS the alkyl chain remains perpendicular to the hydroxide layer and the benzene ring in a tilted position. Therefore, in case of DBS the above equation is modified in the following form.

$$d_L(nm) = 0.129 + 0.127(n_c - 1) \quad (4.2)$$

In the modified LDH usually there exists a layer of adsorbed water molecules in between the hydrocarbon chain end of the surfactant and the metal hydroxide layer, especially in the samples not dried in vacuum [6, 22]. Loss of this layer of water molecules causes a contraction in interlayer spacing by about $0.3 - 0.5 \text{ nm}$ [6]. It has been reported that in LDH-DBS the loss of this adsorbed layer of water molecules causes 0.32 nm contraction in basal spacing. The same value has been used for correcting the basal spacings calculated from equation (4.1) and (4.2). These are shown and compared with experimentally observed value in **Table 4.2**. Except in case of surfactant BEHP, the calculated basal spacings after correction for adsorbed water layer closely resemble the experimentally observed values. The small difference observed can be due to the size of the anionic functional groups present and difference in the tilt angle. In case of LDH-BEHP, the basal spacing calculated based on equation (4.1) show close similarity to the experimental value when no correction is made for adsorbed water layer. Obviously, LDH-BEHP does not contain any adsorbed water in its structure. The absence of water loss peak (below 200°C) in TGA curve of BEHP modified LDH can be taken as the evidence for this proposition.

Table 4.2 Comparison between theoretically calculated and experimentally observed values of the basal spacing in the modified LDH materials

Materials	Equation Used	Calculated d_L <i>nm</i>	Calculated d_L after correction for adsorbed water layer <i>nm</i>	Observed d_L <i>nm</i>
LDH-DS	(4.1)	2.23	2.55	2.68
LDH-DBS	(4.2)	2.69	3.01	2.95
LDH-laurate	(4.1)	2.23	2.55	2.45
LDH-BEHP	(4.1)	1.59	1.84	1.52

4.3.2.2 FTIR Analysis

The FTIR spectra of the modified LDH reveal two types of bands: one corresponding to the anionic species intercalated and other corresponding to host LDH materials. This has been shown in details in **Figure 4.5** and **Table 4.3**. All the modified samples show strong absorption bands in the range $2850 - 2965 \text{ cm}^{-1}$ corresponding to the $-\text{CH}_2-$ stretching vibration of the hydrocarbon tail present in each of the surfactant anions. The bands appear in the range $1000 - 1800 \text{ cm}^{-1}$ are mostly due to the anionic functionalities present in the surfactants and also interlayer water molecules. The band around 428 cm^{-1} originates from the lattice vibration of the hydroxide sheet and the broad band in the range $3200 - 3700$

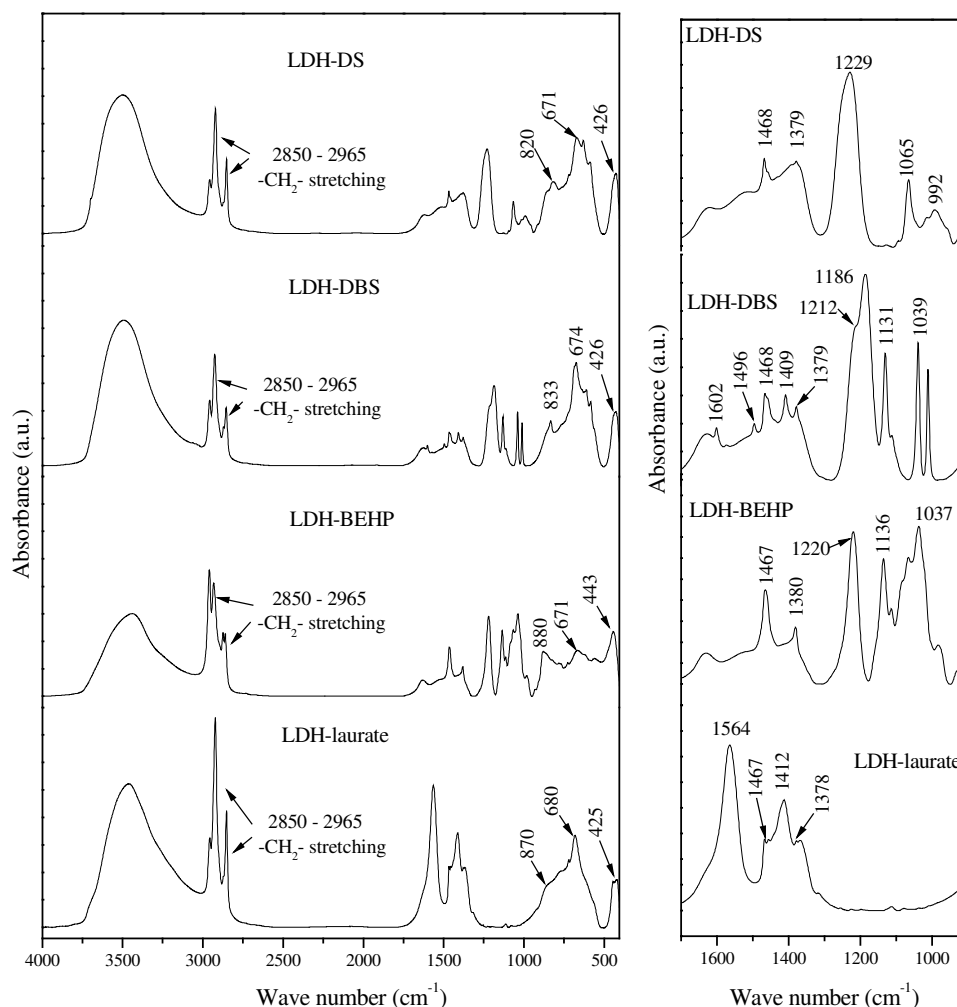


Figure 4.5 FTIR spectra of the LDH modified by different anionic surfactants using regeneration method (the assignments of various bands are given in Table 4.3)

cm^{-1} are mainly from the O–H groups present in metal hydroxide layers. The appearance of characteristic vibration bands for CO_3^{2-} (γ_2 , γ_3 and γ_4) means their exits still some CO_3^{2-} in the interlayer region. However, the absence of the strong 1357 cm^{-1} band in the modified samples is a strong indication of significant decrease in the interlayer CO_3^{2-} content and also of the change of its symmetry in comparison to that observed in unmodified LDH. The lowering of CO_3^{2-} ion's symmetry in the interlayer region is further indicated by the splitting of the γ_3 band into a pair around 1379 cm^{-1} and 1467 cm^{-1} [14, 119]. This is perhaps caused by the partial constraint release on the movement of the CO_3^{2-} ions in a more spacious interlayer region formed by the intercalation of relatively large organic molecules. The source of the CO_3^{2-} ions in the modified samples is partly the unreleased ions still remaining in CLDH and partly atmospheric carbon dioxide, which is incorporated into LDH structure during the regeneration process.

The FTIR spectra of the modified samples do not provide any clear indication of the presence of interlayer water. In this regard, only difference observed is the disappearance of the shoulder in the region $3000 - 3100 \text{ cm}^{-1}$, which is caused by the $\text{H}_2\text{O} \dots \text{CO}_3^{2-}$ interaction in the interlayer region. However, a broad band or shoulder is observed in all the modified sample in the range $1600 - 1640$

Table 4.3 Assignment of FTIR bands in LDH modified with different surfactants by regeneration method [19, 118, 123, 124]

Materials	Band position (cm^{-1})	Tapes of Vibration
LDH-DS	2850–2965	$\nu\text{-CH}_2$
	1229	$\nu_{\text{S=O}}$ (symmetric)
	1065	$\nu_{\text{S=O}}$ (asymmetric)
	630	$\nu_{\text{C-S}}$
	671, 820, 1379 and 1468	Different vibration modes of CO_3^{2-}
	426	M-O(lattice vibration)
LDH-DBS	2850–2965	$\nu\text{-CH}_2$
	1186	$\nu_{\text{S=O}}$ (symmetric)
	1038	$\nu_{\text{S=O}}$ (asymmetric)
	615	$\nu_{\text{C-S}}$
	1602, 1496, 1409 and 1450(w)	$\nu_{\text{C=C}}$ of the benzene ring
	674, 833, 1379 and 1467	Different vibration modes of CO_3^{2-}
	426	M-O(lattice vibration)
LDH-BEHP	2850–2965	$\nu\text{-CH}_2$
	1037 and 1136	$\nu_{\text{P-O-C}}$
	1220	$\nu_{\text{P=O}}$
	671, 880, 1380 and 1465	Different vibration modes of CO_3^{2-}
	443	M-O(lattice vibration)
LDH-Laurate	2850–2965	$\nu\text{-CH}_2$
	1563	$\nu\text{-COO-}$ (asymmetric)
	1412	$\nu\text{-COO-}$ (symmetric)
	680, 870, 1378 and 1467	Different vibration modes of CO_3^{2-}
	425	M-O(lattice vibration)

cm^{-1} , which may indicate the presence of H_2O molecules as the band for its bending vibration appears in this region. The XRD and TGA (see below) analysis show the presence of interlayer water. Therefore, it is logical to interpret that the water molecules present in the modified LDH do not interact with CO_3^{2-} anions rather they bridge the gap between the hydrocarbon tail of the surfactants and the metal hydroxide layers.

The FTIR bands corresponding to the functional groups of the surfactant anions are distinctly visible in all the modified samples. In LDH-DS, the characteristic S=O stretching vibration bands appear at 1229 cm^{-1} (symmetric) and 1065 cm^{-1} (asymmetric). The corresponding bands in LDH-DBS appears at 1186 cm^{-1} and 1038 cm^{-1} respectively. The C–S stretching vibration band is also observed at 630

cm^{-1} in LDH-DS and at 615 cm^{-1} in LDH-DBS. The LDH-DBS additionally shows multiple bands corresponding to the $\text{C}=\text{C}$ vibrations of the aromatic ring in the range $1450 - 1610 \text{ cm}^{-1}$. The LDH-BEHP shows characteristic $\text{P}-\text{O}-\text{C}$ stretching vibration bands at 1136 cm^{-1} (symmetric) and 1037 cm^{-1} (asymmetric). The $\text{P}=\text{O}$ stretching vibration is also indicated by a strong band at 1220 cm^{-1} . The LDH-laurate shows two strong characteristic bands at 1563 cm^{-1} and 1412 cm^{-1} respectively for the asymmetric and the symmetric stretching vibrations associated with the COO^{-1} group [124]. The intercalation imparts some degree of constraints on the various characteristic vibrations of these functional groups. As a result, their corresponding FTIR bands are expected to shift to lower values of wave number in comparison to their free-state values as more energy is required for executing such vibrations under constraints.

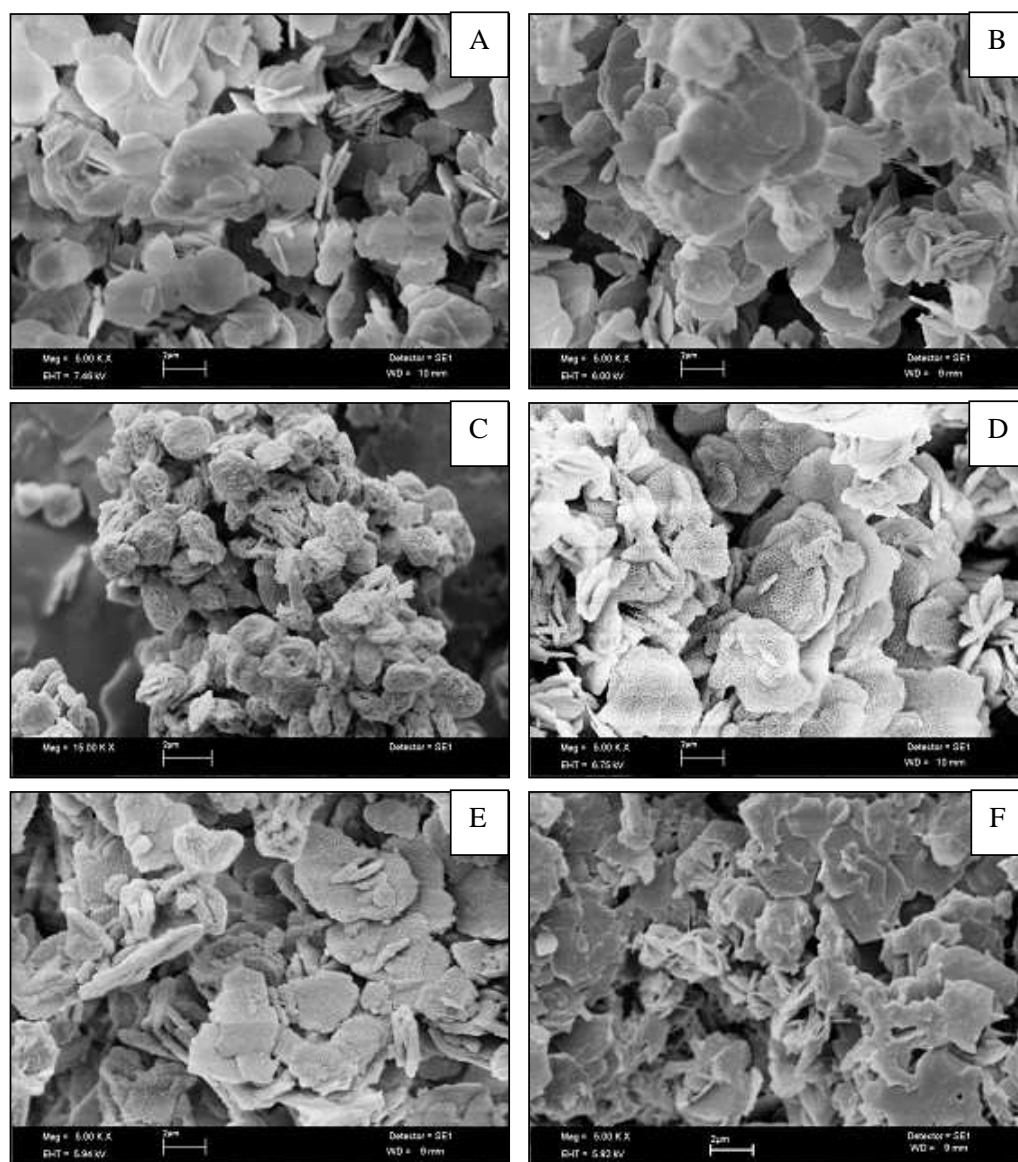


Figure 4.6 SEM micrographs of the LDH samples: A = unmodified Mg-Al-LDH, B = CLDH, C = LDH-laurate, D = LDH-DS, E = LDH-DBS and F = LDH-BEHP (magnification bar $2\mu\text{m}$)

4.3.2.3 Morphological Analysis

Mg-Al-LDH clays have usually plate-like particle morphology. The size distribution of the particles depends mostly on the synthesis conditions and varies from few hundred nm to few micrometer in lateral dimensions. In **Figure 4.6A**, the SEM micrograph of the synthesized LDH shows this particle geometry where the primary plate-like particles are characterized by distinct hexagonal shapes and sharp edges. The highly anisometric nature of these primary particles is also apparent. The lateral dimension of these plate-like particles varies within few micrometer whereas the thickness hardly exceeds few hundred nm. Interestingly, the calcination at about 450°C does not significantly change the overall particle morphology (**Figure 4.6B**). The plate-like appearance of the primary particles still exists in CLDH. The morphological features of the modified LDH are quite similar irrespective of the type of surfactant used in the present study. The regeneration process restores the metal hydroxide sheets of the LDH crystal. However, the particle morphology is somewhat modified after organic modification. As can be observed from **Figure 4.6C to F**, the well defined hexagonal particle shapes are lost. Instead plate-like particle morphology with irregular shapes and edges persists in the modified LDH. This seems quite obvious as the regeneration process, even in presence of carbonate anion, does involve loss of crystallinity (as confirmed from the broadening of XRD peaks in **Figure 4.2**). The surfactant anions being much larger in size than simple inorganic anions perhaps hinder the large scale lateral growth of the LDH layer. All the modified samples except LDH-BEHP show prominent surface irregularities compared to the unmodified LDH. A closer look into the higher magnification SEM images shows that the surface texture of primary particles (platelets) of the three samples (LDH-laurate, LDH-DBS and LDH-DS) is different from that of LDH-BEHP. From **Figure 4.7** it seems that in these three modified clays the particle surface is either

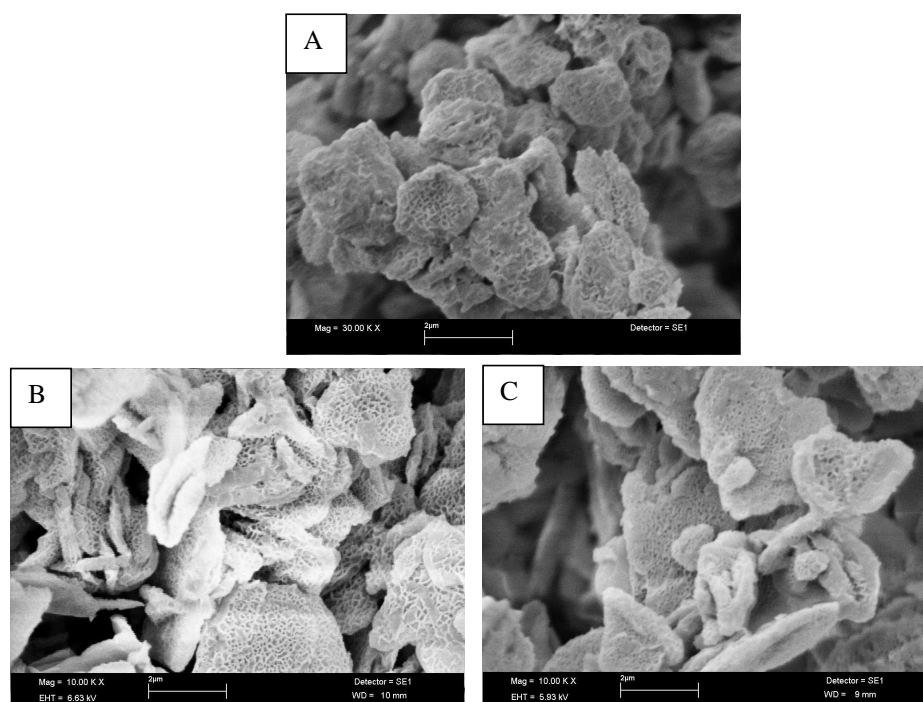


Figure 4.7 High magnification SEM micrographs showing the finer details of the surface morphology of the primary particles in LDH-laurate (A), LDH-DS (B) and LDH-DBS (C). (magnification bar 2 μm)

perforated or contain structural features probably due to secondary layer growth. Also, they appear more floppy compared to unmodified LDH. Whereas, in LDH-BEHP the surface texture resembles unmodified LDH with the presence of sharp edges of the primary particles. The structure of BEHP is quite different from the other surfactants. Although it contains two hydrocarbon tails, the length of each tail is much smaller than those present in other three surfactants. The XRD analysis reveals that the in LDH-DS and LDH-DBS the expansion of the interlayer distance is much higher than that in LDH-BEHP. The size of the surfactant anions may be a potential factor that influence the stacking and the growth of the metal hydroxide layers during regeneration process. However, more critical investigations are necessary for determining the exact mechanism of the regeneration process in presence of organic surfactants.

4.3.2.4 Thermal Analysis

The thermal analysis of the modified LDH is primarily aimed to investigate the decomposition behavior of the organic fraction and also the metal hydroxide layers. This was carried out by identifying various decomposition stage and the corresponding temperature range in the TGA plots. The comparison of the TGA plots of the modified LDH with that of the unmodified one gives an indication how the interlayer surfactants anions influence the decomposition of the host material. Thermal behavior of unmodified Mg-Al-LDH have been studied in details by several researchers. The most widely reported proposition suggests a two-stage decomposition process: a low temperature (up to about 225 °C) dehydration stage due to the loss of interlayer water and a high temperature decomposition (225 – 500 °C) stage due to the loss of interlayer carbonate and dehydroxylation of the metal hydroxide layer [125]. Often the high temperature decomposition occurs in two distinct steps depending upon the $\text{Mg}^{2+}/\text{Al}^{3+}$ ratio [5, 7, 125]. This tendency becomes more prominent as the $\text{Mg}^{2+}/\text{Al}^{3+}$ ratio increases. At $\text{Mg}^{2+}/\text{Al}^{3+}$ equal to 2, these two steps are quite distinctly separated [22, 44]. The first of these two peaks is attributed to the partial loss of OH^- from the brucite-like layer and the second one to the complete loss of OH^- and carbonate ions [5]. However, it has also been observed that release of interlayer carbonate starts as early

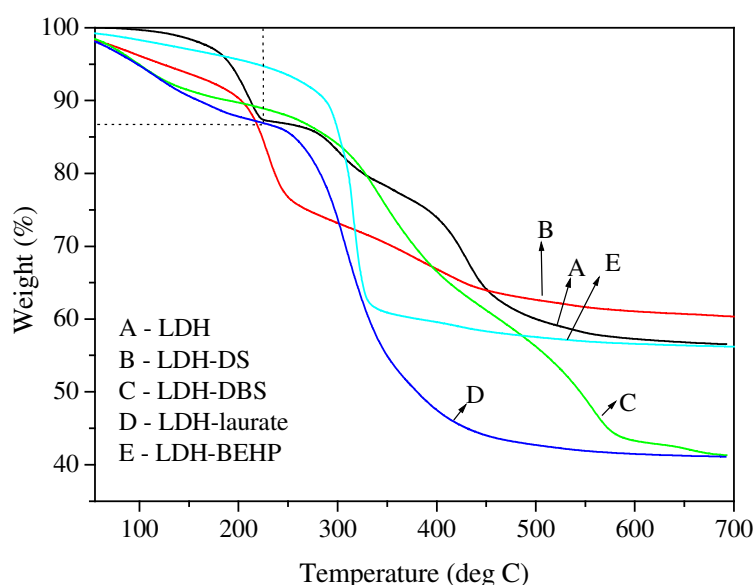


Figure 4.8 TG plots of LDH synthesized by urea method and its various modified forms.

as 250 °C and continues till 500 °C [126].

The thermal decomposition analysis of the unmodified LDH and its modified forms is presented in **Figure 4.8 and 4.9**. The low temperature decomposition step in the unmodified LDH lies below 230 °C with decomposition peak around 210 °C. During this step the loss of interlayer water molecules corresponds to a small (about 10 – 11 wt%) loss in weight in the TGA plot. This weight loss is closely equivalent to the total interlayer water content according to the chemical formula of LDH with Mg^{2+}/Al^{3+} ratio equal to 2. The high temperature decomposition of the unmodified LDH takes place in two distinct steps with decomposition peaks around 300 and 430 °C. The organic modification of the LDH significantly changes its the thermal decomposition behavior in comparison to the unmodified sample, especially the second stage of the decomposition process, which results complete collapse of materials structure. It is also apparent from **Figure 4.8 and 4.9** that the nature of surfactant anions has a strong influence on the thermal stability of the modified LDH. The loss of interlayer water molecules up to temperature about 225 °C in the modified samples are comparable to unmodified LDH, except the sample LDH-BEHP suffering much less weight loss compared to the others. This indicates that in LDH-BEHP much less water molecules are accommodated in the interlayer region. This is also reflected in the XRD analysis, where experimentally observed interlayer distance corresponds to the theoretical value calculated without considering the presence of the water layer in the interlayer region. Unlike other surfactants, BEHP has two

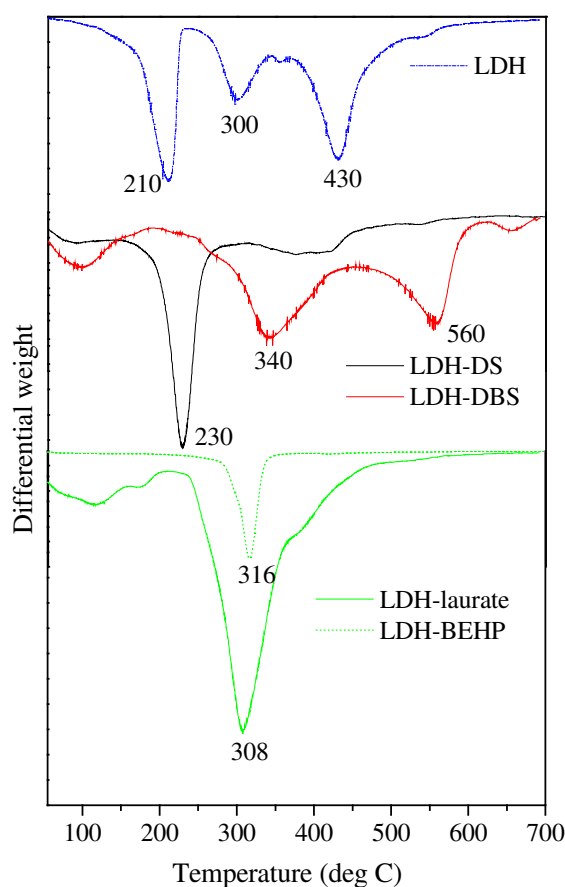


Figure 4.9 DTG curves for LDH and its various modified forms showing major decomposition stages.

branched hydrocarbon tails and thus perhaps, makes the interlayer region in LDH-BEHP too crowded to accommodate a large number of water molecules. The water molecules adsorbed on the non-gallery surfaces of LDH can also undergo desorption during this low temperature weight loss stage [127]. **Figure 4.8** and **4.9** also exhibit that the low temperature decomposition peak shifts to lower temperature in most of the modified samples indicating release of water molecules at lower temperature compared to that in unmodified LDH. In unmodified LDH, interlayer water molecules remain in close interaction with the interlayer carbonate ions and the hydroxide sheets through hydrogen bonding in a relatively constrained environment. After intercalation with surfactants, such interactions are largely reduced due to large decrease in carbonate anion concentration in the interlayer region and accumulation of the water molecules in between hydrocarbon tail of surfactant and hydroxide sheets. Similar shifts in the first decomposition step is also observed with decreasing Mg^{2+}/Al^{3+} ratio, which causes reduction in carbonate anion proportion in LDH composition [22].

The second decomposition stage is also changed significantly after organic modification. The two-step decomposition is only distinctly observed in LDH-DBS in the range 240 – 600 °C. However, both the peaks shift to higher value compared to the unmodified LDH. The decomposition of the dodecylbenzenesulfonate also takes place during this phase and probably interferes with the decomposition of the host material. The decomposition of benzene ring and long hydrocarbon chain in absence of free oxygen can delay the overall thermal decomposition process. LDH-DS shows lower thermal stability compared to other samples with greater weight loss up to temperature 230 °C. The decomposition of dodecylsulfate ion takes place in the range 210 – 250 °C [128] and therefore, a greater loss is observed below 250 °C compared to other modified LDH samples. The loss of the remaining carbonate and dehydroxylation of the host layer in LDH-DS takes place at slower rate over a wide temperature range of 280 – 300 °C resulting in a broad peak in DTG plot. Thermal decompositions of LDH-laurate and LDH-BEHP are characterized by the presence of a large proportion of weight loss step, which in case of former ranges within 250 – 350 °C and later within 280 – 350 °C. This is caused by the decomposition of the interlayer surfactant anions in these regions. However, major dehydroxylation process of the host materials occurs or starts around 300 °C. Therefore, largest proportion of weight loss for these two modified samples takes place in this region.

4.3.2.5 SDBS Modified LDH or LDH-DBS

Since LDH-DBS has the largest interlayer distance among all the modified samples studied, this organically modified LDH was chosen for the preparation of PE/LDH based nanocomposites. The characterization of LDH-DBS in the previous section though provides many important information on its structure, a further analysis using FTIR and XRD at various temperatures can be helpful to understand the changes in structure of LDH and LDH-DBS with increasing temperature. These information may also be important during processing and melt rheological analysis of the nanocomposites as they are carried out at a elevated temperature.

I. XRD analysis at different temperatures

Figure 4.10 shows the XRD patterns of both unmodified LDH and LDH-DBS at different temperatures. The XRD measurements were carried out by heating the sample within the sample holding unit in XRD instrument under nitrogen atmosphere. In **Figure 4.10**, the unchanged positions of the

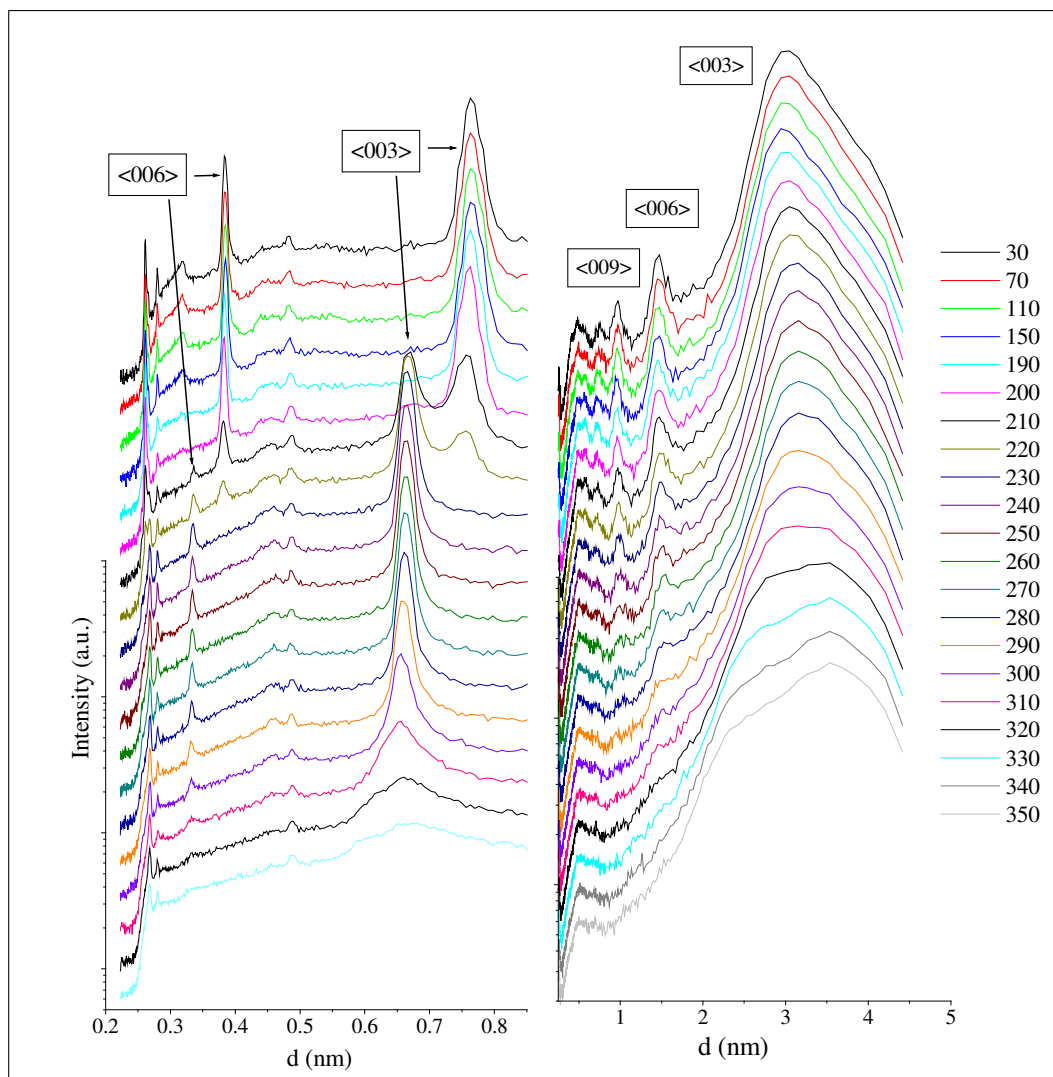


Figure 4.10 XRD patterns of unmodified LDH (left) and LDH-DBS (right) measured at different temperature showing the change in structure with temperature

first order and subsequent basal reflections of $\langle 00l \rangle$ series in the unmodified LDH indicates no significant change occurs in the crystal structure of LDH up to about 200 °C. Beyond this temperature, the intensity of the first order basal reflection $\langle 003 \rangle$ becomes progressively weaker and there appears a second reflection at slightly higher value of 2θ (from 11.7 to 13.2 degree), which corresponds to about 0.10 nm decrease in interlayer distance. The similar shifts in 2θ also take place in cases of the higher order basal reflection ($\langle 006 \rangle$, $\langle 009 \rangle$, etc). Above 220 °C, all the basal reflection peaks observed in LDH below 200 °C are lost at their original position, but a new similar set of basal reflections appears at somewhat shifted 2θ value. From the thermal analysis shown previously and also from numerous references from literature, it is well known that loss of interlayer water in LDH occurs below 225 °C. This loss in water causes a reduction in interlayer distance, but interestingly does not destroy the crystal structure of the LDH materials. In case of LDH-DBS, the loss of interlayer water molecules can not be identified so distinctly from the XRD spectra. When the XRD pattern of this materials obtained at different temperatures are compared side by side, the basal reflections starts broadening above about 100 °C. Since the decrease in in-

terlayer distance due to such water loss is only about 0.3 nm, corresponding decrease in first basal reflection ($< 003 >$) from 2.96 nm to about 2.66 nm appears in the form of a weak shoulder in the XRD pattern above 100 °C in **Figure 4.10**.

In the unmodified LDH, the sharp basal reflection of the $< 00l >$ series are observed even up to 300 °C. This means the layered structure remains undisturbed up to this temperature. Above 300 °C, all the XRD reflections become progressively weaker and broader with increasing temperature indicating a breakdown of the layered structure. Around 320 to 330 °C, the material becomes predominantly amorphous. In case of LDH-DBS, above 280 to 290 °C, the different XRD reflections become indistinguishable. During processing and melt analysis of PE/LDH nanocomposites, temperatures is hardly reached above 250 °C. So the physical and the chemical integrity of the clay material during such processes remain practically unaffected.

II. TGA analysis under inert and oxygen atmosphere

TGA analysis of Mg-Al-LDH and LDH-DBS discussed earlier were based on the results obtained from the measurements carried out under oxygen atmosphere. The same measurement when carried out under an inert atmosphere and the results are compared, interesting information regarding the thermal stability of various species/moieties are obtained and distinct regions of their thermal degradation can be identified. **Figure 4.11** reveals such comparison between TGA results obtained under oxygen and nitrogen environments. Interestingly, in case of unmodified LDH the nature of TGA and hence the DTG plots remain exactly identical under both the environment. This means thermal decomposition of unmodified LDH simply involves the loss of interlayer species and then endothermic decomposition of metal hydroxide layer. The complete loss of interlayer water takes place within 210 – 220 °C which is indicated by strong peak 'a' in the DTG curve. The second large decomposition stage occurs around 300 °C (indicated by the peak 'b' in DTG plot), which involves

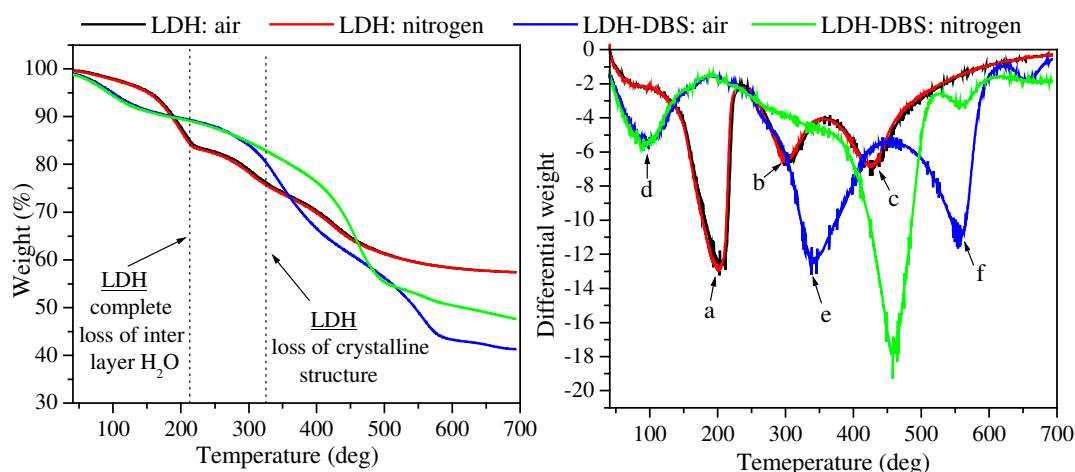


Figure 4.11 TGA analysis of LDH and LDH-DBS in different atmospheres

mostly the loss of interlayer carbonate causing collapsing of the layered structure as confirmed from **Figure 4.10**. The decomposition of the metal hydroxide sheets also begins at this stage, but to a very insignificant extent as the residual weight still remains about 80 %. The final decomposition peak 'c' in the DTG plot of the unmodified LDH is observed around 430 °C. During this stage, the

hydroxide layers are decomposed to form metal oxide releasing water vapour. The equal amounts of residue are left after heating LDH above 700 °C in both the atmospheres. This also indicates the similar nature of the residue obtained. However, in case of LDH-DBS, thermal decomposition under nitrogen and oxygen atmospheres follows different paths and also yields different extents of residue. The two TGA plots are virtually identical below about 300 °C indicating no oxidative degradation occurs below this temperature. However, when compared with the unmodified LDH, low temperature decomposition though spans up to 200 to 210 °C, the decomposition peak is observed at much lower temperature (around 100 °C). Since the weight loss in this range is mostly due to the release of interlayer water molecules, it can be said that in LDH-DBS, the interlayer water is more loosely bound as compared to that in the unmodified LDH. One may argue that this weight can be due to desorption of the physically adsorbed water molecules on the non-gallery surfaces of LDH crystallites. However, this seems unlikely as LDH-DBS has highly hydrophobic surface with low surface energy (discussed later).

From above 300 °C to 600 °C, decomposition of LDH-DBS under oxygen atmosphere is characterized by two peaks one at around 340 °C (e) and other at around 560 °C (peak 'f'). When decomposition is carried out under nitrogen atmosphere, the second peak does not show any change in position, but the first one shifts from about 340 °C to about 460 °C. It is believed that this shift in decomposition peak in DTG is associated with the decomposition of the intercalated DBS anion. In presence of oxygen, DBS anion undergoes oxidative decomposition liberating oxides of carbon and water vapour whereas under inert atmosphere, it undergoes non oxidative degradation through bond scission, which usually occur at higher temperature than their oxygen supported combustion temperature. Also the non oxidative decomposition of hydrocarbon species produces carbonaceous solid residue, which may account for the higher amount of residue left after thermal analysis under nitrogen atmosphere.

III. FTIR investigation at elevated temperatures

The FTIR analysis of unmodified LDH and LDH-DBS at different temperature provides useful information regarding the changes in structure of the host material with increasing temperature. **Figure 4.12 A–C** shows the selected regions of FTIR spectra measured with increasing temperature up to 235 °C for unmodified LDH. The most interesting change observed on heating is the gradual disappearance of the shoulder around 3100 cm⁻¹, which stands for hydrogen bonding between interlayer water molecules and carbonate anion. This is due to loss of major portion of interlayer water molecules below about 250 °C. This also reduces the intensity of the broad peak observed in the region 1550 - 1750 cm⁻¹ associated with the bending vibration of the interlayer water. The presence of strong γ_3 peak around 1357 cm⁻¹, even at 235 °C, indicates most of the CO₃²⁻ ions are still retained in the interlayer region (**Figure 4.12C**). The FTIR spectra of LDH-DBS at different temperatures shows how the interlayer water molecules are released with increasing temperature. The broad peak around 1640 cm⁻¹ due to H₂O bending vibration nearly disappears as early as 100 °C in **Figure 4.12D** and is released at much lower temperature than that in the unmodified LDH.

IV. Surface Tension Measurement

Interfacial tension is a very important parameter that controls the miscibility of filler particles into a polymer matrix. If the surface tensions of these two components differ largely from each other,

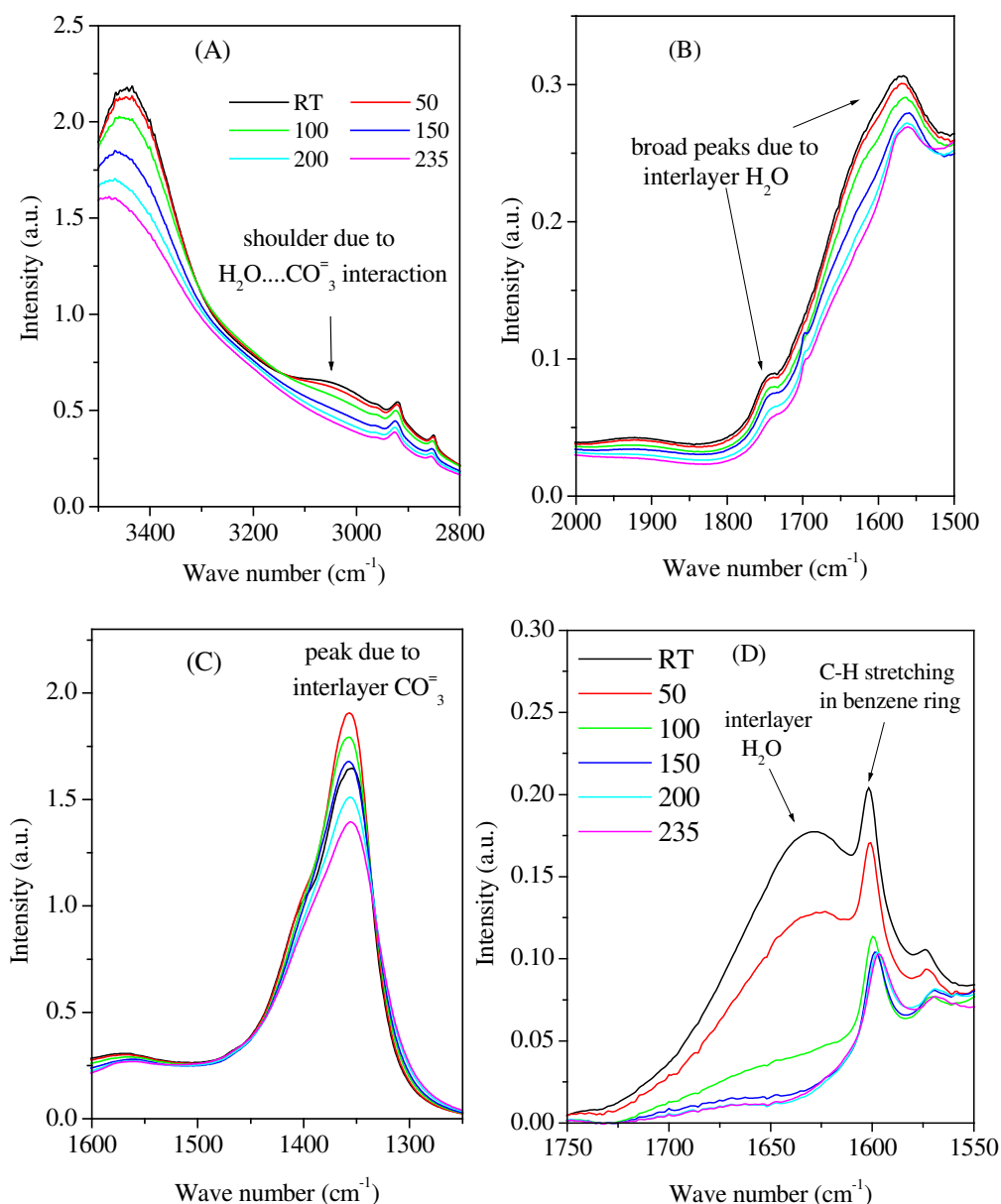


Figure 4.12 FTIR spectra of unmodified LDH (A-C) and LDH-DBS (D) taken at different temperatures showing changes in the structure of the unmodified clay material.

interfacial tension becomes very high and the filler particle cannot disperse well in the matrix. Therefore, the prerequisite condition for obtaining a good dispersion of an inorganic filler in a non-polar polymer is the reduction of its surface tension difference with the polymer. The pristine unmodified LDH has highly hydrophilic surface similar to that of $\text{Mg}(\text{OH})_2$. The modification of LDH with surfactants not only brings about the enlargement of interlayer distance in LDH, but also makes it more hydrophobic. This is important as it prevents large scale aggregate formation by the filler particles when mixed with non-polar polymers. The technique used for measuring the surface tension of LDH materials is the capillary penetration method based on modified Washburn equation [129, 130]. The powdered LDH materials were packed in a glass capillary tube having one end closed with a piece of filter paper. At the other end, the filled capillary was hanged to a microbalance. The close end was then brought in contact with several test liquids of different

surface tensions and allowed to rise along the packed column in the capillary. The increase in weight of the the capillary was then measured with time in every case. The capillary penetration of the test liquid is related to the wetting tension $\gamma_{lv}\cos\theta$ through the modified Washburn equation as shown below (equation 4.3), where γ_{lv} and $\cos\theta$ represent the liquid surface tension and the contact angle of the liquid respectively.

$$\gamma_{lv} \cos\theta = \left[\frac{1}{K} \right] \left[\frac{\eta}{\rho^2} \right] \left[\frac{M^2}{t} \right] \quad (4.3)$$

The first term on the right hand side of equation 4.3 is an unknown geometric constant of the capillary system, the second term is the property of the test liquid (η and ρ are the viscosity and density of the test liquid respectively) and the third term is experimentally determined (M represents the weight of the test liquid penetrated in time t). The experiments were carried out for several test liquids covering wide range of surface tension and also several measurements with each test liquid were made. Then $K \gamma_{lv} \cos\theta$ (which is equal to $\left[\frac{\eta}{\rho^2} \right] \left[\frac{M^2}{t} \right]$) was plotted against γ_{lv} . According to this approach, the maximum obtained in this plot represent the solid surface tension or γ_{sv} . The detail theoretical background and experimental procedure are described in Appendix C.

Since LDH-DBS has highest interlayer separation and better thermal stability, it was used for nanocomposite preparation. Hence, surface tension measurement was carried out only with this materials and compared with industrially obtained Mg-Al-LDH, its calcined form and also with $\text{Mg}(\text{OH})_2$. Comparison with $\text{Mg}(\text{OH})_2$ here is logical as it matches the surface chemistry of the unmodified and non surface treated Mg-Al-LDH is similar with projecting hydroxyl groups. The

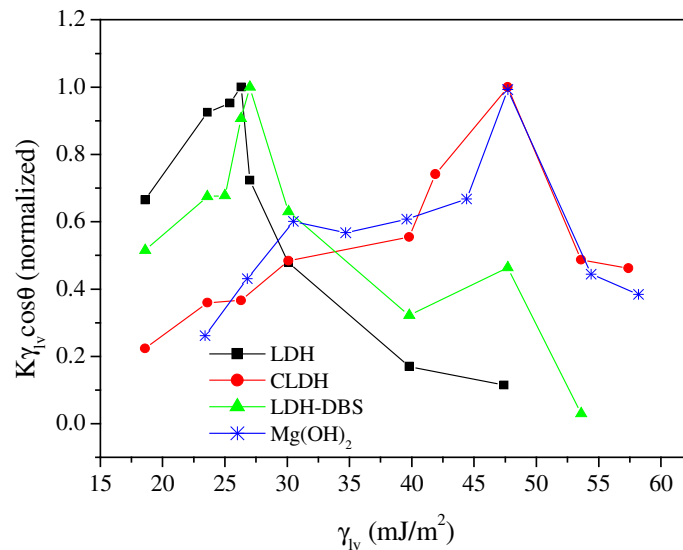


Figure 4.13 $K\gamma_{lv}\cos\theta$ versus γ_{lv} plots of LDH, CLDH and LDH-DBS. The plot for $\text{Mg}(\text{OH})_2$ is also shown for comparison. The maximum in each plot gives a measure of the surface tension of the respective powdered sample. The parameter in the y axis is normalized against the maximum value and the error bar in each points are omitted for having better visibility of the maxima

results from the capillary penetration tests are shown in **Figure 4.13**. Mg-Al-LDH obtained from industry is surface treated and shows low surface energy value, which is around 26.34 mJ/m^2 as shown by the peak position in **Figure 4.13**. After calcination, LDH is converted to its mixed oxide form and become more hygroscopic showing large increase in the surface tension (maximum is shifted to 47.74 mJ/m^2). On treatment with SDBS, the regeneration of the crystal structure of LDH takes place. The XRD pattern indicates that DBS anion are intercalated in between hydroxide sheets. However, no information about the nature of the exposed surface of the LDH crystallites is obtained from the XRD analysis. The modification of LDH with SDBS lowers the surface tension to near about 27 mJ/m^2 . This is much lower than that of magnesium hydroxide. Such significant lowering of surface tension after modification with surfactants having hydrophobic tail(s) has also been reported in case of cationic clays, like montmorillonite using amine based organic surfactants [131].

4.4 Conclusion

The organic modification of Mg-Al-LDH and characterization of the modified clays have been discussed in this chapter. The method used for such modification was based on regeneration effect shown by the LDH materials. This method avoids complicated chemical process, use of organic solvent and external heating. Among the different surfactants investigated SDBS gave the best results in terms of increase of interlayer separation. It provides nearly four fold increase in basal spacing. Another interesting aspects to be noted here that regeneration method works better with anionic surfactants that are highly soluble in aqueous medium. The homogeneity of the product is excellent in these cases. For example, with SDBS and SDS, no unmodified fraction of LDH can be detected in their XRD patterns. On the other hand, surfactants, which are not soluble or sparingly soluble in aqueous medium at room temperature such as laurate, organic phosphate, stearate, etc give significant fraction of unmodified LDH as confirmed from the XRD and FTIR analysis. All the surfactants studied, give mono layer stacking within the interlayer region. However, bi layer arrangements of anionic surfactants can also occur under specific condition and has been reported in literature for stearate [132], sodium octylsulfate [45], etc. In case of LDH-DBS, elemental analysis (Appendix A) confirms that surfactant anion can not completely replace carbonate ions in the interlayer region. However, this can not be confirmed from the FTIR investigation (**Figure 4.5**) as the peaks for interlayer carbonate ion fall in the region where the peaks corresponding to C=C of benzene ring appears. In the industrial sample, where the value of 'x' in chemical structure of LDH is roughly 0.3, the chemical the elemental analysis shows that around 48 – 50% of the carbonate anion are replaced by the DBS ion. The high degree of anion exchange by large surfactants has one disadvantage that it results hybrid with high organic content. The inorganic content of such modified filler, which account for matrix reinforcement, improvement of barrier properties and flammability, etc will be drastically reduced in that case.

CHARACTERIZATIONS OF PE/LDH NANOCOMPOSITE

5.1 Morphological Characterizations

5.1.1 Introduction

In addition to the base matrix PE and the filler particles, the PE/LDH nanocomposite prepared by melt-compounding contain a third component, namely compatibilizer. This compatibilizer is a functionalized polymer containing pendent maleic anhydride groups on a polyethylene backbone. The primary purpose of using a functionalized polymer (PE-g-MAH) is to improve compatibility between the non-polar PE matrix and the highly polar LDH particle surface. Though organic modification makes the clay mostly hydrophobic (see **Figure 4.13** in Chapter 4), use of functionalized polymer is a common practice in the preparation of polyolefin/clay type nanocomposites. This may be due to fact that polar functional groups present in functionalized polymers (like maleic anhydride group in PE-g-MAH) can have favorable interaction with clay surface. The rigorous morphological characterization of a polymer/clay nanocomposite is necessary to understand the state of clay particle dispersion in polymer matrix. The primary approach is to study the changes in the interlayer separation of the clay crystals using X-ray diffraction analysis (XRD) using wide angle X-ray scattering (WAXS) at various stages of material preparation. In case of melt compounding process, such analysis is usually carried out with freshly compounded nanocomposite samples and is compared with that observed in the clay precursor i.e. organically modified clay. However, the XRD analysis alone can not be reliable to draw final conclusion about the dispersion state of clay particle in nanocomposites [133, 134]. This is because of the fact that the nature of reflection (in terms of its position and intensity) in the WAXS pattern not only depend on the interlayer separation, but also on several other factors, like concentration of the clay in the nanocomposites, symmetry in specific crystallographic directions, etc. Besides, inhomogeneity in crystal structure of the clay (i.e. intercalated, exfoliated and unmodified fraction existing in the same sample) may results in a complicated WAXS pattern. Therefore, along with XRD analysis electron microscopic investigations are often coupled to obtain a complete picture of dispersion of the clay particle in polymer nanocomposites. However, the morphological analysis using electron microscopy, like TEM also has certain inherent disadvantage so far as polymer nanocomposite is concerned. First, to view the nanoscopic particle distribution within a polymer matrix one needs to rely on high magnification images, which makes the scan surface area very small not necessarily representing the whole surface area of the sample. Second, it shows only the surface morphology of the particle distribution and not the bulk morphology. In case of molded articles

or test specimen, the nature of particle distribution can be significantly different at the different sections of the samples [135]. To obtain the overview of particle dispersion over large surface area, images of different magnifications starting from low magnification to high magnification should be investigated simultaneously on the same surface.

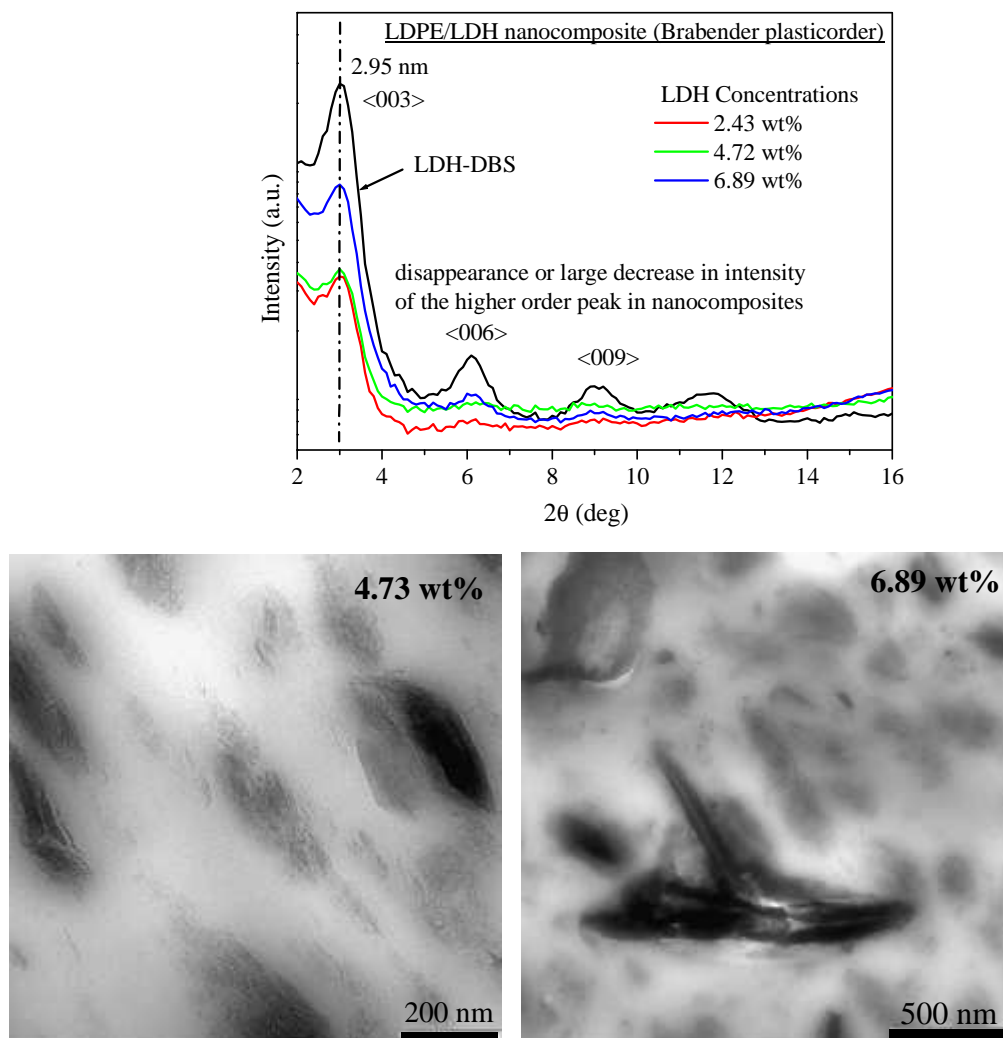


Figure 5.1 WAXS patterns (top) and representative TEM micrographs of PE/LDH nanocomposites (below: LDH concentration are shown) prepared by melt-compounding in Brabender plasticorder.

5.1.2 PE/LDH Nanocomposite Prepared in Small Batch-Mixer

To investigate whether melt-mixing method is suitable or not for preparing PE/LDH nanocomposites, small batches of sample with different LDH contents were prepared in a batch-mixer (Brabender plasticorder). The WAXS pattern and the representative TEM micrographs of these compositions are shown in **Figure 5.1**. For comparison, the WAXS pattern of LDH-DBS is also shown. The WAXS patterns of these trial samples are characterized by the presence of the first order basal reflection ($<003>$) in all the compositions indicating that the LDH layers are not fully exfoliated in the polymer matrix. An-

other interesting point to be noted here is the nature of higher order basal reflection of $< 00l >$ series. They are either disappeared or their intensities are sharply reduced. This is a clear indication of increasing crystal disordering of the LDH particles in the nanocomposites [134]. The first order basal reflection in LDH-DBS corresponds to an interlayer layer separation of about 2.95 nm. In case of the nanocomposites prepared in Brabender plasticorder, there is observed no change in the position of the basal reflection as compared to that in LDH-DBS. Also at low LDH concentrations, intensity of this peak is very weak and higher order reflections can not be detected by the instrument. At high LDH concentrations, the higher order basal reflection peaks become prominent indicating the presence of larger crystallites of LDH. The representative TEM images shown in **Figure 5.1** indicate that the dispersed LDH particles in the nanocomposite matrix have preferentially intercalated morphology with occasional exfoliation of the clay layers from bigger LDH platelets. The primary particles appear swollen and have disordered structure at their surfaces. They also form aggregates at high concentrations (**Figure 5.1B**). The high magnification TEM images reveal that nanoscopic particle fragments (particle size well below 100 nm) are indeed delaminated from the surface of the primary LDH particles. As shown in **Figure 5.2**, the increasing LDH concentration though the primary particles form more aggregates, their partial exfoliation is not suppressed. This kind of morphology resembles those observed in intercalated/exfoliated type polymer clay nanocomposites [133]. The partially exfoliated nature of the LDH particles seems a promising sign toward the possibility of obtaining better dispersion of metal hydroxide type filler in polyolefin matrix and preparing polyolefin/LDH based nanocomposites.

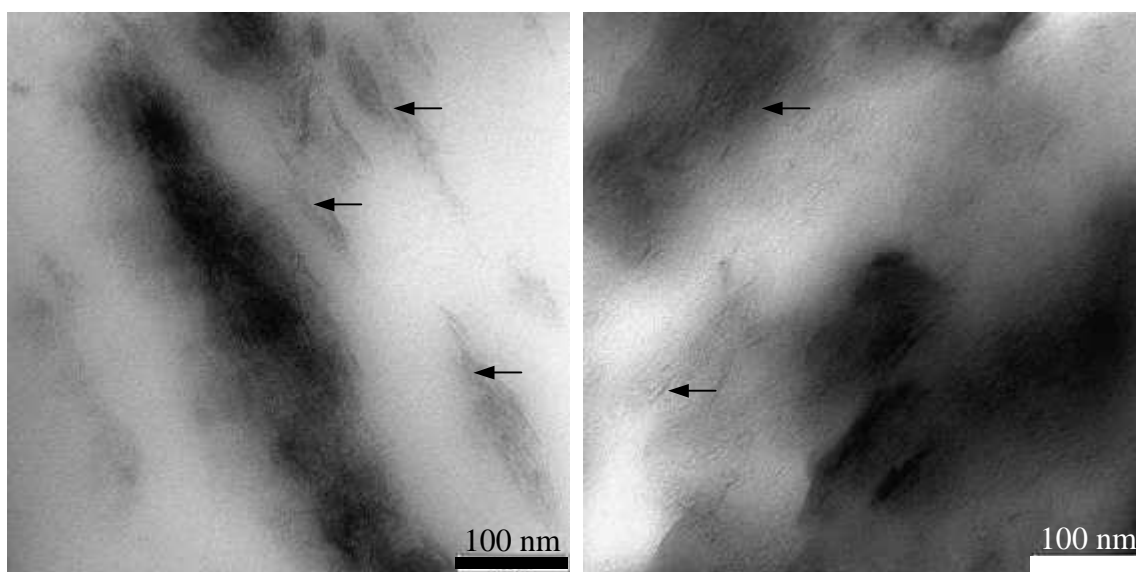


Figure 5.2 High magnification TEM showing exfoliated LDH layers fragments (some indicated by arrow marks) in PE/LDH nanocomposites containing low (left, 4.72 wt%) and high (right, 16.20 wt%) LDH concentration (magnification bar 100 nm).

5.1.3 PE/LDH Nanocomposite Compositions Prepared in Twin-Screw Extruder

The morphological characteristics observed in case of PE/LDH compositions prepared in batch mixture were encouraging enough to prepare similar compositions using more intensive and industry relevant melt-mixing equipment, namely a twin-screw extruder. The WAXS patterns of the extruder mixed samples are shown in **Figure 5.3**. These patterns look virtually similar to those observed in case of the compositions prepared in Brabender plasticorder (**Figure 5.1**). Only difference observed is a small shift of all basal reflection peaks to lower 2θ value and this shift in case of the first order basal reflection ($<001>$) takes place from 2.95 nm to 3.27 nm. This may be due to intercalation of polymer chain segments into the interlayer region of LDH induced by the stronger shearing action during melt-mixing in the extruder.

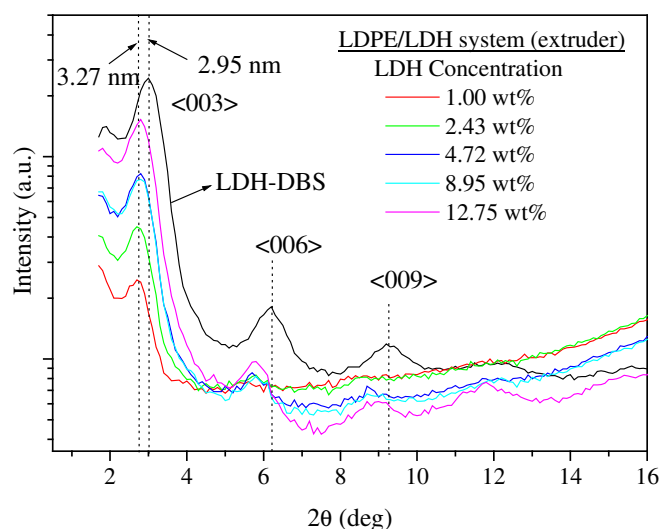


Figure 5.3 WAXS patterns for PE/LDH compositions prepared in twin screw extruder

The changes in the morphological features of the LDH particles induced by the melt-compounding process in extruder is elaborately shown in **Figure 5.4**. The SEM image as shown in **Figure 5.4A**, reveals a plate-like shape of the LDH-DBS particles with lateral dimensions ranging below few μm and thickness within few hundreds nm. These primary particles during melt-compounding suffer significant size reduction as obvious from the TEM images of various PE/LDH nanocomposite composition shown in **Figure 5.4B-E**. These low magnification images though cannot reveal nanoscopic particle structures in the matrix, provide a direct way of inspecting the presence of microscopic particles or their aggregated structures. At the first look to these images, the discrete LDH particles can be detected throughout the matrix, whose dimensions fall roughly within one micrometer scale. These particles are either individual primary particles (platelets/tactoids consisting of multiple metal hydroxide layers) as viewed perpendicular to their lateral face or clusters of primary particles as viewed parallel to the lateral surface. With increasing LDH concentration in the nanocomposites, the size of these particles remains practically unchanged, only their number density increases. Even at LDH concentration about 12.75 wt%, the formation of large aggregates can not be observed to a significant extent. It is also apparent that the shearing action of the extruder during melt-compounding causes significant breakdown of the primary LDH-DBS particles.

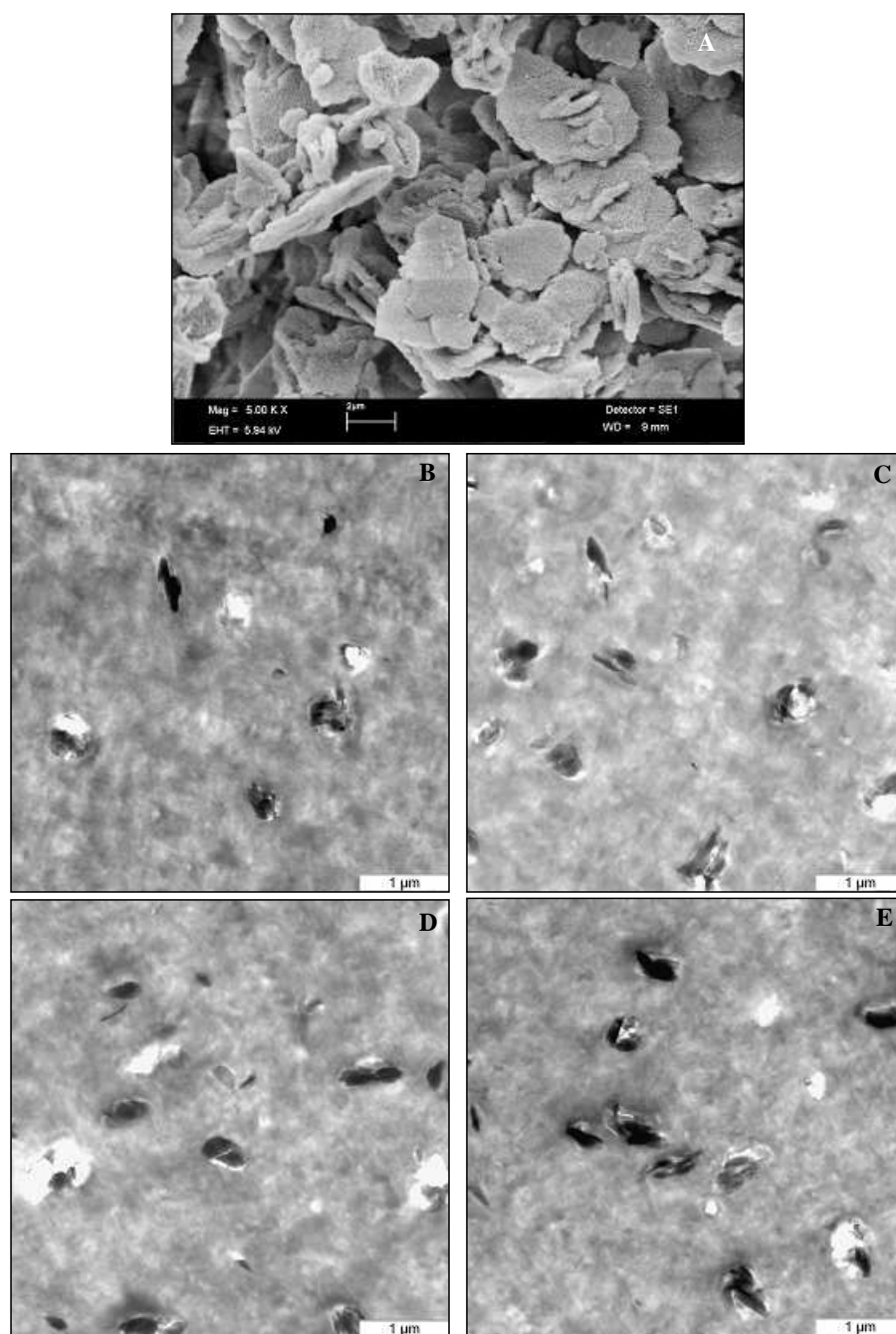


Figure 5.4 Morphological analysis of the LDH particles: A: SEM image of LDH-DBS and B-E: low magnification TEM images of PE/LDH nanocomposites [B: PE-LDH2 (4.72 wt%), C: PE-LDH3 (6.89 wt%), D: PE-LDH4 (8.95 wt%) and E: PE-LDH5 (12.75 wt%)]

When the high magnification TEM images are analyzed, both the nature of the large discrete particles (in **Figure 5.4B-E**) and the region in between them become more distinguishable. **Figure 5.5** shows the magnified view of one such particle and also the surrounding matrix region. It is apparent that the large particle is highly distorted and show ample evidences of crystal layer delamination at the surface. Such particles always show poor long range crystalline symmetry and hence explains the broadening and weakening of reflection maxima in the XRD patterns described in **Figure 5.3**. The morphological features observed in **Figure 5.5B** reveals a clear understanding about how the LDH-DBS particle are

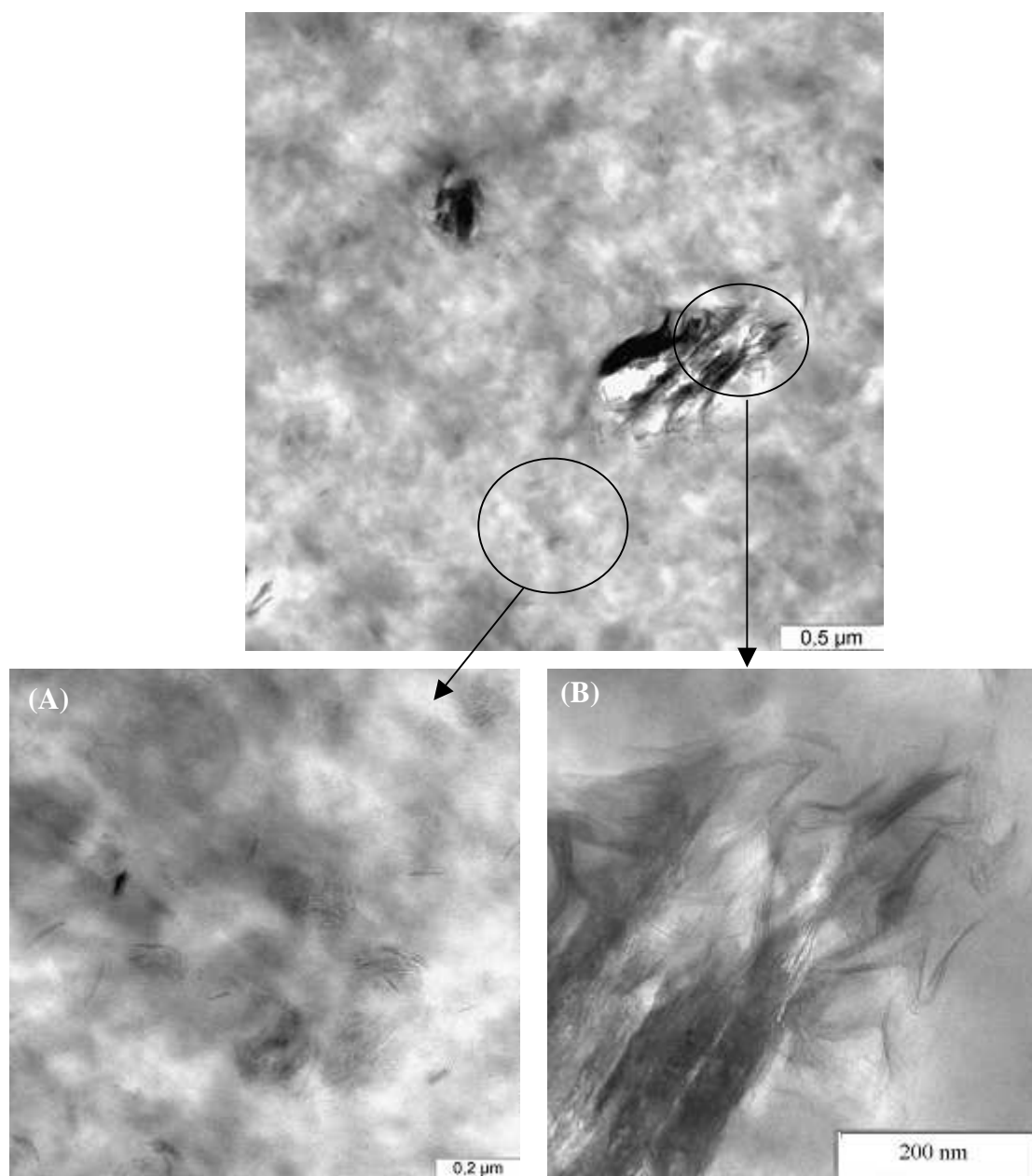


Figure 5.5 TEM micrographs showing that exfoliated LDH particles exist both in the bulk matrix (A) and also in the vicinity of the originating bigger particles (B).

exfoliated during melt-compounding. At first, the polymer chains penetrate within the interlayer region of the LDH-DBS particles and push apart the metal hydroxide sheets. With the course of time within the mixing channel of extruder, more and more polymer chains enter the interlayer region and the shearing action of the screws forces the delamination of the surface layers one by one from the surface of a large LDH-DBS particle. As a result, not only the exfoliated particle fragments are formed, but also the size of the original particles is reduced. This also explains why the average size of the primary particles observed in **Figure 5.4** is much smaller than that observed in case of LDH-DBS prior to melt-compounding. The breakdown of the organically modified primary LDH particles has also been observed during melt-compounding in case of polyamide 6 based nanocomposites [60]. Therefore, it is expected

that conditions employed during the melt-compounding (like, screw speed and geometry, temperature, feed rate, etc) will have a strong influence on the extent of exfoliation of the LDH particles and optimization of these conditions would give the best result in terms of clay particle dispersion [136, 137]. The exfoliated crystal layers may remain either crowded in the vicinity of the parent particles or the shearing action of extruder screw can force them to disperse throughout the matrix. This has been clearly demonstrated in **Figure 5.5A** and **B**. These exfoliated layers are highly anisometric in nature with very large aspect ratio and thickness much smaller than the primary LDH-DBS particles. From the size of the exfoliated particle, it seems obvious that during exfoliation process the crystal layers or small stacking of layers (called tactoids) are not only delaminated from the surface of the primary particles, but also under rupturing. In addition to the shearing action during melt-compounding, the low crystal layer rigidity of the LDH can be a potential reason for such rupturing (LDH has lower crystal layer rigidity as it has three atomic layers in a single sheet as compared to layered silicates, which contains 5 – 7 atomic layers [138]). However, these exfoliated particles are not necessarily the single metal hydroxide sheet, but most often the stack of several such sheets. **Figure 5.6** suggests that a significant fraction of LDH-DBS particle are exfoliated and is indeed dispersed in nanoscale throughout the matrix. These morphological features also proves that the melt-compounding method is certainly a promising method to obtain exfoliated particle morphology, at least partially, of LDH nanofillers in polyethylene. Comparing the morphological features of the PE/LDH nanocomposites prepared in small batch mixture and in extruder indicates that the shearing action experienced by the LDH particles during melt-compounding strongly influence their dispersion in the final composition. The more intense shearing experienced in twin-screw extruder not only promotes higher degree of LDH particle exfoliation, but also prevents the formation of large scale aggregates by the primary particles.

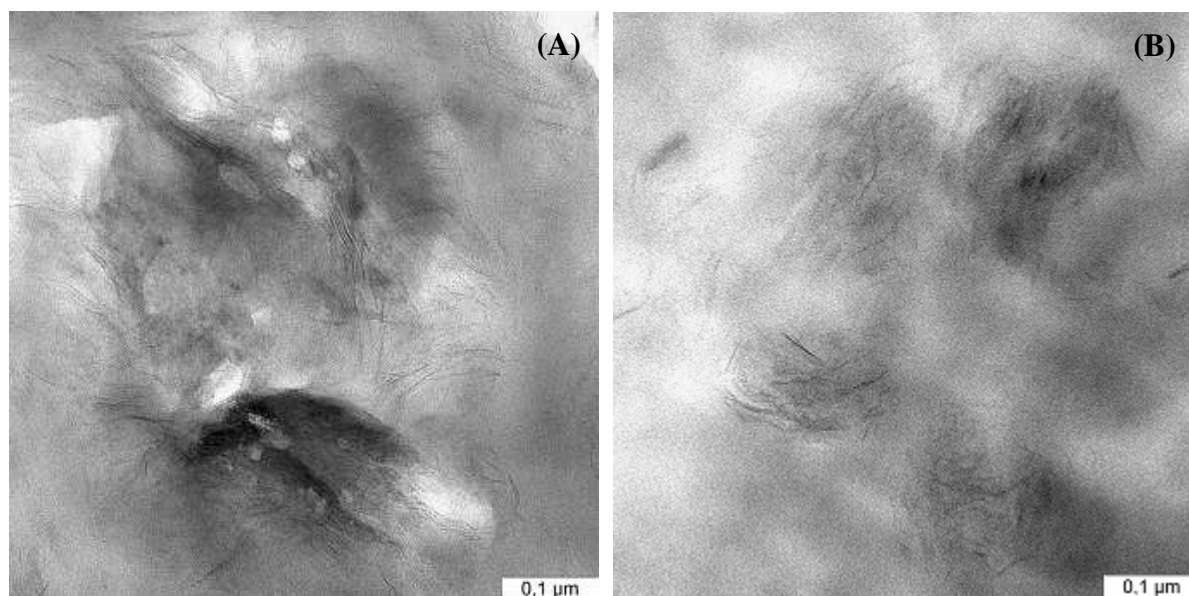


Figure 5.6 High magnification TEM micrograph showing that LDH particles also undergo exfoliation into single layers (A: PE-LDH3 and B: PE-LDH4)

In general, the dispersed LDH particles in the nanocomposite matrix form various structural asso-

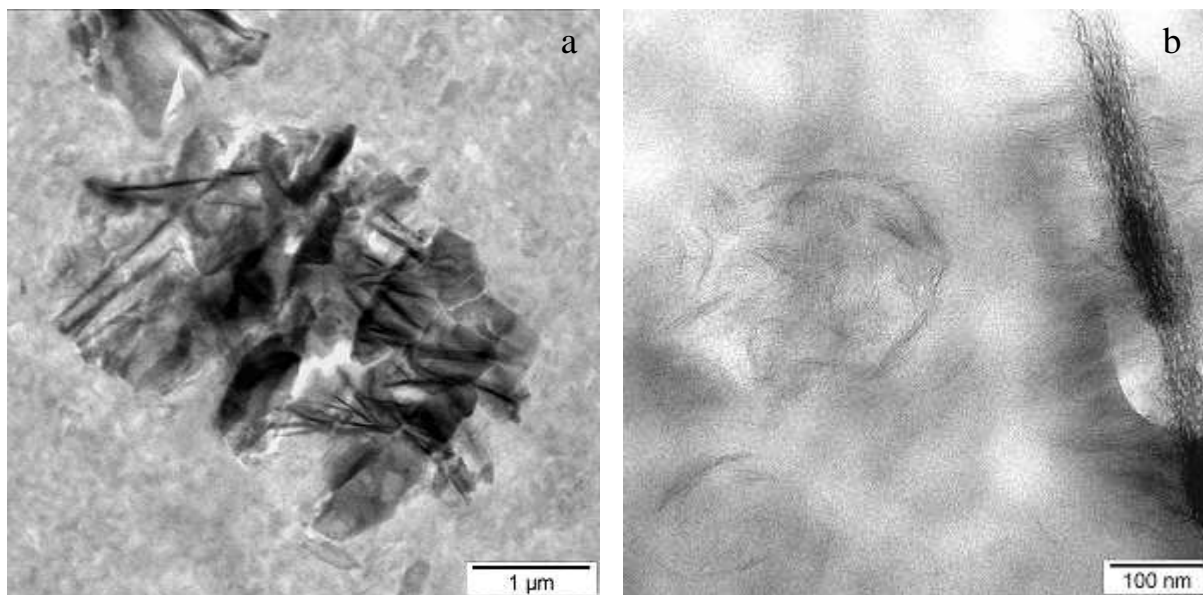


Figure 5.7 TEM images showing different types structural associations formed by the dispersed LDH particle in PE/LDH nanocomposite matrix: (a) formation of aggregates by the primary LDH platelets and (b) structural association among the exfoliated clay layers.

ciations in different scales. In one hand, the primary particles or the platelets may remain scattered throughout the matrix or may form aggregates. These aggregates in true sense are not real hard clusters of particles, rather a region or domain containing large number of individual platelets in close physical association with each other. **Figure 5.7 a** shows a typical LDH particle domain having dimensions in micrometer scales and consists of multiple number of LDH platelets in random orientation. The individual platelets in these aggregates can easily be identified as the dark rod-like structure in the TEM image. The magnified view of such a region reveals that these aggregates are indeed diffused in nature with considerable extent of matrix embedded within. On the other hand, the exfoliated metal hydroxide layers also form physically associated domains throughout the matrix and often in the vicinity of the parent primary particles. **Figure 5.7b** demonstrate a representative case of such state of particle morphology, which shows the delamination of the thinner layers from the surface of a single LDH platelet and also the structural association formed by them. Such morphology is abundant throughout the matrix. It can be argued that the LDH particles (both the primary and exfoliated ones) favors the physically associated morphology in order to stabilize the electrostatic charge imbalance on their surfaces. Therefore, it is highly unlikely that in a non-polar matrix, like polyethylene a highly exfoliated particle morphology can be stabilized, where homogeneous random distribution of the nanoscopic LDH particles would persist throughout the matrix.

The morphological features discussed so far reveal no specific kind of structure or shape of the dispersed LDH particles in the nanocomposite matrix. Rather these nanocomposites are characterized by the presence hierarchy of particle size starting from nanoscopic exfoliated fragments to the structured domains of primary clay particles. Such type of nanocomposites are best described as intercalated/exfoliated or partially exfoliated nanocomposites. The presence of functionalized polymers (PE-

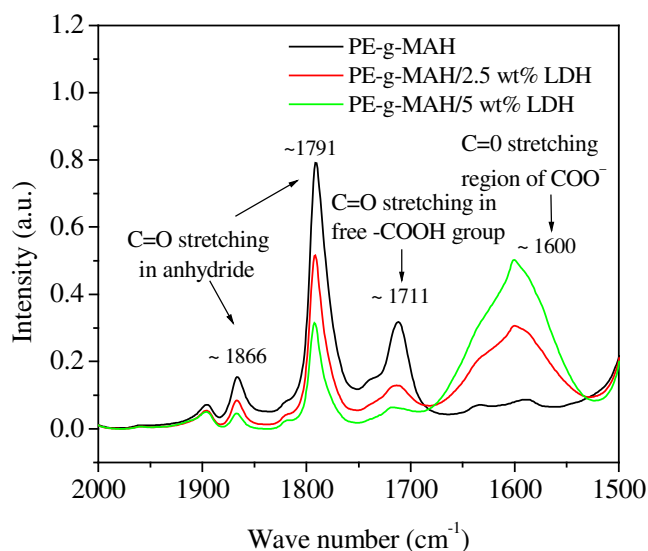


Figure 5.8 FTIR spectra for PE-g-MAH and PE-g-MAH/LDH composites showing changed occurring in peaks characteristics of MAH functional groups in presence of LDH

g-MAH) here plays a major role to facilitate the clay layer exfoliation process and better dispersion. Usually, use of such functionalized polymers is necessary to prepare polyolefin/clay based nanocomposites [139, 140]. Even though the hydrophilic clays are organically modified, they hardly undergo any intercalation or exfoliation process when directly mixed with polyolefins, like polyethylene [139, 140]. It is for sure that a non polar polymer chain has no thermodynamic compatibility with a charged clay surface. Again the hydrocarbon chain in the surfactants is not long enough to push apart the layers by a great distance or to prevent them from coming close to one another. This two factors i.e. high incompatibility and small hydrocarbon chain length of the surfactant hinder the exfoliation process and a stable, nanoscale dispersion of organically modified clays in unmodified polyolefins [141]. The presence of functionalized polymer changes the situation significantly. For example, PE-g-MAH used in the presence case can interact with positively charged LDH clay surface through the maleic anhydride groups. Evidence of such positive interaction can easily be detected from FTIR spectroscopic analysis of LDH-DBS filled PE-g-MAH composites as shown in **Figure 5.8**. Two interesting observations can be made from these spectra:

- I. The intensity of C=O stretching vibrations (1791 cm^{-1} and 1866 cm^{-1}) are significantly reduced with 5 wt% LDH addition without any change in the position of these peaks.
- II. The C=O stretching vibration peak corresponding to free carboxylic acid groups in MAH (1711 cm^{-1}) is broadened and its intensity is also reduced significantly.
- III. A broad peak around 1600 cm^{-1} appears, which is also the region for C=O stretching vibration peaks observed in carboxylate salts.

All these above observation are certainly an indication toward possible chemical changes suffered by the anhydride or acidic functional groups present in PE-g-MAH in presence of LDH. It seems highly probable that basic metal hydroxide surface of LDH undergo acid base reaction with free acidic groups.

Additionally, the interlayer water present in LDH are liberated during melt processing (above 200 °C) causing conversion of some anhydride groups into acid groups which can further react with LDH surface. However, presence of surfactant anions (DBS) on the surface of LDH in large concentration may be an obstructing factor against such reaction. Therefore, addition of functionalized polymer is necessary in preparing polyolefin based nanocomposites to obtain a thermodynamically stable system.

5.2 Thermal Analysis

Thermogravimetric (TGA) analysis of the PE/LDH nanocomposites are shown in **Figure 5.9**. The thermal decomposition of pure polyethylene is characterized by two major temperature regions of weight loss: first a sharp loss in the temperature range 335 – 410 °C (about 70% weight loss takes place in

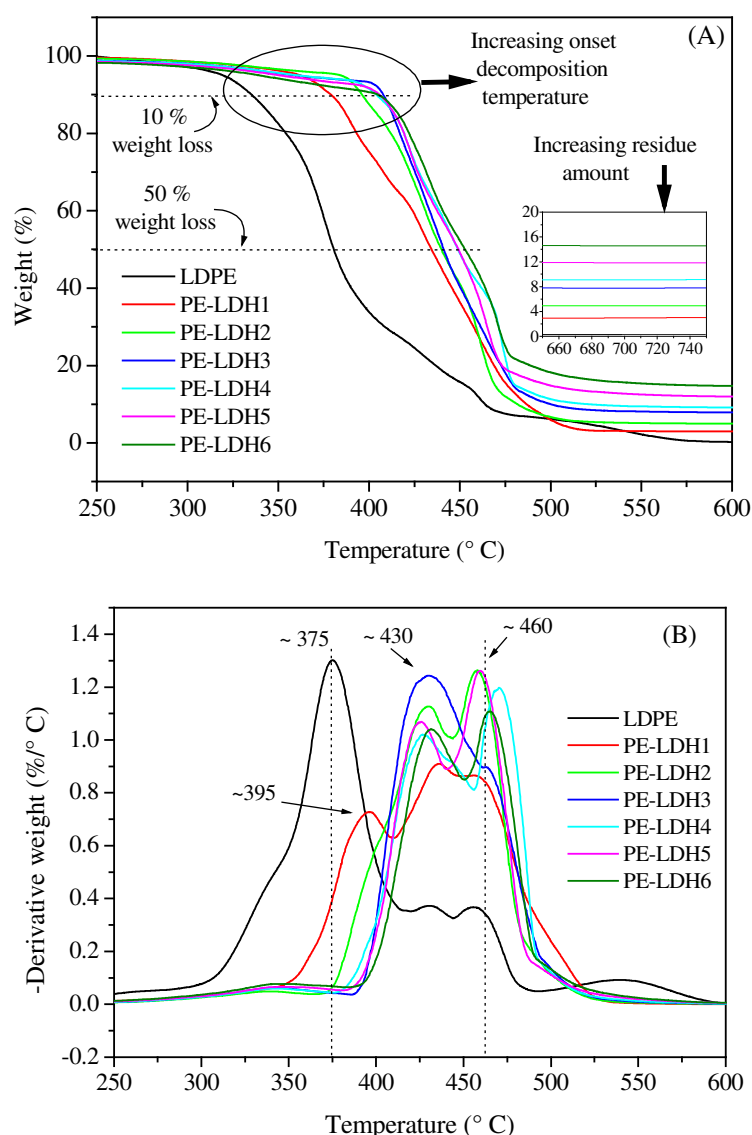


Figure 5.9 Thermogravimetric analysis of polyethylene/LDH nanocomposites prepared by melt-mixing in extruder (the LDH concentration increases from 2.43 wt% in PE-LDH1 to 16.20 wt% in PE-LDH6)

this region) and second a relatively weaker loss in the temperature range $410 - 475^{\circ}\text{C}$ (more than 25% weight takes place) (**Figure 5.9A**). In the differential thermogravimetric (DTG) plot, **Figure 5.9B**, these two regions appear as a sharp decomposition peak at about 375°C and a broad peak respectively. The presence of LDH causes distinct changes in the thermal decomposition behavior in comparison to the unfilled polyethylene. With the addition of only 2.43 wt% LDH, the first decomposition stage in unfilled polyethylene is not only shifted to a higher temperature range (the decomposition peak in DTG shifts from about 375°C to about 395°C), but also the extent of weight loss during this stage decreases from about 70 wt% to about 25 wt% (**Figure 5.9A**). With further increase in LDH concentration, the low temperature decomposition peak is completely suppressed and most of the material contents are decomposed in the higher temperature range starting above 400°C . The broad decomposition peak at higher temperature range observed in unfilled polyethylene becomes more and more sharp and also divided into two decomposition stages around 430°C and 460°C in the nanocomposites containing high concentration of LDH (**Figure 5.9B**). Usually, the comparison of thermal stability for polymeric materials from TGA plots is carried out in terms of two temperatures: one is the onset of decomposition temperature ($T_{0.10}$) referring to 10% weight loss and the other is the decomposition temperature ($T_{0.50}$) referring to 50% weight loss. **Figure 5.10A** shows the comparison of these two temperatures for unfilled polyethylene and LDH filled nanocomposites. The onset of decomposition is delayed significantly by the addition of 2.43 wt% LDH. In fact, with increasing LDH concentration the onset decomposition temperature $T_{0.1}$ increases first and then stabilizes after 5–6 wt% LDH concentration. The decomposition temperature, $T_{0.5}$ also increases with increasing LDH concentration. With about 9.0 wt% LDH concentration $T_{0.5}$ increases by about 70°C as shown in **Figure 5.10**.

The residue left or the char yield after combustion in air is nearly zero for unfilled polyethylene as all the organic contents (hydrocarbon) are converted into gaseous products. If one assumes that the polymeric material and the organic part in LDH-DBS are completely burnt and lost as gaseous products after heating up to 750°C , the amount of residue left after heating during TGA analysis of the nanocomposites can be calculated from the approximate formula of LDH-DBS. This means that whatever residue formed after burning of the composite would come from the LDH and will be consisting of metal oxides only. The calculation of the combustion residue from the approximate composition of LDH-DBS is shown in Appendix A. The calculated value and the experimentally obtained values from TGA of the nanocomposites are compared in **Figure 5.10B**. It is apparent that the experimentally obtained values are significantly higher than the calculated value. Though the calculation was based on approximate formula of LDH-DBS, the difference is quite significant and cannot be considered as simple error due to approximate chemical formula of LDH-DBS. Therefore, it is believed that the presence of LDH facilitates the carbonaceous char formation. This is further supported by the light gray to blackish appearance of the residues of these composites obtained during LOI or UL94 testing, which may be due to some carbonaceous materials associated with the metal oxide.

When the amount of the residues obtained under nitrogen and oxygen atmosphere during TGA experiments are compared, comparable numbers are obtained in case of filled system (**Figure 5.10B**). The comparison of the TGA plots of nanocomposite composition PELDH4 is shown in **Figure 5.11**. It undergoes a two-step decomposition in presence of oxygen whereas under nitrogen atmosphere a single-step decomposition occurs with the low temperature peak around 430°C being completely suppressed. It is obvious that the high amount of residue obtained under non oxidative atmosphere indicates the forma-

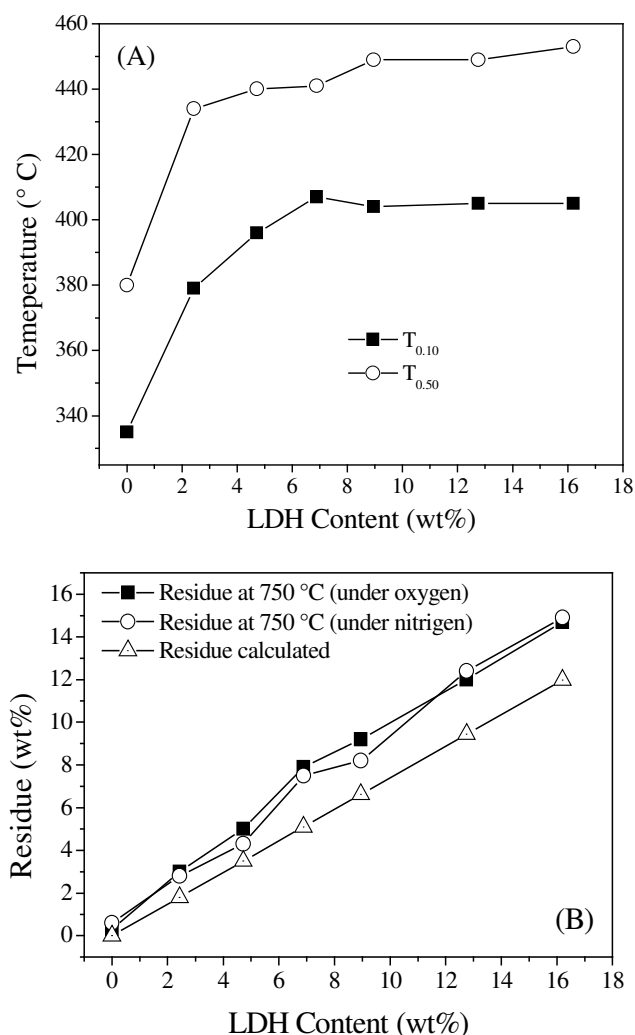


Figure 5.10 The influence of LDH concentration on (A) the decomposition temperatures at 10% weight loss ($T_{0.1}$) and 50% weight loss ($T_{0.5}$) (B) the amount of residue at 750 $^{\circ}\text{C}$ and its comparison with theoretically calculated value

tion of carbonaceous char. But, how can the similar amount of residue be also obtained under oxygen atmosphere? Perhaps the organic species (surfactant anion, polymer chain segments, etc) present within the interlayer region have delayed and less access of oxygen due to their encased position within metal hydroxide layer and the surrounding bulk polymeric matrix. Additionally, the endothermic decomposition of the metal hydroxide layers imparts a cooling effect, which may further affect the combustion process of these constraint organic species. As a result, incomplete combustion is more likely resulting in the formation of carbonaceous char even when combustion is carried out under oxygen atmosphere. In fact, such carbonaceous char formation within clay layers has earlier been proposed in case of combustion of polymer/layered silicate nanocomposites [142]. The basic difference between layered silicate and LDH during combustion is that the later undergoes endothermic decomposition liberating water and metal oxide, which makes reinforcement of the char less probable with LDH.

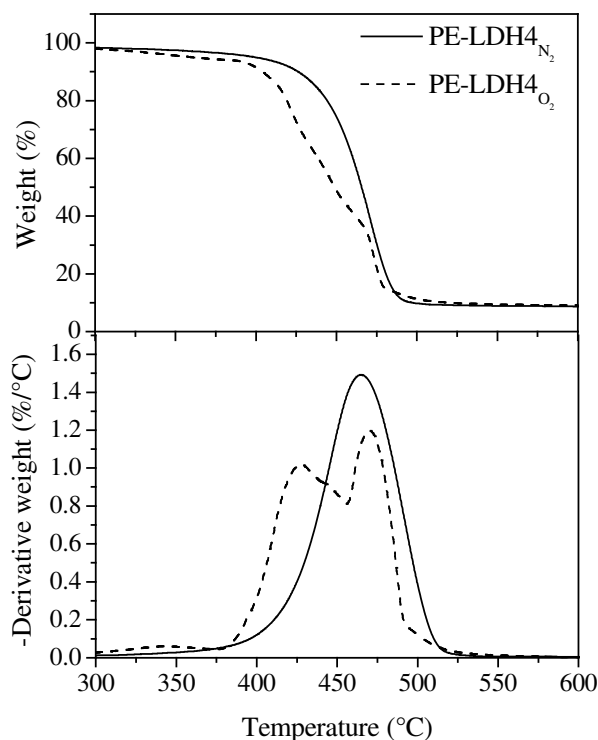


Figure 5.11 Comparison of the Thermogravimetric analysis of PE/LDH nanocomposite under oxygen and nitrogen atmosphere

5.3 Rheological Analysis

5.3.1 Introduction

Rheological analysis of polymeric melts involves the study of the mechanical response of the melt under the action of external mechanical stress or strain. In case of filled polymeric systems, rheological behavior can be drastically different from that of the unfilled melts depending on the nature of filler particles (structure, size, shape, surface characteristics, etc) and the state of their dispersion in the polymer matrix [143, 144]. In fact, rheological analysis is an important tool to investigate the state of filler particle dispersion in filled systems and their response under external force. Though an indirect method, rheological analysis can be treated as a complementary to the direct methods for morphological analysis, like XRD and electron microscopy, which altogether provide a complete picture of the state of filler particle dispersion in polymer matrix. The major advantages of rheological analysis are that it reflects the bulk properties of the matrix and also provides flow behavior of the melt that are often useful in deciding the optimum processing conditions required for the melt processing of polymer composites.

Polymeric melts are viscoelastic systems and their response to shearing depends on the ratio between the time scales of shear experiments and the characteristic relaxation time of microstructures present within such systems. The term microstructure means molecular entanglements in a high molecular weight unfilled melt and additionally structural association the filler particles in a particle filled system. Principally, such microstructures signify structural feature that acts as a physical barrier against flowability of the polymer chains under stress. When the experimental time scale is far below the characteristic relaxation time the microstructure (experienced at high frequencies or shear rates), the system

shows preferably elastic response characterized by high value of storage modulus. Whereas, at large experimental time scale (experienced at low frequencies or shear rates), the system shows viscous response. Again, shearing actions, if sufficiently high can change and even destroy these microstructures resulting in an entirely different material response compared to that observed when shearing does not affect the microstructures. From the scientific point of view, investigations in both these regions are important as they highlight the different mechanism of material's response toward external stress. The polymeric melts are characterized by a critical strain below which stress bears linear relationship with the applied strain and their ratio (known as relaxation modulus) shows a constant value independent of strain. Thus, the rheological behavior of polymeric melts below this critical strain is a linear viscoelastic one. Above the critical strain, due to changes in the microstructures, the relaxation modulus decreases with strain and the stress becomes a non-linear function of strain resulting in a non-linear viscoelastic material response [145]. Therefore, the primary task before carrying intensive rheological analysis is to determine the transition point between linear and non-linear viscoelastic regime. One simple way to determine this critical strain or a range about it, is to subject the polymeric melt to dynamic oscillatory shear using sinusoidal strain at constant frequency and varying strain amplitude. The strain input function looks like

$$\gamma(t) = \gamma_0 \sin(\omega t) \quad (5.1)$$

where oscillatory strain $\gamma(t)$ is applied at constant frequency ω with varying strain amplitude γ_0

The storage modulus, G' , is then monitored against strain amplitude. In the $\log G'$ versus $\log \gamma$ plot, the transition from linear to non-linear regime is indicated by the change of the storage modulus from low strain plateau value to strain dependent values [146]. In case of PE/LDH nanocomposites, this strain amplitude sweep tests were carried out at constant frequency of 10 rad/s and a temperature 240 °C. The results are shown in **Figure 5.12**. It is apparent that unfilled polyethylene melt show linear viscoelastic behavior up to much larger strain compared to PE/LDH nanocomposites and the critical strain for the former in present case lies within 25 – 30 % strain range. In case of nanocomposites, the

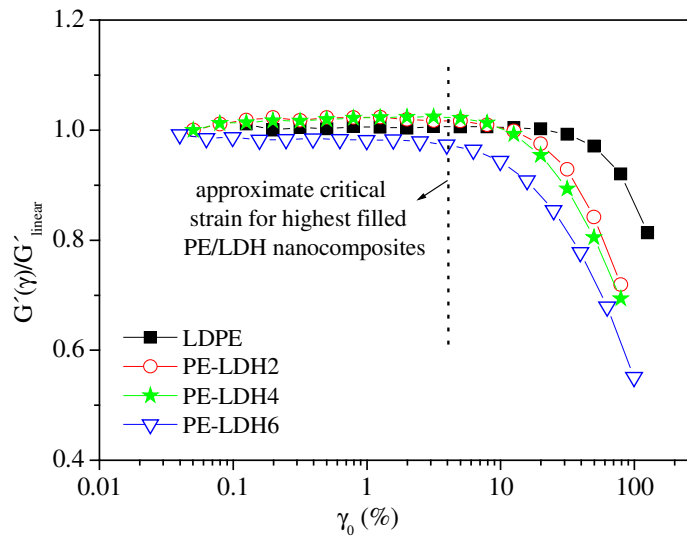


Figure 5.12 Strain dependence of the in-phase component stress response (storage modulus, normalized w.r.t. linear value) during an oscillatory shear experiment

critical strain decreases with increasing LDH content presumably due to specific interactions between the filler particles themselves and also between the particle and polymer chains. However, in the present case, for all the nanocomposites containing LDH concentration up to 20 wt%, the strain range below 5 % can be taken as a safe range for rheological experiments for studying linear viscoelastic behavior.

5.3.2 Linear Viscoelastic Behavior

The linear viscoelastic response of PE/LDH nanocomposites are studied using dynamic oscillatory measurements with a sinusoidal strain input at a constant strain amplitude of 2% and frequency sweep from 0.05 rad/s to 100 rad/s. The temperature range used was 160–240°C. The linear viscoelastic responses of all the nanocomposite compositions are qualitatively similar in this temperature range. But, the time-temperature superposition principle is not fulfilled for the nanocomposites, especially in the low frequency region. This is mainly because of the reason that the modulus shift factors are found to change with LDH concentration [147]. Therefore, construction of the master curves is not possible. All the oscillatory shear experiment data presented in this section corresponds to the measurements carried out at a fixed temperature of 240°C. The material response is interpreted in terms of various parameters, like storage modulus (G'), complex viscosity (η^*), $\tan\delta$, etc. **Figure 5.13** shows the typical features of linear viscoelastic response of the unfilled polyethylene and a nanocomposite melt containing high LDH concentration during such a frequency sweep experiment. Within the experimental frequency range, the storage modulus of the unfilled polyethylene is lower than its loss modulus. This means the viscous component has a dominant effect on the flow behavior of the unfilled polyethylene melt in this frequency range. With increasing frequency the storage modulus increases more compared to the loss modulus and at some higher frequency (which is larger than the highest value of frequency used in the present experiment) G' crosses G'' indicating increasing contribution of the elastic response. This is typical behavior of unfilled thermoplastic melt [145]. On the contrary, PE/LDH nanocomposites having high LDH

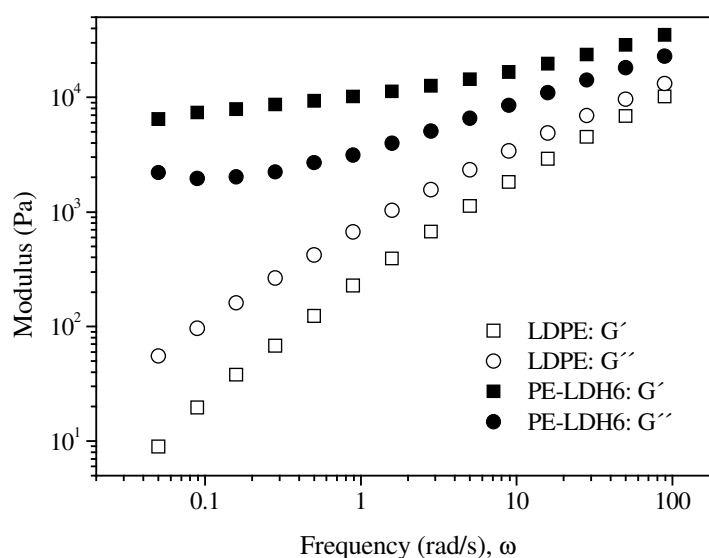


Figure 5.13 Difference in the viscoelastic response (storage modulus, G' and loss modulus G'') of unfilled polyethylene and high LDH filled nanocomposite in a dynamic oscillatory frequency sweep experiment

content show completely different behavior. The storage modulus always remains higher than the loss modulus within the experimental frequency range indicating dominant elastic character of the material. This is typical behavior observed in crosslinked polymer or polymer gel, where viscous flow is restricted by chemical constraints. In the present case, high concentration of LDH particles both in nano- and microscales creates strong physical barrier against the mobility of the polymer chains. The influence of increasing LDH concentration on linear viscoelastic response as discussed in the following sections shows how liquid-like melt is gradually transforms into a solid-like melt.

Figure 5.13 also shows that the difference in viscoelastic response between unfilled melt and the nanocomposite strongly depends on the frequency region at which they are compared. In the high frequency range, due to a small time period in each shear cycle, the dispersed filler particles can not fluctuate in phase with the oscillating shear force field and appears virtually static. As a result their influence is minimized and materials behavior is solely determined the matrix behavior [143]. On the other hand, at low frequencies the influence of the filler particles can be realized as they get more time to follow the oscillating shear force field and if they interfere with flowability of the materials strong effects like that presented in **Figure 5.13** are observed. Therefore, in discussing the linear viscoelastic behavior of nanocomposites the low frequency data are of prime importance.

The ability to store energy by any polymeric melt during shearing depends on its chain relaxation behavior. Lower the relaxation time for a system faster it dissipates the energy and hence shows lower value of storage modulus. In storage modulus versus frequency plot (**Figure 5.14**), the low frequency data for unfilled polyethylene reflect this fact. At low frequencies due to longer time period of shear cycles polymer chains get sufficient time to relax nearly completely showing low value of G' . This is the typical behavior of Newtonian liquids. The addition of LDH filler causes an upward shift of the low frequency G' values, which becomes more prominent with increasing LDH concentration ultimately

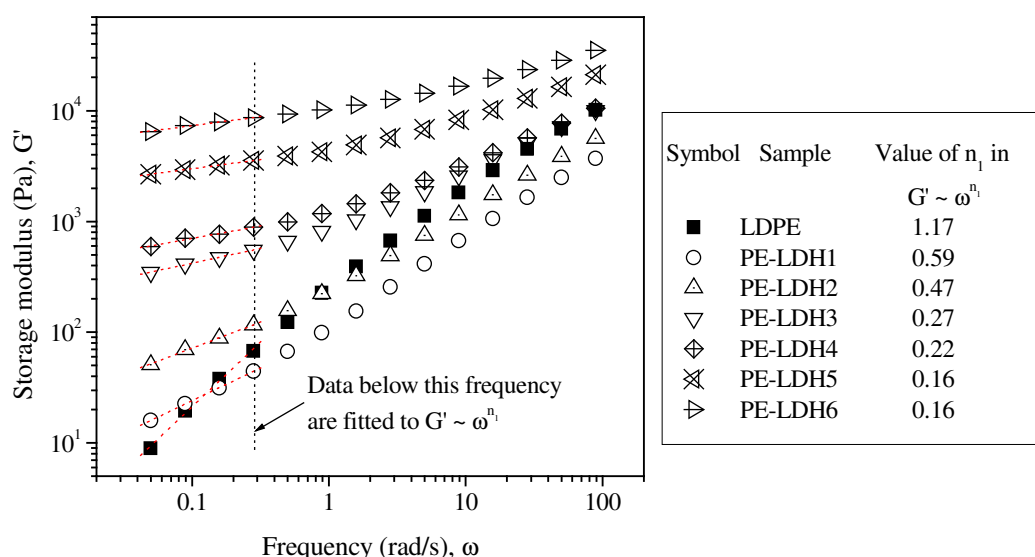


Figure 5.14 Storage modulus (G') versus frequency (ω) plots for unfilled PE and PE/LDH nanocomposite melts based on the results obtained from dynamic oscillatory measurements. The table on right the relaxation exponents obtained by fitting low frequency data to the power law model

leading to a virtually plateau behavior or frequency independence (**Figure 5.14**). The extent by which LDH particles influence the storage modulus can be measured semi quantitatively by the relaxation exponent (n_1) obtained by fitting the low frequency data to power law equation

$$G' \propto \omega^{n_1} \quad (5.2)$$

In case of homopolymers, the complete relaxation at low frequencies results in a characteristic terminal behavior with the value of n_1 equal to 2 [148, 149]. **Figure 5.14** shows how n_1 changes with LDH concentration in case of PE/LDH nanocomposites. The unfilled polyethylene does not show typical homopolymer-like low frequency behavior may be due to its high molecular weight associated with long chain branching and high polydispersity index. Still the value of 1.17 for n_1 indicates high extent of chain relaxation when compared to LDH filled compositions. While the presence of small amount of LDH (2.43 wt%) changes n_1 significantly, the corresponding change in G' is not much. This is attributed to the presence of low molecular weight functionalised polyethylene (PE-g-MAH) as compatibilizer, which lowers the matrix viscosity. Similar effects has also been observed in case of layered silicate based polymer nanocomposites containing a functionalised polymer of lower molecular weight [150]. However, with the further increase LDH concentration (say beyond 5 wt%) the both n_1 and G' at low frequency are changed significantly due to strong influence of LDH particles on the flow behavior of the melt. It is apparent that with increasing LDH concentration, G' shows decreasing frequency dependency in the low frequency region and at very high LDH level (above 10 wt%) a virtually plateau region is reached. This means the system develops more and more solid-like behavior with increasing resistance against relaxation through viscous flow of the polymer chains and segments.

The strong influence of LDH concentration on stress relaxation process of the nanocomposite melt can be directly observed from the variation of stress relaxation modulus [$G(t)$] with time during a step strain experiment. In this experiment, samples are initially equilibrated at experimental temperature at zero shear and then subjected to a sudden strain, which is maintained at a constant value and the changes in relaxation modulus are monitored with time. The results are shown in **Figure 5.15**. In case of unfilled PE, $G(t)$ decays fast indicating small relaxation times. The stress signals beyond 10 s become so small that they fall below the measuring capacity the torque transducer of the rheometer causing a scattering in the $G(t)$ values. This means the unfilled melt undergoes nearly complete stress relaxation within a very short time period (the longest relaxation time being about 26 s). The addition of a small amount of LDH (2.43 wt%) results in a significant slowing down of the decay of $G(t)$ with time. With increasing LDH concentration, $G(t)$ shows a tendency to attain an equilibrium value even after long time (even beyond 500 s). This is certainly an effect induced by the dispersed LDH particles through particle-particle and particle-polymer interactions, which change the relaxation dynamics of the system. This low frequency non-terminal viscoelastic response observed in PE/LDH nanocomposites resembles the layered silicate based exfoliated nanocomposites, where the polymer chain ends are inter-locked at the surface of the highly anisotropic exfoliated silicate layers [151]. On the contrary, such non-terminal behavior is not observed when the polymer chains do not interact with the exfoliated clay layers [148, 151]. It is suggested that the adsorption of polymer chain segments on a rigid surface creates an energetic barrier against the reptation of the polymer chains. As a result, the chain relaxation process is delayed (increasing the relaxation time) and shifts the terminal behavior to very lower frequencies. Interaction between LDH clay surface with polymer chains through maleic anhydride groups present in functionalised polymer

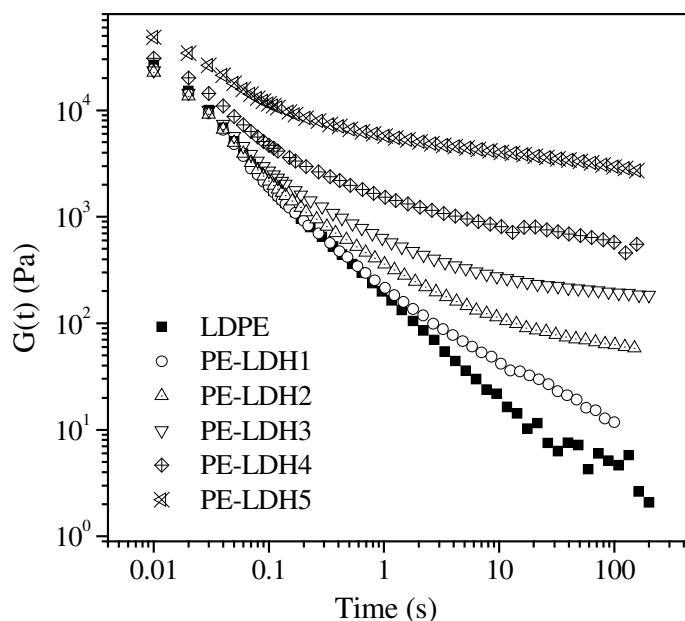


Figure 5.15 Step strain experiment showing how the stress relaxation modulus varies decays with time in unfilled PE and in the PE/LDH nanocomposite melts having different LDH concentrations

has been observed. The morphological analysis of the PE/LDH nanocomposites at different loadings discussed earlier and the fracture surface analysis of these nanocomposites show that polymer chains are indeed adsorbed on the LDH particle surface and are also entrapped within loose particle clusters [152]. The highly anisometric exfoliated LDH layers remains randomly dispersed in the matrix and in the vicinity of larger particle agglomerates. With increasing LDH concentration, the number density of the exfoliated layers increases, which decreases the average inter-particle distance. This may lead to formation of localized domains of physical networked structure, where the nanostructured particles may orient themselves in some preferential direction [147, 151, 153]. The shearing in low frequency region can not generate sufficient force to destroy such structured domain resulting in fluctuation of individual particles to oscillate with the shear force field. Also, close proximity and strong particle-particle interaction cause a kind of physical jamming leading to extremely slow relaxation of the particle phase as well. As a result, this causes strong reinforcement of the melt producing high elastic modulus compared to unfilled melt.

The variation of complex viscosity ($|\eta^*|$) with frequency and LDH concentration is shown in **Figure 5.16**. The unfilled PE melt is characterized by a low frequency Newtonian flow behavior, which transforms to shear thinning characteristic in the high frequency region. This is typical behavior of unfilled polymeric melts (with only differences observed in the frequency region at which transition from Newtonian to shear thinning behavior takes place depending on the molecular weight and the molecular architecture). The presence of nanostructured LDH particles in the melt not only enhances the melt viscosity but also induces shear thinning character in the low frequency region. The frequency independent viscosity of unfilled melt in the low frequency region is an indication that the shear force applied in this region is not sufficient to disentangle the polymer chains and align them in the flow direction. Such Newtonian behavior at low frequencies or low shear rate is also common in polymer composites

containing non interactive filler particles, even at very high filler concentration. Like an unfilled melt, these composite melts are also characterized by the absence of yield stress. However, in case of PE/LDH nanocomposites, completely different low frequency behavior is observed. Like typical polymer/clay based nanocomposites, beyond certain critical concentration of LDH, the low frequency Newtonian behavior changes into a shear thinning behavior.

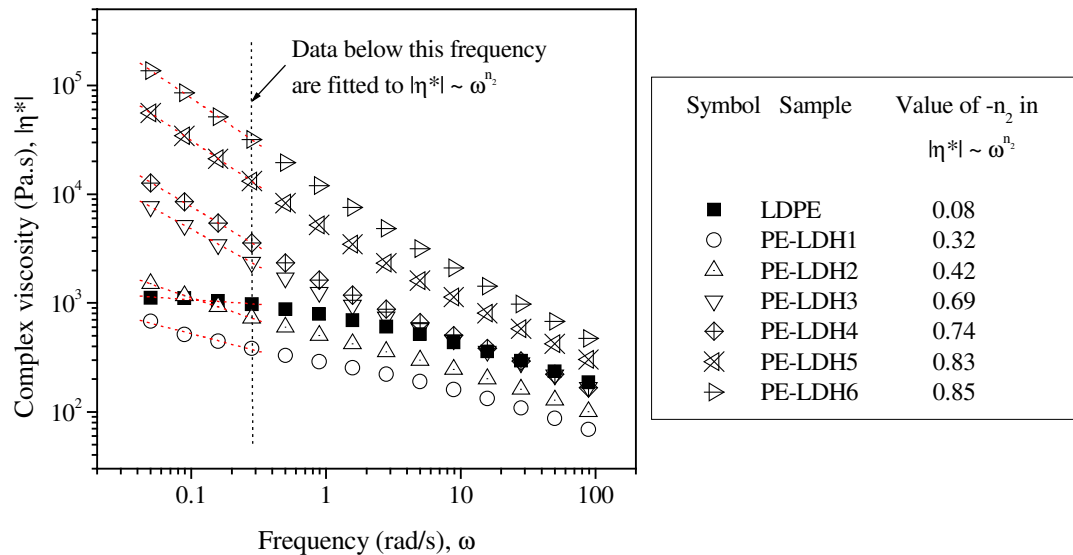


Figure 5.16 Complex viscosity ($|\eta^*|$) versus frequency (ω) plots for unfilled PE and PE/LDH nanocomposite melts obtained from a dynamic oscillatory shear experiments. The table on the right indicates the sample designation and also the value of the corresponding shear thinning exponent n_2 .

The extent of deviation from the low-frequency Newtonian flow behavior is measured by a term called shear thinning exponent (n_2) obtained by fitting the low frequency data in **Figure 5.16** to the power law equation $|\eta^*| \propto \omega^{n_2}$. In case of unfilled PE the value of n_2 is expected to be zero. But, the commercial low density polyethylene used in the present study shows a small negative value (-0.08) of n_2 . The high molecular weight and long chain branching are the factors causing this small increase in shear thinning exponent. In case of PE/LDH nanocomposites the negative value of n_2 increases significantly at a very small LDH concentration and steadily increases with further increase in LDH concentration(**Figure 5.16**). Recently, Wagner et al has proposed this shear thinning exponent as a semi-quantitative measure of degree of exfoliation of the clay particles in polymer/clay nanocomposites [154]. It is suggested that polymer nanocomposites containing exfoliated clay particles show much higher value of n_2 compared to conventional composites, where clay particles form big agglomerates. They observed no change in low-frequency complex viscosity with temperature of the melt, while high-frequency viscosity decreased with increasing temperature. However, the similar explanation does not hold for the PE/LDH nanocomposites and the results shown in **Figure 5.16**. The PE/LDH nanocomposites melts show weaker temperature dependency of the low-frequency complex viscosity compared to that of the high-frequency complex viscosity indicating stronger influence of the dispersed particle in the low frequency response. Besides, the XRD and TEM results of LDH based nanocomposites qualitatively show no significant enhancement in the degree of exfoliation of LDH particles with increasing LDH concentration. Therefore, the change

in the shear-thinning exponent as shown in **Figure 5.16** is not due to enhancement of degree of exfoliation. Rather, the increasing LDH concentration brings about two changes in the system, firstly, more number of polymer chains/segments get interlocked on the LDH platelets surface or in the inter layer region. Secondly, the average distance between the dispersed particles is decreased. These two factors contribute though different mechanisms to the final properties of the nanocomposites. The interlocking of the polymer chains on LDH platelets certainly restricts their mobility and hence delays their relaxation process. This is reflected in so called zero shear viscosity of the melts. In case of unfilled PE and the nanocomposites containing low amount of LDH, the well defined zero shear viscosity can be determined **Figure 5.16** by extrapolating the viscosity versus frequency curve to zero frequency. However, this does not work at high LDH concentration as the complex viscosity versus frequency curves diverge as frequency approaches zero indicating the presence of an yield stress value. Instead of zero shear viscosity, the complex viscosities determined at low frequency (0.05 rad) are compared, an exponential dependence on the LDH concentration is observed, which follows equation 5.3 and is shown in **Figure 5.17**.

$$\eta_0 = \eta_{PE} * \exp(\alpha * \phi) \quad (5.3)$$

where, η_0 is the low frequency complex viscosity, η_{PE} is the low frequency complex viscosity of the unfilled PE and ϕ is the weight fraction of LDH in nanocomposite. Writing equation (5.2), the changes in the matrix viscosity upon addition of the lower molecular weight MAH-g-PE fraction was not consid-

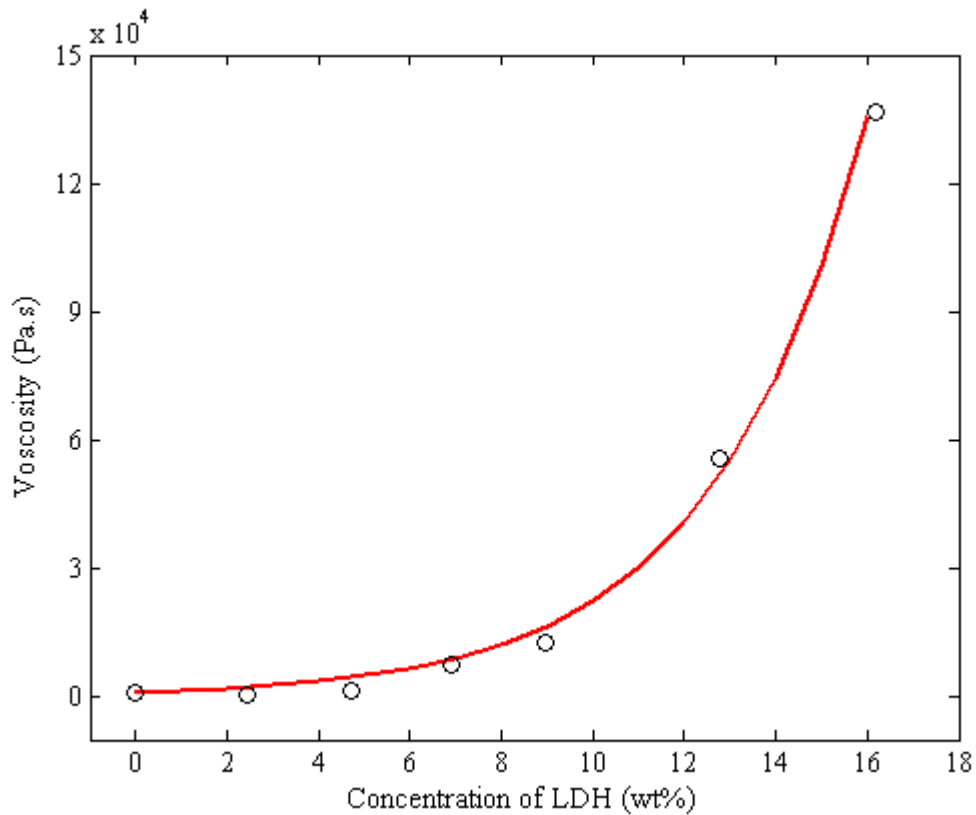


Figure 5.17 Viscosity at low frequency (0.05 rad) as a function of LDH concentration in PE/LDH nanocomposites

ered. The exponent $\alpha \approx 30$ is significantly larger than that expected in the case of pure hydrodynamic reinforcement (2.5 for spheres [155]) and can be explained by a build-up of a filler network structure similar to that in the filled elastomers [156]. This also helps us to understand why nanocomposites show strong shear thinning behavior beyond some critical clay concentration. The formation of network structure (more specifically, sub network structures due to the formation of structured domains) by the nanostructured clay particles beyond certain critical filler concentration induces solid-like behavior in the melt showing high viscosity and elastic modulus. During low-strain and low frequency oscillatory shearing, matrix mobility is severely restricted by such particulate domain. However, as the shearing become more intense with increasing frequency or strain, the network structures start getting disturbed and at sufficiently high frequency or shear rate they may be completely destroyed with shear induced alignment of the clay particles in the flow direction. As a result, melt rheology at this stage is solely influenced by the matrix showing strong temperature dependence. The elastic nature of the melt is also reduced by such alignment [147]. Additionally, the polymer chains which are entrapped between particle clusters or constrained by the clay particles through intercalation and adsorption, experience larger effective strain compared to unconfined chains [157]. This can lead to enhanced shear thinning behavior of the nanocomposite melts at low shear rate experienced during low frequency oscillatory measurements [150, 158].

5.3.3 Non-Linear Viscoelastic Behavior

It is known that shearing polymeric melts within linear viscoelastic regime does not destroy their microstructures, but may cause reorganization with respect to the direction of flow. In many practical situations, however, these materials often experience much severe shearing with high strain or strain rate. For example, during extrusion rotational motion of the extruder screw generates sufficient shear rate that the linear stress-strain relation is hardly followed. Such strong shearing is often necessary to facilitate breakdown of larger filler particles for achieving better dispersion in filled polymer composites. Therefore, characterizing polymer melts in non-linear viscoelastic regime bears direct correspondence to the actual melt processing conditions. The shearing of polymeric melts in non-linear regime causes changes in the internal structure of the system, which can be more pronounced in case of filled system, especially when the filler particles show strong interaction among themselves. Such filled polymeric melts usually exhibit thixotropic effect. This means during shearing, the various microstructures suffer structural breakdown whose extent depends on the magnitude and duration of the shear force and when shearing is stopped regeneration of the structures takes place with time [143]. The breakdown and regeneration of the microstructures both being time dependent processes introduce additional time constants in the response behavior of the melt toward non-linear shearing. To investigate this structural breakdown and regeneration processes in case of present system, the sample melts were subjected to shear cycles constituted of three steps as follows:

- I. In the first step sample was sheared at a constant steady shear rate ($+\dot{\gamma}$) till an apparent steady state is reached. This step is called preshearing cycle.
- II. In the second step, the shearing was stopped and the sample was allowed stay in quiescent state for variable time. This step is called rest period.

III. In the third and final step samples were sheared using the same shear rate as in the first step, but in opposite direction (i.e. $-\dot{\gamma}$). This step is called flow reversal step.

To provide identical flow history, all the test samples were equilibrated at the test temperature for about 10 minutes before the preshearing cycle. The purpose behind carrying out such step-wise shearing, was to subject the system to high strain shearing in the first step so that the microstructures present within the system are ruptured and during the rest period shearing force was withdrawn in order to ensure the structural regeneration under static condition. The length of the rest period was varied expecting its influence on the extent of structural rebuild-up. The flow reversal step was carried out to observe the effect of the regenerated structure and its response during steady shear. This type of step shearing has previously been employed to study similar effects in solutions of liquid crystalline polymers by Walker and co-workers [159] and later applied by others in case of polymer/layered silicate nanocomposites [150, 160]. In the present case, unfilled polyethylene was first characterized to understand the behavior of PE matrix alone during steady shear and rest period, especially with different shear rates and rest periods.

5.3.3.1 Non-linear rheological behavior of unfilled PE

The PE used in the present investigation is a low density and high molecular weight commercial polymer. This type of PE is characterized by long chain branching and multiple branch points on a single polymer chain. Therefore, it is obvious that the polymer chains form much higher extent of entanglements compared to the polyethylenes having no or very small number of branching. The multiple long chain branching causes more steric hindrance against the chain disentanglement process under the influence of applied stress. These chain entanglements are viewed as the microstructures acting as the energetic barrier against the viscous flow and are the root cause of non-linear rheological response during shearing at high shear rate and high strain. The response of this polyethylene melt during steady shearing is shown in **Figure 5.18**.

In **Figure 5.18A**, stress response of unfilled polyethylene at low constant shear rate is characterized by a monotonous increase in stress with time until a steady state is reached. With increasing shear rate a tendency to form a stress maximum (more specifically a broad maximum) before attaining the steady state is observed. With further increase in shear rate, this stress maximum (stress overshoot) becomes more prominent and its position is shifted to the left on the time axis. Such non-linear flow behavior is well known and theoretically described in case of high-molecular-weight polymer melts and concentrated polymer solutions [161–163].

Under the influence of shear flow, the process of stress development and its relaxation in a polymeric melt can be explained in terms of the various kinds of motions, their relative time scales and the influence of chain entanglements. In a concentrated solution or melt of a high molecular weight polymer, each polymer chain forms entanglements with the neighboring chains and itself. The molecular weight of the chain segment between two adjacent entanglement points (M_e) is very important parameter in understanding the polymer chain dynamics. According to Doi-Edward's theory the movements of such entangled polymer chains are described by two different kinds of motion [163, 164]. The first kind is the small scale wriggling motion confined within the chain segments between the entanglements originating from the changing conformational topology of the monomer units. The characteristic time scale of this

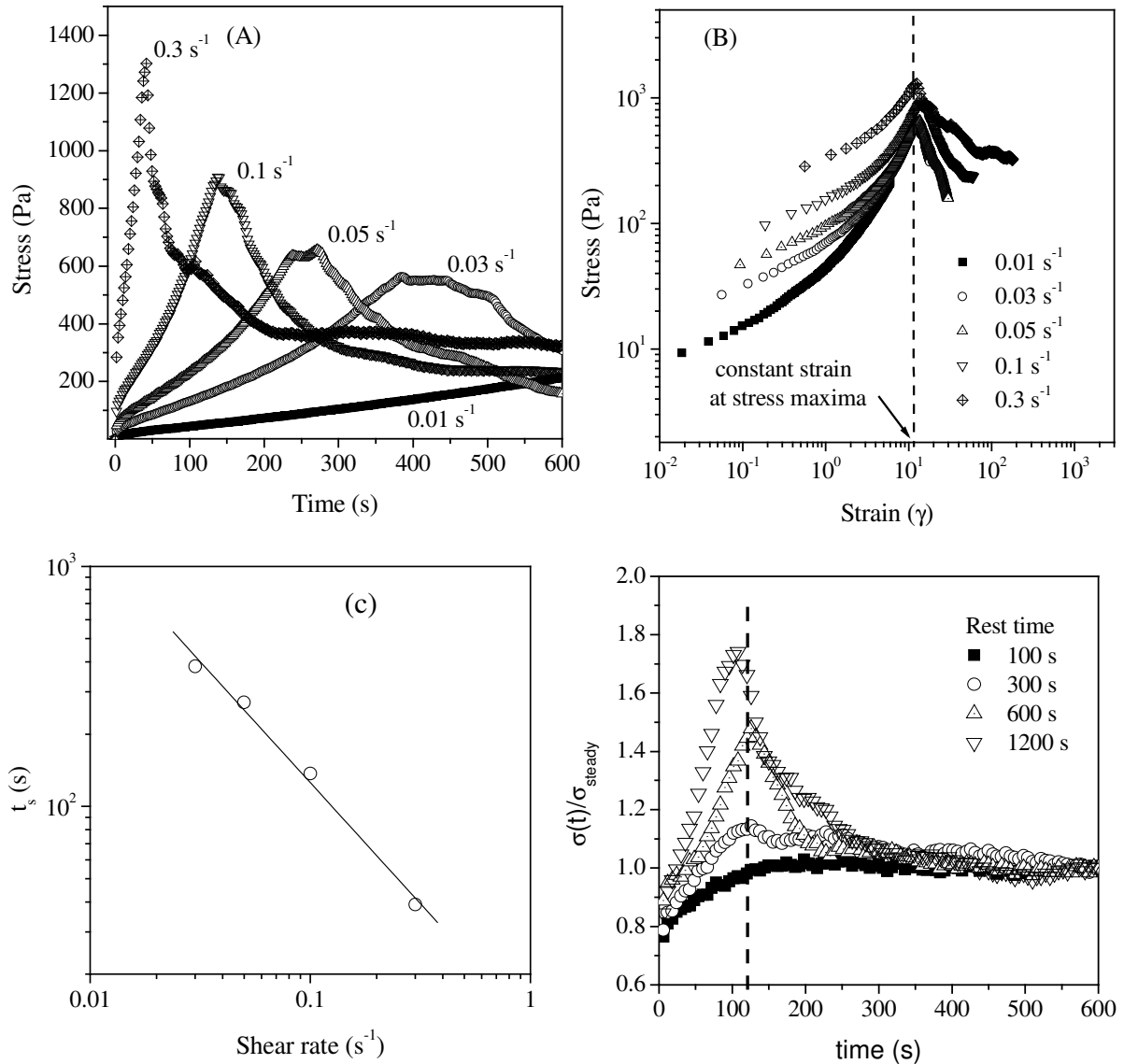


Figure 5.18 Steady shear flow behavior of unfilled PE melt. (A) The influence of shear rate, (B) corresponding strain scaling of the stress at different shear rates, (C) the inverse relation between the shear rate and the time (t_s) at which stress overshoot occurs and (D) the influence of rest period prior to shearing on the steady shear response. The melt temperature was 240 °C.

motion is of the order of Rouse time τ_{eq} and is proportional to the square of M_e . This kind of motion does not affect the topology of chain entanglements. The second kind is the large scale diffusive motion along the chain axis, which involves slippage of the chain along the entanglement points. This motion is characterized by a time scale τ_d called the disentanglement time or the reptation time and is proportional to the square of the molecular weight of polymer. During this diffusive motion, the contour length of a polymer chain remains unaffected, but the average path of the chain segments (called primitive chain segments) in between the entanglement points orients to an equilibrium position with respect to the shear flow field. In practice, there exists a spectrum of time scales for this diffusive or orientational motion and τ_d represents the longest one. The relaxation through the first kind of motion is so fast that within the

time scale of practical rheological experiments its influence is never realised. Therefore, the theoretical explanation of the non-linear rheological response of concentrated polymer solutions or melts is based only on the orientation effects of the primitive chain segments under applied stress [162–164].

In the present case, with unfilled PE melt, the strain scaling of stress developed during steady shear (**Figure 5.18B**) indicates that the strain at which stress maximum is observed is independent of the shear rate within the experimental range. This means that within the limit of experimental shear rate, the polymer chains always maintain their equilibrium contour length and do not suffer chain length extension [162, 164, 165]. At low shear rates, when $\tau_d * \dot{\gamma} \ll 1$, the relaxation of the primitive chain segments to the new equilibrium position at the steady state takes place within the experimental time scale. As a results, monotonous increase in the stress is observed with time till the steady state is reached when all the chains attains their equilibrium orientation with respect to the shear flow field. With the unfilled PE, such monotonous increase in stress with steady shear was observed below $\dot{\gamma} < 0.03 s^{-1}$.

At moderate shear rates ($\tau_d * \dot{\gamma} \gg 1$), when diffusive or orientational relaxation time (τ_d) is comparable or less than the experimental time scale ($1/\dot{\gamma}$), the rate of chain relaxation is smaller than the rate at which they gain energy by the applied shear stress [165]. This results in an excessive stress build up in the polymer chains compared to the steady state, which is manifested as the stress overshoot at the beginning of flow during steady shearing as observed in **Figure 5.18A** above $\dot{\gamma} > 0.03 s^{-1}$. As the shear rate is further increased within the limit $\tau_{eq} * \dot{\gamma} < 1$, the appearance of the stress overshoot peak becomes more intense and at shorter time, but necessarily at the same constant strain **Figure 5.18B**.

Doi-Edward's theory also predicts a constant strain $\gamma (= \dot{\gamma} * t)$ equal to 2 at which stress overshoot appears for linear polymers. However, in the present case γ has been observed at about 12, which can not be explained by original Doi-Edwards theory [162, 164]. The similar deviation have also been reported in case of commercial PE and other high molecular weight branched polymers [166]. The experimental results shows that t_s (the time at which stress overshoot appears) varies inversely with $\dot{\gamma}$ as shown in **Figure 5.18C**, which resemble the observation made by Wagner [167] in case of highly branched low density PE. He also reported a constant strain of $\dot{\gamma} * t = 7$ for stress maximum during steady shear. Such deviation is attributed mainly to extensive chain branching and much more complex and energy intensive chain dynamics associated with commercial low density PE melts [166, 168].

In addition to the influence of shear rate, another important aspect, namely shear history of the melt, strongly influences the non-linear response of the melt. In case of unfilled PE, this was investigated through flow reversal experiment described earlier. The shear rate applied during this experiment was $0.3 s^{-1}$ and melt temperature of $240^\circ C$. The effect of rest period on the stress growth during the flow reversal step was examined and the results are presented in **Figure 5.18D**. It is interesting to note that at low rest period (300 s or below), unfilled PE melt does not show any overshoot. When the rest period is increased, a distinct overshoot appears at the beginning of steady shearing in the flow reversal step, whose magnitude increases with increasing duration of the rest period. It seems also apparent that the time at which stress overshoot appears remains independent of the rest period, which means the strain at stress maximum is also independent of the rest period. Similar behavior has also been observed previously in case of polyisobutylene (PIB) solution [161]. The physical interpretation of the dependence of stress overshoot can be given in terms of relaxation from the equilibrium orientation of the primitive chain segments with respect to the applied shear flow field. In absence of shearing, the equilibrium state is characterized by the random orientation of the primitive chain segments. The preshearing step during

the flow reversal experiment causes orientation of these randomly arranged primitive chain segments in the direction of applied shear and a new equilibrium is achieved at the steady state. As soon as the shearing is stopped and the melt is allowed to rest, the oriented primitive chain segments start to relax and retract to the state persisting in absence of shear. But, this retraction involves diffusional motion of the chain backbone and is not instantaneous as the chain entanglements create energetic barrier against the diffusion of the chain backbone. Therefore, it is expected that the extent of this relaxation depends on the duration of the rest period during flow reversal experiment. Longer the rest period, nearer is the average orientation of the primitive chain segments to that exists in absence of shear. The complete relaxation during the rest period would certainly results strongest stress overshoot in the flow reversal step.

The average molecular weight and polydispersity index of any polymeric material play an important role in determining its rheological behavior and also the transition from linear to non-linear behavior. The appearance of stress overshoot at the a beginning of steady shearing is taken as a strong indication of its non-linear response. The PE matrix used in the present investigation is a commercially available material with high average molecular weight and polydispersity index and is known to have multiple long-chain branching on a single chain. When this material is blended with a low molecular weight functionalized polymer of similar kind, the average molecular weight of the blend becomes lower than that of the original PE and also polydispersity index increases. Such a blend exhibits stress overshoot at higher shear rate compared to the higher molecular weight component of the blend. In the flow reversal experiment, the unfilled PE and its blend with a low molecular weight functionalized polyethylene (PE-g-MAH) were characterized at $\dot{\gamma} = 0.3s^{-1}$ and rest time of 600 s. The stress response during the flow reversal step is shown in **Figure 5.19**. It is obvious that the PE melt exhibits distinct overshoot, whereas the blend shows monotonous increase in stress with time till the steady state is reached. Therefore, it is logical to conclude that at the given shear rate, blend still exhibits linear viscoelastic response.

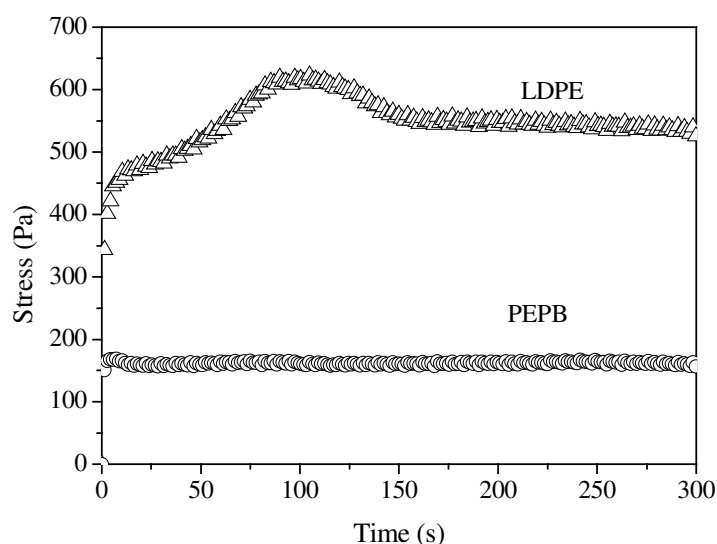


Figure 5.19 Influence of low molecular weight functionalized polymer (PE-g-MAH) on the steady shear viscosity of the unfilled PE melt ($\dot{\gamma} = 0.3s^{-1}$).

5.3.3.2 Non-Linear Rheological Behavior of PE/LDH Nanocomposites

The response of PE/LDH nanocomposites containing different amounts of LDH and PE-g-MAH (ratio of LDH to PE-g-MAH is always constant) at $\dot{\gamma} = 0.3s^{-1}$ and two different rest periods (100 s and 600 s) is shown in **Figure 5.20**, where the stress growth during the flow reversal step has been plotted against the time of shearing. When the rest period is small (100 s), the nanocomposites endow qualitatively similar behavior irrespective of LDH concentration i.e. the stress increases monotonously with time till the steady state is reached. However, the steady state viscosity of the melt increases with LDH concentration, whose effect is partly counter balanced by the simultaneously increasing amount of PE-g-MAH. This means that LDH particles have definite reinforcing effect on the polyethylene melt. At large rest period, for example 600 s, both the PE and the nanocomposites exhibit stress overshoot at the

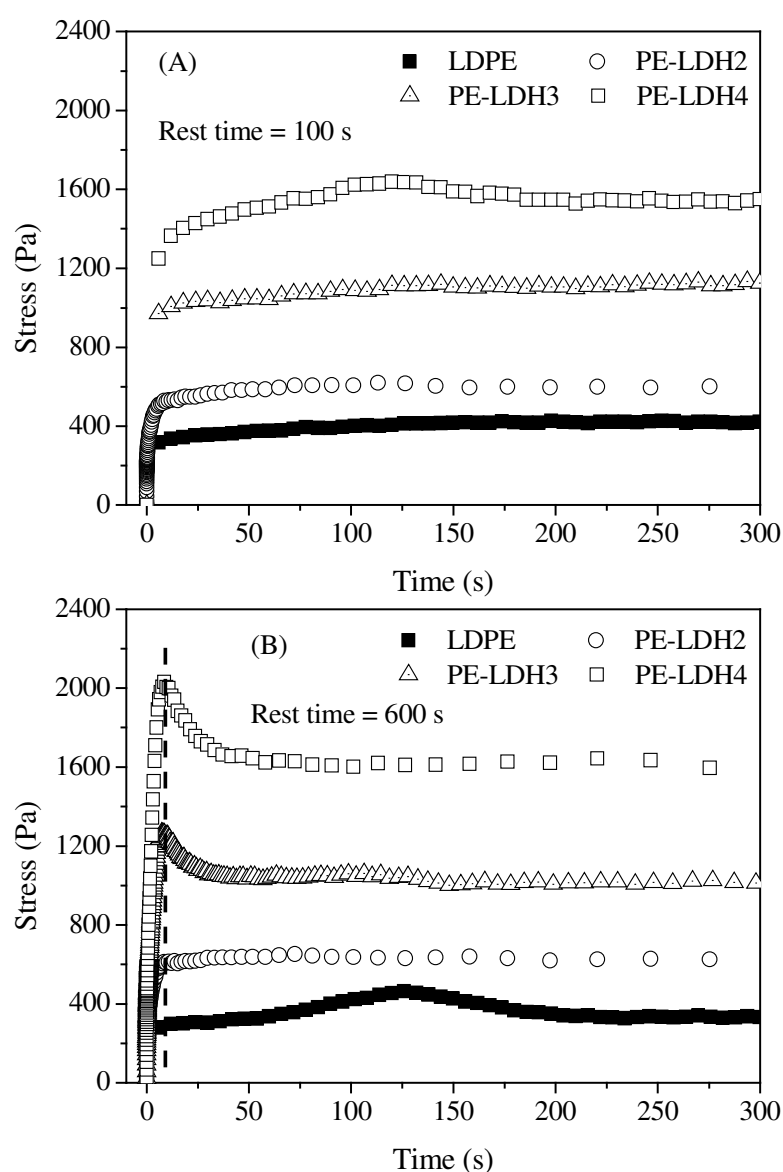


Figure 5.20 Effect of LDH concentration on the stress growth during the flow reversal step in the flow reversal experiment (shearing was carried out for 600 s, but the steady state is reached within 300 s; ($\dot{\gamma} = 0.3s^{-1}$)).

beginning of the flow in the flow reversal step. The nature of stress overshoot peak in nanocomposites (both in terms of its position and magnitude) is completely different from that observed in PE. In later it is rather broad and the time at which it appears (t_{max}) is at around 125 s after the beginning of the flow. Whereas, in case of nanocomposites, the stress overshoot peaks are much more well defined and sharper. Also the t_{max} is at around 8 s and the magnitude of the stress overshoot peak increases with increasing LDH concentration.

When the stress growth shown in **Figure 5.20B** is scaled against the strain ($\dot{\gamma} * t$), the strain at which stress maximum appears is found to be much smaller in the nanocomposites. This means that in the nanocomposites, the microstructures are disturbed at much lower strain in comparison to the unfilled melt. Similar behavior is also observed during dynamic oscillatory shearing with increasing strain amplitude at constant low frequency. The linear relation between the storage modulus and strain amplitude is transformed to a non-linear one at much lower strain amplitudes in the nanocomposites depending on the LDH concentration (**Figure 5.12**). Again, while comparing with the unfilled melt, the influence of PE-g-MAH should also be considered, whose presence shifts the critical shear rate (at which stress overshoot appears) to a higher value. It is thus apparent that this difference in shear growth observed during flow reversal step between the nanocomposites and the unfilled PE is due to the presence of LDH particles. Such unusual flow behavior during steady shearing is not common in conventional particle filled composites at so low filler concentrations, where particle-particle and particle-polymer interactions are not very strong. The significant difference in the t_{max} values between the unfilled and the LDH filled melts is an indication that the LDH particles, even in small concentration, considerably alters the flow dynamics of the polymer chains. Additionally, the contribution from the particle phase alone plays an important role in determining the stress developed in the nanocomposite melts during steady shearing. The linear viscoelastic behavior and the morphological features of PE/LDH nanocomposites discussed earlier showed that the dispersed LDH particles not only interact among themselves, but also with the polymer chains. As a result, in addition to chain entanglements, possible polymer-filler interaction imposes another degree of energetic barrier against the movement of the polymer chains under shear. The relaxation process in the nanocomposite melt becomes slower, which causes higher stress build-up at the beginning of steady shearing. The net outcome of all these effects is the appearance of stronger stress overshoot peak at much shorter time in PE/LDH nanocomposites in the flow reversal step.

Several researchers have tried to explain this type of stress overshoot behavior both qualitatively and theoretically in case of filled polymer melts [144, 150, 169, 170]. It is generally accepted that this stress overshoot is related to the accumulation of stress in the particle phase and its subsequent release due to rupture of these various particulate structures. In case of polymer/clay nanocomposites, such particulate structures mainly consist of physically associated particulate domains or localized network structures both in microscale (formed by the primary clay particles) and in nanoscale (formed by the exfoliated clay layers) [150]. When the nanocomposite melt is subjected to shearing, both the particle phase and the matrix phase respond according to their characteristic structural rigidities. The elastic modulus of the particulate structure is certainly much higher than that of the polymer matrix. This is because the force that facilitates the formation of various particulate structures in the melt state is usually of electrostatic in nature coupled with thermodynamic incompatibility between the particle and the polymer phases. In case of LDH clay particles, this is indeed very strong because of its high surface charge density. Whereas, in case of unfilled PE melt, the elasticity is mostly related to the chain entanglement and its degree,

which are topological constraints. Therefore, at the inception of shearing, the phase with higher elastic modulus i.e. particle phase responds first. Leonov [144] had explained that as the shearing begins, the networked particle domains or 'flocs' accumulate energy up to the limit of their critical strain energy. This results into a stress overshoot built up in the system, which is manifested as a stress overshoot at the beginning of steady shear. When the critical strain energy level is exceeded, the 'flocs' are ruptured to form smaller 'flocs', which suffer similar fate. The rupturing process is associated with release of strain energy. This process continues till the steady state is reached, when the ruptured particles are arranged in an equilibrium orientation with respect to the flow direction. According to Solomon et al. [150] at the beginning of steady shear the average orientation of the particles and the particle distribution about that average orientation are changed to a new equilibrium state under the action of flow field. During such change in particle orientation, the network structure formed by the dispersed clay particles are ruptured and the particles are oriented in the flow direction.

Similar to the behavior observed in case of unfilled PE melt in **Figure 5.18D**, the magnitude of the stress overshoot peak in the nanocomposites is strongly dependent on the duration of the rest period. **Figure 5.21** shows how the rest period influences the stress overshoot peak in nanocomposite composition containing 5.0 and 7.5 wt% LDH. This dependence indicates the reversibility of the structural breakdown of the particle phase i.e. under the quiescent condition the regeneration of the particulate structure takes place. The driving force behind this regeneration process is the electrostatic attractive interaction among the inorganic particle fragments in a sea of non-polar polymer matrix. Such electrostatic interaction facilitates forced diffusion of the highly anisotropic clay particles even in a highly viscous medium. Simple Brownian relaxation process cannot explain the kinetics of this regeneration process. This is because the time scale for diffusion due to Brownian motion of the disc shaped particles with an average lateral dimension of 500 nm in a polymer matrix of viscosity about 4000 Pa.s is of the order of 10^5 s [171]. Whereas the effect of the structural regeneration is observed within few hundred seconds.

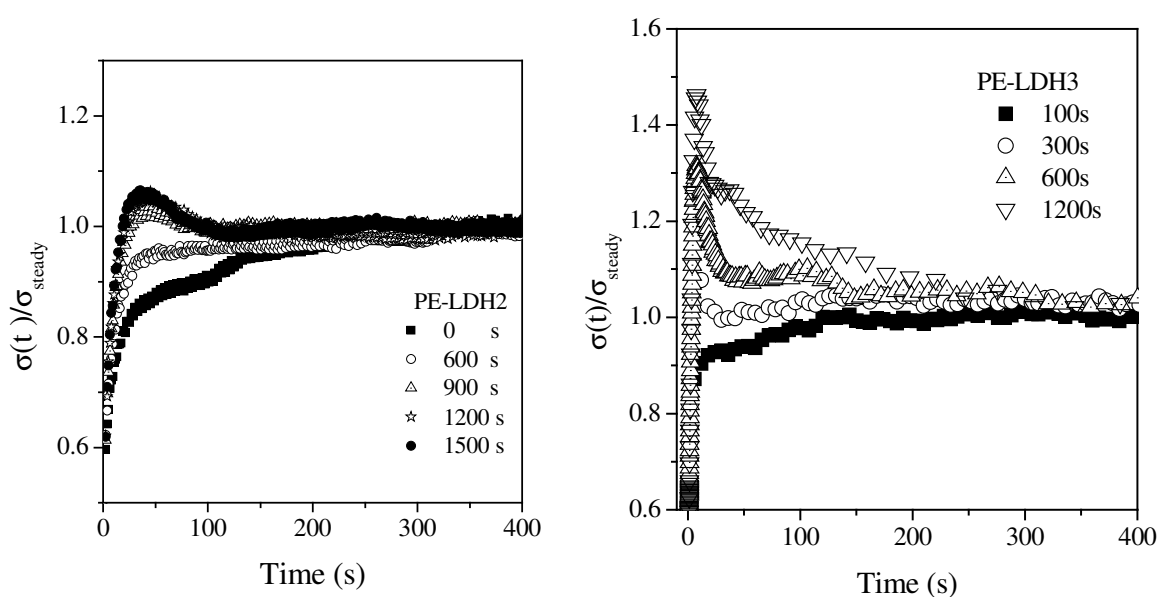


Figure 5.21 Effect of rest period on the stress overshoot during start-up flows in the second steady shear step in a flow reversal experiments.

The structural regeneration associated with the dispersed particle phase under quiescent condition

and the effect of the regenerated structure on the transient response during steady shearing followed immediately after the quiescent period was also studied in case of flocculated suspension of TiO_2 by Lapasin et al. [172]. They used oscillatory time sweep at a low strain amplitude and a low frequency during the quiescent period to monitor the change in storage modulus of the melt with time. The idea behind this experiment was stemmed from the fact that shearing at low strain and frequency does not disturb the particulate structure in the suspension. Similar investigation has been carried out with unfilled polyethylene melt and the PE/LDH nanocomposites during flow reversal experiment. The results are shown in **Figure 5.22**. The oscillatory shear measurement during a long rest period shows striking difference between the unfilled PE and the nanocomposites. In the former, the storage modulus increases marginally with increasing rest time whereas, in the nanocomposites an exponential increase of the storage modulus is observed that does not reach the steady value within the experimental time. The strong increase in storage modulus under nearly quiescent condition shows a direct evidence of the structural build-up in the system. It is obvious that the ruptured LDH particles oriented in the preshearing step start to reorganize from their stress induced equilibrium state and approach to a new equilibrium dispersion state that prevails in absence of shear. In case of PE/LDH nanocomposite and similar systems

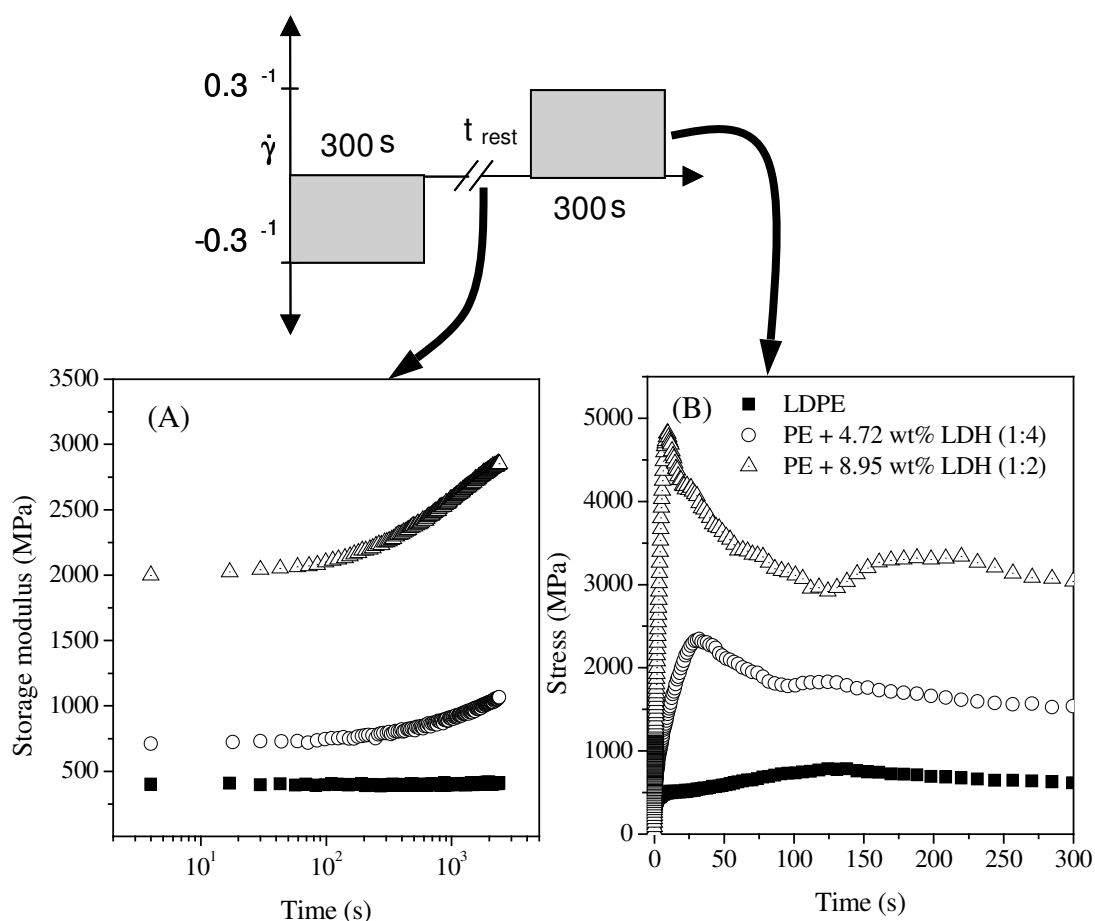


Figure 5.22 The experimental results showing how the storage modulus (measured by applying low amplitude (1.0%) and low frequency (1 rad/s) dynamic oscillatory shearing during rest period t_{rest}) changes with time (A) and the corresponding transient steady shear response followed after the rest period (B). (The ratio shown in bracket indicates the ratio of LDH and functionalized polymer in the nanocomposites)

this reorganization of the particle phase means the regeneration of the physically associated particulate domains. Since these domains act as the pockets for energy storage during shearing, the elastic nature of the melt increases with time and the storage modulus increases steadily. In case of unfilled PE melt, the scenario is completely different as no particle phase is involved. In the quiescent state, chain segments undergo relaxation from their shear induced oriented state to the random orientation observed in absence of shear. The response during subsequent steady shearing followed after the rest period is also obvious. The stress overshoot in the nanocomposites is much stronger and appears at much shorter time indicating higher elastic nature of the melt compared to the unfilled melt. Again, the concentration of LDH also influences the relative increase in the storage modulus of the nanocomposites. For a given rest period, the composition containing 7.5 wt% LDH shows much higher increase in storage modulus compared to the composition having 5.0 wt% LDH. This also explains why the magnitude of the stress overshoot during steady shear followed after a constant rest period increases with LDH concentration (**Figure 5.20**).

The dynamic oscillatory shearing at a low frequency showed previously (**Figure 5.12**) that at low

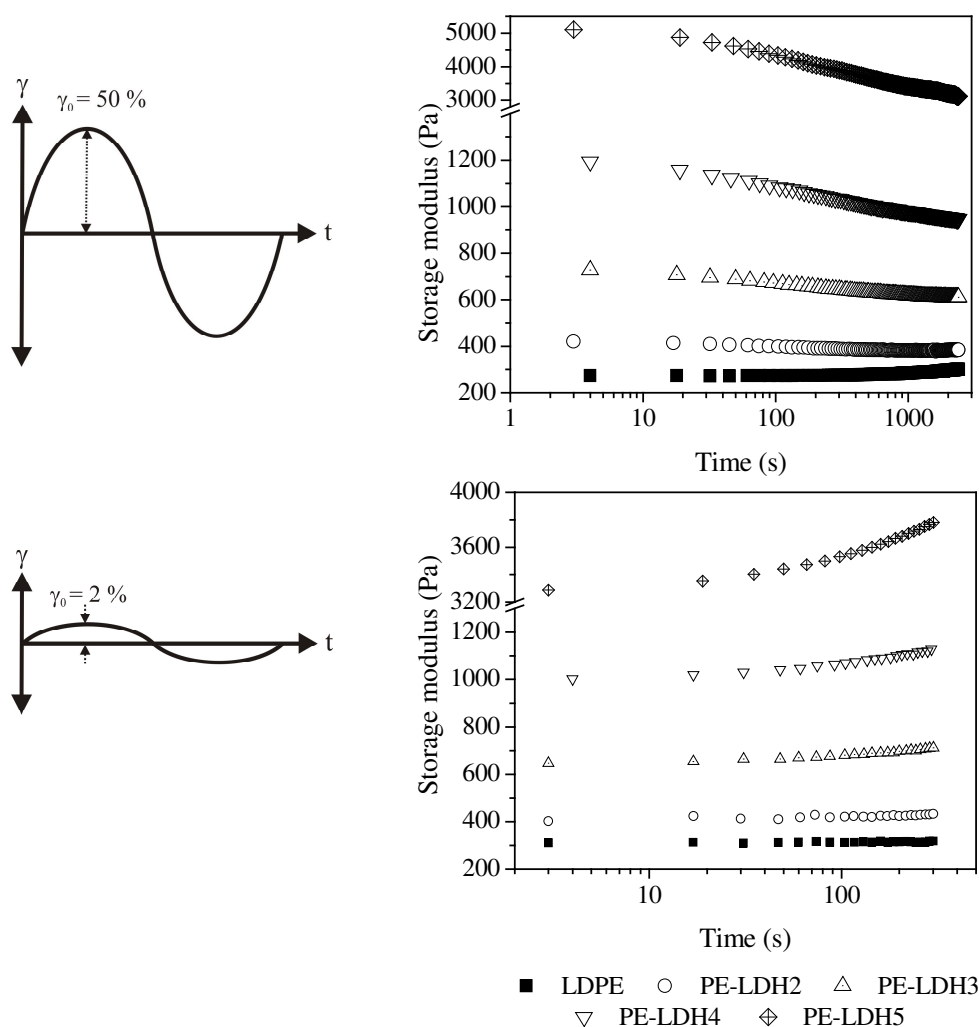


Figure 5.23 Plots showing the variation of storage modulus with time during oscillatory shearing in the non-linear viscoelastic regime (carried out at 50% strain amplitude and 1 rad/s frequency) (A) and linear viscoelastic regime (carried out at 2% strain amplitude and 1 rad/s frequency) (B).

strain amplitude the storage modulus of the nanocomposite melts remains constant and independent of the applied strain. But, above a certain critical strain (dependent on the LDH concentration), it decreases with increasing strain. This critical strain defines the strain limit at which linear viscoelastic response of the melt is transformed into non-linear one. Therefore, in principle, the kinetics of the structural breakdown of the microstructures and their regeneration processes can be investigated by subjecting the melts to two consecutive oscillatory shearing steps at constant frequency. First in the non-linear viscoelastic regime at strain 50 % (at a strain amplitude when both unfilled polyethylene and the nanocomposites shows strain dependent modulus) to study the structural breakdown with time and second in the linear viscoelastic regime at strain 2 % (at a strain when modulus is independent of strain amplitude) to study the regeneration of the structures. During both the shearing steps, storage modulus was monitored with time and the results are shown in **Figure 5.23**.

In **Figure 5.23A**, it can be observed that in case of PE/LDH nanocomposites, the storage modulus decreases with time. The continuous shearing at high strain amplitude causes structural breakdown in the nanocomposites resulting in a loss of their elastic character. It is also apparent that during the initial phase storage modulus decreases at faster rate and then approaches a steady state. At the beginning of shearing, the nanocomposite melts are in a state where relatively large aggregated structures and structured domains prevail and the rate of structure breakdown depends on their size and the shear rate [173]. As the shearing continues the average size of these microstructures is progressively reduced and hence also the rate of structure breakdown. When the steady state is achieved, there exists an equilibrium between structure breakdown and regeneration process. At this stage, the size of the particle aggregates and the structured domains are determined solely by the applied shear rate. The effect of LDH concentration on the rate of structure breakdown is also obvious as it determines both the extent and size of the structural association among the dispersed particles. Higher is the concentration of LDH, larger is the size and number density of particle aggregates and structured domains. On the contrary, in **Figure 5.23** the changes in storage modulus of the unfilled polyethylene is insignificant in comparison to the nanocomposites. It shows a small increase in shear modulus after prolonged period of shearing. This can be due to increase in molecular weight due to continuous shearing in the rheometer chamber at elevated temperature for long period. This seems logical as such increase in molecular weight is also observed in case of unfilled polyethylene after extrusion in twin screw extruder at 200 °C.

In **Figure 5.23B**, the effect of structure regeneration on the storage modulus of the nanocomposite melts is apparent. Since the shearing at low amplitude and low frequency does not affect the microstructures within a polymeric melt, the second shearing step can be treated as equivalent to the rest period previously described in the flow reversal experiment. During this shearing step the diffusion kinetics of the dispersed LDH particles are not affected by the small strain amplitude. As a result, the structure break down process stops and the force that generates elastic strain within particulate structure (ultimately leading to their breakdown) disappears. Consequently, the separated and oriented particles start to regenerate the structural features characteristic of the zero shear equilibrium state. Simple Brownian motion can not be held responsible for this regeneration process as the actual time scale of this regeneration process is much shorter as compared to the one obtained from Brownian dynamics involving highly anisotropic clay particles. Rather, a strong attractive interaction among the dispersed clay particles and thermodynamic incompatibility between the particle and polymer phase facilitate such fast diffusion of the clay particles within a highly viscous medium [150]. The structure regeneration causes exponential

increase in the storage modulus of the melt, which did not achieve steady state within the applied time period during the experiment. The effect of LDH concentration is also evident. May be the increasing particle concentration reduces the average inter-particle separation after structure breakdown, which results a relatively shorter diffusion path length during regeneration process. Hence, the rate of recovery increases with increasing LDH concentration in the nanocomposites.

5.3.3.3 Modeling of non-linear rheological behavior of PE/LDH nanocomposites

The rheological behavior of PE/LDH nanocomposite described in the previous sections provides a qualitative physical interpretation of the materials response during a steady shear experiment in the non-linear flow regime. These interpretations are not sufficient for the predictions of the magnitude and the time scale of the response. For example, to predict the magnitude of the stress overshoot peak and the time of its appearance (t_{max}) at an arbitrary shear rate, one needs accurate mathematical description of the materials response as a function of the applied shear rate. Such predictions are often very useful in proper designing of the processing parameters for polymeric melts that strongly depend on the flow behavior. Therefore, in the present section this has been tried based on the knowledge available in literatures for describing the flow behavior of polymeric melts. In analysing the PE/LDH nanocomposite compositions, the stress overshoot effect from the matrix alone was neglected primarily because its magnitude (not the normalized value) is negligible in comparison to the filled systems and also it appears at much higher time scale at a given shear rate. Secondly, the increasing amount of low molecular weight functionalized polymer reduces the stress overshoot tendency of the matrix phase. Thus, as the first approximation, the nonlinear viscoelastic response in filled PE/LDH nanocomposites system studied here may be ascribed to the presence of LDH agglomerate structures in various scales.

The appearance of overshoot can be readily described using the Wagner model [174, 175]:

$$\tau(t) = \int_{-\infty}^t M(t-t') \exp(-\beta|\dot{\gamma}(t,t')|) \dot{\gamma}(t,t') dt' \quad (5.4)$$

Here, the first term under integral is the memory function and the second exponential term is the damping function with the parameter β describing the strength of non-linearity. The term

$$\dot{\gamma}(t,t') = \int_{t'}^t \dot{\gamma}(t'') dt'' \quad (5.5)$$

depends on the history of strain rate for all past times $-\infty < t' \leq t$. For the sake of simplicity, we consider here the memory function to be in a form of the Maxwell model with only one relaxation mode:

$$M(t-t') = \left[\frac{\eta}{\lambda_0^2} \right] \exp[-(t-t')/\lambda_0] \quad (5.6)$$

where η and λ_0 are the viscosity and the relaxation time, respectively. Then for the start up of the shear flow one obtains a following solution:

$$\left[\frac{\tau(t)}{\dot{\gamma}_0} \right] = -\eta_i \left[\frac{\lambda_{\dot{\gamma}}^2}{\lambda_0^2} (1 - e^{-t/\lambda_{\dot{\gamma}}}) + \frac{t}{\lambda_0} e^{-t/\lambda_{\dot{\gamma}}} \left(1 - \frac{\lambda_{\dot{\gamma}}}{\lambda_0} \right) \right] \quad (5.7)$$

where the first term describes a monotonic increase of the shear stress and the second term describes the stress overshoot. The relaxation time of sheared system is given by:

$$\lambda_\gamma = \frac{\lambda_0}{1 + \beta |\dot{\gamma}_0| \lambda_0} \quad (5.8)$$

whereby λ_γ decreases with the increase in $\dot{\gamma}_0$. The decrease of a characteristic relaxation time with increasing shear rate in the case of filled nanocomposites can be interpreted as the decrease in the dimensions of an average filler agglomerate. Thus, the Wagner model implicitly assumes that the system structures become finer under the application of shear flow. It is clear that in reality a filled polymer system undergoes gradual breakage of its structure after the start up of the shear flow. Therefore, Lion et al. proposed a model in which the relaxation time undergoes a gradual decrease from the rest value of λ_0 till the stationary value of λ_{st} [176]. In the following, it is assumed that the relaxation time used in equation (5.3) is simply an average value between λ_0 and λ_{st} .

In the stress relaxation experiment, when the step strain γ_0 is applied at time $t = 0$, the Wagner model gives the following solution

$$\tau(t) = -\gamma_0 G(t) e^{\beta \gamma_0} \quad (5.9)$$

where,

$$G(t) = \int_{-\infty}^0 M(t - t') dt' \quad (5.10)$$

is the linear viscoelastic relaxation modulus determined at $\gamma \rightarrow 0$. Equation (5.9) expresses the principle of time-strain factorization, i.e. that the nonlinear relaxation modulus

$$G(t, \gamma_0) = G(t) e^{\beta \gamma_0} \quad (5.11)$$

can be factored into a function of time alone and a function of strain alone. This factorization is indeed observed experimentally for silicate-based intercalated nanocomposites, except at very short times (about 10s), thus justifying the estimation of long relaxation times from the stress relaxation curves.

The Wagner model proved itself over years to be quite useful for description of the nonlinear viscoelastic properties of commercial polymer melts. However, polymer nanocomposites represent much more complex systems than the pure melts due to the presence of inhomogeneous filler structure and possible filler-polymer and filler-filler interaction. The first problem confronted in this study is that behavior of the samples strongly depends on the history of their preparation. Further, the filler structure has been found to change constantly in non-linear shear experiments and this cannot be described in the frame of original Wagner model with β equal to a constant. Therefore, to describe the non-linear rheological behavior of the present nanocomposite system, modification of Wagner model was necessary.

In order to explain the experimentally observed behavior in the nanocomposites melts, the non-linearity parameter β in original Wagner model was considered to vary with time during steady shear until a steady value is reached at equilibrium. This parameter can now be given a special name i.e. structural variable. The instantaneous value of $\beta(t)$ as a function of time during steady shear can be written as

$$\beta(t) = \beta_{st} + (\beta_0 - \beta_{st}) \exp\left(-\frac{t}{T_b}\right) \quad (5.12)$$

where, β_0 and β_{st} represent the initial and the steady state values, respectively. T_b is the relaxation time under steady shear, which can be extracted from the steady shear experiment. During flow reversal experiments, there occurs structural regeneration during the rest period and hence to describe this behavior β was allowed to increase with time following the equation

$$\beta(t_{rest}) = \beta_{st} + (\beta_R - \beta_{st}) \left[1 - \exp\left(-\frac{t_{rest}}{T_R}\right) \right] \quad (5.13)$$

where $\beta_R < \beta_0$ is the maximal value of structural variable which can be achieved after the recovery process and T_R is the regeneration time of the LDH structure. T_R , which is at least one order of magnitude larger than the longest relaxation time in the presence of shear flow, is presumably defined by the diffusion kinetics of the filler particles in the melt in a quiescent state.

Further, it is observed that stationary viscosity of the nanocomposites during steady shear is only slightly affected by the rest time. Thus, one has to eliminate the shear thickening effect caused by the increase of structural variable. In the present modification of Wagner model, it was assumed that viscosity in the second shearing cycle also depends on the rest time:

$$\eta(t_{rest}) = \eta_i \frac{\lambda_0^2}{\lambda_y^2 (\beta(t_{rest}))} \quad (5.14)$$

It is plausible to assume that the filler structure will undergo further breakage in the shearing cycle followed after the rest period, which can be described by the decrease of structural variable from $\beta(t_{rest})$ to some smaller value β_{end} :

$$\beta(t - t_2) = (\beta(t_{rest}) - \beta_{end}) \exp\left(-\frac{t - t_2}{T_B}\right) + \beta_{end} \quad (5.15)$$

where, t_2 is the sum of first shear cycle time and the rest period. This decrease is found to be much less pronounced than that in the preshearing cycle: theoretical curves can be only fitted to the experimental data (**Figure 5.24**) if one assumes that $\beta(t_{rest}) - \beta_{end} \leq 0.02$; moreover, this value seems to be independent on the rest time. Presently, this puzzling behavior is not clearly understood and can be guessed that during the rest time the filler clusters reorganize themselves in some other kind of superstructure that can not be broken as easily as the initial structure in freshly prepared samples.

Figure 5.24 shows a fit of the flow reversal experiment for the PE/LDH nanocomposite (LDH concentration about 5.0 wt%) using equations (5.12)-(5.15). The main discrepancy is observed for $t_{rest} = 0$ when the sample is immediately sheared (zero rest period) in the reverse direction. The stress calculated theoretically grows much slower than that measured experimentally (similar discrepancy for $t_{rest} = 0$ has been obtained in the frame of structure network model [177]). Otherwise, the modified Wagner model provides a reasonably good fit of the flow reversal experiment that can be improved further assuming a multi-exponential dependence of the β recovery.

To interpret the nonlinear shear experiments, the Wagner model was chosen and allowed the nonlinear parameter β to change with the history of shear application. This approach is capable to interpret the change in the microstructure in the nanocomposite melts in terms of a macroscopic structure parameter, which changes with the changing filler structure both under steady shear and quiescent condition. The PE/LDH nanocomposites, like many polyolefin/layered silicate based nanocomposites, represent however a highly inhomogeneous system with almost unknown interactions between the silicate particles and

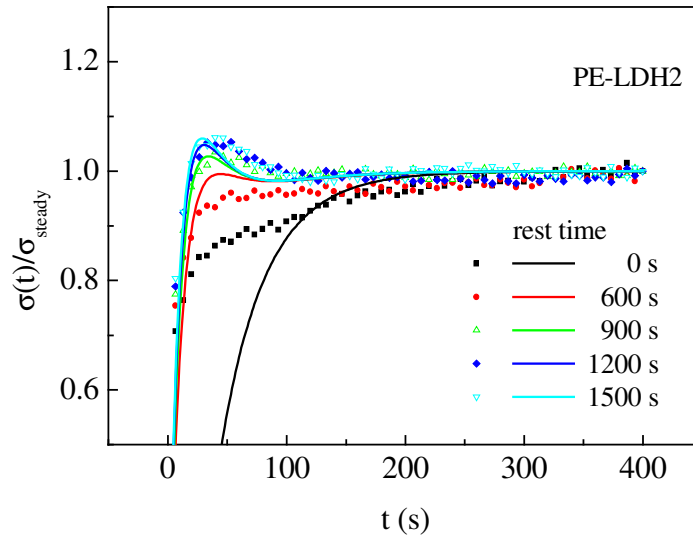


Figure 5.24 Reverse shear flow experiment for the nanocomposite PE-LDH2: $|\dot{\gamma}|$. Symbols - experiment; lines - modified Wagner model in which $\beta(t)$ is given by eq. (5.11). $\beta_R = 0.14$, $\beta_{st} = 0.02$, $T_R = 500s$, $\beta(t_{rest}) - \beta_{end} = 0.02$, $T_B = 50s$, $\lambda_0 = 30s$

the particles and polymer matrix. Therefore, this has not been intended to provide a microscopic description of the structural evolution in the PE/LDH nanocomposites, but rather to extract some regularities. It is clear that the structural variable β correlates with an average dimension of the filler aggregates. It was found that the structural β changes differently depending on the direction of approaching the steady state. In overall, structural behavior of the PE/LDH nanocomposites under shear flow is similar to the behavior of filled elastomers for which breakdown of filler clusters at increasing strain and their re-aggregation with decreasing strain was observed under oscillatory shear (Payne effect [153]). In both cases, only partial recovery of the initial structure has been observed.

5.4 Mechanical Properties and Fracture Behavior

The mechanical properties of PE/LDH nanocomposites are shown in details in **Figure 5.25**. It is apparent that, LDH clay does not act as a reinforcing filler for PE matrix. The yield strength value steadily decreases with increasing LDH concentration. Whereas the tensile modulus increases significantly in the nanocomposites. Up to about 10.0 wt% LDH concentration, the changes in mechanical properties, especially the yield strength and elongation at break are not very significant. The nanocomposites at low LDH concentrations show similar mechanical and fracture behavior as compared to the unfilled PE. However, beyond 10 wt% LDH concentration, the materials undergo brittle failure with low yield strength and elongation at break.

In comparing the mechanical properties based on **Figure 5.25** one important factor should be kept in mind. The influence of low molecular weight functionalized polymer (PE-g-MAH) on the mechanical properties can be very significant [152]. It has been observed that such low molecular weight fraction reduces the tensile strength and yield strength of the unfilled matrix. In the present case, each nanocomposite composition contains functionalized polymer twice the amount of LDH. Therefore, comparison

of the mechanical properties of the nanocomposite compositions with that of the unfilled PE does not reflect the true information on the reinforcing nature of the LDH clay. Because, the reference unfilled material in every case is not pure PE rather a blend of PE and PE-g-MAH with increasing proportion of the latter. In fact, when a nanocomposite composition is compared with corresponding blend matrix, significant improvement in tensile strength is observed [152].

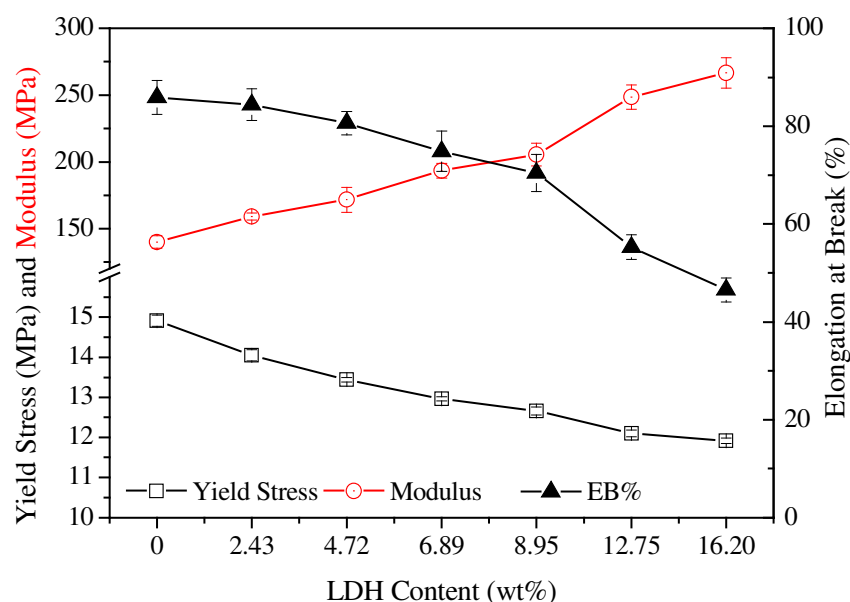


Figure 5.25 Mechanical properties of PE/LDH nanocomposites

Investigation of the nature of fracture surface morphology of the tensile fractured is useful in gaining information not only about the nature of filler particle distribution, but also how the failure takes place within the matrix, within filler particle aggregates and especially at the particle-polymer interface. **Figure 5.26** shows the general overview of the tensile fractured surfaces of unfilled PE and the PE/LDH nanocomposite compositions. The unfilled PE shows very uniform morphological features of the fractured surface with characteristic shear band formation indicating ductile failure of the matrix. The long parallel bands are observed throughout the fractured surface (**Figure 5.26a**). In presence of both nano and microscopic LDH particles, the fracture behavior changes gradually from a ductile nature at low LDH concentration to a highly brittle nature at high LDH concentration. The volume of polymer that undergoes yielding determines the total energy absorption and the ultimate mode of fracture in case of filled thermoplastics. At low LDH concentrations (for example PE-LDH1 and PE-LDH2), the fractured surface reveals the presence of isolated and non-aggregated primary LDH particles (platelets) in large numbers. The similar morphological feature is also observed in TEM analysis of these compositions at low LDH concentrations. These isolated LDH particles show poor adhesion to the PE matrix on their surface resulting in the formation of voids around them during tensile deformation of the sample. As a result, a small concentration the LDH particles cannot affect the ductile failure of the matrix. However, with increasing concentration, formation of secondary structures by these primary particles are noticed in the fractured surface morphology and the polymer matrix in the vicinity of these particle aggregates mainly undergo brittle failure. The interface also appears rough with clear sign of adhesion of the matrix on the particle surface. This becomes more prominent and more frequent at high LDH concentration such

as in PE-LDH4, PE-LDH5 and PE-LDH6. As a result, the large scale plastic flow characteristics as observed on the fractured surfaces of unfilled PE and the PE/LDH nanocomposite composition having low LDH concentration are greatly reduced in case of the nanocomposites having high LDH concentration **Figure 5.26d-f**.

The low magnification SEM images of the composition PE-LDH2 as shown in **Figure 5.27a**), reveals that the sub-micron sized LDH primary particles are discretely dispersed throughout the matrix. In addi-

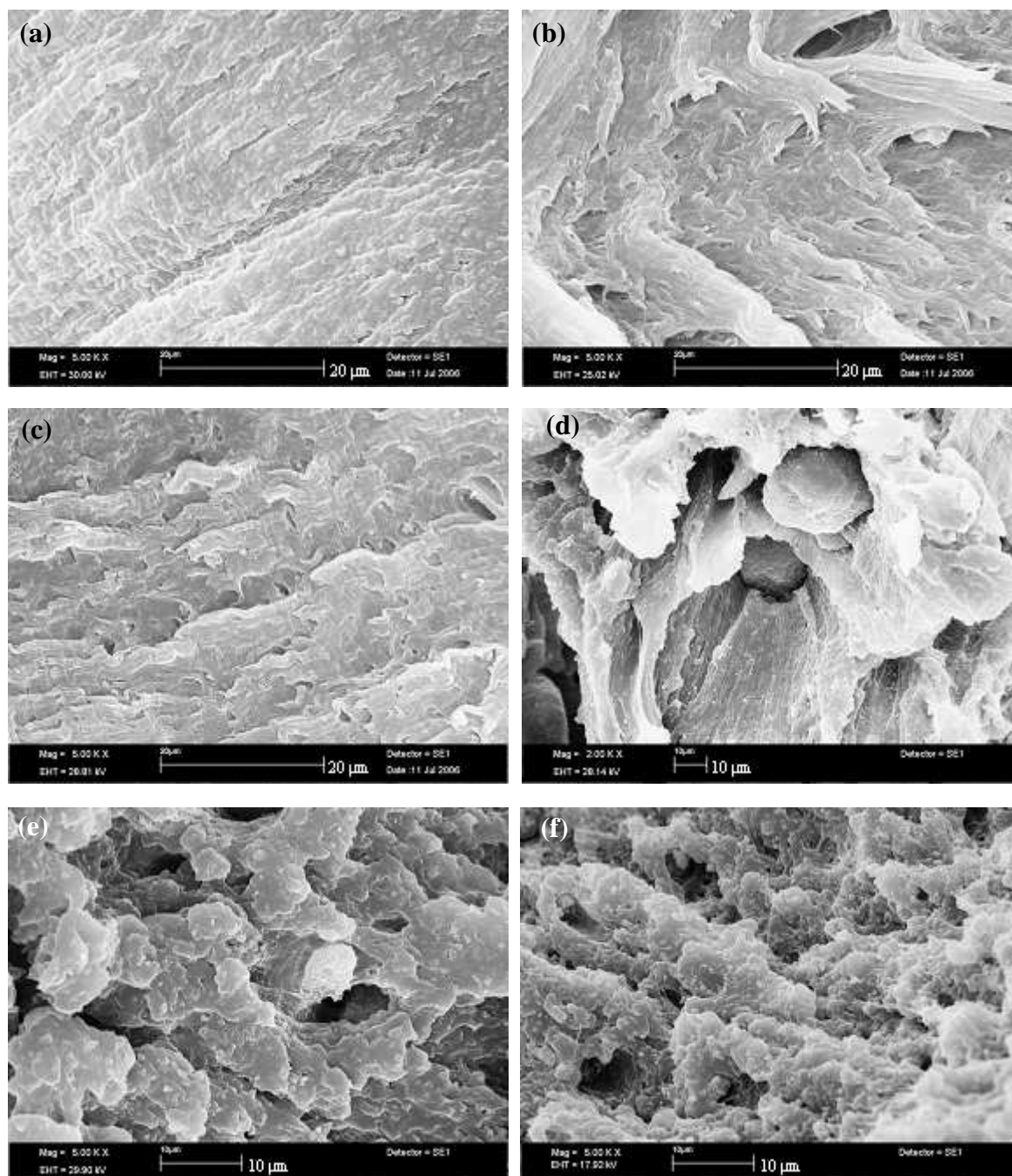


Figure 5.26 SEM micrographs showing the fracture surface morphology of PE/LDH nanocomposite: (a) unfilled PE, (b) PE-LDH1, (c) PE-LDH2, (d) PE-LDH3, (e) PE-LDH4 and (f) PE-LDH5

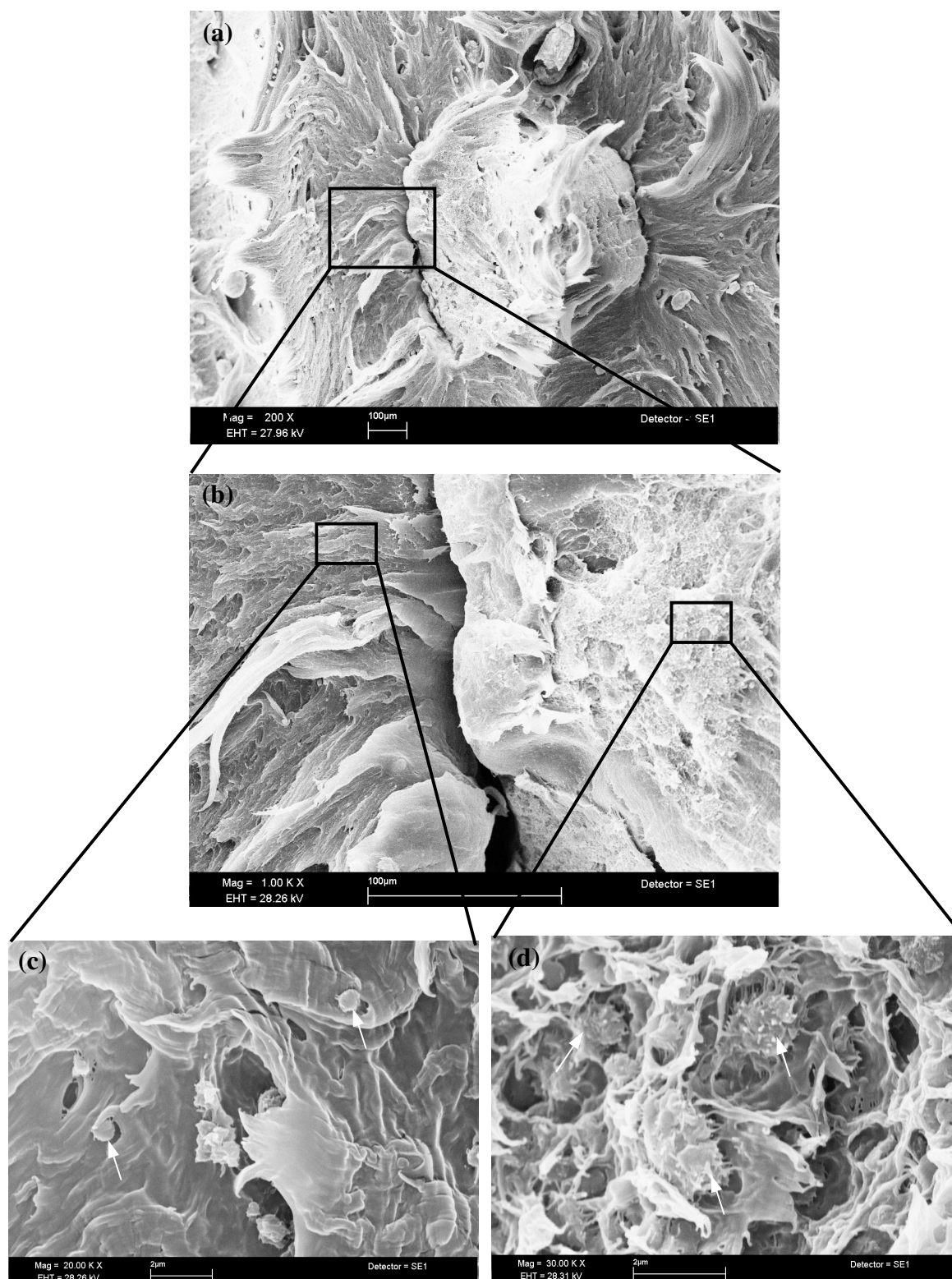


Figure 5.27 SEM images of fractured surface of PE-LDH2 sample showing morphology at different region of the matrix: (a) overall morphology (magnification 200X), (b) at the interface of particle rich and particle devoid regions (magnification 1KX), (c) particle devoid region (magnification 20KX) and (d) particle rich region (magnification 30KX) (the black arrows show the individual or small stacks of LDH platelets)

tion, they also form large particle clusters of sizes ranging from few micrometer to above 100 micrometer (similar features are observed more frequently at higher LDH concentration). The formation of large cracks during tensile fracture at the interface between these clusters and the bulk matrix is also apparent (**Figure 5.27b**). However, the high magnification SEM images show that these large clusters are actually the regions or the domains of high concentration of LDH particles. These particles are present either as single or small stacks of platelets in these domains and show strong adherence to the matrix. This can be speculated from the nature of the interface in this region (**Figure 5.27d**). During the tensile yielding, the particle-polymer interface is strained substantially and this causes the pulling out of the matrix adhered to the LDH particle surface or entrapped withing large particle clusters. This often results in the formation of pullout matrix strands that bridge the widening gap at the interface, which has been clearly demonstrated in **Figure 5.27d** and **Figure 5.28**. The failures of matrix in the LDH particle rich domains and the bulk matrix are distinctly different. In case of former, the failure is apparently brittle type and show

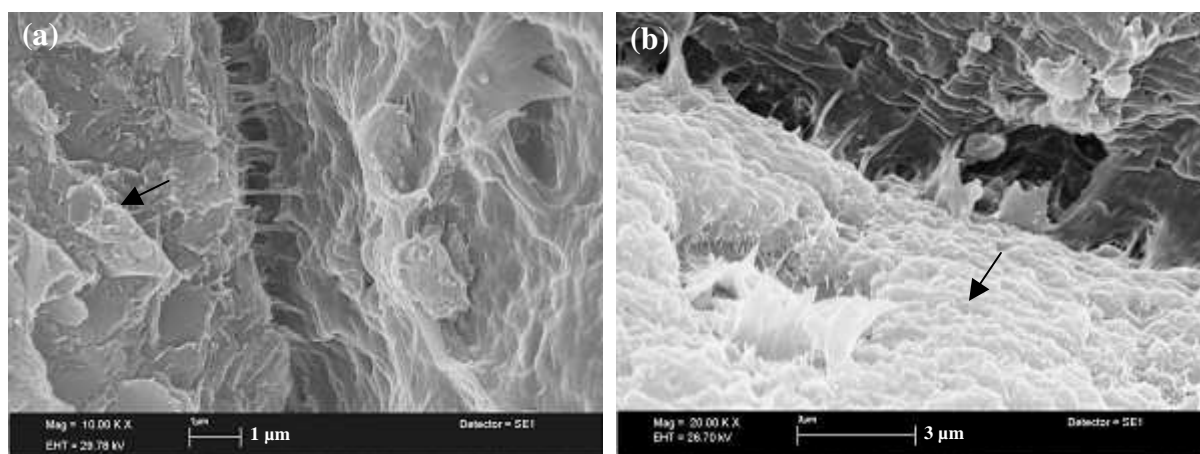


Figure 5.28 The bridging effects at the interface between the particle rich region (indicated by arrow) and particle devoid region in PE/LDH nanocomposite compositions containing (a) 4.72 wt% and (b) 16.20 wt % LDH

no large scale plastic flow around the LDH particles. In contrast, the bulk matrix, where discrete LDH particles are dispersed suffers preferably a plastic deformation. The weak particle-polymer interaction in these regions is evident from the appearance of smooth interface (**Figure 5.27c**). During tensile failure, cracks are easily developed between these two regions indicating a weak interface that undergoes easy failure during under stress. With increasing LDH concentration number of such concentrated particulate domains increases, which may be the major cause of significant lowering of mechanical strength. The question is what causes the formation of such concentrated particulate domains in the nanocomposite. The answer probably lies in the preparation technique of these materials. Since, LDH is added to PE not directly, but as its masterbatch (which is again the principle behind the most widely used techniques for polyolefin based nanocomposite preparation by melt compounding) with functionalized polyethylene (PE-g-MAH). The granules of LDH masterbatch and unfilled PE are melted and mixed in extruder. May be the shearing action of the extruder screw cannot force homogeneous distribution of strongly associated LDH particles (present in a masterbatch containing 50.0 wt% LDH) between PE-g-MAH and PE phases. Though, PE-g-MAH is used as the compatibilizer between LDH and matrix, homogeneous dis-

tribution of LDH in the final composite matrix requires the complete melting of the masterbatch granules and subsequent breakdown of the particle clusters present in the masterbatch followed by the distribution of LDH/PE-g-MAH association within PE matrix. Since, PE-g-MAH bonds more strongly to LDH particle surface than polyethylene chains [178], a fraction of LDH/PE-g-MAH cluster might still remain unbreakable after the extrusion process. It is therefore obvious that the extrusion conditions (temperature, feed rate, screw geometry and screw speed) should strongly influence the particle morphology in polymer/clay nanocomposites [137]. In addition, during the injection molding process (used to prepare tensile test specimen), a part of the fragmented or exfoliated LDH particles formed during extrusion may undergo reagglomeration or orientation creating particle concentrated domains.

The nature of failure at the interface between a particulate domains and the bulk matrix varies widely. Sometimes, the interface fails abruptly (as evident in **Figure 5.27b**) showing poor stress transfer between these two regions. Often considerable extent of interpenetration of the matrix is also observed between them. The typical representation of this is given in **Figure 5.28**. The bridging of the fractured interface by stressed matrix strands is a clear evidence of interpenetration of the PE matrix within the particulate regions or clusters, which is helpful for efficient stress transfer between the two regions. However, the large size of these clusters along with strong particle-particle and particle-polymer interactions make them brittle and thus explain lower mechanical strength of the composite as a whole,

FLAMMABILITY PROPERTIES OF LDH BASED COMPOSITES

6.1 PE/LDH Nanocomposites

6.1.1 Flammability Study by LOI

One of the major objectives of the present investigation is to study the efficiency of LDH nanofiller as a potential flame retardant for polymers, especially polyethylene. In this regards, the evaluation of the composite materials in terms of limited oxygen index (LOI) provides the first hand information on the effectiveness of fire retardant additives or so called flame-retardants [4]. For PE/LDH nanocomposites containing LDH up to 16.20 wt%, the LOI values are shown in **Figure 6.1**. The unfilled PE has a

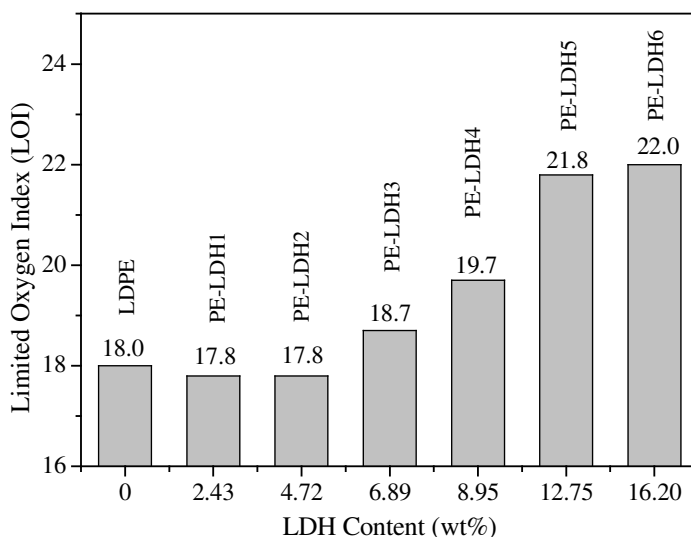


Figure 6.1 Limited oxygen index (LOI) of PE/LDH nanocomposites (the value shown have ± 0.5 unit variation)

LOI value of 18.0 and the addition of small amount of LDH (as in PE-LDH1, PE-LDH2) results in no significant change in the LOI value. Rather, a small decrease is observed below the LDH concentration of 5.0 wt% . However, at higher level of LDH content (as in PE-LDH3 and the above), the LOI value increases with increasing LDH content. The nanocomposite containing 16.2 wt% LDH shows an LOI value around 22.0, which is significantly higher than that of the unfilled PE, but still further improvement

is necessary for industrial acceptance.

Although the LOI value is merely expressed as a number indicating the minimum percentage of oxygen required for self-sustained combustion of a polymeric material, this test method can also be used to analyze how the materials burn at oxygen concentration corresponding to LOI value and also close (from lower side) to it. During the LOI test measurements, flame propagates vertically downward along the burning test specimen. The propagation first takes place through the surface layer and then finally reaches the core of the sample. The basic difference between burning of unfilled PE and PE/LDH nanocomposites is that in case of former no char/burn residue is formed. During burning, the unfilled PE is first converted into melt, which burns like candle with continuous dripping of the melt till the whole sample is lost. The burning behavior of the LOI test piece in case of the PE/LDH nanocomposites is quite different. While burning, three distinct regions can be identified on the burning surface. The top or the skin layer consists of the burn residue/char, which remains supported by melt region beneath. In the melt region, convective material flow and the decomposition of LDH particles lead to bubbling of gaseous materials (most probably water vapor and carbon di/mono oxide) through the melt layer. The third region is the unburnt bulk material below the molten layer and on this the above two regions (i.e. the char and the molten layer) rest. Sufficient heat energy from the flame-front must be conducted through the char layer to the melt region for sustaining the burning process. Thus, the char layer acts as a physical barrier against the propagation of the flame downward along the LOI sample. At low LDH concentration, the amount of char layer formed and hence its thickness on the burning surface is very small. As a result, the char can not provide efficient barrier effect and the test piece burns quite easily at similar oxygen concentration as that for unfilled PE. With the increasing LDH concentration both thickness of the char layer and the endothermic decomposition contribution of the clay increases. This makes the self-sustained burning of the sample more and more difficult at low oxygen concentration, thus increasing the LOI value with LDH concentration. The influence of the char layer is also dependent on the melt region formed beneath. The ability of the char layer to remain fixed and integrated on the burning test piece not only depends on its structural rigidity, but also on the flowability (in other word viscosity) of the melt region. At low LDH concentration, the viscosity of melt is not sufficient to hold the residue on the vertically placed test specimen. As a result, it falls down and a fresh unburnt surface is continuously exposed to flame resulting in spontaneous burning of the test specimen at relatively lower oxygen concentration. However, at higher LDH concentration, the high viscosity of the melt prevents the easy slippage of the char layer from the sample stock. Therefore, the melt viscosity plays an important role in determining the LOI value of the PE/LDH nanocomposites. In fact, this is also true for the conventional polyolefin/metal hydroxide type flame-retardant composites. To obtain similar LOI value with these conventional metal hydroxides, much higher filler loading is required. The inefficient char formation as described above can be a potential reason for this. The melt viscosity of these conventional composites at similar filler loading is much lower compared to LDH based nanocomposites. The later shows an abrupt increase in low shear viscosity beyond 5 wt% LDH concentration in comparison to the unfilled melt (**Figure 5.17**). The contribution from the char during flame inhibition is a part of the story. The endothermic decomposition of the LDH particles also play vital role as it reduces the supply of heat for the combustion process. As a result, more oxygen is required to sustain the flame, i.e. the LOI value increases. While burning at oxygen concentration lower than that indicated by the LOI value of the respective nanocomposite sample, the test piece though catches the flame, but the flame is extinguished

after some time whereas it burns continuously at LOI.

6.1.2 Flammability Study by UL94

UL94 testing was carried out using two norms one vertical burn test (UL94V) and the other horizontal burn test (UL94HB). The PE/LDH nanocomposites containing LDH up to 16.20 wt% did not pass any of the UL94V test specification. All the samples start burning spontaneously after first 10 s flame application, which continued until the test specimen was completely burned up to the sample holding clamp. However, the UL94V burn test provides useful information regarding the dripping behavior of these composite materials. The dripping of the burning melts can accelerate the spread of flame through secondary flaming during a real life burning situation. Although all the PE/LDH nanocomposite samples show dripping while burning, the time at which dripping starts is significantly delayed by the presence of LDH. A parameter called time to start dripping is defined as the time after the first 10 s-flame-application at which the dripping starts and the the piece of cotton kept underneath is ignited by the dripping melt. As shown in **Figure 6.2**, the time to first dripping increases steadily with increasing LDH concentration

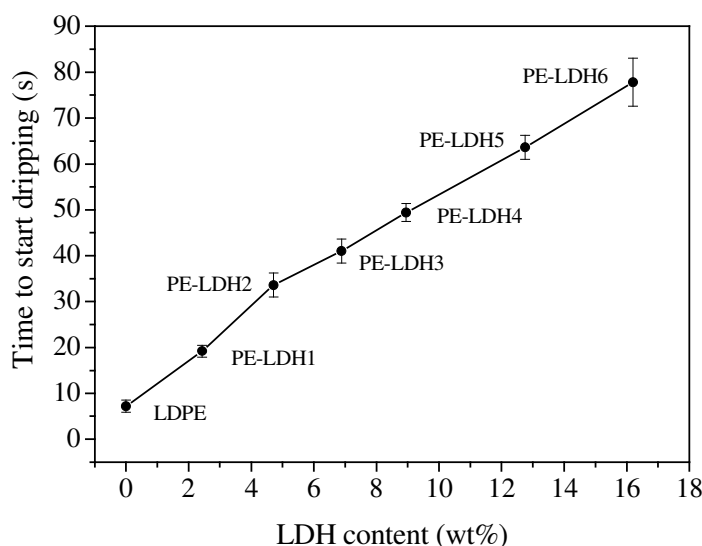


Figure 6.2 The effect of LDH loading on the dripping tendency of the PE/LDH nanocomposites (Time to start dripping is the time after first 10 second flame application at which first dripping occurs that ignites a piece of cotton underneath during UL94V testing)

in the nanocomposites and becomes more than ten times at 16.20 wt% LDH in PE-LDH6. Similar, trend was also observed in case of polypropylene/layered silicate based nanocomposites, where the nanocomposite showed improved dripping behavior compared to unfilled polypropylene [68]. The slow and much delayed dripping tendency in PE/LDH nanocomposites are caused by the high melt viscosity of the nanocomposites, which increases with increasing LDH concentration. While in case of unfilled PE dripping starts in the form of a continuous stream of burning melt, that in presence of LDH takes place in the form of chunks of glowing residue. **Figure 6.3** shows the typical dripping behavior of the unfilled PE and a PE/LDH composition (PE-LDH5) at comparable time after the first 10s-flame-application. The UL94 horizontal burn test showed better flammability performances of the PE/LDH nanocomposites as compared to the pure polyethylene. The nanocomposites containing 4.72 wt% (PE-LDH2) or higher

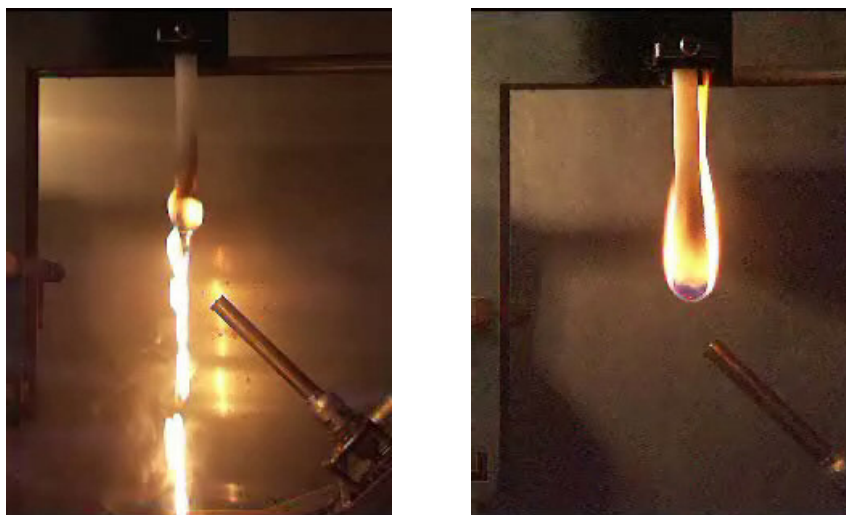


Figure 6.3 Dripping behavior of unfilled PE (left) and PE/LDH nanocomposite containing 12.75 wt% LDH (PE-LDH5) (right) (pictures were taken approximately after the same time period from the cessation of first 10 s flame application during UL94V test)

LDH easily passed the UL94 HB rating. This test method is also used to determine the rate of burning (expressed as mm/min) of the testing material. In PE/LDH nanocomposites, increasing LDH concentration significantly delays the burning rate as can be observed in **Figure 6.4**. When LDH concentration is increased above 10.0 wt%, the specimen burns extremely slowly.

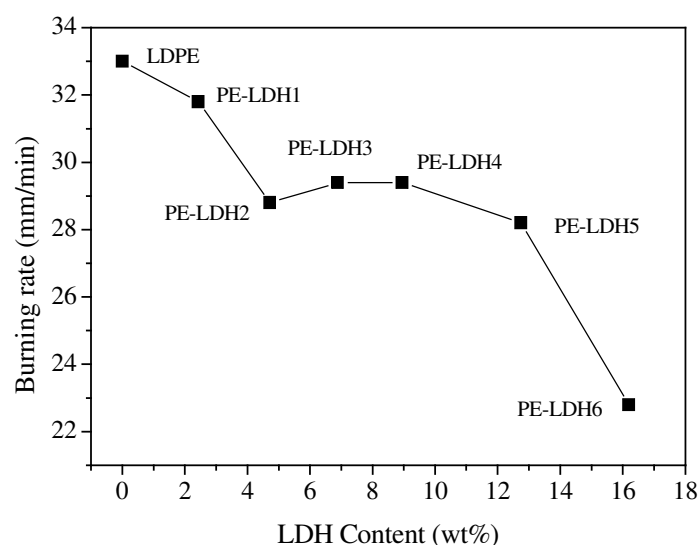


Figure 6.4 Influence of LDH loading on the rate of burning during UL94 HB test (at each composition average of three measurements were taken)

6.1.3 Flammability Study by Cone Calorimetry

The cone calorimeter investigation is a very popular and standard method for ranking and comparing the flammability properties of polymeric materials. During a cone calorimeter investigation, the test

specimen is burned under a forced flaming scenario using a constant external heat flux to maintain the sustained combustion of the test sample. Therefore, the test results from cone calorimeter are more significant in practical flammability evaluation of the specimen compared to the results obtained from tests that depend on material's heat of combustion for sustaining the combustion process, like LOI and UL94 test methods. The results from the cone calorimeter investigations for PE/LDH nanocomposites

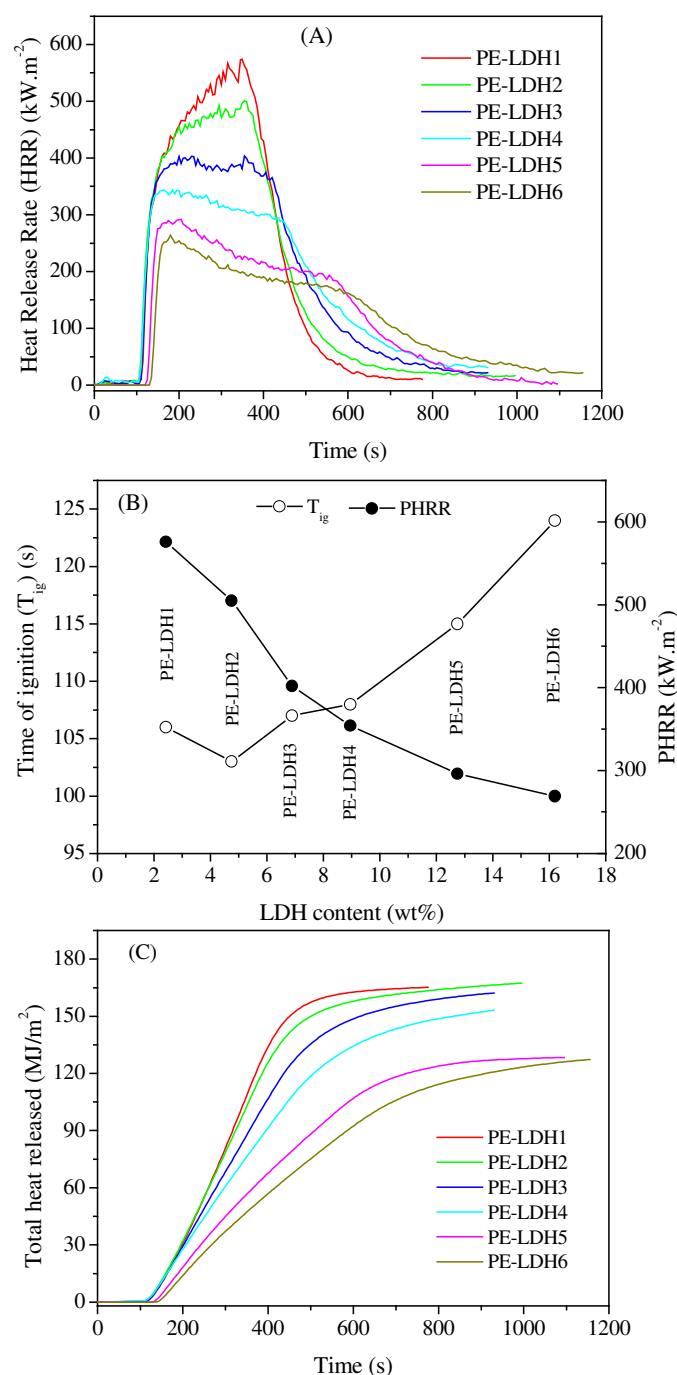


Figure 6.5 Cone-calorimeter investigation results showing (A) variation of heat release rate (HRR) with time, (B) total heat released (THR) with time and (C) variation of time of ignition (t_{ig}) and peak heat release rate (PHRR) with LDH concentration in the PE/LDH nanocomposites.

are summarized in **Figure 6.5 to 6.9**. The testing unfilled polyethylene was deliberately avoided as during its combustion mass loss occurred due to melt dripping, which was not possible to eliminate with the used experimental set up. This mass loss due to melt dripping resulted incomplete combustion of the test sample and hence results obtained were not conclusive.

Heat release rate (HRR) is the single most important variable, which controls how fast a fire can reach an uncontrollable stage. This single parameter provides information regarding the size of the fire and how fast it grows. The effectiveness of a fire retardant additive in polymer can also be assessed with respect to this parameter. **Figure 6.5 A and B**, show that with increasing concentration of LDH in PE/LDH nanocomposites, the maximum of HRR (called peak heat release rate or PHRR) is significantly reduced. In addition to that, the HRR versus time plots shows a plateau effect with longer combustion time with lower HRR. This means that the burning rate of the nanocomposites decreases significantly with increasing LDH concentration. In case of unfilled PE, cone calorimeter investigation under similar external heat flux (30 kW/m^2 and 35 kW/m^2) results in a PHRR value over 800 kW/m^2 [179, 180]. The addition of small amount of LDH causes a reduction in PHRR value below 600 kW/m^2 . At higher LDH concentration (as in PE-LDH4, PE-LDH5 and PE-LDH6) the PHRR is further reduced to below 300 kW/m^2 . The ignition of unfilled PE is followed by the formation of molten surface layer on which the flame floats. The ignition time (t_{ig}), parameter defined as the time at which the test specimen catches the flame and it is sustained over the entire surface of the specimen, is also significantly increased with increasing LDH content. A t_{ig} value below 100 s is observed in case of unfilled PE, which increases to above 120 s with 16.20 wt% of LDH content in the nanocomposites (PE-LDH6) (**Figure 6.5B**). This indicates that the resistance against ignition is improved in presence of LDH and with increasing LDH concentration. The total heat released (THR) is a parameter that determines the size of a fire. Once the ignition takes place, THR steadily increases with burning time and attains a steady state before the flameout occurs. The variation of THR with burning time is shown in **Figure 6.5C**. It is clear that THR is progressively reduced with increasing LDH content. At 10 min, THR reduced by about 17.0 % and 44.0 % in the samples PE-LDH4 and PE-LDH6 in comparison to the sample PE-LDFH1.

The efficiency of a flame-retardant can be evaluated in terms of relative change of THR and the ratio PHRR/t_{ig} with increasing flame-retarding concentration in the composite. The total heat released (THR) is often taken as the measure of the propensity to sustain a long duration fire. An efficient flame-retardant should reduce THR effectively when incorporated into a polymer. In this respect, LDH fillers have definite advantage over layered silicate type nano fillers as flame-retardants. The presence of layered silicate nano fillers in a polymer nanocomposite does not cause any significant change in the THR value in comparison to unfilled polymer even if the concentration of the filler is increased [181]. This is because the layered silicates are chemically inert and its inorganic content is not changed much during the combustion of the composites. Hence the heat of combustion of the layered silicate based composites remains the same as that of the unfilled polymer. They simply act as a physical barrier between the flame front and the burning surface. On the other hand, LDH takes part actively in combustion process through endothermic decomposition, which act as the heat sink reducing the total heat generated during combustion. So it significantly reduces the total heat released. The ratio PHRR/t_{ig} gives a measure of how fast a fire can grow during burning process or more precisely related to the propensity to cause fast growth of fire. Like, having low THR, an efficient flame-retardant should also give a low value of this ratio. In fact, when THR is plotted against PHRR/t_{ig} , the position of a good flame-retardant composites would

be close to origin [107]. **Figure 6.6** shows a comprehensive assessment of PE/LDH nanocomposites using this principle. It is obvious that increasing LDH concentration not only reduces the THR, but also the PHRR/t_{ig} ratio. Beyond certain LDH concentration, the position of the nanocomposites in THR versus PHRR/t_{ig} co-ordinate system, sharply bend toward origin with increasing LDH concentration. This is certainly a promising development in comparison to the performances of layered silicate based nanocomposites. In case of polyolefin/layered silicate based composites, it has been observed that with increasing filler concentration PHRR/t_{ig} ratio decreases significantly. But, since the THR value remain roughly constant, the positions of this system lies parallel to PHRR/t_{ig} axis in similar plots as in **Figure 6.6**. These results shows LDH has definite advantage over inactive layered silicate type nanoclay as flame-retardant in polymer.

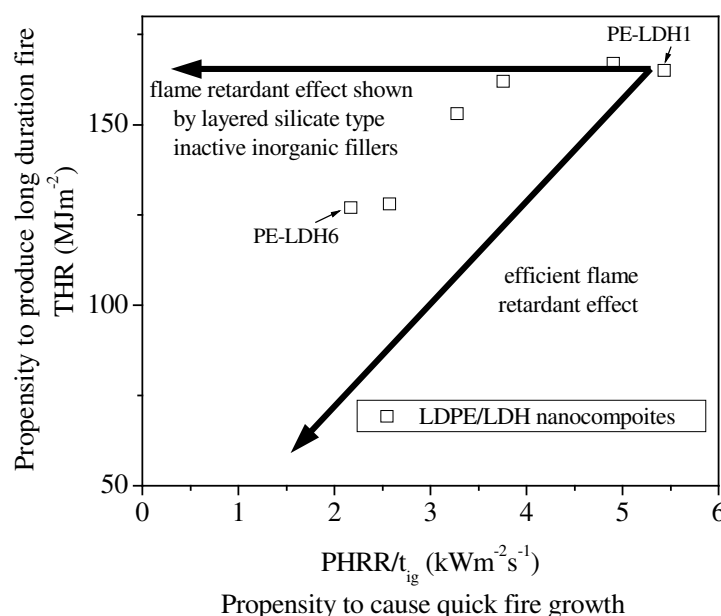


Figure 6.6 Graphical assessment of fire risk associated with PE/LDH nanocomposites, plotting THR against PHRR/t_{ig} for different LDH concentration (the LDH concentration increases from right to left as shown)

Figure 6.7 shows the influence of LDH loading on rate of carbon dioxide (CO_2) and carbon monoxide (CO) emission during combustion. During first 500 s of combustion of the nanocomposites in cone-calorimeter, the rates of release of CO_2 and CO are reduced significantly with increasing LDH concentration. But, beyond 500 s, the unfilled PE and the PE/LDH compositions with low LDH concentration show drastic drop in the release rates of these two gases. This is attributed to the increase in the burn time with increasing LDH concentration, which results a steady but prolonged release of these two gases. For examples the total burn time (the time at which flame-out takes place during cone-calorimeter combustion test) in PE-LDH1 is about 660 s and that in case of PE-LDH6 is above 1000 s.

Like HRR, mass loss during combustion is an important aspect that indicate how fast the material is burning. Usually, unfilled PE shows very rapid mass loss after the ignition of the test specimen. The material first undergoes melting followed by the decomposition into volatile fragments, which escape from the surface to the flame zone causing rapid mass loss. In presence of LDH, the endothermic decomposition of hydroxide layer produces the cooling effect in the surrounding, which slows down the

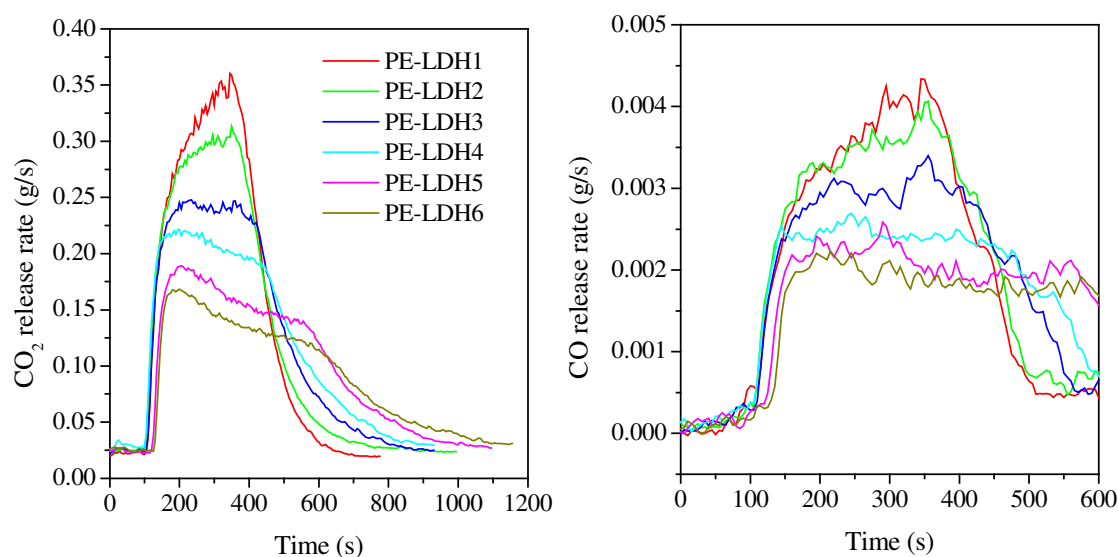


Figure 6.7 The variation of carbon dioxide (CO₂) and carbon monoxide (CO) release rate during combustion in a cone calorimeter chamber with burning time.

thermal decomposition of the hydrocarbon chain resulting in lower rate of mass loss. The residue formed after decomposition of LDH creates barrier effects against heat flow from the flame zone to the burning surface and also against the diffusion of oxygen and volatiles. All these effects together cause reduction in mass loss with increasing LDH content in the nanocomposites. **Figure 6.8** shows the mass loss with time (left) and variation of average specific mass loss rate with LDH content. It is obvious that mass loss rate is maximum immediately after the ignition and then slows down. With increasing LDH content,

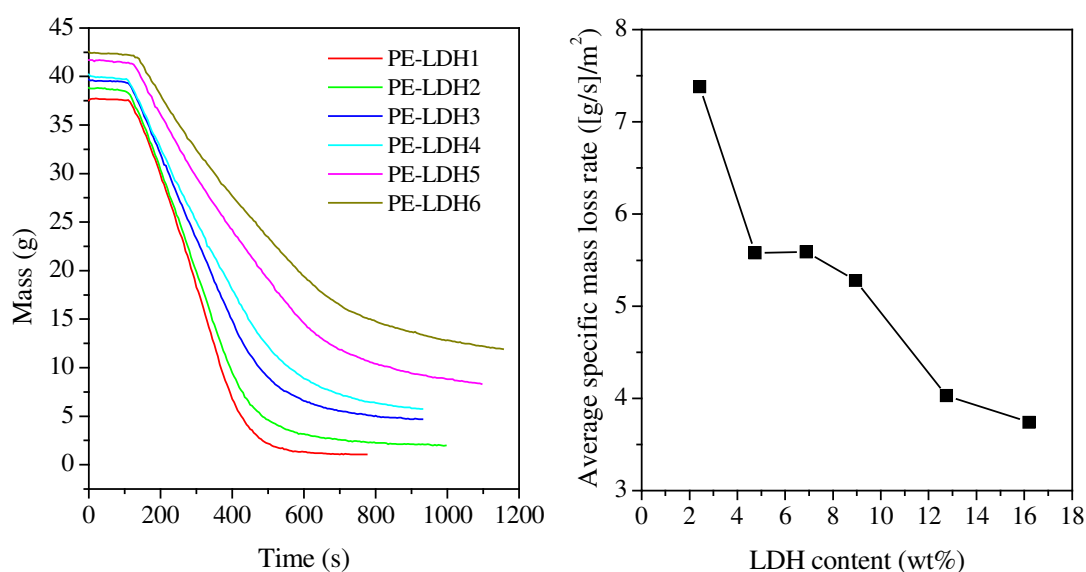


Figure 6.8 Cone calorimeter investigation results showing changes in mass of sample with combustion time (left) and average specific mass loss rate with increasing LDH concentration (right).

besides increase in flame inhibition effects, the amount of combustible polymeric material decreases that further causes slower mass loss. At higher LDH content, substantial amount of residue is left, which is important for having better flame-retardant performance through the physical barrier effect of the char.

To obtain self-sustained combustion process during burning, heat released due to combustion should be able to trigger the chemical reaction between the combustible material at the normal concentration (about 20 volume%) of oxygen. For materials having LOI value lower than 20, heat released during combustion is more than sufficient to sustain this combustion process in air and so they burn spontaneously once ignited. When LOI value becomes high, the heat released may not be sufficient to sustain the combustion reaction in air and materials show self extinguishing nature. Heat release rate during combustion is reduced when the combustion process is inhibited though inactivation of the flame propagating radicals or some endothermic reaction takes place during combustion (specially, in presence of metal hydroxide type flame-retardants). Therefore materials showing low flammability i.e. higher LOI value, usually show low heat release rate [182]. In fact, **Figure 6.9** shows, in case of PE/LDH nanocomposites, it has also been observed that PHRR decreases with increasing LOI value.

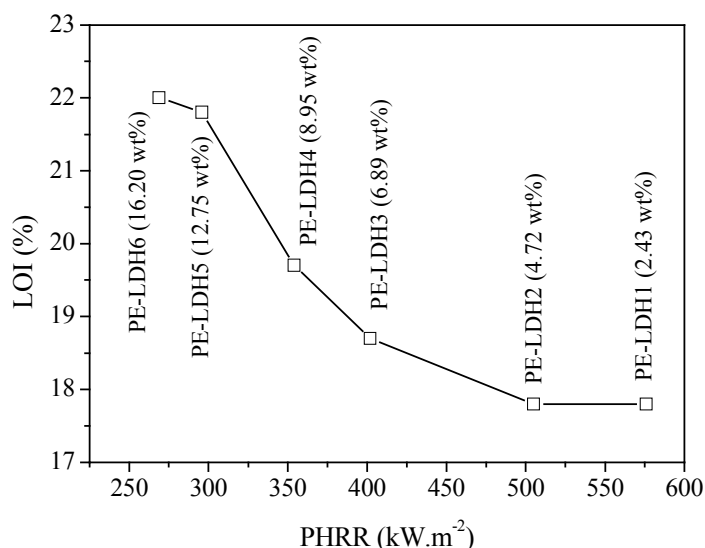


Figure 6.9 Variation of LOI values in the polyethylene/LDH nanocomposites with increasing PHRR, the number shown after the label of every data point indicates the LDH concentration in the respective sample.

As observed during LOI test, the residue formed after combustion process plays a major role in improving the flame retardancy of polymeric materials. The same is also apparent from the cone-calorimeter investigation. One basic advantage of the mineral fillers as flame-retardant in polymer composites is that they leave a large proportion of their mass as residue after complete combustion. In case of LDH, decomposition produces mixed metal oxide and MgO. This MgO being highly non-conducting to heat, the residue can act as thermal insulator depositing on the burning surface. However, the barrier effect shown by combustion residue is also dependent on its physical nature. A highly compact residue usually provide better barrier effect than a residue having pores, cracks, etc. In **Figure 6.10**, the nature of the combustion residue for PE/LDH nanocomposites has been shown. The unfilled PE does not leave any residue. Whereas, nanocomposites containing low LDH concentration (PE-LDH1 and PE-LDH2)

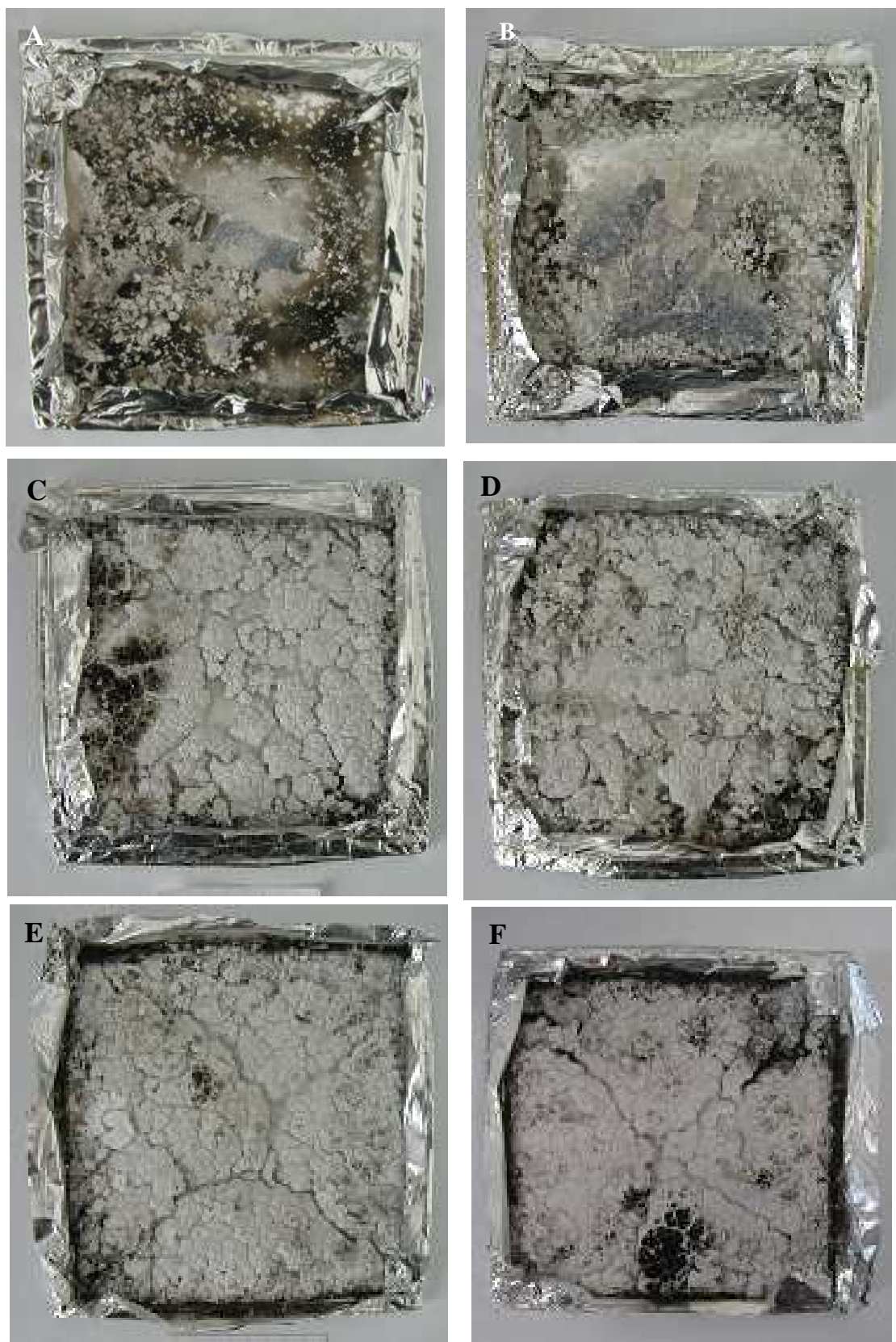


Figure 6.10 Pictures showing the nature of the residue after complete combustion of the PE/LDH nanocomposite samples during cone calorimeter testing: A - PE-LDH1, B - PE-LDH2, C - PE-LDH3, D - PE-LDH4, E - PE-LDH5 and F - PE-LDH6.

yield very small amount of residue and hence not effective to impart barrier effect during combustion (**Figure 6.10A and B**). On further increase in LDH content, both the amount and compactness of the residue improves (**Figure 6.10C to F**). The surface colour of the residue turns from white to gray. The residue just beneath the surface layer appears darker may be due to presence of carbonaceous char, which was also indicated in thermal analysis of these materials.

The amount of residue obtained from PE/LDH nanocomposites can be determined theoretically from the approximate chemical composition of LDH-DBS and its decomposition chemistry. But the theoretically calculated values are always lower than the values obtained from combustion during thermogravimetric analysis. This difference provides an indication of the formation of carbonaceous char during combustion. The residue obtained in a cone-calorimeter combustion experiments perhaps represents more closely the actual amount of char yield in case of real fire scenario. **Table 6.1** shows the comparison of combustion residue obtained from thermogravimetric analysis, cone-calorimeter and theoretical calculation.

Table 6.1 Comparison of the combustion residue obtained from thermogravimetric analysis (TGA), cone-calorimeter and theoretical calculation

Sample	Hydroxide	Combustion residue			Carbonaceous residue	
	content	TGA	cone-calorimeter	calculated	TGA	cone-calorimeter
	wt%	wt%	wt%	wt%	wt%	wt%
PE-LDH1	2.43	3.00	2.77	1.79	1.21	0.98
PE-LDH2	4.72	5.00	5.10	3.47	1.53	1.63
PE-LDH3	6.89	7.90	11.80	5.07	2.83	6.73
PE-LDH4	8.95	9.20	14.25	6.59	2.61	7.66
PE-LDH5	12.75	12.00	19.97	9.39	2.61	10.58
PE-LDH6	16.20	14.70	27.97	11.92	2.78	16.05
PE15MH	15.00	11.25	18.01	10.35	0.90	7.67

The combustion of the nanocomposites in cone-calorimeter yields much higher residue in comparison to those obtained from TGA and the theoretical calculation. This means that even though a constant external heat flux is maintained throughout the experiment, the nanocomposites undergo incomplete combustion yielding a large amount of char. From the appearance of these chars as shown in **Figure 6.10**, it seems they contain significant amount of carbonaceous residue. Since in the theoretical calculation the metal oxides formed after complete combustion is considered as the char, the amount of carbonaceous char can be taken as the difference between the experimentally obtained value and the calculated one. **Table 6.1** also shows the amount of carbonaceous char calculated using this principle. The TGA analysis mentioned previously shows that the yield of carbonaceous char attains a steady

value after certain LDH concentration (PE-LDH3). Whereas, in case of cone-calorimeter combustion, the amount of carbonaceous char increases with increasing LDH content in the nanocomposites. This may be due to the difference in the sample size and geometry used in these two experiments. In case of TGA, a very small amount of the sample (a few mg) is subjected to combustion using an external heat flux. This small size of the sample cannot yield a sufficient amount of combustion residue at the sample surface to cause effective thermal and gas barrier effect. On the other hand, large and very thick sample size produces a large amount of residue on the surface, which can drastically reduce the heat and oxygen supply to the interior of the sample resulting in an incomplete combustion. **Table 6.1** also shows a comparison between PE/LDH nanocomposite composition (PE-LDH6, containing 16.20 wt% LDH) and polyethylene/Mg(OH)₂ conventional microcomposite (PE15MH) containing comparable amount of metal hydroxide. The TGA experiment shows that PE15MH yields nearly similar amount of char as theoretically predicted one, whereas PE-LDH6 yields much higher amount of char. This difference is much more pronounced in case of cone-calorimeter results. In this case, both PE-LDH6 and PE15MH yield significantly higher amount of char compared to the theoretically calculated value. But, the nanocomposite yields more than 50.0% higher amount of char compared to the conventional composites. This large increase in char yield occurs due to much higher amount of carbonaceous (more than double) char formation in case of the nanocomposite composition. This means the nanocomposite compositions are more efficient char former than the conventional composites.

6.2 PE/LDH/Mg(OH)₂ Composites: Synergistic Effect

The use of metal hydroxides, like Mg(OH)₂ (MH) and aluminum trihydrate (ATH) as flame-retardants in polyolefins is a very common practice. But to obtain satisfactory flame retardant effect concentration often in excess of 60.0 wt% of these metal hydroxide is required. Such high concentration of filler, on the other hand, deteriorates the mechanical properties and processibility of the composites [108, 109]. These metal hydroxides exhibit flame-retardant effect mainly through endothermic decomposition and barrier effect of the metal oxide residue. Because of their very mechanism of flame inhibition, they are far less efficient as flame-retardant compared to halogenated flame-retardants, which directly terminate the flame propagating reactive radical species in the flame zone. As a result, these metal hydroxide are required in large quantity for effective flame retardation. Along with that, their poor compatibility with non polar polymer matrices creates further difficulties in terms of inhomogeneous dispersion, which further reduces their efficiency as flame-retardant. Therefore, extensive researches have been made and still continuing to improve dispersion through reducing the interfacial tension between metal hydroxide filler and non polar polymer matrix [110, 111, 183–186]. Mg-Al-LDH with its potential as nanofiller can be a certain development in this regard. The problem of inhomogeneous particle dispersion can be addressed to a greater extent through reduced particle size and metal hydroxide layer exfoliation in LDH based nanocomposites. However, LDH alone may not be sufficient for improving flammability, especially the test results, like LOI and UL94 revealed this fact in the previous sections. This is due to the indirect mechanism of flame retardation (similar to MH) and lower limit of maximum filler concentration in clay based polymer nanocomposites in general in comparison to microcomposites. The latter is very important criteria because LDH beyond a concentration of 10.0 wt% makes the nanocomposite extremely brittle. The alternative way of utilizing the flame-retardant potential of LDH can be its use in combination

with MH with an aim to reduce the overall filler loading in a PE/MH type conventional flame-retardant composites. In the present work, MH was partially replaced by an increasing amount of LDH and the flammability performance of the composites were investigated. The maximum amount of LDH used for such investigation was 10.0 wt%.

The LOI results for composites based on 40.0, 50.0 and 60.0 wt% MH are shown in **Figure 6.11**. In each of these composites, MH is progressively replaced by LDH keeping the total amount of MH and LDH concentration constant. The composites containing only MH are considered as the control compounds for the respective series. It is apparent that as the combined systems show higher LOI values than the control compounds and with increasing LDH proportion the LOI value also increases. **Figure 6.11** also shows that the composition PE/10LDH/30MH has similar LOI value as that of the composition PE/50MH and the similar is true also in case of PE/10LDH/40MH and PE/60MH. This means that overall filler loading in a PE/MH composite can be significantly reduced in presence of LDH to obtain desired LOI values. The explanation of such synergism can be obtained if the burning process is observed carefully. In case of composites containing only MH, the burn residue/char is held less firmly with the sample stock. As a result, with increasing volume, the char falls down under its own weight exposing fresh sample surface for burning. On the other hand, presence of LDH enhances the viscosity of the melt, which support the growing char on its top and hence an efficient barrier effect is obtained. Additionally, the improved dispersion of LDH particles causes better distribution of cooling effects throughout the matrix through endothermic decomposition during burning .

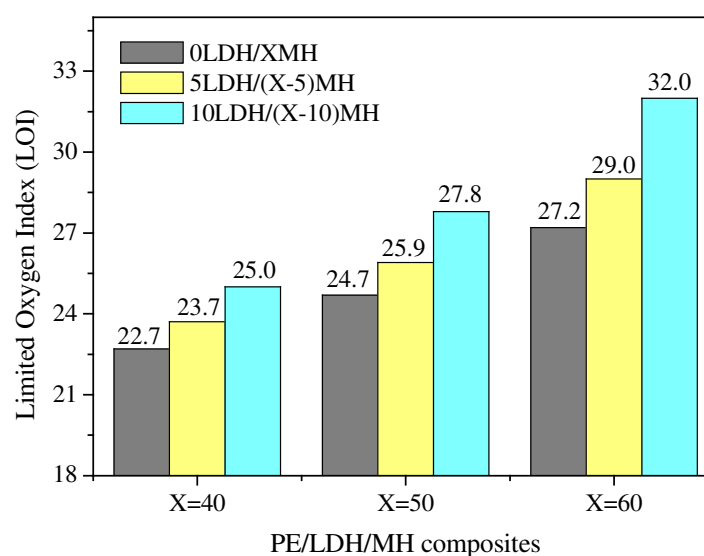


Figure 6.11 Synergistic effect of LDH in $\text{Mg}(\text{OH})_2$ filled PE composites: LOI values have compared between composites where magnesium hydroxide is being progressively replaced by LDH (X represent total weight percent of filler i.e. $\text{Mg}(\text{OH})_2 + \text{LDH}$)

Thermogravimetric analysis shows that the thermo-oxidative degradation of PE/MH composites containing 40 wt% MH starts at about 375 °C and continues up to about 475 °C (**Figure 6.12**). This decomposition takes place in two distinct stages characterized by two decomposition peaks in differential plot (**Figure 6.12**) at 400 °C and 460 °C. During the first decomposition stage, which spans over an approximate range 375 – 425 °C, PE/MH composites (containing 40.0 wt% MH) loses less than 25.0% of

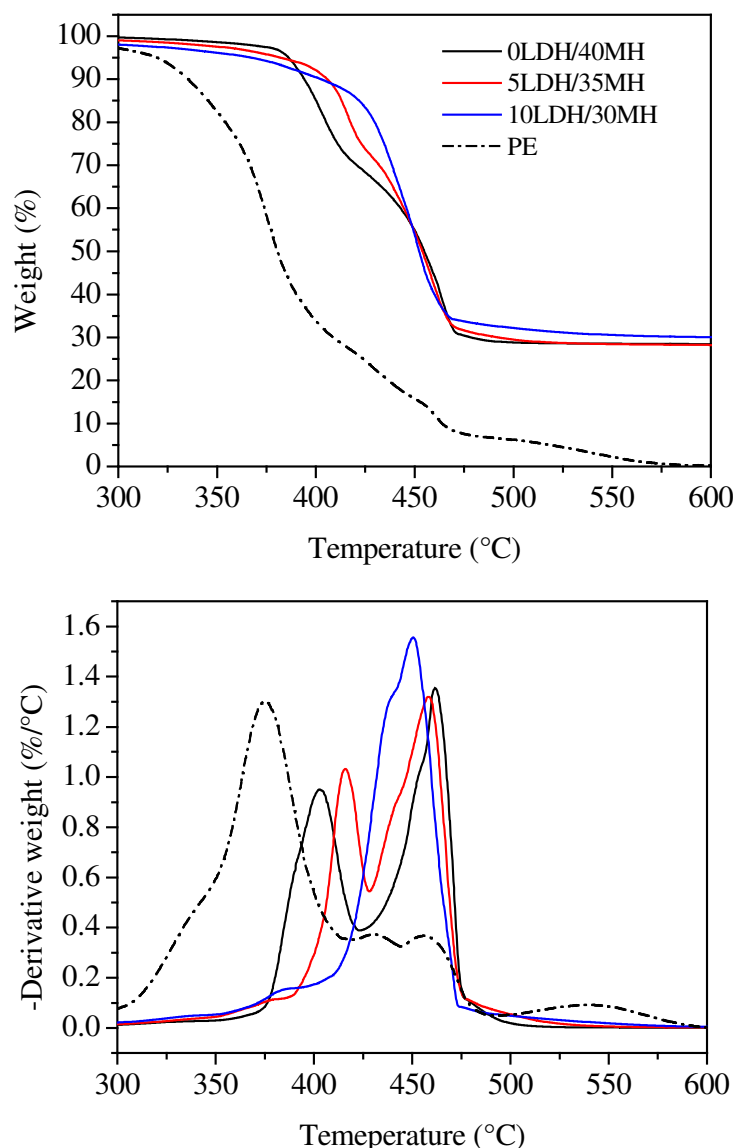


Figure 6.12 Thermogravimetric analysis of PE/MH and PE/LDH/MH composites.

its weight. By the temperature of 425 °C, the unfilled PE itself loses more than 70.0% and MH itself more than 28.0% of their respective weight. So, principally, PE/MH composite containing 40.0 wt% MH should lose more than 53.0 wt% ($\approx 0.70 \times 60 + 0.28 \times 40$) at a temperature of 425 °C. But, in practice **Figure 6.12** shows it is less than 30.0 wt%. Therefore, it can be concluded that the endothermic decomposition of MH suppresses the first decomposition stage of the PE matrix in PE/MH to a significant extent and a major part of the matrix decomposition takes place above 425 °C. When MH in PE/MH composite is partially replaced by increasing amount of LDH, distinct changes in the thermal decomposition behavior can be observed. The first decomposition peak, which corresponds to the decomposition of the filler and a part of the matrix, shifts to higher temperature with increasing LDH loading and ultimately merges with the second decomposition stage. This means that the two stage decomposition observed in PE/40MH is changed to a single stage decomposition in PE/10LDH/30MH. This is a clear indication of improvement of thermal stability of the composites in presence of LDH.

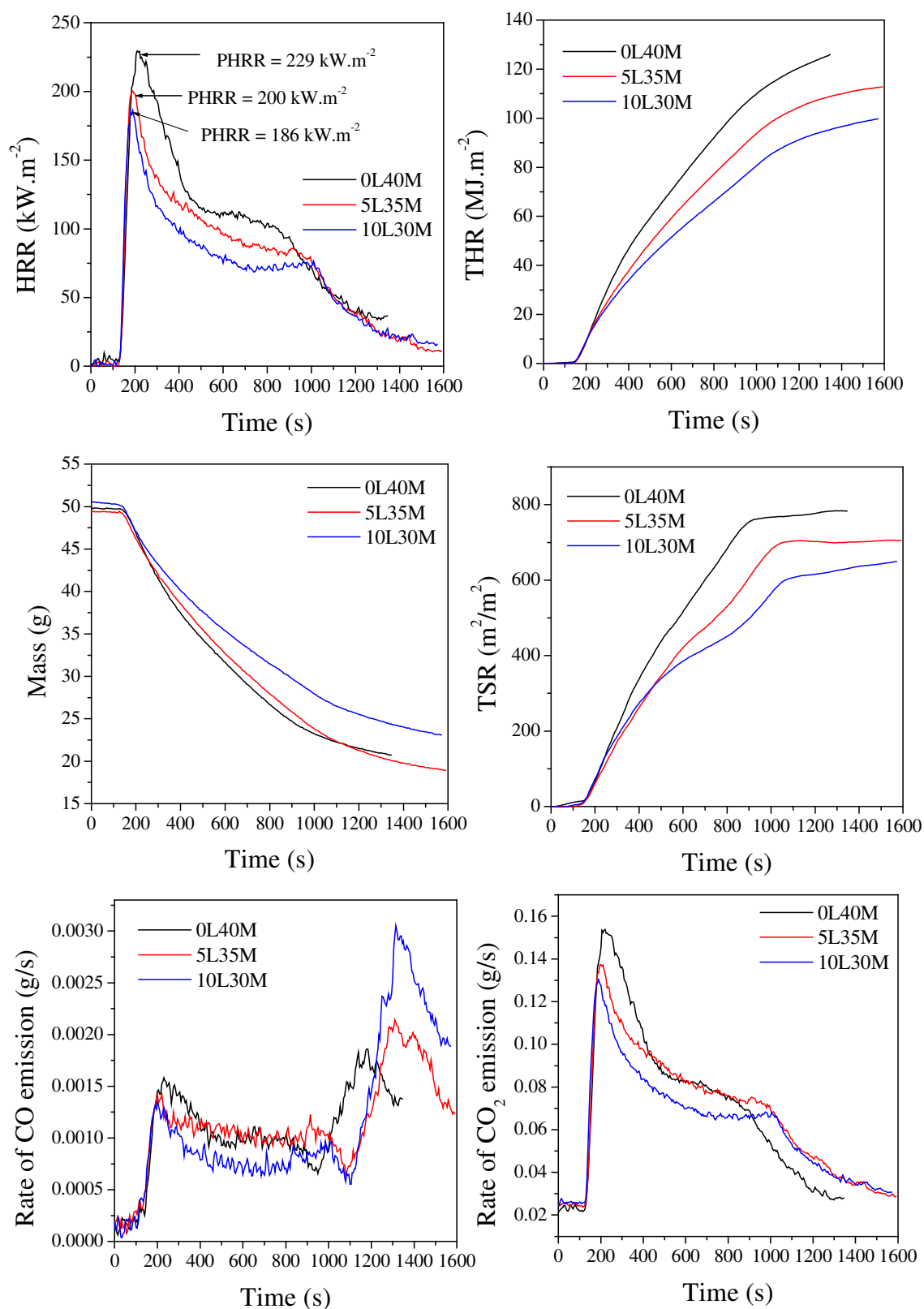


Figure 6.13 Cone-calorimeter investigation results for the PE/MH and the PE/LDH/MH composites, showing synergistic effect of LDH with MH (L and M stands for LDH and MH respectively and the number before them indicate the weight percentage)

The summary of the cone-calorimeter investigation results for PE/MH and PE/LDH/MH composites is shown in **Figure 6.13**. Again, the mixed systems of the flame-retardants show better performance in comparison to the control system. The both heat release rate (HRR) and its peak value (PHRR) decreases as the amount of LDH increases in the combined system. The burning time is also extended resulting in slower burning process. However, introduction of LDH does not change the time of ignition, may be due to their similar mechanism of flame inhibition. The heat released during combustion is also lowered by the addition of LDH. The slower burning rate in presence of LDH also accounts for the slower mass loss with time as compared to the PE/MH control composites. Interesting, although the net amount of metal hydroxide remains constant in all the three composites, the increasing amount LDH causes reduced smoke generation. Perhaps, LDH facilitates carbonaceous char formation resulting in less smoke generation. The formation of carbonaceous char is also responsible for increase in CO emission rate during the last stage of the combustion process. The carbonaceous residue may undergo slow oxidation liberating CO and other volatile materials. Similar observation of increased CO production after flame-out has also been observed in case of polyamide/carbon nanotube based nanocomposites [187]. The slow thermo-oxidation of carbon nanotube residue has been held responsible for increased CO production in such composites. Contrarily, similar increase in CO₂ emission was not observed.

Table 6.2 Summary of UL94 vertical burn test for PE/MH and PE/LDH/MH composites (sample size: 125 mm x 10 mm x 4 mm)

sample	LDH	MH	t ₁ ^a	Dripping	t ₂ ^a	Dripping	t ₃ ^b	UL rating
	wt%	wt%	s	-	s	-	s	-
0L40MH	0	40	A, B	Yes	-	-	68 ^c	No
0L40MH	5	35	A, B	Yes	-	-	125 ^c	No
10L30MH	10	30	8	No	A, B	Yes	83 ^d	No
0L50MH	0	50	A, B	Yes	-	-	151 ^c	No
5L45MH	5	45	11	No	A, B	Yes	66 ^d	No
10L40MH	10	40	2	No	4	No	-	Yes, VO
0L60MH	0	60	2	No	6	No	-	Yes, VO
5L55MH	5	55	0	No	2	No	-	Yes, VO
10L50MH	10	50	0	No	0	No	-	Yes, VO

^a t₁ and t₂ are burning time after first and second heating respectively. A: Drips and the cotton below burns, B: sample burns up to the sample holder.

^b t₃ is the time at which dripping starts.

^c t₃ is counted from the end of first heating.

^d t₃ is counted from the end of second heating.

The flammability performance of PE/MH and PE/LDH/MH composites were also compared in terms of their performances in the UL94 vertical burn test, which are summarized in **Table 6.2**. From the results shown in **Table 6.2**, the improved flame retardant effect of the mixed filler system on once again apparent. In the system containing 40.0 wt% filler no positive rating is obtained even after introduction of 10.0 wt%. However, the dripping resistance of the material improves significantly as more and more LDH is incorporated. The sample containing 40 wt% MH shows continuous melts dripping after first heating. While, the sample containing 30.0 wt% MH and 10.0 wt% LDH (10L30MH) does not show any melt dripping after first heating, as the flame extinguishes after some time. However, this samples burns continuously and show dripping after the second heating step. In the second system, the control compound containing 50.0 wt% MH also do not show positive UL94V rating and the sample burns continuously with melt dripping after first heating. However, replacement MH in this system with LDH results in significant improvement and the composite containing 10.0 wt% LDH and 40.0 wt% MH (i.e., 10L40MH in Table 6.2) shows positive UL94V rating with V0 classification. In the third system with 60.0 wt% filler content, all the compositions are self-extinguishing and show UL94V0 rating. However, when MH is replaced by LDH, burning time after each heating steps in UL94V testing are decreased significantly.

The main purpose of substituting magnesium hydroxide by Mg-Al-LDH in polyethylene based composites was to reduce the overall metal filler content to obtain satisfactory flame retardancy. But, in doing

Table 6.3 Summary of mechanical properties of PE/MH and PE/LDH/MH composites

Sample	Modulus	SD ^a	Yield stress	SD	EB ^b	SD
	MPa	-	MPa	-	%	-
0L40M	379.6	16.9	12.64	0.09	39.57	3.24
5L35M	368.0	22.6	13.19	0.21	34.51	2.96
10L30M	424.9	24.2	13.36	0.25	21.29	2.46
0L50M	540.4	59.0	12.73	0.15	18.0	3.76
5L45M	484.1	15.8	13.76	0.13	19.49	1.69
10L40M	539.2	36.4	13.72	0.19	10.06	0.86
0L60M	672.9	42.2	13.71	0.26	9.25	1.2
5L55M	682.8	60.6	14.55	0.29	7.84	0.73
10L50M	741.5	47.4	14.45	0.33	4.65	0.57

^a SD is the standard deviation

^b EB is elongation at break

so the effects on other properties should also be considered, such as mechanical properties and processibility. In fact the deterioration of these properties in the composites containing mixed filler system, is not encouraging for their final applications. Therefore, increase in proportion of LDH in a MH/LDH combination is limited by the processibility and the mechanical properties of the composites. **Table 6.3** shows the summary of the mechanical properties of various PE/LDH/MH compositions investigated in the present work.

The incorporation of LDH up to 10.0 wt% does not deteriorate the modulus and yield strength of the composites rather a small increase in both the properties were observed. However, at 10.0 wt% LDH content, especially in composites with high total filler concentration (as in 10L50M), the flexibility of final composites is affected significantly indicating the lowering of the impact strength of the materials. To obtain a optimum combination of LDH and MH in polyethylene and other polyolefin matrices more rigorous and detail investigation are necessary. May be the use of some compatibilizer or impact modifier would be a potential solution for this limitation.

CONCLUSIONS AND OUTLOOKS

The present investigation is primarily aimed to investigate the potential of layered double hydroxide based on aluminum and magnesium (Mg-Al-LDH) as a flame-retardant and nanofiller in a polyolefin matrix, like low density polyethylene. The reason behind selection of Mg-Al-LDH is manifold. For example, Mg-Al-LDH can be treated as a novel metal hydroxide type filler, which has close similarity to both conventional metal hydroxides, like $\text{Mg}(\text{OH})_2$, $\text{Al}(\text{OH})_3$, etc (with respect to its endothermic decomposition) and layered silicate type of nanofillers (with respect to its ability to intercalate with large organic species). The similarity with $\text{Mg}(\text{OH})_2$ makes it a suitable material to improve the flame retardancy of the filled polymeric composites mainly through endothermic decomposition and large amount of non-conducting char formation. On the other hand, the similarity with layered silicate type of conventional nanofillers can be explored through intercalation and exfoliation by the polymer chains to obtain better dispersion of the filler particle in polymer matrix in comparison to the conventional metal hydroxide. Besides, Mg-Al-LDH is a naturally occurring minerals and can also be synthesized in laboratory in large scale by easy methods to obtain more homogeneity in structure and compositions. The bio-compatible nature of this anionic clay is also suitable for designing an environment friendly flame-retardant for polymers.

To make the unmodified Mg-Al-LDH clay a suitable precursor for the preparation of polymer nanocomposite, modification by anionic surfactants is necessary. In fact, a number of such surfactants were used in the present study to modify Mg-Al-LDH in order to enlarge the interlayer distance and to render it more organophilic. The surfactants were selected based on their functionality, chain length, etc. Although there are several method reported in literature for organic modification of LDH in general, the regeneration technique was deliberately chosen because of its higher efficiency and simple procedure. Other methods, like co-precipitation in presence of surfactant anions, direct ion exchange, etc would be the better alternative can also be used for this purpose. The characterization of the organically modified Mg-Al-LDH was carried out extensively using various analytical techniques, like XRD, FTIR, TGA, SEM and surface tension measurements. The XRD analysis of the modified clay reveals that the surfactant anions are arranged as monolayer within the interlayer region of Mg-Al-LDH and enlarge the interlayer distance according to the length of their hydrocarbon chain. Some water molecules are also found to be present in the interlayer region in the modified LDH, which are usually arranged as monolayer in between surfactant and metal hydroxide sheet. However, in case of the surfactant having more crowded hydrocarbon chain (for example, containing two hydrocarbon chains as in BEHP) no interlayer water was detected in the modified sample. From the various functionalities of the surfactants, Mg-Al-LDH shows more affinity to sulfate and sulfonate, which was confirmed from the purity of their WAXS

pattern. In case of LDH-DS and LDH-DBS, no peak corresponding to the unmodified clay was detected. However, with phosphate and carboxylate, formation of some unmodified LDH during regeneration process was indicated from the presence its characteristic reflection maximum in WAXS pattern of the modified materials. The original plate-like particle morphology of the unmodified LDH materials is not changed after organic modification except the appearance surface roughness and disordered edges. The intercalation of bigger anionic species into the interlayer space results swelling of the LDH platelets. The thermal analysis reveals that unmodified Mg-Al-LDH show large decomposition peaks below 300°C due to the complete loss of interlayer water molecules and the partial loss of carbonate anions. The organic modification, especially with SDBS, either significantly suppresses these peaks or shifts them to higher temperature. The modified LDH materials in addition to modifying surfactant anions, also contain some interlayer water and carbonate anions, which are incorporated during regeneration process. Surface energy measurements using capillary penetration method reveal that the organic modification makes the LDH clay more hydrophobic, which results lowering of surface energy significantly in comparison to a similar unmodified metal hydroxide particles ($\text{Mg}(\text{OH})_2$).

The primary aim of organic modification of unmodified Mg-Al-LDH was to render it suitable for the polymer nanocomposite preparation. In this regard, LDH-DBS was chosen because it has the largest interlayer distance among all the modified sample prepared. Also DBS shows higher efficiency of intercalation compared to the other surfactants. Besides, the presence of aromatic moiety in its structure facilitates the formation of higher amount of carbonaceous char after combustion of the PE/LDH nanocomposite. This becomes more important when modified clay contains large fraction of the intercalated surfactant, which is above 40% incase of LDH-DBS. To prepare nanocomposite based on PE matrix using melt compounding method, conventional masterbatch technique was followed. This was an obvious choice rather than an arbitrary one as a highly nonpolar PE matrix hardly intercalate itself within the interlayer space of inorganic clays. Therefore, a functionalized polymer (PE-g-MAH) was used as compatibilizer between the two. However, mixing in batch-mixture, like Brabender plasticorder, where shearing force was less intense resulting in a lower degree of intercalation/exfoliation of the clay particles by polymer chains. The WAXS pattern of these nanocomposite did not show any change in position of the basal reflection peaks corresponding to LDH-DBS. The TEM images reveal the partial exfoliated and intercalated structure of the dispersed clay particles and also the presence of aggregated structures among the primary clay particles. On the other hand, compounding in a co-rotating twin-screw extruder results in a better dispersion of clay particles with higher degree of intercalation and exfoliation of the clay platelets. Overall, in the nanocomposites hierarchy of structural features of the dispersed LDH particles was observed. The primary particles, which are single LDH platelet containing large number of metal hydroxide sheets, not only undergo breakdown in smaller fragments through delamination of thinner stacks from their surface, but also form aggregates that look more precisely like domains of closely associated platelets. The exfoliated fragments or clay layers either remain scattered in the matrix or form localized region of physically network structures.

The melt rheological analysis of PE/LDH nanocomposite shows flow behavior typical of polymer/layered silicate nanocomposites, which have extensively been reported in literatures. This was not only helpful to understand the flow behavior of the composite melts under different shearing conditions, but was also useful in understanding the nature of LDH particle dispersion and possible filler-filler and filler-polymer interaction in the nanocomposites. The dynamic oscillatory shearing in linear viscoelastic

regime reveals that with increasing LDH concentration, the nanocomposite melts progressively deviate from the low-frequency Newtonian behavior to a strong shear thinning behavior. Also the pseudo-solid like behavior becomes more and more prominent with the appearance of apparent yield stress. Such deviation in the low frequency flow behavior is caused by the dispersed LDH particles and their physical networked structures, which creates an energy barrier against the relaxation of the polymer chains. This also gives indirect evidence that polymer chains are interlocked on the LDH particle surface or within clusters. The morphological analysis shows that the dispersed LDH particles form physically associated structures in different scales. As a result, the response of these nanocomposite melts during shearing in non-linear regime differs significantly from that of the unfilled PE melt. It is observed that steady shearing causes breakdown of the filler structures until a steady state is reached. This is manifested in the form of stress overshoot at the start-up flows during steady shear. Such behavior is also observed in unfilled PE melt, but the time scale and magnitude of stress overshoot differ drastically from the nanocomposites. Also, the non-linear behavior in the nanocomposite melts appear at lower shear rate and strain. The ruptured filler structures are regenerated with time when shearing is stopped and the melts are allowed to equilibrate. The structural regeneration progressively enhances the elastic nature of the melt as indicated by a steady increase in storage modulus of the melt with time. This kind of non-linear behavior is not commonly observed in conventional micro- or macrocomposites containing inactive filler particles. To predict these non-linear flow behavior theoretically Wagner model was used as starting tool as it quite satisfactorily describes the non-linear behavior of unfilled PE melt. The modification of the original model is made considering the non-linear parameter β being dependent on the structure build-up in the nanocomposite melts. This parameter changes with time during steady shear and upon cessation of steady shear. This gives a quantitative prediction of the stress overshoot behavior of the nanocomposite melts and its dependence on rest period during a flow reversal experiment. However, to describe the experimentally observed behavior more precisely further investigation is necessary regarding the dependence of β on shear rate, filler loading and temperature during steady shear.

The flammability studies of the PE/LDH nanocomposites showed improved flame retardancy in comparison to the unfilled PE. The LOI value was progressively improved with increasing LDH concentration. Though the nanocomposite compositions did not pass any UL94 testing standard, they exhibit stronger resistance against the dripping tendency of the melt during burning process. The cone-calorimeter investigation results showed that LDH can suppress the combustion process and significantly reduces the burning rate in comparison to unfilled PE. This is important as this type of behavior provides a longer escape time during real life fire accidents. The peak heat release rate (PHRR) was significantly reduced in nanocomposite compositions containing over 5 wt% LDH. The LDH materials also show synergistic effect in presence of conventional flame-retardant $\text{Mg}(\text{OH})_2$ in PE. When the later is partially replaced by organically modified Mg-Al-LDH (up to 10 wt% of the total composition was tried), the LOI index is improved significantly. In comparison to only $\text{Mg}(\text{OH})_2$ based composites, such combinations also results satisfactory flammability rating in UL94 testing at lower net filler concentrations. The mechanical properties of the composites based on mixed system also show marginal improvement compared to their counterparts. This is certainly a promising development as this may lead to the lowering filler concentration required in the conventional metal hydroxide based flame-retardant polyolefin composites without any compromise in flammability ratings and mechanical properties. This synergistic approach has certainly a tremendous potential in reducing the total flame retardant concentration in polymer com-

posites. The char forming ability of LDH has been demonstrated in this study, which might be very useful in combination with conventional active flame-retardants, like phosphates.

The potential of the Mg-Al-LDH clay as nanofiller in non-polar polymer, like polyethylene has been demonstrated in the present study. The very target behind such application is to obtain high degree of exfoliation of the clay layers. However, the use of non-polar polymers always makes this task a challenging one. The unfavorable thermodynamic compatibility between the clay particles and non-polar matrix always acts as a strong barrier not only against the penetration of the polymer chain within the clay layers, but also against the formation of stable homogeneous distribution of the exfoliated clay layers throughout the matrix. This is also common in case of various layered silicate based polyolefin nanocomposites. In spite of these difficulties some degree of exfoliation and better clay particle dispersions are achieved with polyolefin in comparison to conventional inorganic fillers, like $\text{Mg}(\text{OH})_2$, hydrated $\text{Al}(\text{OH})_3$, etc. The use of LDH as flame-retardant has certain advantage over layered silicate type cationic clays. Unlike layered silicate, LDHs actively take part in flame inhibition through its endothermic decomposition, which in addition to the physical barrier effect obtained from the inorganic combustion residue provides extra measure against flame inhibition. Again, the inherent bio-compatible nature of the Mg-Al-LDH may also make it attractive to flame-retardant industries as alternative to halogen containing chemicals. The present study highlighted these perspectives with some significant property improvements, especially the flame retardancy at lower filler concentration. This study has also opened new possibilities of investigations regarding the use of LDH type clays in polymer as nanofiller. The improvement of LDH particle dispersion in polymer matrix is certainly desired for further improvement in properties, especially mechanical properties. Such improvements will certainly be helpful to develop flame-retardant composites showing satisfactory mechanical properties and processibility, which are compromised in case of conventional metal hydroxide type flame-retardants.

The selection of surfactants for organic modification needs more critical attention with respect to their structural and chemical variations. Very low molecular weight functionalized polymer containing carboxylate (like, copolymers of acrylic acids), sulfonate, etc can also be potential candidates for this purpose. The cationic nature of the metal hydroxide layers in LDH makes the choice of organic species more flexible. Organic species containing functional groups -OH, -COOH, -SO₃H, etc shows favorable interaction with LDH clays. Therefore, LDH can be modified with wide range of organic species. Such flexibility in selecting modifying anionic species makes LDH a suitable candidate for designing a multifunctional nanohybrids filler for polymers. For example, LDH can be modified by organic species having specific properties, like UV absorption [188], photo stabilization [189], antimicrobial effect [190], fluorescent effect [85], etc. All these nanohybrids can be potential functionalized fillers for polymers to develop novel composite materials.

References

- [1] National fire protection association fire loss in the U.S. during 2005 abridged report (<http://www.usfa.dhs.gov/statistics/national/>).
- [2] A. R. Horrocks and D. Price (ed). *Fire Retardant Materials*. Woodhead Publishing Limited, Cambridge, England, 2001.
- [3] G. E. Zaikov and S. M. Lomakin. Ecological issue of polymer flame retardancy. *Journal of Applied Polymer Science*, 86:2249 – 2462, 2002.
- [4] S. M. Lomakin and G. E. Zaikov. *Modern Polymer Flame Retardancy*. VSP Publishers, Netherlands, 2003.
- [5] F. Cavani, F. Trifiro, and A. Vaccari. Hydrotalcite-type anionic clays: Preparation, properties and applications. *Catalysis Today*, 11:173 – 301, 1991.
- [6] M. Meyn, K. Beneke, and G. Legaly. Anionic-exchange reactions of layered double hydroxides. *Inorganic Chemistry*, 29:5201 – 5207, 1990.
- [7] S. Miyata. Physico-chemical properties of synthetic hydrotalcites in relation to composition. *Clays and Clay Minerals*, 28:50 – 56, 1980.
- [8] M. D. Arco, E. Cebadera, S. Gutierrez, C. Martin, M. J. Montero, V. Rives, J. Rocha, and M. A. Sevilla. Mg,Al layered double hydroxides with intercalated indomethacin: Synthesis, characterization, and pharmacological study. *Journal of Pharmaceutical Sciences*, 93:1649 – 1658, 2004.
- [9] T. S. Stanimirova, G. Kirov, and E. Dinolova. Mechanism of hydrotalcite regeneration. *Journal of Material Science Letter*, 20:453 – 455, 2001.
- [10] W. T. Reichle. Synthesis of anionic clay minerals (mixed metal hydroxides, hydrotalcite. *Solid State Ionics*, 22:135 – 141, 1986.
- [11] O. Clause, M. Gazzano, F. Trifiro, A. Vaccari, and L. Zatroski. Preparation and thermal reactivity of nickel/chromium and nickel/aluminium hydrotalcite-type precursors. *Applied Catalysis*, 73:217 – 236, 1991.
- [12] O. Clause, B. Rebours, E. Merlen, F. Trifir, and A. Vaccari. Preparation and characterization of nickel-aluminium mixed oxides obtained by thermal decomposition of hydrotalcite-type precursors. *Journal of Catalysis*, 133:231 – 246, 1992.

- [13] M. Sychev, R. Prihodko, K. Erdmann, A. Mangel, and R. A. van Santen. Hydrotalcites: relation between structural features, basicity and activity in the wittig reaction. *Applied Clay Science*, 18:103 – 110, 2001.
- [14] U. Costantino, F. Marmottini, M. Nocchetti, and R. Vivani. New synthetic routes to hydrotalcite-like compounds- characterization and properties of the obtained materials. *European Journal of Inorganic Chemistry*, pages 1434 – 1446, 1998.
- [15] M. Ogawa and H. Kaiho. Homogeneous precipitation of uniform hydrotalcite particles. *Langmuir*, 18:4240 – 4242, 2002.
- [16] P. Yang, J. Yu, Z. Wang, Q. Liu, and T. Wu. Urea method for the synthesis of hydrotalcites. *Reac. Kinetics Catal. Lett.*, 83:275 – 282, 2004.
- [17] A. I. Khan and D. O'Hare. Intercalation chemistry of layered double hydroxides: recent developments and applications. *Journal of Materials Chemistry*, 12:3191 – 3198, 2002.
- [18] K. E. Malki, M. Guenane, C. Forano, A. De Roy, and J. P. Besse. Inorganic and organic anionic pillars intercalated in lamellar double hydroxides. *Material Science Forum*, 91 – 93:171 – 176, 1992.
- [19] R. P. Bontchev, S. Liu, J. L. Krumhansi, J. Voigt, and T. M. Nenoff. Synthesis, characterization, and ion exchange properties of hydrotalcite $Mg_6Al_2(OH)_{16}(A)_x(A')_{2-x}4H_2O$ ($A, A' = Cl^-, Br^-, I^-$, and NO_3^- , $2 \geq x \geq 0$) derivatives. *Chemistry of Materials*, 15:3669 – 3675, 2003.
- [20] G. Mascolo. Synthesis of anionic clays by hydrothermal crystallization of amorphous precursors. *Applied Clay Science*, 10:21 – 30, 1995.
- [21] V. Prevot, C. Forano, and J. P. Besse. Hybrid derivative of layered double hydroxides. *Applied Clay Science*, 18:3 – 15, 2001.
- [22] S. Carlino. The intercalation of carboxylic acids into layered double hydroxides: A critical review of the different methods. *Solid State Ionics*, 98:73 – 84, 1997.
- [23] F. Leroux and J. P. Besse. Polymer interleaved layered double hydroxide: A new emerging class of nanocomposites. *Chemisty of Materials*, 13:3507 – 3515, 2001.
- [24] N. T. Whilton, P. J. Vickers, and S. Mann. Bioinorganic clays: synthesis and characterization of amino- and polyamino acid intercalated layered double hydroxide. *Journal of Materials Chemistry*, 7:1623 – 1629, 1997.
- [25] C. Vaysse, L. Guerlou-Demourgues, E. Duguet, and C. Delmas. Acrylate intercalation and in situ polymerization in iron-, cobalt-, or manganese-substituted nickel hydroxides. *Inorganic Chemistry*, 42:4559 – 4567, 2003.
- [26] W. F. Lee and Y. C. Chen. Superabsorbent polymeric materials. xiv. preparation and water absorbancy of nanocomposite superabsorbents containing intercalated hydrotalcite. *Journal of Applied Polymer Science*, 94:2417 – 2424, 2004.

- [27] E. M. Moujahid, J. P. Besse, and F. Leroux. Synthesis and characterization of a polystyrene sulfonate layered double hydroxide nanocomposite. in-situ polymerization vs. polymer incorporation. *Journal of Materials Chemistry*, 12:3324 – 3330, 2002.
- [28] J. P. Besse E. M. Moujahid, M. Dubois and F. Leroux. Role of atmospheric oxygen for the polymerization of interleaved aniline sulfonic acid in LDH. *Chemistry of Materials*, 14:3799 – 3807, 2002.
- [29] M. Tanaka, I. Y. Park, K. Kuroda, and C. Kato. Formation of hydrotalcite-acrylate intercalation compounds and their heat treated product. *Bull. Chem. Soc. Jpn.*, 62:3442, 1989.
- [30] V. P. Isupov, L. E. Chupakhina, M. A. Ozerova, V. G. Kostrovsky, and V. A. Poluboyarov. Polymerization of $m\text{-NH}_2\text{C}_6\text{H}_4\text{COO}$ anions in the intercalation compounds of aluminium hydroxide $[\text{LiAl}_2(\text{OH})_6][m\text{-NH}_2\text{C}_6\text{H}_4\text{COO}]\cdot n\text{H}_2\text{O}$. *Solid States Ionics*, 141-142:231 – 236, 2001.
- [31] L. Vieille, C. Taviot-Gueho, J. P. Besse, and F. Leroux. Hydrocalumite and its polymer derivatives. 2. polymer incorporation versus in situ polymerization of styrene-4-sulfonate. *Chemistry of Materials*, 15:4369 – 4376, 2003.
- [32] L. Vieille, E. M. Moujahid, C. Taviot-Gueho, J. Cellier, J. P. Besse, and F. Leroux. In situ polymerization of interleaved monomers: a comparative study between hydrotalcite and hydrocalumite host structures. *Journal of Physics and Chemistry of Solids*, 65:385 – 393, 2004.
- [33] C. Roland-Swanson, J. P. Besse, and F. Leroux. Polymerization of sulfopropyl methacrylate, a surface active monomer, withing layered double hydroxide. *Chemistry of Materials*, 16:5512 – 5517, 2004.
- [34] G. A. Wang, C. C. Wang, and C. Y. Chen. The disorderly exfoliated LDHs/PMMA nanocomposite synthesized by in situ bulk polymerization. *Polymer*, 46:5065 – 5074, 2005.
- [35] G. A. Wang, C. C. Wang, and C. Y. Chen. Preparation and characterization of layered double hydroxides - PMMA nanocomposites by solution polymerization. *Journal of Inorganic and Organometallic Polymers and Materials*, 15:239 – 251, 2005.
- [36] T. Challier and R. C. T. Slade. Nanocomposite materials: Polyaniline-intercalated layered double hydroxides. *Journal of Materials Chemistry*, 4:367 – 371, 1994.
- [37] Y. Sugahara, N. Yokoyama, K. Kuroda, and C. Kato. Preparation and properties of silica and silicate gels by the alkoxide, colloidal and amine-silicate methods. *Ceramic International*, 14:163 – 167, 1988.
- [38] H. B. Hsueh and C. Y. Chen. Preparation and properties of LDHs/polyimide nanocomposites. *Polymer*, 44:1151 – 1161, 2003.
- [39] S. O'Leary, D. O'Hare, and G. Seely. Delamination of layered double hydroxides in polar monomers: new ldh-acrylate nanocomposites. *Chemical Communication*, 14:1506 – 1507, 2002.
- [40] P. B. Messersmith and S. I. Stupp. High-temperature chemical and microstructural transformations of a nanocomposite organoceramic. *Chemistry of Materials*, 7:454 – 560, 1995.

- [41] C. O. Oriakhi, I. V. Farr, and M. M. Lerner. Incorporation of poly (acrylic acid), poly (vinyl-sulfonate) and poly (styrenesulfonate) within layered double hydroxides. *Journal of Materials Chemistry*, 6:103 – 107, 1996.
- [42] O. C. Wilson Jr., T. Olorunyolemi, A. Jaworski, L. Borum, D. Young, A. Siriwat, E. Dickens, C. Oriakhi, and M. Lerner. Surface and interfacial properties of polymer-intercalated layered double hydroxide nanocomposites. *Applied Clay Science*, 15:265 – 279, 1999.
- [43] F. Leroux, P. Aranda, J. P. Besse, and E. Ruiz-Hitzky. Intercalation of poly(ethylene oxide) derivatives into layered double hydroxides. *Eur. J. Inorg. Chem.*, 6:1242 – 1251, 2003.
- [44] M. Meyn, K. Beneke, and G. Legaly. Anionic-exchange reactions of hydroxy double salts. *Inorganic Chemistry*, 32:1209 – 1215, 1993.
- [45] Y. You, H. H. Zhao, and G. F. Vance. Surfactant-enhanced adsorption of organic compounds by layered double hydroxide. *Collid and Surf. A: Phys. Engg. Asp.*, 205:161 – 172, 2002.
- [46] Y. You, H. H. Zhao, and G. F. Vance. Hybrid organic-inorganic derivatives of layered double hydroxides and dodecylbenzenesulfonate: Preparation and adsorption characteristics. *Journal of Materials Chemistry*, 12:907 – 912, 2002.
- [47] W. Chen and B. Qu. Structural characteristics and thermal properties of PE-g-MA/MgAl-LDH exfoliation nanocomposites synthesized by solution intercalation. *Chemistry of Materials*, 15:3208 – 3213, 2003.
- [48] W. Chen, L. Feng, and B. Qu. Preparation of nanocomposites by exfoliation of ZnAl layered double hydroxides in nonpolar LLDPE solution. *Chemistry of Materials*, 16:368 – 370, 2004.
- [49] L. Qui, W. Chen, and B. Qu. Structural characterisation and thermal properties of exfoliated polystyrene/ZnAl layered double hydroxide nanocomposites prepared via solution intercalation. *Polymer Degradation and Stability*, 87:433 – 440, 2005.
- [50] G. A. Buniak, W. H. Schreiner, N. Mattoso, and F. Wypych. Preparation of a new nanocomposite of $Al_{0.33}Mg_{0.67}(OH)_2(C_{12}H_{25}SO_4)_{0.33}$ and poly(ethyleneoxide). *Langmuir*, 18:5967 – 5970, 2002.
- [51] C. S. Liao and W. B. Ye. Enhanced ionic conductivity in poly(ethyleneoxide)/layered double hydroxide nanocomposite electrolytes. *Journal of Polymer Research*, 10:241 – 246, 2003.
- [52] B. Li, Y. Hu, J. Liu, Z. Chen, and W. Fan. Preparation of poly(methyl methacrylate)/LDH nanocomposite by exfoliation-adsorption process. *Colloidal Polymer Science*, 281:998 – 1001, 2003.
- [53] H. B. Hsueh and C. Y. Chen. Preparation and properties of LDHs/epoxy nanocomposites. *Polymer*, 44:5275 – 5283, 2003.
- [54] Q. Z. Yang, D. J. Sun, C. G. Zhang, X. J. Wang, and W. A. Zhao. synthesis and characterization of polyoxyethylene sulfate intercalated Mg-Al-nitrate layered double hydroxide. *Langmuir*, 19:5570 – 5574, 2003.

- [55] A. S. Costa, T. Imae, K. Takagi, and K. Kikuta. Intercalation of dendrimers in the interlayer of hydrotalcite clay sheets. *Progress in Colloidal Polymer Science*, 128:113 – 119, 2004.
- [56] L. van der Ven, M.L.M. van Gemert, L.F. Batenburg, J.J. Keern, L.H. Gielgens, T.P.M. Koster, and H.R. Fischer. On the action of hydrotalcite-like clay materials as stabilizers in polyvinylchloride. *Applied Clay Science*, 17:25 – 34, 2000.
- [57] S. Miyata. Halogen-containing polyolefin composition, and methods for inactivating halogen therein. *US Patent*, 4 379 882, 1983.
- [58] S. Miyata, T. Hirose, and N. Iizima. Fire-retarding thermoplastic resin composition. *US Patent*, 4 085 088, 1978.
- [59] K. L. Nichols and C. J. Chou. Polymer composite comprising a inorganic layered material and a polymer matrix and a method for its preparation. *US Patent*, 5 952 093, 1999.
- [60] M. Zammarano, S. Bellayer, J. W. Gilman, M. Franceschi, F. L. Beyer, R. H. Harris a, and S. Meriani. Delamination of organo-modified layered double hydroxides in polyamide 6 by melt processing. *Polymer*, 47:652 – 662, 2006.
- [61] W. D. Lee, S. S. Im, H.-M. Lim, and K.-J. Kim. Preparation and properties of layered double hydroxide/poly(ethyleneterephthalate) nanocomposites by direct melt compounding. *Polymer*, 47:1364 – 1371, 2006.
- [62] P. Ding and B. Qu. Synthesis of exfoliated PP/LDH nanocomposites viamelt-intercalation: Structure, thermal properties, and photo-oxidative behavior in comparison with pp/mmt nanocomposites. *Polymer Engineering and Science*, 10:1153 – 1159, 2006.
- [63] L. Du and B. Qu. Structural characterization and thermal oxidation properties of LLDPE/MgAl-LDH nanocomposites. *Journal of Material Chemistry*, 16:1549 – 1554, 2006.
- [64] U. Costantino, A. Gallipoli, M. Nocchetti, G. Camino, F. Bellucci, and A. Frache. New nanocomposites constituted of polyethylene and organically modified znal-hydrotalcites. *Polymer Degradation and Stability*, 90:586 – 590, 2005.
- [65] G. A. Wang, C. C. Wang, and C. Y. Chen. The disorderly exfoliated LDHs/PMMA nanocomposite synthesized by in situ bulk polymerization : The effects of LDH-U on thermal and mechanical properties. *Polymer Degradation and Stability*, 91:2443 – 2450, 2006.
- [66] J. C. A. A. Roelofs, J. A. van Bokhoven, A. Jos van Dillen, J. W. Geus, and K. P. de Jong. The thermal decomposition of Mg-Al hydrotalcites: effects of interlayer anions and characteristics of the final structure. *Chem. Eur. J.*, 8:5571 – 5579, 2002.
- [67] J. W. Gilman. Flammability and thermal stability studies of polymer-layered silicate (clay) nanocomposites. *Applied Clay Science*, 15:31 – 49, 1999.
- [68] U. Wagenknecht, B. Kretschmar, and G. Reinhardt. Investigation of fire retardant properties of polypropylene-clay nanocomposites. *Macromolecular Symposium*, 194:207 – 212, 2003.

- [69] M.S. Cho, B. Shin, S.D. Choi, and K.G. Song Y. Lee. Gel polymer electrolyte nanocomposites PEGDA with MgAl layered double hydroxides. *Electrochimica Acta*, 50:331 – 334, 2004.
- [70] C. S. Liao and W. B. Ye. Structure and conductive properties of poly(ethylene oxide)/layered double hydroxide nanocomposite polymer electrolytes. *Electrochimica Acta*, 49:4993 – 4998, 2004.
- [71] D. Tichit and B. Coq. Catalysis by hydrotalcites and related materials. *Cattech*, 7:206 – 217, 2003.
- [72] C. D. Hoyo. Layered double hydroxides and human health: An overview. *Applied Clay Science*, doi:10.1016/j.clay.2006.06.010, 2006.
- [73] W. F. Lee and Y. C. Chen. Effect of hydrotalcite on the physical properties and drug-release behavior of nanocomposite hydrogels based on poly[acrylic acid-co-poly(ethylene glycol) methyl ether acrylate] gels. *Journal of Applied Polymer Science*, 94:692 – 699, 2004.
- [74] J. H. Choy, S. Y. Kwak, J. S. Park, Y. J. Jeon, and J. Portier. Intercalative nanohybrids of nucleoside monophosphates and dna in layered metal hydroxide. *Journal of the American Chemical Society*, 121:1399 – 1400, 1999.
- [75] D. Shan, S. Cosnier, and C. Mousty. Layered double hydroxides: An attractive material for electrochemical biosensor design. *Analytical Chemistry*, 75:3872 – 3879, 2003.
- [76] J. V. de Melo, S. Cosnier, C. Mousty, C. martelet, and N. Jaffrezic-Renault. Urea biosensors based on immobilization of urease into two oppositely charged clays (laponite and zn-al layered double hydroxides). *Analytical Chemistry*, 74:4037 – 4043, 2002.
- [77] Y. Lin, J. Wang, D. G. Evans, and D. Li. Layered and intercalated hydrotalcite-like materials as thermal stabilizers in pvc resin. *Journal Physics and Chemistry of Solids*, 67:998 – 1001, 2006.
- [78] L. Perioli, V. Ambrogi, C. Rossi, L. Latterini, M. Nocchetti, and U. Costantino. Use of anionic clays for photoprotection and sunscreen photostability: Hydrotalcites and phenylbenzimidazole sulfonic acid. *Journal of Physics and Chemistry of Solids*, 67:1079 – 1083, 2006.
- [79] T. Kuwahara, H. Tagaya, and K. Chiba. Photochromism of spiropyran dye in Li-Al layered double hydroxide. *Microporous Materials*, 4:247 – 250, 1995.
- [80] S. Guo, D. G. Evans, and D. Li. Preparation of C.I. pigment 52:1 anion-pillared layered double hydroxide and the thermo- and photostability of the resulting intercalated material. *Journal of Physics and Chemistry of Solids*, 67:1002 – 1006, 2006.
- [81] Y. Feng, D. Li, Y. Wang, D. G. Evans, and X. Duan. Synthesis and characterization of a UV absorbent-intercalated Zn-Al layered double hydroxide. *Polymer Degradation and Stability*, 91:789 – 794, 2006.
- [82] Y. Tian, G. Wang, F. Li, and D. G. Evans. Synthesis and thermo-optical stability of o-methyl red-intercalated NiFe layered double hydroxide material. *Materials Letters*, 61:1662 – 1666, 2007.

- [83] C. Taviot-Guehoa, A. Illaïk, C. Vuillermoz, S. Commereuc, V. Verney, and F. Leroux. LDHdye hybrid material as coloured filler into polystyrene: Structural characterization and rheological properties. *Journal of Physics and Chemistry of Solids*, 68:1140 – 1146, 2007.
- [84] N. G. Zhuravleva, A. A. Eliseev, A. V. Lukashin, U. Kynast, and Y. D. Tretyakov. Luminescent materials based on Tb- and Eu-containing layered double hydroxides. *Doklady Chemistry*, 396:87 – 91, 2004.
- [85] D. Evans Z. Chang and, X. Duan, P. Boutinaud, M. de Roy, and C. Forano. Preparation and characterization of rare earth-containing layered double hydroxides. *Journal of Physics and Chemistry of Solids*, 67:1054 – 1057, 2006.
- [86] E. P. Giannelis. Polymer layered silicate nanocomposites. *Advanced Materials*, 8:29 – 35, 1996.
- [87] J. W. Gilman, T. Kashiwagi, and J. D. LichtenhanD. Nanocomposites: A revolutionary new flame retardant approach. *SAMPE Journal*, 33:40 – 46, 1997.
- [88] J. W. Gilman, C. L. Jackson, A. B. Morgan, R. H. Harris (Jr.), E. Manias, E. P. Giannelis, M. Wuthenow, D. Hilton, and S. H. Phillips. Flammability properties of polymer-layered-silicate nanocomposites, polypropylene and polystyrene nanocomposites. *Chemistry of Materials*, 12:1866 – 1873, 2000.
- [89] A. B. Morgan, L.-L. Chu, and J. D. Harris. A flammability performance comparison between synthetic and natural clays in polystyrene nanocomposites. *Fire Mater*, 29:213 – 229, 2005.
- [90] J. Zhu and C. A. Wilkie. Thermal and fire studies on polystyrene-clay nanocomposites. *Polym International*, 49:1158 – 1163, 2000.
- [91] M. Biswas and S. S. Ray. Recent progress in synthesis and evaluation of polymer- montmorillonite nanocomposites. *Advances in Polymer Science*, 155:167 – 221, 2001.
- [92] S. S. Ray and M. Okamoto. Polymer/layered silicate nanocomposites: a review from preparation to processing. *Progress in Polymer Science*, 28:1539 – 1641, 2003.
- [93] Y. Kojima, A. Usuki, M. Kawasumi, A. Okada, Y. Fukushima, T. Kurauchi, and O. Kamigaito. Mechanical properties of nylon 6-clay hybrid. *Journal of Material Research*, 8:1185 – 1189, 1993.
- [94] A. Blumstein. Polymerization of adsorbed monolayers: II. thermal degradation of the inserted polymers. *Journal of Polymer Science*, 3:2665 – 2673, 1965.
- [95] E. P. Giannelis. Polymer-layered silicate nanocomposites: synthesis, properties and applications. *Appl Organomet Chem*, 12:675 – 680, 1998.
- [96] S. D. Burnside and E. P. Giannelis. Synthesis and properties of new poly(dimethylsiloxane) nanocomposites. *Chemistry of Materials*, 7:1597 – 1600, 1995.
- [97] T. Agag, T. Koga, and T. Takeichi. Studies on thermal and mechanical properties of polyimideclay nanocomposites. *Polymer*, 42:3399 – 3408, 2001.

- [98] H.-L. Tyan, Y.-C. Liu, and K.-H. Wei. Thermally and mechanically enhanced clay/polyimide nanocomposite via reactive organoclay. *Chemistry of Materials*, 11:1942 – 1947, 1999.
- [99] Y. W. Chen-Yang, H. C. Yang, G. J. Li, and Y. K. Li. Thermal and anticorrosive properties of polyurethane/clay nanocomposites. *Journal of Polymer Research*, 11:275 – 283, 2005.
- [100] B. Lepoittevin, M. Devalckenaere, N. Pantoustier, M. Alexandre, D. Kubies, C. Calberg, R. Jerome, and P. Dubois. Poly(1-caprolactone)/clay nanocomposites prepared by melt intercalation: mechanical, thermal and rheological properties. *Polymer*, 43:4017 – 4023, 2002.
- [101] F. Dietsche and R. Muelhaupt. Thermal properties and flammability of acrylic nanocomposites based upon organophilic layered silicates. *Polymer Bulletin*, 43:395 – 402, 1999.
- [102] J. W. Gilman, T. Ksahiwagi, E. P. Giannelis, E. Manias, S. Lomakin, J. D. Lichtenhan, and P. Jones. *Flammability properties of polymer-layered silicate nanocomposites*. In: Al-Malaika S, Golovoy A, Wilkie CA, editors. *Chemistry and technology of polymer additives*. Oxford: Blackwell Science, 1999.
- [103] J. W. Gilman, T. Ksahiwagi, A. B. Morgan, R. H. Harris Jr., L. D. Brassell, M. R. VanLandingham, and C. L. Jackson. Flammability of polymer clay nanocomposites consortium: Year one annual report, July 2000.
- [104] S. Miyata. Stabilized polyvinyl chloride resin composition. *US Patent*, 4751261, 1988.
- [105] M. Zammarano, M. Franceschib, S. Bellayera, J. W. Gilmana, and S. Meriani. Preparation and flame resistance properties of revolutionary self-extinguishing epoxy nanocomposites based on layered double hydroxides. *Polymer*, 46:9314 – 9328, 2005.
- [106] L. Qiu, W. Chen, and B. Qu. Morphology and thermal stabilization mechanism of LLDPE/MMT and LLDPE/LDH nanocomposites. *Polymer*, 47:922 – 930, 2006.
- [107] M. Bartholmai and B. Schartel. Layered silicate polymer nanocomposites: new approach or illusion for fire retardancy? investigation of the potentials and the tasks using a model system. *Polymers for Advanced Technology*, 15:355 – 364, 2004.
- [108] R. N. Ronthon (ed). *Particle-filled polymer composites*. Longman Scientific, London, UK,, 1995.
- [109] S. Zhu, Y. Zhang, and Y. Zhang. Deformation and fracture of $Mg(OH)_2$ -filled polyolefin composites under tensile stress. *Journal of Applied Polymer Science*, 89:3248 – 3255, 2003.
- [110] B. Howarth, C. L. Raymond, and I. Sutherland. Polyethylene compounds containing mineral fillers modified by acid coatings. 2: Factors influencing mechanical properties. *Polymer Engineering Science*, 41:1345 – 1364, 2001.
- [111] S. Kim. Flame retardancy and smoke suppression of magnesium hydroxide filled polyethylene. *Journal Polymer Science, Part B: Polymer Physics*, 41:936 – 944, 2003.
- [112] H. Hausmann and V. Flaris. Polymeric coupling agents as property enhancers in highly filled polymer systems. *Polym. Polym. Comp.*, 5:113 – 119, 1997.

- [113] S. Lipponen and J. Seppaelae. Ethylene/silane copolymers prepared with a metallocene catalyst as polymeric additives in polyethylene/aluminum trihydroxide composites. *Journal of Polymer Science Part A: Polymer Chemistry*, 43:5597 – 5608, 2005.
- [114] S. M. Lomakin, S. V. Usachev, E. V. Koverzanova, L. V. Ruban, I. G. Kalinina, and G. E. Zaikov. An investigation of thermal degradation of polymer flame retardant additives: triphenylphosphine and modified/intercalated trimethylphosphine. In *10th annual conf. Recent Advances in the Fire Retardancy of Polymeric Materials*, Business Communication Co, Norwalk, USA, 1999.
- [115] L. Ruban, S. Lomakin, and G. E. Zaikov. *Polymer nanocomposites with participation of layer aluminium silicates* in Zaikov G E and Khalturinski N A (eds), *218 Fire retardant materials 'Low Flammability Polymeric Materials*. Nova Science Publishers, New York, 1999.
- [116] C. Huggett. Estimation of rate of heat release by means of oxygen consumption measurements. *Fire and Materials*, 4:61 – 65, 1980.
- [117] V. Babrauskas. Development of the cone calorimeter-a bench-scale heat release rate apparatus based on oxygen consumption. *Fire and Materials*, 8:81 – 95, 1984.
- [118] L. J. Bellamy. *The Infrared Spectra of Complex Molecules*, volume 1. Chapman and Hall, 3rd edition, 1986.
- [119] D. L. Bish and G. W. Brindley. A reinvestigation of takovite, a nickel aluminumhydroxy-carbonate of the pyroaurite group. *Amer. Min.*, 62:458, 1977.
- [120] K. Fuda, N. Sudo, S. Kawai, and T. Matsunaga. Preparation of zn/ga-layered double hydroxide and its thermal decomposition behavior. *Chemistry Letters*, 22:777 – 780, 1993.
- [121] M. J. Hernandez-Moreno, M. A. Ulibarri, J.L. Rendon, and C. J. Serna. Ir characteristics of hydrotalcite-like compounds. *Phys. Chem. Minerals*, 12:34 – 38, 1985.
- [122] J. T. Klopogge, D. Wharton, L. Hickey, and R. L. Frost. Infrared and raman study of interlayer anions CO_3^{2-} , NO_3^- , SO_4^{2-} and ClO_4^- in Mg/Al hydrotalcite. *American Mineralogist*, 87:623 – 629, 2002.
- [123] J. Coates. *Interpretation of Infrared Spectra, A Practical Approach in Encyclopedia of Analytical Chemistry*, R. A. Meyers (Ed). Jonh Wiley & Sons Ltd. Chichester, 2000.
- [124] M. Borja and P. K. Dutta. Fatty acids in layered metal hydroxides: membrane-like structure and dynamics. *Journal of Physical Chemistry*, 96:5434 – 5444, 1992.
- [125] E. Kanezaki. Effect of atomic ratio mg/al in layers of mg and al layered double hydroxide on thermal stability of hydrotalcite-like layered structure by means of in situ high temeperature powder x-ray diffraction. *Materials Research Bulletin*, 33:773 – 778, 1998.
- [126] P. Bera, M. Rajamathi, M. S. Hegde, and P. V. Kamath. Thermal behavior of hydroxides, hydroxysalts and hydrotalcites. *Bulletin of Material Science*, 23:141 – 145, 2000.
- [127] S. K. Yun and T. J. Pinnavaia. Water content and particle texture of synthetic hydrotalcite-like layered double hydroxides. *Chemisty of Materials*, 7:348 – 354, 1995.

- [128] F. Leroux, M. A. Pagano, M. Intissar, S. Chauviere, C. Rorano, and J. P. Besse. Delamination and restacking of layered double hydroxides. *Journal of Materials Chemistry*, 11:105 – 112, 2001.
- [129] K. Grundke, T. Bogumil, T. Gietzelt, H. J. Jacobasch, D. Y. Kwok, and A. W. Newman. Wetting measurements on smooth, rough and porous solid surfaces. *Prog. Colloid Polym. Sci.*, 101:58 – 68, 1996.
- [130] K. Grundke and A. Augsburg. On the determination of the surface energetics of porous polymer materials. *Journal of Adhesion Science and Technology*, 14:765 – 776, 2000.
- [131] A. Leuteritz, D. Pospiech, B. Kretzschmar, D. Jehnichen, U. Jentzsch, K. Grundke, and A. Janke. Characterization and comparison of organically modified clay compounds and their nanocomposites with polypropylene. In *Proc. Second World Congress Nanocomposites, San Diego, USA*, 2002.
- [132] T. Itoh, N. Ohta, T. Shichi, T. Yui, and K. Tagaki. The self-assembling properties of stearate ions in hydrotalcite clay composites. *Langmuir*, 19:9120 – 9126, 2003.
- [133] A. B. Morgan and J. W. Gilman. Characterization of polymer-layered silicate (clay) nanocomposites by transmission electron microscopy and x-ray diffraction: A comparative study. *Journal of Applied Polymer Science*, 87:1329 – 1338, 2003.
- [134] R. A. Vaia and W. Liu. X-ray powder diffraction of polymer/layered silicate nanocomposites: Model and practice. *Journal of Polymer Science, Part B: Polymer Physics*, 40:1590 – 1600, 2002.
- [135] K. Wang, S. Liang, R. Du, Q. Zhang, and Q. Fu. The interplay of thermodynamics and shear on the dispersion of polymer nanocomposite. *Polymer*, 45:7953 – 7960, 2004.
- [136] H. R. Dennis, D. L. Hunter, D. Chang, S. Kim, J. L. White, J. W. Cho, and D. R. Paul. Effect of melt processing conditions on the extent of exfoliation in organo-clay based nanocomposites. *Polymer*, 42:9513 – 9522, 2001.
- [137] W. Lertwimolnun and B. Vergnes. Influence of compatibilizer and processing conditions on the dispersion of nanoclay in a polypropylene matrix. *Polymer*, 46:3462 – 3471, 2005.
- [138] S. A. Solin, D. Hines, S. K. Yun, T. J. Pinnavaia, and M. F. Thorpe. Layer rigidity in 2D disordered Ni-Al layer double hydroxides. *Journal of Non-Crystalline Solids*, 182:212 – 220, 1995.
- [139] G. Liang, J. Xu, S. Bao, and W. Xu. Polyethylene/maleic anhydride grafted polyethylene/organic-montmorillonite nanocomposites. i. preparation, microstructure, and mechanical properties. *Journal of Applied Polymer Science*, 91:3974 – 3980, 2004.
- [140] T. G. Gopakumar, J. A. Lee, M. Kontopoulou, and J. S. Parent. Influence of clay exfoliation on the physical properties of montmorillonite/polyethylene composites. *Polymer*, 43:5483 – 5491, 2002.
- [141] A. C. Balazs, C. Singh, and E. Zhulina. Modeling the interaction between polymers and clay surfaces through self-consistent field theory. *Macromolecules*, 31:8370 – 8381, 1998.

- [142] J. W. Gilman, A. B. Morgan, and R. Harris (Jr.). Polymer layered silicate nanocomposites: Polyamide-6, polypropylene and polystyrene. In *Proc. New Advances in Flame Retardant Technology. Proceedings. Fire Retardant Chemicals Association, Lancaster, PA, USA*, pages 9 – 22, 1999.
- [143] H. A. Barnes. Thixotropy - a review. *Journal of Non-Newtonian Fluid Mechanics*, 70:1 – 33, 1997.
- [144] A. I. Leonov. On the rheology of filled polymers. *J. Rheology*, 34:1039 – 1068, 1990.
- [145] C. W. Macosko. *Rheology Principles, Measurements and Applications*. VCH Publishers, USA, 1993.
- [146] T. G. Mezger. *The Rheology Handbook for users of rotational and oscillatory rheometer, edited by Dr. Ulrich Zroll*. Curl R. Vincentz Verlag, Hannover, Germany, 2002.
- [147] J. Ren, A. S. Silva, and R. Krishnamoorti. Linear viscoelasticity of disordereed polystyrene-polypropylene block copolymer based layered-silicate nanocomposites. *Macromolecules*, 33:3739 – 3746, 2000.
- [148] R. Krishnamoorti, R. A. Vaia, and E. P. Giannelis. Structure and dynamics of polymer-layered silicate, nanocomposites. *Chemisty of Materials*, 8:1728 – 1734, 1996.
- [149] K. M. Lee and C. D. Han. Effect of hydrogen bonding on the rheology of polycarbonate/organoclay nanocomposites. *Polymer*, 44:4573 – 4588, 2003.
- [150] M. J. Solomon, A. S. Almusallam, K. F. Seefeldt, A Somwangthanaroj, and P. Vardan. Rheology of polypropylene/clay hybrid materials. *Macromolecules*, 34:1864 – 1872, 2001.
- [151] R. Krishnamoorti and E. P. Giannelis. Rheology of end-thethered polymer layered silicate nanocomposites. *Macromolecules*, 30:4097 – 4102, 1997.
- [152] F.R. Costa, B.K. Satapathy, U. Wagenknecht, R. Weidisch, and G. Heinrich. Morphology and fracture behaviour of polyethylene/MgAl layered double hydroxide (LDH) nanocomposites. *European Polymer Journal*, 42:2140 – 2152, 2006.
- [153] M. Klueppel. The role of disorder in filler reinforcement of elastomers on various length scales. *Advances in Polymer Science*, 164:1 – 86, 2003.
- [154] R. Wagner and T. J. G. Reisinger. A rheological method to compare the degree of exfoliation of nanocomposites. *Polymer*, 44:7513 – 7518, 2003.
- [155] R.G. Larson. *The structure and rheology of complex fluids*. Oxford University Press, New York, Oxford, 1999.
- [156] G. Heinrich and M. Klueppel. Recent advances in the theory of filler networking in elastomers. *Advances in Polymer Science*, 160:1 – 44, 2002.
- [157] A. Subbotin, A . Semenov, E. Manias, G. Hadziioannou, and G. ten Brinke. Rheology of confined polymer melts under shear flow: Strong adsorption limit. *Macromolecules*, 28:1511 – 1515, 1996.

- [158] R. Krishnamoorti, J. Ren, and A. S. Silva. Shear response of layered silicate nanocomposites. *J. Chem. Phys.*, 114:4968 – 4973, 2001.
- [159] L. M. Walker, N. L. Wagner, R. G. Larson, P. A. Mirau, and P. Moldenaers. The rheology of highly concentrated PBLG solutions. *Journal of Rheology*, 39:925 – 952, 1995.
- [160] K. M. Lee and C. D. Han. Rheology of organoclay nanocomposites: Effects of polymer matrix/organoclay compatibility and the gallery distance of organoclay. *Macromolecules*, 36:7165 – 7178, 2003.
- [161] R. A. Stratton and A. F. Butcher. Stress relaxation upon cessation of steady flow and the overshoot effect of polymer solutions. *Journal of Polymer Science: Polymer Physics Edition*, 11:1747 – 1758, 1973.
- [162] M. Doi and S. F. Edward. Dynamics of concentrated polymer systems. part 4.-rheological properties. *Journal of the Chemical Society, Faraday Transactions 2: Molecular and Chemical Physics*, 75:38 – 54, 1979.
- [163] M. Doi and S. F. Edwards. *The theory of polymer dynamics*. University Press, Oxford, 1986.
- [164] M. Doi and S. F. Edwards. Dynamics of concentrated polymer systems part 2.-molecular motion under flow. *Journal of the Chemical Society, Faraday Transactions 2: Molecular and Chemical Physics*, 74:1802 – 1817, 1978.
- [165] K. Osaki, T. Inoue, and T. Isomura. Stress overshoot of polymer solutions at high rates of shear. *Journal of Polymer Science Part B: Polymer Physics*, 38:1917 – 1925, 2000.
- [166] K. Osaki. On the damping function of shear relaxation modulus for entangled polymers. *Rheologica Acta*, 32:429 – 437, 1993.
- [167] M. H. Wagner. Analysis of time-dependent non-linear stress-growth data for shear and elongational flow of a low-density branched polyethylene melt. *Rheological Acta*, 15:136 – 142, 1976.
- [168] T. C. B. McLeish and R. G. Larson. Molecular constitutive equations for a class of branched polymers: The pom-pom polymer. *Journal of Rheology*, 42:81 – 110, 1998.
- [169] M. Sobhanie and A. I. Isayev. Modelling and experimental investigation of shear flow of a filled polymer. *Journal of Non-Newtonian Fluid Mechanics*, 85:189 – 212, 1999.
- [170] J. Ren and R. Krishnamoorti. Nonlinear viscoelastic properties of layered -silicate-based intercalated nanocomposites. *Macromolecules*, 36:4443 – 4451, 2003.
- [171] J. Li, C. Zhou, G. Wang, and D. Zhao. Study on rheological behavior of polypropylene/clay nanocomposites. *Journal of Applied Polymer Science*, 89:3609 – 3617, 2003.
- [172] M. Barut, R. Lapasin, A. Zupancic, and M. Zumer. Time dependent rheological behaviors of tio₂ suspensions. In *Proc. XIIth Congr. on Rheology, August 18-23, Quebec City, Canada*, page 578, 1996.

- [173] A. Mujumdar, A. N. Beris, and A. B. Metzner. Transient phenomena in thixotropic systems. *Journal of Non-Newtonian Fluid Mechanics*, 102:157 – 178, 2002.
- [174] M. Wagner. Zur Netzwerktheorie von Polymer-Schmelzen. *Rheological Acta*, 18:33 – 50, 1979.
- [175] R.B.Bird, R. C. Armstrong, and O. Hassager. *Dynamics of polymeric fluids*, volume 1. John Wiley and Sons, New York, 2nd edition, 1987.
- [176] A. Lion, C. Kardelky, and P. Haupt. On the frequency and amplitude dependence of the Payne effect: Theory and experiments. *Rubber Chemistry and Technology*, 76:533– 547, 2002.
- [177] D. Acierno, F.P. La Mantia, G. Marruca, G. Rizzo, and G. Titomanlio. A non-linear viscoelastic model with structure-dependent relaxation times ii. comparison with l.d. polyethylene transient stress results. *Journal of Non-Newtonian Fluid Mechanics*, 1:147 – 157, 1976.
- [178] F. R. Costa, U. Wagenknecht, Dieter Jehnichen, M. Abdel-Goad, and G. Heinrich. Nanocomposites based on polyethylene and Mg-Al layered double hydroxide: II. rheological characterization. *Polymer*, 47:1649 – 1660, 2006.
- [179] Z. Wang, B. Qu, W. Fan, and P. Huang. Combustion characteristics of halogen-free flame-retarded polyethylene containing magnesium hydroxide and some synergists. *Journal of Applied Polymer Science*, 81:206 – 214, 2001.
- [180] M. J. Scudamore, P. J. Briggs, and F. H. Prager. Cone calorimetry-a review of tests carried out on plastics for the association of plastic manufacturers in europe. *Fire and Materials*, 15:65 – 84, 1991.
- [181] C. Zhao, H. Qin, F. Gong, M. Feng, S. Zhang, and M. Yang. Mechanical, thermal and flammability properties of polyethylene/clay nanocomposites. *Polymer Degradation and Stability*, 87:183 – 189, 2005.
- [182] J. Rychly and L. Costa. Modelling of polymer ignition and burning adopted for cone calorimeter measurements: The correlation between the rate of heat release and oxygen index. *Fire and Materials*, 19:215 – 220, 1995.
- [183] J. H. Yeh, M. J. Yang, and S. H. Hsieh. Combustion of polyethylenes filled with metallic hydroxides and ethylene vinyl acetate copolymer. *Polymer Degradation and Stability*, 61:465 – 472, 1998.
- [184] H. Hippi, J. Mattila, M. Korhonen, and J. Seppälä. Compatibilization of polyethylene/aluminum hydroxide (PE/ATH) and polyethylene/magnesium hydroxide (PE/MH) composites with functionalized polyethylenes. *Polymer*, 44:1193 – 1201, 2003.
- [185] S. Vornov, V. Tokarev, K. Oduola, and Y. Lastukhin. Polyperoxide surfactants for interface modification and compatibilization of polymer colloidal systems. I. synthesis and properties of polyperoxide surfactants. *Journal of Applied Polymer Science*, 76:1217 – 1227, 2000.

- [186] S. Vornov, V. Tokarev, V. Datsyuk, V. Seredyuk, O. Bednarska, K. Oduolar, H. Adler, C. Puschke, A. Pich, and U. Wagenknecht. Polyperoxidic surfactants for interface modification and compatibilization of polymer colloidal systems. II. design of compatibilizing layers. *Journal of Applied Polymer Science*, 76:1228 – 1239, 2000.
- [187] B. Schartel, P. Poetschke, U. Knoll, and M. Abdel-Goad. Fire behaviour of polyamide 6/multiwall carbon nanotube nanocomposites. *European Polymer Journal*, 41:1061 – 1070, 2005.
- [188] Y. Feng, D. Li, Y. Wang, D. G. Evans, and X. Duan. Synthesis and characterization of a UV absorbent-intercalated Zn/Al layered double hydroxide. *Polymer Degradation and Stability*, 91:789 – 794, 2006.
- [189] S. Guo, D. G. Evans, and D. Li. Preparation of C.I. pigment 52:1 anion-pillared layered double hydroxide and the thermo- and photostability of the resulting intercalated material. *Journal of Physics and Chemistry of Solids*, 67:1002 – 1006, 2006.
- [190] W-. Z. Li, J-. S. Chen J. Lu, G-. D. Li, Y-. S. Jiang, L-. S. Li, and B-. Q. Huang. Phenoxymethylpenicillin-intercalated hydrotalcite as bacteria inhibitor. *Journal of Chemical Technology and Biotechnology*, 81:89 – 93, 2006.

List of Figures

1.1	Schematic representation of polymer combustion process [2].	2
1.2	Schematic flame spread during of polymer combustion process [2].	3
2.1	Schematic Representation comparing the crystal structure of brucite (A) and LDH (B) .	6
2.2	Schematic pathways of in-situ polymerization within LDH layers to synthesize polymer-LDH nanocomposites	9
2.3	Preparation of LDH-polyimide (LDH-AB/PI) nanocomposites (LDH-AB: aminobenzoate intercalated LDH, ODA: 4,4'-oxydianiline, PMDA: pyromellitic anhydride [38]. .	11
2.4	XRD patterns of LDH and LDH nanocomposites: (a) LDH-PSS, (b) LDH-PVS and (c) LDH-CO ₃ [41].	14
2.5	(left) The x-ray diffraction patterns of LDHs-aminolaurate (a), LDHs/Epoxy resin (b - e) [(b) - stirred at room temperature for 60 min, (c) - at 55°C for 30 min, (d) - at 55°C for 60 min and (e) - 55°C for 180 min] and LDHs/Epoxy/Curing agent (f - k) [(f) - stirred at room temperature for 60min, (g) - at 75°C for 30 min, (h) - at 75°C for 60 min, (i) - at 75°C for 120 min, (j) - at 135°C for 30 min and (k) - at 135°C for 60 min.] [53]. (right) The XRD patterns of at different stages during two-step bulk polymerization of MMA in presence of organically pillared LDH (LDH-U) and catalysts (a) unmodified LDH-U; (b) mixture of LDH-U, MMA and catalyst stirring at room temperature; at various conversions of MMA during the prepolymerization process (c) 6.3 wt%, (d) 8.4 wt%, (e) 10.5 wt%, (f) 13.2 wt%, (g) 16.2 wt%, (h) 17.1 wt%, (i) 18.3 wt%, (j) 19.6 wt% and (k) LDHs/PMMA nanocomposite [34].	15
2.6	Change of XRD patterns with the different contents of LDH content in polystyrene/LDH nanocomposite sample: (a) 100 wt%, (b) 50 wt%, (c) 20 wt%, (d) 10 wt%, (e) 5 wt% [49].	16
2.7	TEM micrographs showing LDH particle dispersion in different polymer (a) PMMA [34], (b) epoxy [53], (c) polyamide 6 [60] and (d) polystyrene containing 5 wt% LDH [49]	16
2.8	SEM micrographs of Zn-Al LDH prepared by co-precipitation method (A) and Zn-Al/polystyrene sulfonate nanocomposites prepared by (a) in situ polymerization, (b) reconstruction, (c) direct exchange and (d) restacking. The bars represent 2 μ m. [23]	17
2.9	Effects of the LDHs content on the tensile properties (tensile strength, Young's modulus and strain at break) of the epoxy/LDH nanocomposites. [53]	18
2.10	Left: TGA curves of LDH/polyimide nanocomposites with various LDH loadings, Right: Effects of LDH content on the decomposition temperatures at 5 and 10 % weight loss of LDH/polyimide nanocomposites [38].	20

2.11	The effect of LDH on ionic conductivity of Poly(ethylene glycol diacrylate)/Mg-Al-LDH/ LiClO ₄ based polymer nanocomposite [69].	20
2.12	Various fields of application of LDH materials [5].	21
2.13	Dependence of the effective activation energy (E _a) on the extent of conversion (α) for the thermo-oxidative degradation of virgin LLDPE and its nanocomposites. (MMT NC 10 = LLDPE/montmorilinite, ZnAlNC 10 = LLDPE/Zn-Al-LDH and MgAlNC 10 = LLDPE/Mg-Al-LDH; the filler contents are 10 wt%) [106]	26
3.1	Brabender plasticorder: (left) the mixing chamber and (right) sigma type screw used for melt-compounding	31
3.2	Shear cycle used during non-linear shear or flow reversal experiments	35
3.3	A typical LOI measuring instrument	36
3.4	Schematic representation of a cone calorimeter unit	37
3.5	Schematic representation of a UL-94 VB (top) and UL-94 HB (bottom) test methods	39
4.1	Different surfactants used for intercalation within the LDH gallery	41
4.2	XRD patterns of different Mg-Al-LDH clay materials without interlayer modification (* indicates the unknown reflections in the industrial samples).	42
4.3	Comparison of the FTIR spectra of synthesized Mg-Al-LDH, CLDH, LDHR and an industrial Mg-Al-LDH showing the recovery of original structure LDH after regeneration process.	43
4.4	XRD patterns of modified LDH obtained using regeneration methods in presence of various surfactants.	44
4.5	FTIR spectra of the LDH modified by different anionic surfactants using regeneration method (the assignments of various bands are given in Table 4.3)	47
4.6	SEM micrographs of the LDH samples: A = unmodified Mg-Al-LDH, B = CLDH, C = LDH-laurate, D = LDH-DS, E = LDH-DBS and F = LDH-BEHP (magnification bar 2μm)	49
4.7	High magnification SEM micrographs showing the finer details of the surface morphology of the primary particles in LDH-laurate (A), LDH-DS (B) and LDH-DBS (C). (magnification bar 2μm)	50
4.8	TG plots of LDH synthesized by urea method and its various modified forms.	51
4.9	DTG curves for LDH and its various modified forms showing major decomposition stages.	52
4.10	XRD patterns of unmodified LDH (left) and LDH-DBS (right) measured at different temperature showing the change in structure with temperature	54
4.11	TGA analysis of LDH and LDH-DBS in different atmospheres	55
4.12	FTIR spectra of unmodified LDH (A-C) and LDH-DBS (D) taken at different temperatures showing changes in the structure of the unmodified clay material.	57
4.13	Kγ _h cosθ versus γ _h plots of LDH, CLDH and LDH-DBS. The plot for Mg(OH) ₂ is also shown for comparison. The maximum in each plot gives a measure of the surface tension of the respective powdered sample. The parameter in the y axis is normalized against the maximum value and the error bar in each points are omitted for having better visibility of the maxima	58

5.1	WAXS patterns (top) and representative TEM micrographs of PE/LDH nanocomposites (below: LDH concentration are shown) prepared by melt-compounding in Brabender plasticorder.	61
5.2	High magnification TEM showing exfoliated LDH layers fragments (some indicated by arrow marks) in PE/LDH nanocomposites containing low (left, 4.72 wt%) and high (right, 16.20 wt%) LDH concentration (magnification bar 100 nm).	62
5.3	WAXS patterns for PE/LDH compositions prepared in twin screw extruder	63
5.4	Morphological analysis of the LDH particles: A: SEM image of LDH-DBS and B-E: low magnification TEM images of PE/LDH nanocomposites [B: PE-LDH2 (4.72 wt%), C: PE-LDH3 (6.89 wt%), D: PE-LDH4 (8.95 wt%) and E: PE-LDH5 (12.75 wt%)] . . .	64
5.5	TEM micrographs showing that exfoliated LDH particles exist both in the bulk matrix (A) and also in the vicinity of the originating bigger particles (B).	65
5.6	High magnification TEM micrograph showing that LDH particles also undergo exfoliation into single layers (A: PE-LDH3 and B: PE-LDH4)	66
5.7	TEM images showing different types structural associations formed by the dispersed LDH particle in PE/LDH nanocomposite matrix: (a) formation of aggregates by the primary LDH platelets and (b) structural association among the exfoliated clay layers. . .	67
5.8	FTIR spectra for PE-g-MAH and PE-g-MAH/LDH composites showing changed occurring in peaks characteristics of MAH functional groups in presence of LDH	68
5.9	Thermogravimetric analysis of polyethylene/LDH nanocomposites prepared by melt-mixing in extruder (the LDH concentration increases from 2.43 wt% in PE-LDH1 to 16.20 wt% in PE-LDH6)	69
5.10	The influence of LDH concentration on (A) the decomposition temperatures at 10% weight loss ($T_{0.1}$) and 50% weight loss ($T_{0.5}$) (B) the amount of residue at 750 °C and its comparison with theoretically calculated value	71
5.11	Comparison of the Thermogravimetric analysis of PE/LDH nanocomposite under oxygen and nitrogen atmosphere	72
5.12	Strain dependence of the in-phase component stress response (storage modulus, normalized w.r.t. linear value) during an oscillatory shear experiment	73
5.13	Difference in the viscoelastic response (storage modulus, G' and loss modulus G'') of unfilled polyethylene and high LDH filled nanocomposite in a dynamic oscillatory frequency sweep experiment	74
5.14	Storage modulus (G') versus frequency (ω) plots for unfilled PE and PE/LDH nanocomposite melts based on the results obtained from dynamic oscillatory measurements. The table on right the relaxation exponents obtained by fitting low frequency data to the power law model	75
5.15	Step strain experiment showing how the stress relaxation modulus varies decays with time in unfilled PE and in the PE/LDH nanocomposite melts having different LDH concentrations	77

5.16	Complex viscosity ($ \eta^* $) versus frequency (ω) plots for unfilled PE and PE/LDH nanocomposite melts obtained from a dynamic oscillatory shear experiments. The table on the right indicates the sample designation and also the value of the corresponding shear thinning exponent n_2	78
5.17	Viscosity at low frequency (0.05 rad) as a function of LDH concentration in PE/LDH nanocomposites	79
5.18	Steady shear flow behavior of unfilled PE melt. (A) The influence of shear rate, (B) corresponding strain scaling of the stress at different shear rates, (C) the inverse relation between the shear rate and the time (t_s) at which stress overshoot occurs and (D) the influence of rest period prior to shearing on the steady shear response. The melt temperature was 240 °C.	82
5.19	Influence of low molecular weight functionalized polymer (PE-g-MAH) on the steady shear viscosity of the unfilled PE melt ($\dot{\gamma} = 0.3s^{-1}$).	84
5.20	Effect of LDH concentration on the stress growth during the flow reversal step in the flow reversal experiment (shearing was carried out for 600 s, but the steady state is reached within 300 s; ($\dot{\gamma} = 0.3s^{-1}$).	85
5.21	Effect of rest period on the stress overshoot during start-up flows in the second steady shear step in a flow reversal experiments.	87
5.22	The experimental results showing how the storage modulus (measured by applying low amplitude (1.0%) and low frequency (1 rad/s) dynamic oscillatory shearing during rest period t_{rest}) changes with time (A) and the corresponding transient steady shear response followed after the rest period (B). (The ratio shown in bracket indicates the ratio of LDH and functionalized polymer in the nanocomposites)	88
5.23	Plots showing the variation of storage modulus with time during oscillatory shearing in the non-linear viscoelastic regime (carried out at 50% strain amplitude and 1 rad/s frequency) (A) and linear viscoelastic regime (carried out at 2% strain amplitude and 1 rad/s frequency) (B).	89
5.24	Reverse shear flow experiment for the nanocomposite PE-LDH2: $ \dot{\gamma} $. Symbols - experiment; lines - modified Wagner model in which $\beta(t)$ is given by eq. (5.11). $\beta_R = 0.14$, $\beta_{st} = 0.02$, $T_R = 500s$, $\beta(t_{rest}) - \beta_{end} = 0.02$, $T_B = 50s$, $\lambda_0 = 30s$	94
5.25	Mechanical properties of PE/LDH nanocomposites	95
5.26	SEM micrographs showing the fracture surface morphology of PE/LDH nanocomposite: (a) unfilled PE, (b) PE-LDH1, (c) PE-LDH2, (d) PE-LDH3, (e) PE-LDH4 and (f) PE-LDH5	96
5.27	SEM images of fractured surface of PE-LDH2 sample showing morphology at different region of the matrix: (a) overall morphology (magnification 200X), (b) at the interface of particle rich and particle devoid regions (magnification 1KX), (c) particle devoid region (magnification 20KX) and (d) particle rich region (magnification 30KX) (the black arrows show the individual or small stacks of LDH platelets)	97
5.28	The bridging effects at the interface between the particle rich region (indicated by arrow) and particle devoid region in PE/LDH nanocomposite compositions containing (a) 4.72 wt% and (b) 16.20 wt % LDH	98

6.1	Limited oxygen index (LOI) of PE/LDH nanocomposites (the value shown have ± 0.5 unit variation)	100
6.2	The effect of LDH loading on the dripping tendency of the PE/LDH nanocomposites (Time to start dripping is the time after first 10 second flame application at which first dripping occurs that ignites a piece of cotton underneath during UL94V testing)	102
6.3	Dripping behavior of unfilled PE (left) and PE/LDH nanocomposite containing 12.75 wt% LDH (PE-LDH5) (right) (pictures were taken approximately after the same time period from the cessation of first 10 s flame application during UL94V test)	103
6.4	Influence of LDH loading on the rate of burning during UL94 HB test (at each composition average of three measurements were taken)	103
6.5	Cone-calorimeter investigation results showing (A) variation of heat release rate (HRR) with time, (B) total heat released (THR) with time and (C) variation of time of ignition (t_{ig}) and peak heat release rate (PHRR) with LDH concentration in the PE/LDH nanocomposites.	104
6.6	Graphical assessment of fire risk associated with PE/LDH nanocomposites, plotting THR against PHRR/ t_{ig} for different LDH concentration (the LDH concentration increases from right to left as shown)	106
6.7	The variation of carbon dioxide (CO_2) and carbon monoxide (CO) release rate during combustion in a cone calorimeter chamber with burning time.	107
6.8	Cone calorimeter investigation results showing changes in mass of sample with combustion time (left) and average specific mass loss rate with increasing LDH concentration (right).	107
6.9	Variation of LOI values in the polyethylene/LDH nanocomposites with increasing PHRR, the number shown after the label of every data point indicates the LDH concentration in the respective sample.	108
6.10	Pictures showing the nature of the residue after complete combustion of the PE/LDH nanocomposite samples during cone calorimeter testing: A - PE-LDH1, B - PE-LDH2, C - PE-LDH3, D - PE-LDH4, E - PE-LDH5 and F - PE-LDH6.	109
6.11	Synergistic effect of LDH in $\text{Mg}(\text{OH})_2$ filled PE composites: LOI values have compared between composites where magnesium hydroxide is being progressively replaced by LDH (X represent total weight percent of filler i.e. $\text{Mg}(\text{OH})_2 + \text{LDH}$)	112
6.12	Thermogravimetric analysis of PE/MH and PE/LDH/MH composites.	113
6.13	Cone-calorimeter investigation results for the PE/MH and the PE/LDH/MH composites, showing synergistic effect of LDH with MH (L and M stands for LDH and MH respectively and the number before them indicate the weight percentage)	114
B.1	ARES rheometer with parallel plate geometry used for rheological analysis	145
C.1	Experimental setup for surface tension measurement of LDH materials using capillary penetration method	148

List of Tables

2.1	Selected cone calorimeter investigation results for polymer/layered silicate nanocomposites at 35 kW/m ² heat flux [67]	25
3.1	Various technical details of the commercial Mg-Al-LDH used in the present study	28
3.2	Various technical details of the surfactants used for the modification of Mg-Al-LDH	29
3.3	Description of the different polymeric materials used	30
3.4	Designation of PE/LDH nanocomposite composition and the actual metal hydroxide content in each composition	32
3.5	Different parameters measured during cone calorimeter tests	38
3.6	UL-94 vertical and horizontal test criteria	38
4.1	Assignment of various XRD reflections obtained for LDH and its modified forms	45
4.2	Comparison between theoretically calculated and experimentally observed values of the basal spacing in the modified LDH materials	46
4.3	Assignment of FTIR bands in LDH modified with different surfactants by regeneration method [19, 118, 123, 124]	48
6.1	Comparison of the combustion residue obtained from thermogravimetric analysis (TGA), cone-calorimeter and theoretical calculation	110
6.2	Summary of UL94 vertical burn test for PE/MH and PE/LDH/MH composites (sample size: 125 mm x 10 mm x 4 mm)	115
6.3	Summary of mechanical properties of PE/MH and PE/LDH/MH composites	116
A.1	Compositional analysis of LDH materials	143

Appendices

THEORETICAL CALCULATION OF COMBUSTION RESIDUE

The general chemical formulation of Mg-Al-LDH or hydrotalcite is $[\text{Mg}_{1-x}\text{Al}_x(\text{OH})_2](\text{CO}_3)_{x/2} \cdot n\text{H}_2\text{O}$, where the value of n is usually taken as 0.4 and that of x lies between 0.25 to 0.33. The molar ratio of MgO and Al_2O_3 in the commercial Mg-Al-LDH used in this study is about 2.3, which corresponds to a value of x equal to 0.30. In SDBS modified LDH, the extent of SDBS intercalated was calculated from the sulfur content of the modified sample. The C and H content of the sample was also compared, but these values are less reliable as their values are influenced by the physically adsorbed H_2O and CO_2 . In doing compositional analysis based on sulfur content in the modified samples, one assumption was made that DBS (dodecylbenzenesulfonate) content in the modified LDH corresponds to the stoichiometric content. This means that all the DBS anions attached to LDH sheets to neutralize their unbalanced charge. Table A1 shows the compositional analysis of Mg-Al-LDH and its SDBS modified form.

Table A.1 Compositional analysis of LDH materials

Material	Molar mass	C content	H content	S content
	g/mol	%	%	%
Calculated				
$[\text{Mg}_{1-x}\text{Al}_x(\text{OH})_2](\text{CO}_3)_{x/2} \cdot n\text{H}_2\text{O}$	75.31	2.39	3.71	0.00
$[\text{Mg}_{1-x}\text{Al}_x(\text{OH})_2](\text{DBS})_x \cdot n\text{H}_2\text{O}$	163.81	35.16	5.31	5.86
Observed				
Mg-Al-LDH	-	2.37	3.92	0.00
SDBS modified Mg-Al-LDH	-	30.39	6.11	4.45

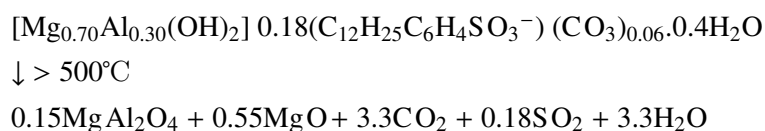
From Table A1, it is obvious that the theoretical calculation of unmodified LDH shows close resemblance to the experimentally observed values (the observed values shown are the average of three mea-

surements, which showed small variation). But, in case of SDBS modified form, the calculated values for 100 % CO_3^{2-} substitution by DBS anion are higher than that observed experimentally. This means that modification by SDBS using regeneration method results partial substitution of CO_3^{2-} by DBS anions. Therefore, the probable chemical formula of the modified LDH can be written as $[\text{Mg}_{1-x}\text{Al}_x(\text{OH})_2](\text{DBS})_y(\text{CO}_3)_{(x-y)/2} \cdot n\text{H}_2\text{O}$, where $y < x$. The value of y can be obtained by trial and error method to show closest similarity to the sulphur content in the modified sample determined experimentally. A value of y equal to 0.18 gives sulphur content in the modified sample equal to 4.49 %, which is close to 4.45 % observed experimentally. The corresponding values for C and H contents are 30.84 % and 6.25 %. Therefore, the chemical composition of the SDBS modified LDH can be written as $[\text{Mg}_{0.70}\text{Al}_{0.30}(\text{OH})_2](\text{DBS})_{0.18}(\text{CO}_3)_{0.06} \cdot 0.4\text{H}_2\text{O}$. According to this chemical composition the metal hydroxide content in the SDBS modified LDH is about 46.0 wt% and based on this metal hydroxide content PE/LDH nanocomposites were prepared.

Mg-Al-LDH on thermal decomposition above 500 °C gives metal oxides, carbon dioxide and water vapor. The generally accepted decomposition products of Mg-Al-LDH after thermal decomposition are given below



For the SDBS modified Mg-Al-LDH (LDH-DBS), if it is assumed that similar metal oxides are formed after complete thermal decomposition in presence of oxygen, then following reaction scheme can be written for LDH-DBS.



In case of complete combustion of PE/LDH nanocomposite, it can be assumed that the residue left is constituted by these metal oxides and all organic contents are converted into gaseous products, like CO_2 , H_2O , etc. Therefore from the above decomposition reaction of SDBS modified LDH one can easily calculate the amount of residue formed after combustion of a nanocomposite combustion. For example, the composition PE10LDH contains 8.95 g metal hydroxide per 100 g of the sample (see Table 3.4, page). According to the above chemical scheme for thermal decomposition of SDBS modified LDH, 1.0 g metal hydroxide in LDH-DBS yields about 73.61 wt% metal oxide residue. Therefore, the LDH-DBS amount containing 8.95 g metal hydroxide would yield 6.59 g metal oxide residue. If, it is considered that in case of nanocomposite compositions, all organic contents are lost after complete combustion, PE10LDH would produce 6.59% of its initial weight as combustion residue. Using the similar procedure and Table 3.4, the combustion residue in other nanocomposite composition can also be calculated. Obviously, the accuracy of this calculation depends on many factors, like the accuracy of metal hydroxide determination in LDH and its modified form, the exact nature of the metal oxide residue and also the standard deviation in the elemental analysis data.

RHEOLOGICAL MEASUREMENTS

The rheological analysis for the present thesis work were carried out in ARES rheometer using the parallel plate geometry of the sample holding unit. Both dynamic oscillatory and steady shear experiments were performed. The instrument was used under shear strain controlled mode. The general outlook of the instrument and the sample holding unit are shown in Figure B1.

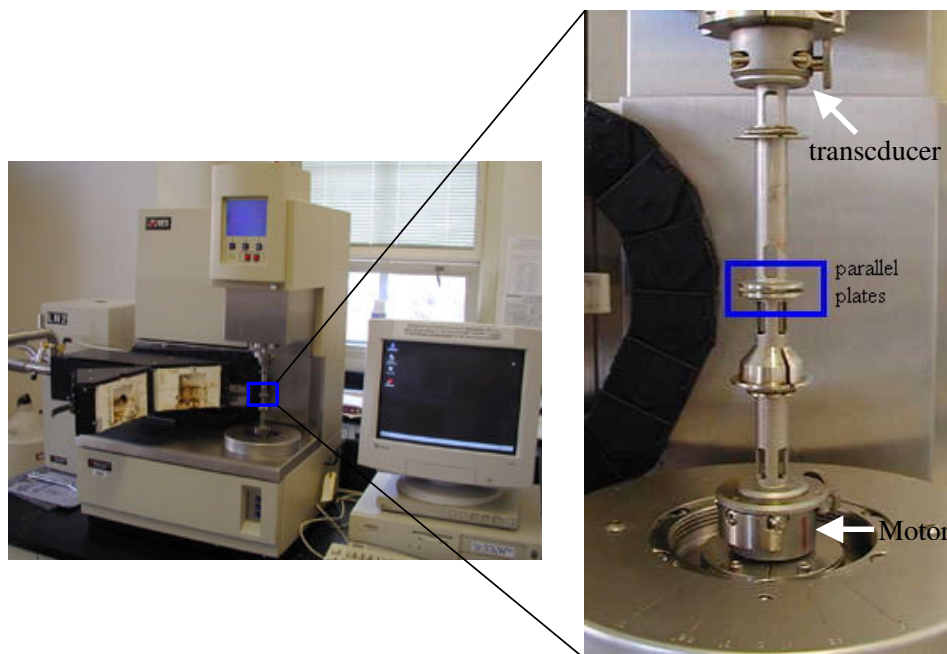


Figure B.1 ARES rheometer with parallel plate geometry used for rheological analysis

The sample holding unit in the rheometer chamber consists of two similar plates of radius R fitted parallel in vertical position. The lower plate is connected to a motor via a cylindrical shaft and the upper plate is connected to a torque-balance transducer. The lower plate is driven by the motor and rotates about its axis maintaining a constant separation with the upper plate during experiment. The upper plate remains fixed, but the transducer connected to it measures the torque experienced by it. The transducer works according to torque-balance principle. This means during experiment, when the sample melt within the parallel plate is sheared by the rotating lower plate, the melt also exerts a force on the upper plate. But, to keep the upper plate in zero position the transducer applies a torque on the upper plate,

which balances the force exerted by the sample.

During both steady and dynamic measurement, the motor applies angular displacement to the upper plate. The calculation of commanded strain and the corresponding stress developed are done using two geometry dependent parameters: stress constant (K_γ) and stress constant (K_τ).

$$\gamma = \theta K_\gamma \quad (\text{B.1})$$

$$\tau = MK_\tau \quad (\text{B.2})$$

where, γ is the commanded strain (desired sample deformation), θ is the angular displacement, τ is the stress (force generated by the torque per unit area of the upper plate surface) and M is the torque.

For parallel-plate geometry of the instrument, with radius of the plates equal to R and distance between them equal to H , the strain and the stress constants are given by

$$K_\gamma = \frac{R}{H} \quad (\text{B.3})$$

$$K_\tau = \frac{2(G_c)}{\pi \left(\frac{R}{10}\right)^3} \quad (\text{B.4})$$

where, G_c is the gravitational constant

In case of dynamic oscillatory measurements, rheological responses are interpreted in terms of parameters, like storage modulus (G'), loss modulus (G''), loss tangent ($\tan\delta$), etc. These parameters are expressed as a function of stress (τ) and strain (γ) as follows.

$$G' = \cos\delta \left(\frac{\tau}{\gamma}\right) \quad (\text{B.5})$$

$$G'' = \sin\delta \left(\frac{\tau}{\gamma}\right) \quad (\text{B.6})$$

where, δ is the phase angle indicating the shift between the stress and strain vectors.

One disadvantage of using parallel-plate configuration is the inhomogeneous shear rate experienced by the sample. From Equations B1 and B3, it is apparent that the shear rate is a function of R . As a results, the value of shear varies in the radial direction from zero at the center of the plate to the maximum at the edge. The calculations are usually based on the maximum shear rate experienced at the edge. This problem can be easily avoided using cone-plate geometry of the instruments. But, with high viscous melts, like those experienced in the present case with high LDH concentration, the sample should be kept for long times often more than hours within the sample chamber at measuring temperature for equilibration. This long exposure may often be detrimental to the materials, especially at high melt temperature (say, 240°C used in the present study). So the choice of parallel-plate geometry was obvious in the present study. Also, the non-linear experiments with unfilled melt has shown, the operating shear rate range does not exceeds the value where the position of the stress overshoot peak with respect to the applied strain during the steady shearing does not vary with shear rate.

SURFACE ENERGY MEASUREMENT USING CAPILLARY PENETRATION METHOD

The principle of the measurement of the surface tension of a porous medium using capillary penetration method is based on Washburn equation, which describes dependence of the height rise with time of a liquid into a porous materials column packed in a single vertical capillary of circular cross section. The relation is given by equation

$$h^2 = \frac{rt}{2\eta} \gamma_{lv} \cos\theta \quad (\text{C.1})$$

where, h is the height of the liquid front, t is the time required for the liquid to rise a distance h above the liquid, r is the radius of the capillary, η is the viscosity of the liquid, θ is the contact angle, γ_{lv} is the total surface tension of the liquid. To apply this relation one has to neglect the influence of the gravity and assume the laminar flow of the liquid within the packed column.

The equation C.1 can be modified by replacing the height h with the weight M of the liquid that penetrates into the capillary of cross sectional area A and density ρ . The modified equation looks like

$$\frac{M^2}{\rho^2 A^2} = \frac{rt}{2\eta} \gamma_{lv} \cos\theta \quad (\text{C.2})$$

which after rearranging becomes

$$\gamma_{lv} \cos\theta = \left[\frac{2}{A^2 r} \right] \left[\frac{\eta}{\rho^2} \right] \left[\frac{M^2}{t} \right] \quad (\text{C.3})$$

The terms $2/(A^2 r)$ and η/ρ^2 in equation C.3 are the geometric factor of the capillary tube and the property of the test liquid used respectively. Whereas, the term M^2/t is an experimentally measurable quantity.

While measuring the surface tension of powdered materials like clay particles, the geometric factor of the packed column is not known. However, if precise care is taken geometry of the packed column made of powdered materials can be maintained roughly constant during preparation of such packed column. In such case, the term $2/(A^2 r)$ can be replaced by an unknown constant K and rewrite equation C.3 as

$$K \gamma_{lv} \cos\theta = \left[\frac{\eta}{\rho^2} \right] \left[\frac{M^2}{t} \right] \quad (\text{C.4})$$

Equation C.4 is the modified Washburn equation used for measuring the surface tension of LDH materials with the assumptions: (1) laminar flow of the liquid within the capillary, (2) insignificant

gravitational effect and (3) constant geometry of the packed capillary column.

The experimental setup used for measuring surface tension of powdered LDH materials using equation C.4 is shown in Figure C.1. The powdered samples were packed in a glass capillary tube of constant diameter and one end of the capillary was closed with a piece of filter paper. Special care were taken to obtain a constant and homogeneous packing. The filled capillary was then hanged with its open end from an electro-balance. While, the closed end was brought in contact with the test liquid kept in the reservoir with help of the movable platform. As soon as the end of the capillary tube comes in contact with the test liquid, the liquid starts penetrating into packed column and the weight of the capillary tube increases with time. This increase in weight with time is measured. Several test liquids covering a wide range of surface tensions are used and for each test liquid, several experimental runs are carried out to obtain a statistical average.

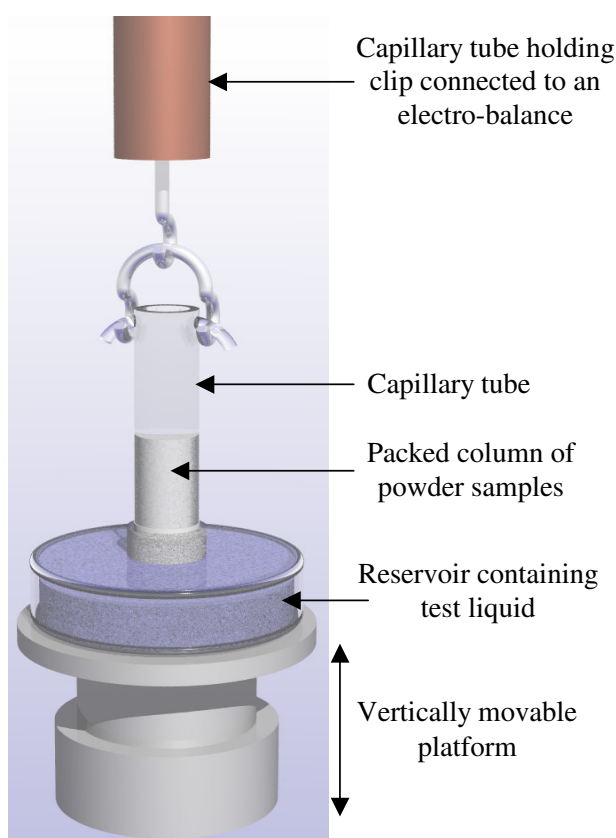


Figure C.1 Experimental setup for surface tension measurement of LDH materials using capillary penetration method

For a given test liquid, from the several measurements, the plots of M^2 against t were constructed and slopes were calculated during the initial phase of weight rise, where the slope remain nearly constant. The average of these slopes was then normalized with η/ρ^2 to get the average value of $K\gamma_{lv}\cos\theta$. These steps are repeated for test liquids with different γ_{lv} to obtain a series of $K\gamma_{lv}\cos\theta$ values. When $K\gamma_{lv}\cos\theta$ is plotted against γ_{lv} , it passes through a maximum at which the γ_{lv} closely resembles the surface tension of the powder material used for the experiment.

CURRICULUM VITAE OF FRANCIS RENY COSTA



Personal Details:

Last Name	Costa
First Name	Francis Reny
Date of Birth	17th January, 1976
Nationality	Indian
Marital Status	Married to Swapna Costa Sarkar and has one daughter
Present Address	Leibniz-Institute for Polymer Research Hohe Strasse 6 01069 Dresden Germany
Permanent Address	221B/1 M. G. Road Prantik, P. O. Thakurpukur Kolkata - 700063 West Bengal, India
Email Address	costa@ipfdd.de, francis_rc@yahoo.com

Research Interests:

1. Polymer nanocomposites synthesis and characterization
2. Rheological analysis of polymeric materials using both experimental and theoretical approach
3. Layered double hydroxide type clay synthesis, organic modification and their applications as multifunctional filler in polymers
4. Flame retardancy of polymeric materials
5. Fracture mechanics

Academic Records:

Ph.D. Dissertation: Mg–Al Layered Double Hydroxide: A Potential Nanofiller and Flame-Retardant for Polyethylene
(2003 – 2007) Supervisor: Prof. Dr.rer.nat.habil. Gert Henrich
Pursued at *Leibniz-Institute of Polymer Research Dresden, Germany* and as a registered student of Faculty of Mechanical Engineering, Technische Universität Dresden, Germany

M.Tech. Rubber Technology
(2000 – 2002) *Indian Institute of Technology, Kharagpur, India*, (Result: First Class, Rank 1)
Worked in Germany at *Institute for Plastic Processing (IKV), RWTH Aachen* for M. Tech. project, which dealt with the application of PECVD (Plasma Enhanced Chemical Vapor Deposition) technique to form gas barrier coating on PET film and its characterization.

B.Tech. Polymer Science and Technology
(1997 – 2000) *University of Calcutta, India*, (Result: First Class).

B. Sc. Chemistry (as major), Physics and Mathematics
(1994 – 1997) *St. Xavier's College, Calcutta (under University of Calcutta), India*, (Result: First Class).

Work Experience:

2002 – 2003 Worked as project assistant in a consultancy project under Sponsored Research and Industrial Consultancy (SRIC) at Indian Institute of Technology, Kharagpur, India (Principal project invigilator Prof. A. K. Bhowmick).
The project dealt with the development of radiation curable NBR/CR based rubber compounds for O-ring, gaskets and diaphragms for application in Indian railways.

Academic Awards:

1. DAAD-Leibniz Scholarship: For Ph.D. research at Leibniz-Institute of Polymer Research, Dresden, Germany (2003 -2007)
2. DAAD Scholarship: Under sandwiched program (between Indian Institute of Technology and German Academic Exchange Service) for Master Project in Germany (2001-2002)
3. Incab Rubber Prize: For the best CGPA in M.Tech. in Rubber Technology Center, Indian Institute of Technology, Kharagpur (2002)
4. Modi Rubber Prize: For best Master project work in Rubber Technology Center Indian Institute of Technology, Kharagpur (2002)

Publications:

Book Chapter:

1. 'Industrial relevant Preparation, Characterization and Application of Polymer Nanocomposites' by Andreas Leuteritz, Bernd Kretzschmar, Doris Pospiech, Francis Reny Costa, Udo Wagenknecht and Gert Heinrich; Chapter 19 in "Polymeric Nanostructures and Their Applications" edited by H. S. Nalwa, American Scientific Publisher, 2006.
2. 'Thermoplastic Elastomers' by F. R. Costa, N. K. Datta, N. Roy Choudhury, and A. K. Bhowmick in "Current Topics Of Elastomer Research" edited by A. K. Bhowmick, CRC Press-Taylor and Francis Group, LLC.

Journals:

1. Layered Double Hydroxide Based Polymer Nanocomposites. F. R. Costa, M. Saphiannikova, U. Wagenknecht and G. Heinrich; **Advances in Polymer Science**, 210 (2008) 101 - 168, online from October 2007.
2. Nonlinear Behaviour of Polyethylene/Layered Double Hydroxide Nanocomposites Under Shear Flow; M. Saphiannikova, F. R. Costa, U. Wagenknecht, G. Heinrich; 2007, accepted in *Polymer Science*.
3. Intercalation of Mg–Al based layered double hydroxide by anionic surfactants containing different functionalities using regeneration method; F. R. Costa, A. Leuteritz, U. Wagenknecht, D. Jehnichen, L. Häussler and G. Heinrich; 2007, article in press in *Applied Clay Science*.
4. LDPE/Mg–Al layered double hydroxide nanocomposite: Thermal and flammability properties; F. R. Costa, U. Wagenknecht and G. Heinrich; *Polymer Degradation and Stability*, 92 (2007) 1813 – 1823.
5. Polyethylene/Mg–Al Layered Double hydroxide Based Nanocomposites: II. Rheological Characterization; F. R. Costa, M. A. Goad, U. Wagenknecht and G. Heinrich; *Polymer*, 47 (2006) 1649 – 1660.

6. Microwave Assisted HMDSO/Oxygen Plasma Coated Polyethyleneterephthalate Films: Effects of Process Parameters and Uni-axial Strain on Gas Barrier Properties, Surface Morphology and Chemical Composition; E. Schmachtenberg, F. R. Costa and S. Goebel, *J. Appl. Polym. Sci.*, 99 (2006) 1485 – 1495.
7. Morphology and fracture behaviour of polyethylene/Mg–Al layered double hydroxide (LDH) nanocomposites; F. R. Costa, B. K. Satapathy, U. Wagenknecht, R. Weidisch and G. Heinrich; *European Polymer Journal*, 42 (2006), 2140 – 2152.
8. Nanocomposites Based on Polyethylene and Mg–Al Layered Double Hydroxide: Characterization of the Modified Clay, Morphological and Rheological Analysis of the Nanocomposites; F. R. Costa, U. Wagenknecht and G. Heinrich; *Plastic Rubber and Composites: Macromolecular Engineering*, 35 (2006), 139 – 148.
9. Polyethylene/Mg–Al Layered Double hydroxide Based Nanocomposites: I. Synthesis and Characterization; F. R. Costa, M. A. Goad, U. Wagenknecht and G. Heinrich; *Polymer*, 46 (2005) 4447 – 4453.
10. Structural Kinetics in Filled Elastomers and PE/LDH Composites, G. Heinrich, V. Hrtel, J. Tschimmel, M. Klüppel, F. R. Costa, M. Abdel-Goad, U. Wagenknecht, A. L. Sviskov, B. Lauke; *Kautschuk Gummi Kunststoffe*, 4 (2005) 163 – 167.
11. Influence of electron beam irradiation as one of the mixed crosslinking systems on the structure and properties of nitrile rubber, V. Vijaybaskar, F. R. Costa and Anil K. Bhowmick; *Rubber Chemistry and Technology*, 77 (4) (2004), 624 – 645.

Conference:

1. Strain Behavior of Plasma-Polymerized Permeation Barrier Layers on Plastics Films; W. Michaeli, S. Gbel, F. Costa; PPS 18 (18th Annual Meeting of Polymer Processing Society), Portugal, June 2002 (Proceeding).
2. Flame Retardancy plus Mechanical Improvement - a New Way of Materials Design; U. Wagenknecht and F. R. Costa; PPS 20, 2004, Akron, USA (Proceeding).
3. Structural Kinetics in Filled Elastomers and PE/LDH composites; G. Heinrich, F. R. Costa, M. A. Goad and U. Wagenknecht; 6th Fall Rubber Colloquium (KHK), Hanover (G), November 10th -13th, 2004 (Proceeding).
4. Nanocomposites Based on Polyethylene and Mg-Al-Layered Double Hydroxide - Potential Environment Friendly flame-retardant Composites; F. R. Costa and U. Wagenknecht; Polymerwerkstoffe 2004, Halle, Germany (Proceeding).
5. Nanocomposites Based on Polyethylene and Mg–Al-Layered Double Hydroxide: Rheological Characterization; F. R. Costa, M. A. Goad, U. Wagenknecht and G. Heinrich; PPS 21 (21th Annual Meeting of Polymer Processing Society), Leipzig, Germany, June 2005 (Proceeding).

6. Flame-Retardant Polyolefin Composites with Improved Mechanical Properties using Reinforcing flame-retardants; U. Wagenknecht and F. R. Costa; PPS - 2005, America's Regional Meeting, August 14 - 17, 2005, Quebec City, Canada (Proceeding).
7. Layered Double Hydroxides (LDH) als verstärkende Flammhemmer; F. R. Costa, U. Wagenknecht, G. Heinrich, S. Reinemann; TECHNOMER 2005 (19th Fachtagung ber Verarbeitung und Anwendung von Polymeren), 10 - 12th November, Chemnitz, Germany (Proceeding).
8. Nonlinear shear response of the PE-LDH nanocomposites; M. Grenzer, F. R. Costa, U. Wagenknecht and G. Heinrich; Euromech Colloquium 487 "Structure sensitive mechanics of polymer materials: physical and mechanical aspects", 10 – 13th October, 2006 Strasbourg, France (Proceeding).
9. Flame Retardancy and Mechanical Properties of $Mg(OH)_2$ Filled Polyethylene Composites: Potential Development on an Unavoidable Compromise; F. R. Costa, U. Wagenknecht and G. Heinrich; European Meeting on Fire Retardancy and Protection of Materials (FRPM'05) (10th European Conference on Fire Retardant Polymers) BAM, Berlin, Germany, 7 - 9th September, 2005 (Poster).
10. Polyolefin-inorganic filler based flame-retardant composites: prospective development in improvement in mechanical properties; U. Wagenknecht, F. R. Costa and G. Heinrich; 8th European Symposium on Polymer Blends (Eurofillers 2005), May 9 to 12, 2005, Bruges, Belgium (Poster).
11. Complex shear response of the PE-LDH nanocomposites; M. Grenzer, F. R. Costa, U. Wagenknecht and G. Heinrich; Jlich soft matter days 2006, 14 – 17th November, 2006, Bonn, Germany (Poster).